TNO innovation for life

# MMU

## UNRAVELLING THE STRATIGRAPHIC AND STRUCTURAL DEVELOPMENT OF THE STRATA FOUND UNDERNEATH AND ABOVE THE MID-MIOCENE UNCONFORMITY

*by Geert de Bruin, Kees Geel, Sander Houben, Dirk Munsterman, Hanneke Verweij, Jeroen Smit, Nico Janssen, Susan Kerstholt-Boegehold, and Vincent Vandeweijer*

*Frontpage: Crossbedding in a Miocene outcrop, Denmark*

TNO Report 2017 R10425

Final report

# MMU

## UNRAVELLING THE STRATIGRAPHIC AND STRUCTURAL DEVELOPMENT OF THE STRATA FOUND UNDERNEATH AND ABOVE THE MID-MIOCENE UNCONFORMITY

Geert de Bruin, Kees Geel, Sander Houben, Dirk Munsterman, Hanneke Verweij, Jeroen Smit, Nico Janssen, Susan Kerstholt-Boegehold, and Vincent Vandeweijer

Sponsors: Wintershall Noordzee B.V.
EBN B.V.
ENGIE B.V.
TAQA Energy B.V.
Rosewood Resources

Project name: MMU
Project number: 060.18855
Date: 30 March 2017



This project is executed with subsidy from the Ministry of Economic Affairs, National Regulations EA-subsidies, Topsector Energy executed by the Netherlands Enterprise Agency

## Acknowledgements

We would like to express our greatest appreciation to the sponsors of this project. Especially, Wintershall has been a driving force behind this project by providing great feedback and provisioning valuable data. We would like to offer a special thanks to Fred Kluin (Wintershall) for his assistance with the collection of the data and Henk van Lochem (Wintershall) for reviewing the report.

# CONTENT

*The Netherlands from the ISS by Jeff Williams*

# 1. INTRODUCTION AND SCOPE

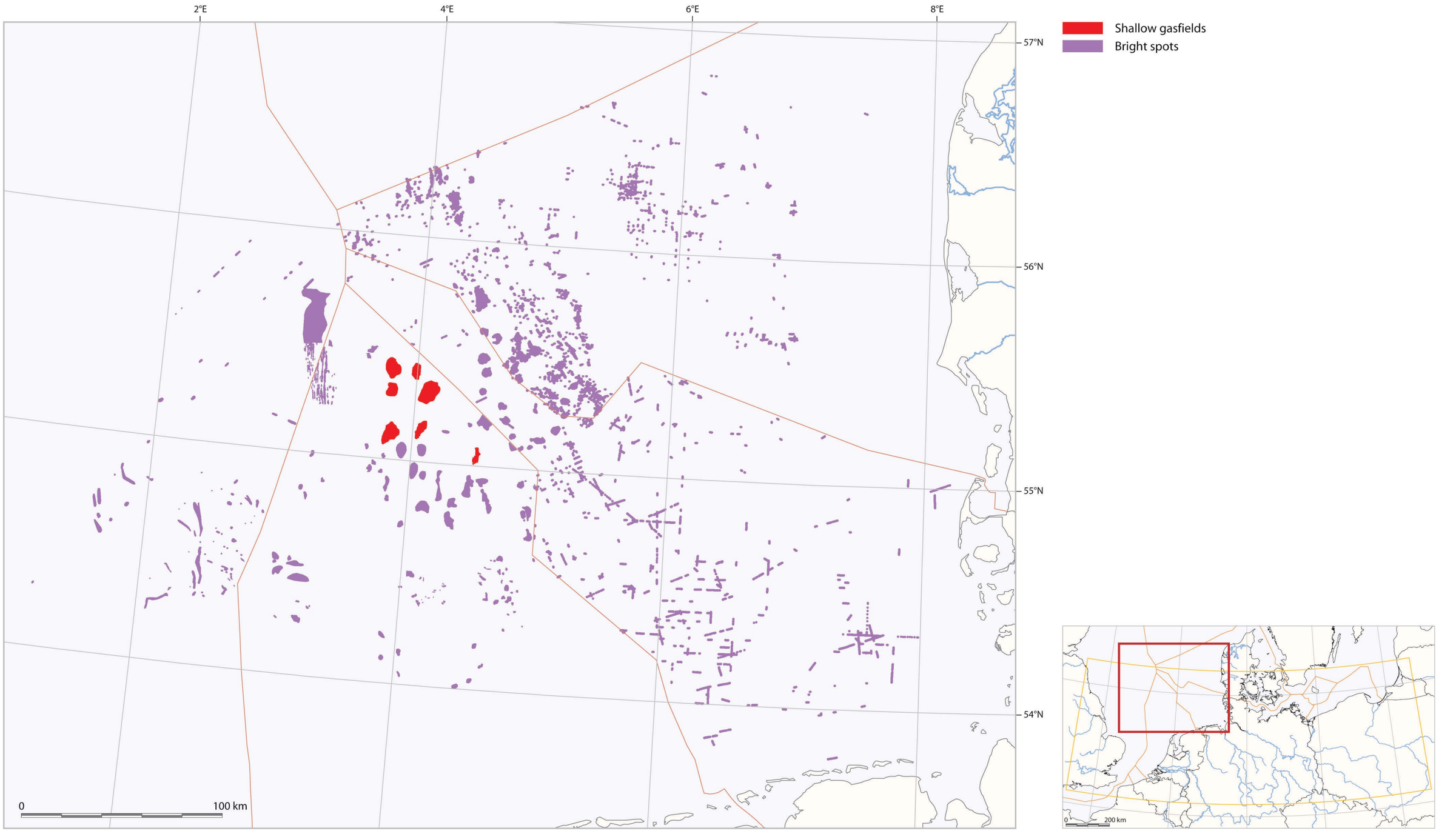


**Figure 1.1: "Distribution of bright spots and amplitude anomalies in the southern North Sea. Bright spots are observed on 2D- and 3D-seismic data as high amplitudes, probably caused by microbial or thermogenic gas in the pore fluid. Most bright spots were found at the top of Pliocene sands. Linear alignments of some bright spots in the English and German North Sea sectors are related to the locations of the 2D-seismic lines used rather than to geological structures." From SPBA**

## Introduction

The recent discovery of hydrocarbons in the “Little John” structure in the Danish sector of the North Sea led to a renewed interest in the Neogene. In similar aged strata in the Netherlands, that are found in the interval around the Mid Miocene Unconformity (MMU), indications for hydrocarbons are found (see figure 1.2). Furthermore, the MMU petroleum play seems to be present in the same area where the Neogene gas fields are found. Whether this play is linked to other petroleum systems (deeper or shallower) was unclear at the start of this project, but since multiple prospects can be found overlying each other, risks of drilling failures are spread and, Neogene prospects (figure 1.1), that are deemed uneconomical, could become economical.

The interval was never studied in great detail since most operators considered drilling (and logging) through the Cenozoic section to be a necessary evil to get to deeper targets. This study will increase or knowledge of the interval around the MMU’s in order to understand the potential of this interval as a petroleum play, multiple aspects of this system are studied in several work packages.

## Aim of the project

The aim of this project is to unravel the stratigraphic and structural development of the strata that are found underneath and above the Mid-Miocene Unconformities, with the goal to better understand and predict the presence of reservoir sands. This could potentially lead to a complete new petroleum play by itself  or result increased production, by taking additional layers into production.

## Main research questions:

- What stratigraphic level(s) contain reservoir sands (with recorded HC shows)?
- What is the depositional environment?
- What are the ages of the deposits that are found below, in between, and above the unconformities?
- What is the difference between the lithostratigraphic and seismic definition of the base of the Upper North Sea Group?
- What is the series of events (sedimentation, erosion, tectonic movements) that led to the development of the strata around the MMU?
- What causes the lateral and vertical pressure differences observed?
- The interpretation of headspace gas analyses in order to study the gas-migration conditions, origin of the gas, and the influence of the MMU on migration.

## Approach

The project will start with a literature review of the tectonic evolution of the North Sea. The project is centred on three regional seismic lines that run through the entire Dutch Northern offshore. After seismic interpretation of these seismic lines, Wheeler diagrams are made out of them. Ten wells that are along these transects are analysed to identify reservoir facies (petrophysics) and to establish the age of the sediments (palynology). Furthermore, pressure, gas composition and isotopes are studied. All results are integrated to answer the research questions mentioned above.

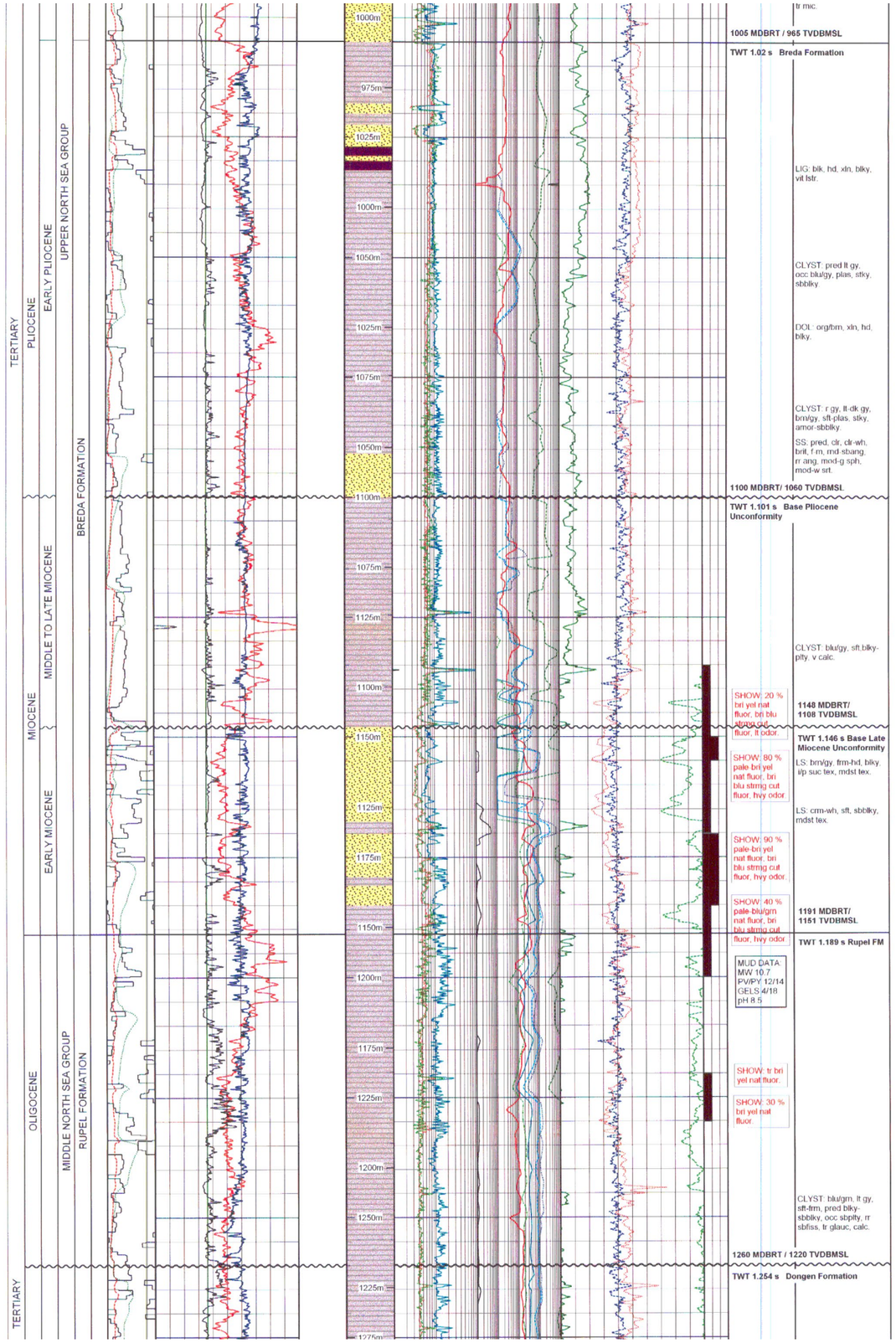


**Fugure 1.2: Composite log of well F02-06 showing the interval around the MMU**

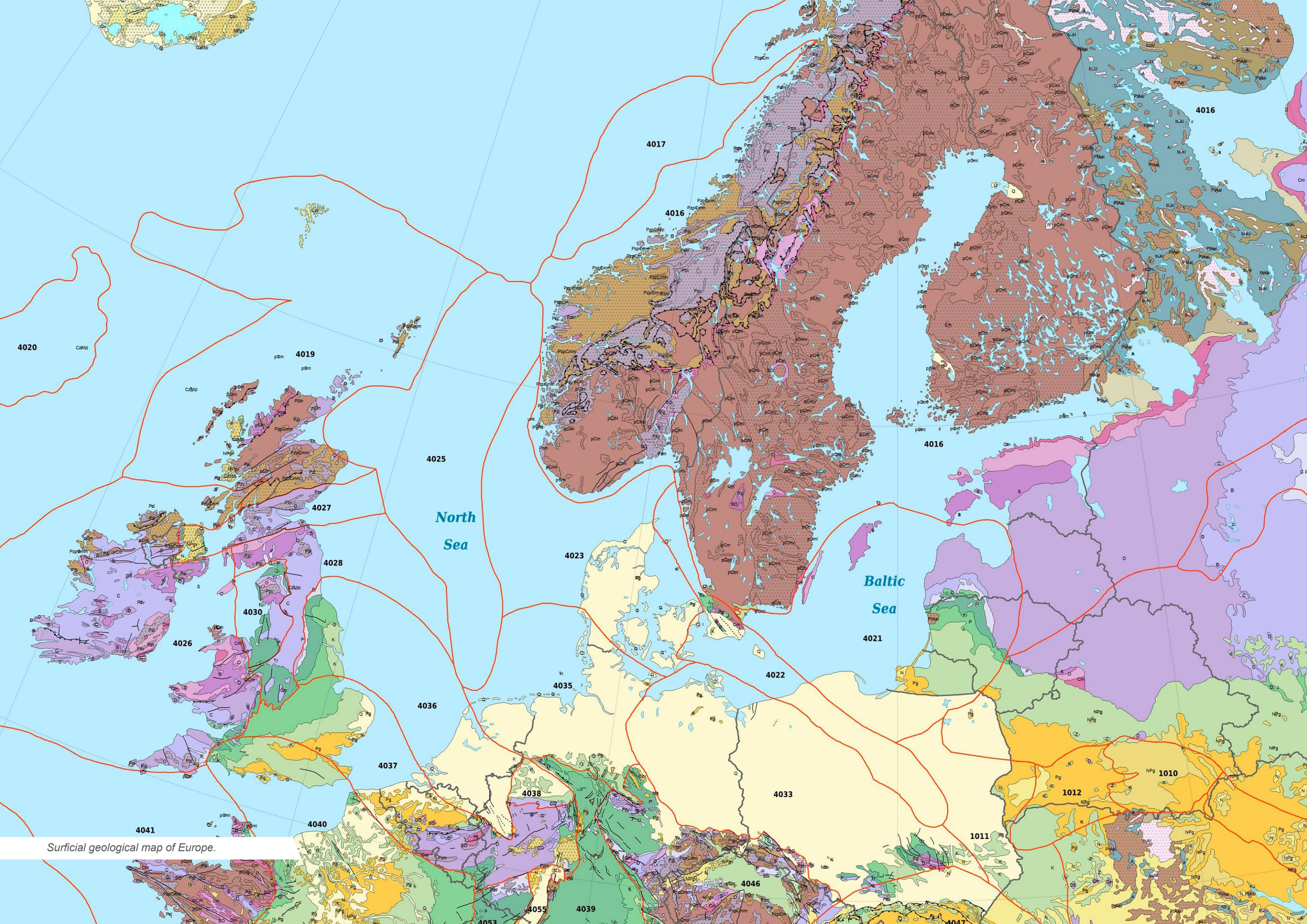


*Surficial geological map of Europe.*

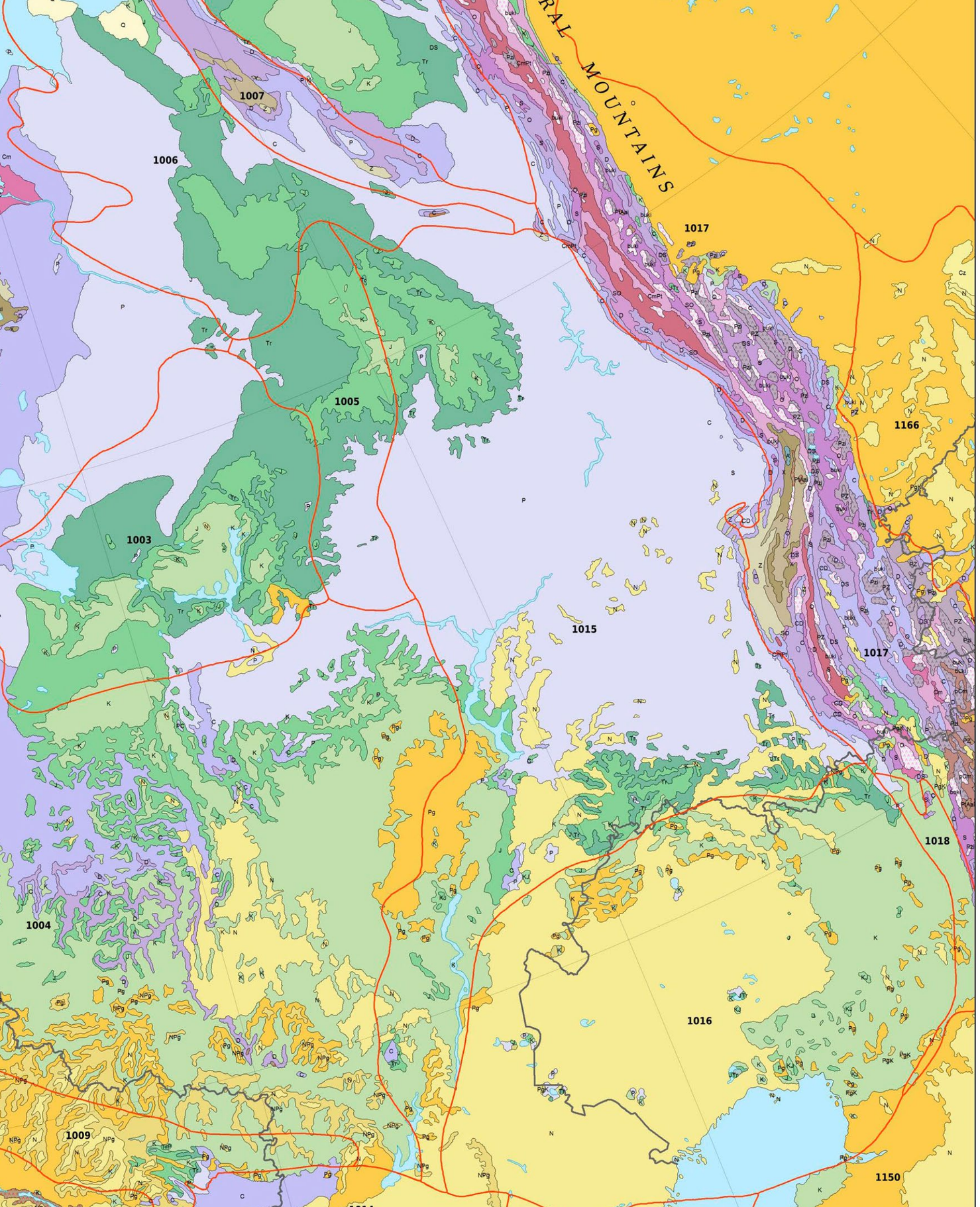


## 2. Geological Background

## Introduction

The Neogene succession of the southern North Sea is characterized by the westward prograding Eridanos delta of Mid Miocene to Pleistocene age. Fed with erosional products from Scandinavia, mainly southern Sweden, the early middle to late Miocene Eridanos delta was located along the southern Norwegian and Danish shore. Westward progradation continued into the Pliocene and Pleistocene with a lateral shift of the depocentre towards the Dutch northern offshore. With most research focussing on either the Danish or Dutch part, the distinction between early, Norwegian/Danish and the late, Dutch Eridanos deltas is not always made in literature leading to confusion. Furthermore, characterisation of sedimentary units, and stratigraphic boundaries is only valid locally and subject to lateral variability. For instance, a package with high angle clinoforms and erosional truncation at the top in Denmark, may laterally change into a low angle package with a conformable top in the Netherlands.

This section contains the summary of a literature study of the Neogene southern North Sea with a focus on the relationship between Eridanos delta and the Miocene unconformities, with the focus on the MMU and the nature of that MMU. Further discussion includes the relative role of climate and tectonics and possible explanations for the presence of glauconite-bearing sands beneath the Dutch Eridanos.

## Overview of the Miocene & Pliocene and its unconformities

The sedimentary succession of the Dutch northern offshore (Figure 2.1) consists of (I) a relatively thin early Miocene (Pre Eridanos) part, (II) a toe-of-slope facies of the early Eridanos (Mid-Late Miocene, Kuhlmann et al., 2006) and (III) a relatively thick Late Eridanos (Pliocene-Pleistocene) part.

The Miocene is bounded by the Savian Unconformity at its base and the Late Miocene unconformity (LMU) at its top. it contains the Early (EMU) and Mid Miocene unconformities (MMU). These main sequence boundaries represent numerous time gaps that can be traced over tens to hundreds of kilometres. In the German G-11-1 borehole (Figure 2.2) located very close to the border with the Dutch Northern offshore (Figures 2.2 and 2.3), ditch cuttings from Neogene and Paleogene sequences of the G-11-1 borehole from the German North Sea were analysed for dinoflagellate cysts and calcareous nannoplankton (Köthe, 2007; Köthe et al., 2008). The record displays several time gaps (Late Thanetian to Middle Ypresian, Bartonian to Middle Priabonian, earliest Oligocene, within the Middle Rupelian, Chattian to earliest Aquitanian (Savian), Middle Burdigalian (EMU) and Late Tortonian to Early Zanclean (LMU)). These time gaps can be traced for at least 30 kilometres in seismic lines.

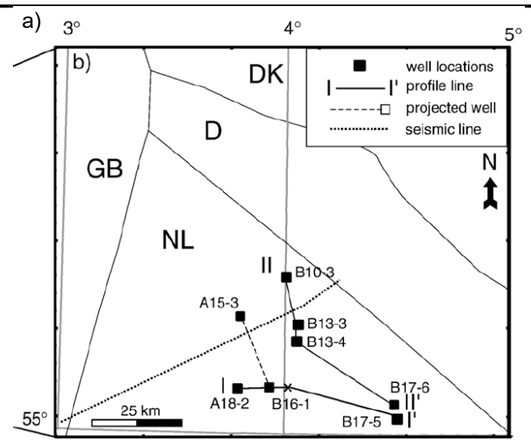


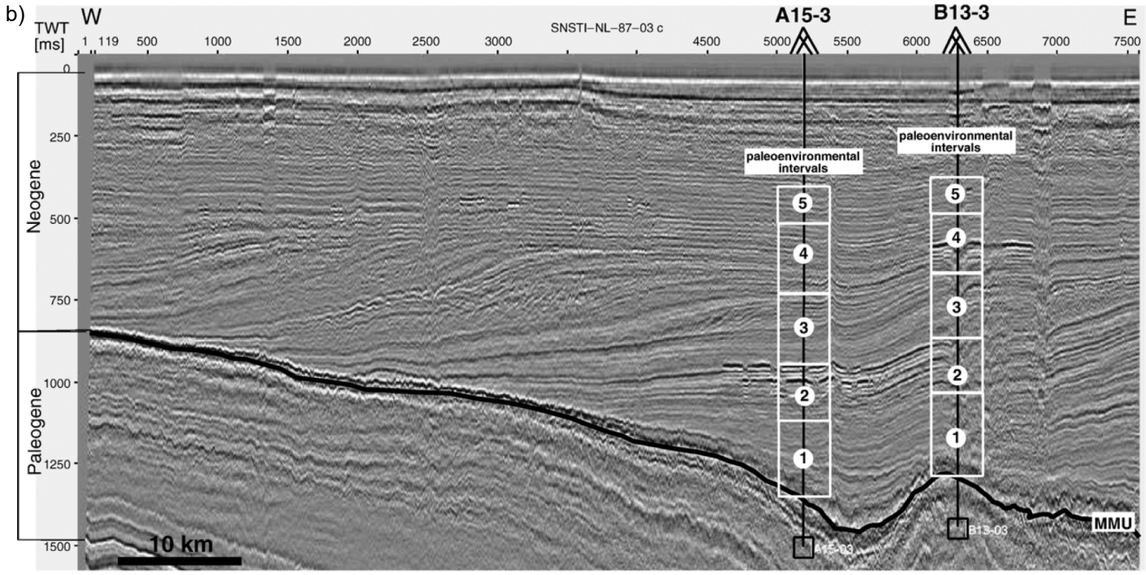


c)

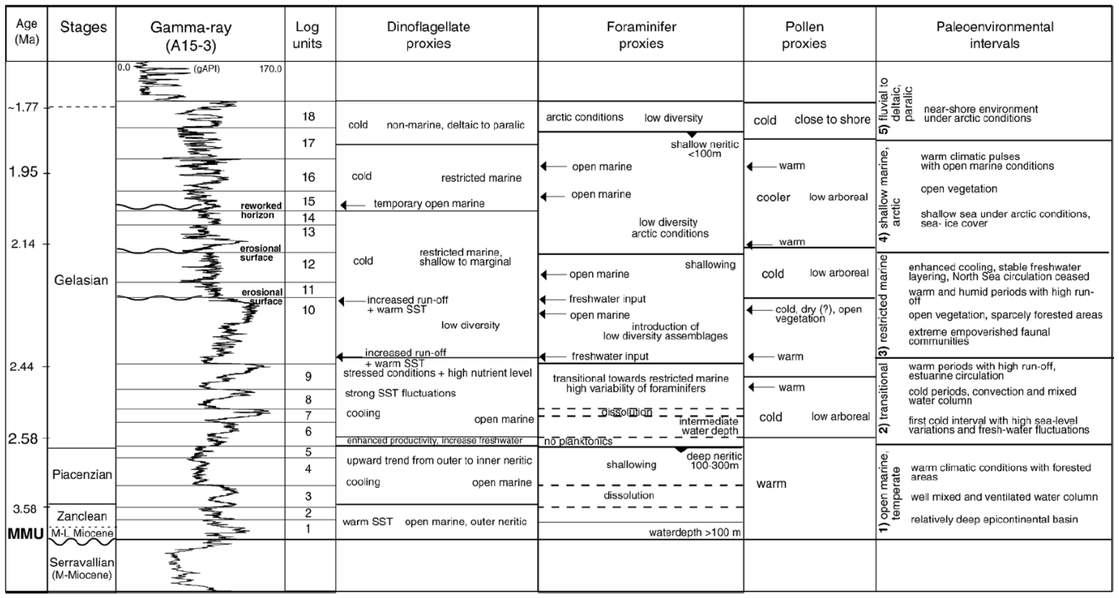


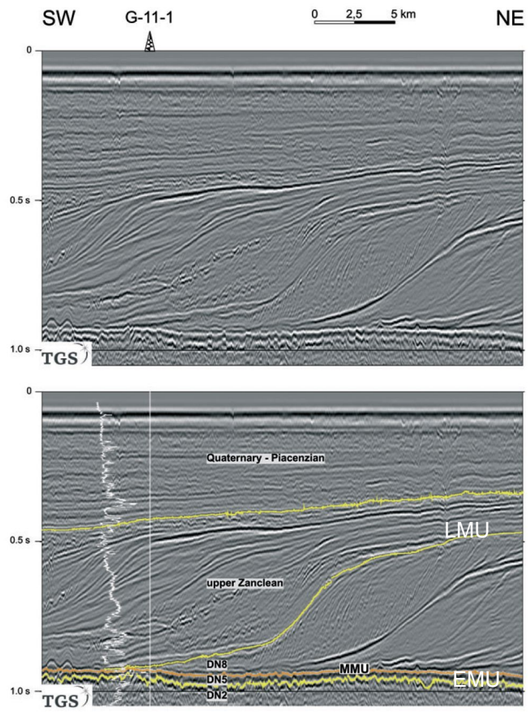


**Figure 2.2 Top: time migrated seismic line showing the early and late Eridanos deltas. Bottom: seismic with the gamma-ray log and the ages of the sediments in terms of dinoflagellate cyst zones Köthe (2007). The yellow lines separate intervals of different ages and are respectively time gaps (hiatuses or condensed sections). The orange line indicates the MMU, the yellow line above it represents the Late Miocene unconformity, while the line below it represents the Early Miocene unconformity. Note how the reflectors of LMU and MMU merge, still east of the DE/NL border.**

**Figure 2.1 Chronostratigraphic interpretation for the Neogene of the northern Dutch offshore (Kuhlmann et al., 2006). a) Map with location of seismic profile and the locations for the eighth wells used for biostratigraphic analyses are shown with closed squares. b) EW-trending seismic profile showing the progradational environment above the Mid-Miocene Unconformity (MMU) and the inferred paleoenvironmental intervals for two boreholes (A15-3, B13-3). The lower boundary of the interpreted interval is the Mid-Miocene Unconformity (MMU). Unit S1 represents Mid-Late Miocene (post-MMU) sediments of the Danish-German Eridanos delta. The top of Unit S1 represents the Late Miocene Unconformity (LMU). Units 2-13 represent the Pliocene (Dutch) Eridanos Delta. In the western half of the profile, beyond Unit S1, the LMU and MMU become one. The authors draw the Paleogene-Neogene boundary at the MMU. c) Integrated environmental interpretation of dinoflagellates, foraminifers and pollen, related to the log units. The resulting five paleoenvironmental intervals are indicated on the right (Kuhlmann et al., 2006).**

## Pre Eridanos

### The Eocene-Oligocene Transition and Top Rupelian

During the Middle-Late Eocene (Bartonian-Priabonian), the study area was the locus of open marine, claystone deposition (Dongen Fm. - Asse Mb.). Across the Eocene-Oligocene boundary, a substantial glacioeustatic sea-level fall led to erosion and non-deposition. Subsequent Early Oligocene trangsgression, following this phase of rapid Antarctic ice-sheet expansion led to re-establishment of the inner-outer neritic overall claystone deposition of the Rupel Fm. Subsequently, the Lower-Upper Oligocene (Rupelian-Chattian) boundary marks another phase of glacial expansion (Van Simaeys, 2004), causing the upper Rupelian and early Chattian to be often incomplete and recognition of the “Top Rupel”-surface.

### Savian

At the base of the Neogene (Miocene), the Savian Unconformity represents a gap separating Chattian from early Aquitanian or younger age deposits (Köthe, 2007). This Savian unconformity is related to a glacioeustatic event at the top of the Oligocene (Miller et al., 2008).

### Early Miocene Unconformity

The lower Miocene sequence of glauconite-bearing sands (Rasmussen and Dybkjær, 2014), is interrupted by the Early Miocene Unconformity (EMU) of Burdigalian, possibly early Langhian age (Dinocysts zone DN3, possibly DN4). These sands are separated from the  Early Eridanos delta (mid-late Miocene) by the MMU.

## Early Eridanos

The early Eridanos delta developed above the Mid Miocene Unconformity (MMU, e.g. Cameron et al., 1992; Anell et al., 2012; Gołędowski et al., 2012). In the Dutch northern offshore, the post-MMU toe-of-slope sediments form a condensed sequence that consists of Tortonian fine grained siliciclastics. This condensed section (Interval 1 in Figure 2.1) corresponds to the distal parts of the sedimentary system that started deposition onto the MMU (Kuhlmann and Wong, 2008). Because of the westward progradation of the Eridanos delta, the Early Eridanos is thicker in the Danish/German sector.

### Mid Miocene Unconformity (MMU)

The MMU (Fig. 2.4) forms the lower (seismic) stratigraphic boundary of the Eridanos delta. It is clearly one of the main (seismic) horizons. The nature of the MMU changes throughout the North Sea. It was described as a transgressive surface, appearing as an onlap surface on seismics towards the north-eastern part of the North Sea Basin. In contrast, it is characterized by a downlap surface within the southern North Sea region and as a conformable surface in the Central Graben area (Anell et al., 2012) Cameron et al., 1993; Huuse and Clausen, 2001; Kuhlmann and Wong, 2008).

A detailed study of a Danish offshore well provided the most complete picture of the MMU in the southern North Sea (Rasmussen and Dybkjær, 2014) and is therefore of prime interest. Results show that, instead of an unconformity, there is a continuous sedimentation dominated by glaucony-rich mud where a ca. 3 m thick mud layer spans several millions years and thus are below seismic resolution (Rasmussen and Dybkjær, 2014). In the eastern North Sea basin (the Danish and Norwegian sectors of the North Sea) the ‘mid-Miocene unconformity’ represents a distinct shift from prograding delta/slope systems to deposition of deeper marine hemipelagic mud, and thus provides a distinct seismic marker horizon (Rasmussen and Dybkjær, 2014). According to the Danish litho-stratigraphy , the so-called ‘mid-Miocene Unconformity’ refers to the top of the Hordaland Group (the base of the Nordland Group) sensu Eidvin & Rundberg (2007) and to the base of the fully marine Hodde Formation (Rasmussen et al. 2008, 2010).

Although the Lower and mid Miocene transgressions may have been among the largest during the Cenozoic, Miocene sediments are largely absent in the western, British part of the southern North Sea basin (Cameron et al., 1992). Instead large-scale incision along the MMU into the Paleogene sequences indicate that the MMU is a real unconformity in the western North Sea. Either southern Scandinavia was the only major sediment source or Miocene sediments have been eroded in the western, British part of the southern North Sea basin

An early Serravalian age for onset of the MMU is proposed by Köthe (2007) (Figure 2.3), based on the early Serravalian age, 14.8 Ma, of sediments below the MMU (dinoflagellate cyst zone DN5, calcareous nannoplankton zone NN5). This age is in agreement with the first consistent correlation and dating both onshore and offshore Denmark and Norway that suggests a mid Miocene age (ca. 15 Ma) (Dybkjær and Piasecki, 2010). The oldest sediments above the MMU are early Tortonian, ca. 11 Ma (dinoflagellate cyst zone DN8) (Köthe, 2007). The onset of sedimentation onto the MMU is estimated at 12 Ma (Middle Miocene) in the Dutch Northern offshore (Kuhlmann et al., 2006a). In conclusion, the MMU spans most of the Serravalian.

## Late Eridanos

The Dutch Pliocene-Pleistocene Eridanos delta is deposited westward of the early Eridanos and after the late Miocene Unconformity (e.g.Overeem et al., 2001; Kuhlmann et al., 2006; Kuhlmann and Wong, 2008; Benvenuti et al., 2012). The Late Eridanos was subdivided into 3 mega sequences in the Netherlands by Ten Veen et al., 2013

### LMU

The Late Miocene Unconformity is of Messinian to early Zanclean age and forms the upper  seismic sequence boundary to the early, DK/DE Eridanos delta and the lower seismic sequence boundary to the young, Dutch Eridanos delta (Downlapping surface).

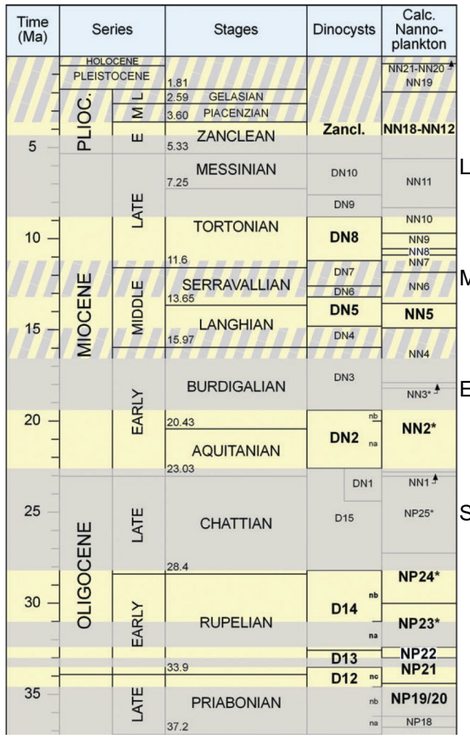


**Figure 2.3: Hiatuses of the G-11-1 borehole. Yellow, stratigraphic intervals; grey: time gaps (hiatuses or condensed sections) Koëthe 2007**

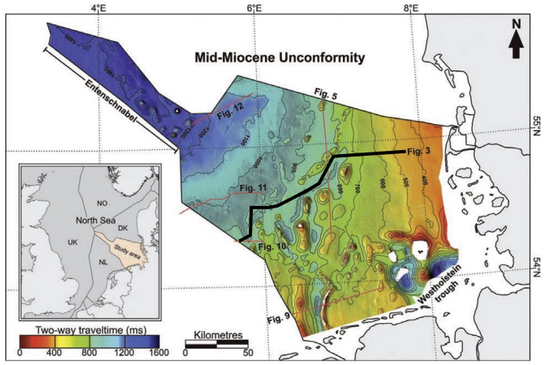


**Figure 2.4: Below: Interpreted composite seismic line in the German offshore showing the MMU as the base of the Eridanos Delta (Thöle et al., 2014).  Right: The orientation of the composite line is shown on a time-structure map of the Mid-Miocene Unconformity (MMU)  for the German North Sea sector (Thöle et al., 2014). Contour lines are every 100 ms (TWT).**

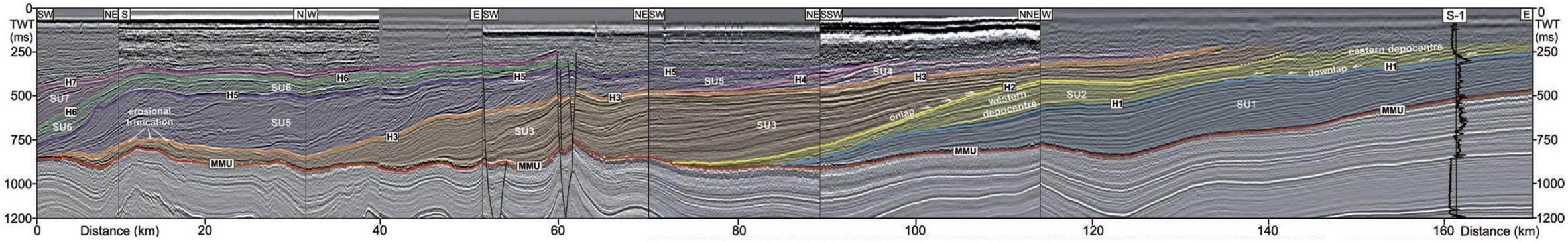

## Neogene detrital influx: driven by tectonics or climate?

Understanding the factors that led to the MMU is of key importance for the stratigraphic architecture of the Neogene in the North Sea. Whether climate changes or regional tectonics are responsible for the MMU remains a matter debate. The main factors included in this debate are outlined in this section.

### Regional Tectonics

The regional tectonics of the circum North Sea during the Cenozoic are marked by vertical motions (Japsen, 1997; Japsen et al., 2008; Holford et al., 2009; Anell et al., 2010; Japsen et al., 2015). Paleogene and Neogene long wave-length vertical motions caused km-scale uplift of areas surrounding the North Sea such as the UK and Ireland, Southern Norway and Southern Sweden and contemporaneous km-scale subsidence of the Southern North Sea basin (Figure 2.5).
Different phases of tectonic activity related to Atlantic opening and Africa-Europe convergence have played a role in the Cenozoic vertical movement of the North Sea (Hillis et al., 2008; Holford et al., 2009, see Figure 2.6).

### Local tectonics: salt diapirism

Growing salt diapirs may create seafloor local topography consisting of relatively local and fast growing domes potentially surrounded by rim synclines. These domes are particularly prone to (submarine) erosion that quickly reaches deeper stratigraphic levels due to the small surface to volume ratio of these ‘domes’. The rim synclines surrounding the diapirs ensures local redeposition, i.e. short transport distances. Thöle et al. (2016) point to the possible relation of salt diapirs and (mass transport) deposits in the southern North Sea.

### Climate

With the inception of global cooling and Antarctic ice-growth across the Eocene-Oligocene Transtion, deteriorating climate left a marked sedimentary response, with glacioeustatic sea-level variations becoming prominent. The primary tool to track such changes is by means of benthic oxygen isotope records that herald the effects of temperature and global ice-volume. During the Oligocene, the most pronounced glacial maxima occur in the Early Chattian. A next major glacial maximum (and sea-level drop) is found at the Oligocene-Miocene boundary (the Mi-1 Event, Miller et al., 1991). Hence, the Savian Unconformity is to some extent associated with glacioeustasy. During the Miocene, several phases of glacioeustatic variation are reflected by recurring Miocene Isotope Events (Mi’s, see Figure 2.7). Remarkably, a transition to higher sea-level happened during the Early-Middle Miocene transition, leading to the recognition of the Mid-Miocene Climatic Optimum, culminating in the Langhian. During the Serravalian, a relatively large glacioeustatic sea-level fall is imposed, after which the Late Miocene is relatively stable. Hence, the MMU might some extent be associated with glacioeustatic sea-level fall. A next major change is of course the onset of Northern Hemisphere glaciation at the base of the Pleistocene.

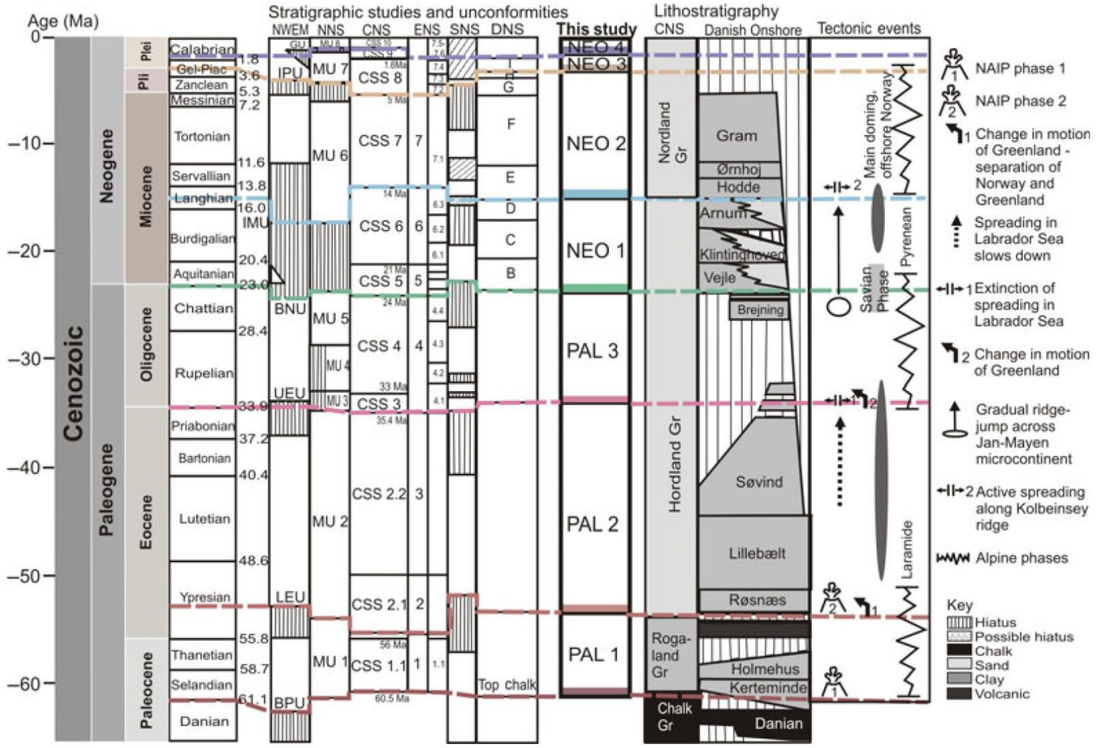


Figure 2.6: Seismic stratigraphy and lithostratigraphy for the North Sea according to Anell et al. (2012), Main tectonic events adapted from (Praeg et al., 2005) and (Lundin and Doré, 2011). Pli, Pliocene; Plei, Pleistocene; Gel-Piac, Gelasian-Piacenzian; NWEM, Northwest European margin; CNS, Central North Sea; ENS, Eastern North Sea; NNS, Northern North Sea; SNS, Southern North Sea; DNS, Danish Sector North Sea (GEUS reference lines); BPU, Base Palaeogene Unconformity; LEU, Lower Eocene Unconformity; UEU, Upper Eocene Unconformity; BNU, Base Neogene Unconformity; IMU, Intra Miocene Mnconformity; IPU, Intra Pliocene Unconformity; GU, Glacial Unconformity; Mf: Moray Firth; NW NS, northwest North Sea; NNS, northern North Sea; M, Moray group; B, Beauly Formation; D, Dornoch Formation (from Anell et al., 2012).

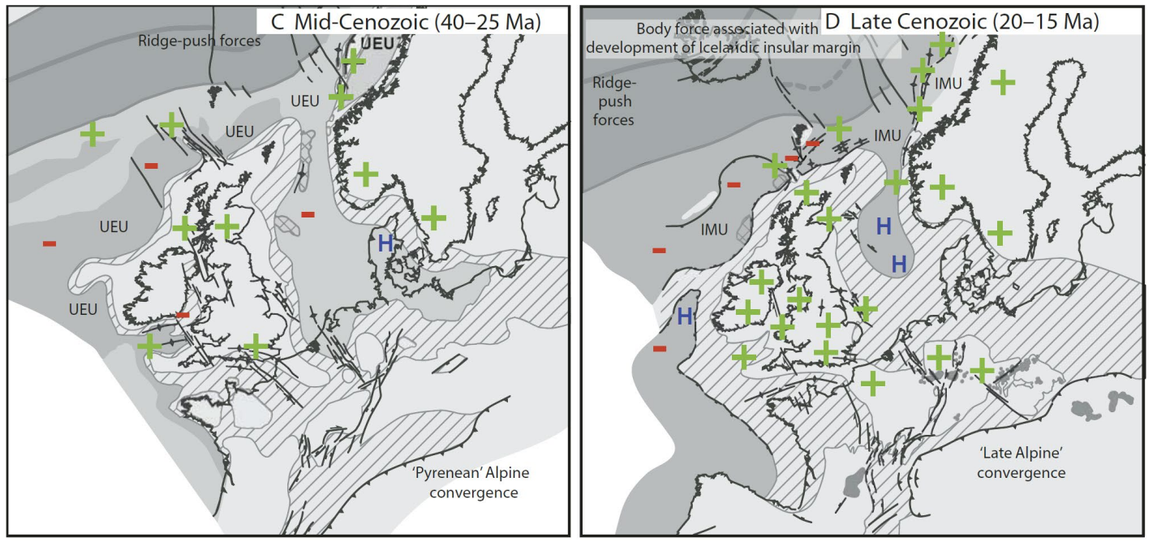


Figure 2.5: Paleogeographic reconstructions of NW Europe (Holford et al., 2009) with superimposed patterns of vertical motions (from this study) during the a) mid-Cenozoic (40–25 Ma) and b) late Cenozoic (20–15 Ma). Plus and minus symbols indicate areas undergoing uplift/exhumation or subsidence/burial, respectively, during the indicated time windows. h—hiatus; IMU: Intra-Miocene unconformity (MMU); UEU: Upper Eocene unconformity.

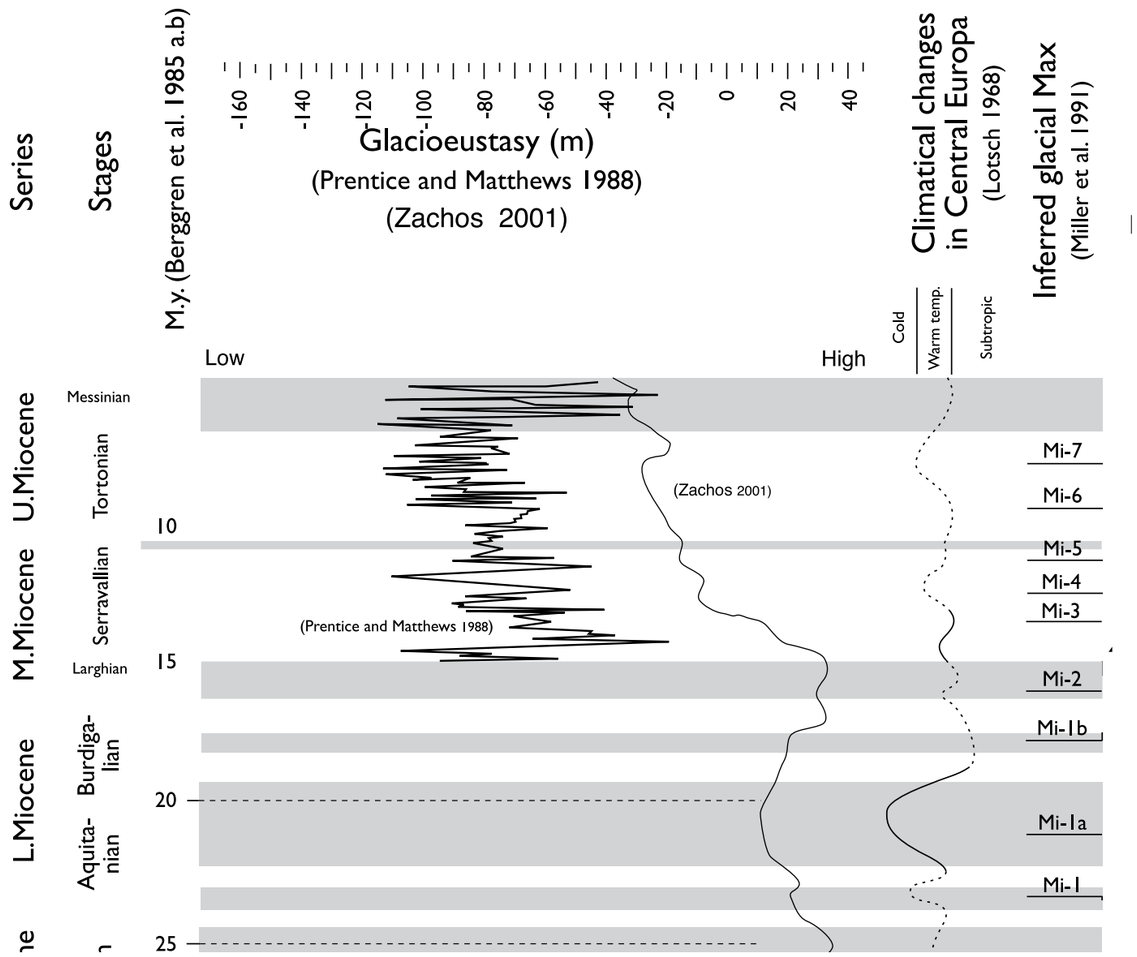


**Figure 2.7: Comparison of (global) glacio-eustatic sea-level changes (derived from oxygen isotope records), climatic change and timing of maximum glaciations (Mi-events). Modified after Rasmussen, 2008.**

### The MMU Climate vs Tectonics

The correlation between (Mid) Miocene sedimentation in the North Sea and climate shifts is the matter of a strong debate. The pro's and contra's for climate driven sedimentation and formation of unconformities can be summarised by the following discussion between Danish research groups.

Gołędowski et al., (2012) compiled the sediment flux from a combination of seismic and borehole data and results from other publications to discuss the relative importance of tectonics, climate and climate change. They conclude that variations in the sediment flux from western Scandinavia correlate better with climate and climate change from the Eocene and onward, possibly related to the increased seasonality that stimulated the sediment flux. Significant climatic cooling episodes correlate with Oligocene deposits in the North Sea, the mid-late Miocene formations of the Norwegian Shelf, the southern North Sea delta system (the early Eridanos) and large volumes of the Late Pliocene-Holocene Formation (the late Eridanos). Gołędowski et al., (2012) notice that the Cenozoic sediment flux from Scandinavia is in general agreement with the detrital flux to the world's oceans.

The occurrence of the prograding deposits with higher depositional rates than underlying deposits above the Mid-Miocene Unconformity is consistent with the cooling following the Mid-Miocene Climatic Optimum (Gołędowski et al. 2012). These authors see herein confirmation for their theory of major climate control on erosion rates during the Cenozoic. Furthermore, these authors argue that the increase in sediment yield during Late Pliocene to Pleistocene times is fully explained by the increased importance of glaciers and their ability to overstep fluvial drainage divide (Gołędowski et al., 2012). The western Scandinavian highlands and surrounding basins show similar features to other glaciated orogens with regards to an increased sediment output during cold climates. (Gołędowski et al. 2012).

According to Rasmussen and Dybkjær (2014), the conclusions from Gołędowski et al. (2012) are not supported by the geological record. They stress that the 'mid-Miocene unconformity' is not a regional hiatus in the Danish and Norwegian sectors of the North Sea basin, but represents a distinct shift from prograding delta/slope systems to deposition of deeper marine hemipelagic mud. Rasmussen and Dybkjær, (2014) mention that a warm climate and dense vegetation cover in southern Scandinavia during the mid-Miocene Climatic Optimum were not able to hinder the progradation of a major siliciclastic wedge from Scandinavia into the North Sea basin. The distinct temperature decrease in the Serravallian does not correlate with the aforementioned progradation either, but on the contrary, correlate with the culmination of a major flooding event and deposition of a condensed succession of marine glaucony-rich clay.

In their answer to the comments by Rasmussen and Dybkjær (2014), (Gołędowski et al., 2014) stress that there are multiple factors that may explain the mismatch between the vegetation cover, inferred from palaeo-climate data and the sediment influx in what they call a very small area of the North Sea. These encompass variations in precipitation, sediment routing, redeposition of older sediments and sediment depositories in the hinterland or variable erosional potential of rivers. they stress that what they describe as a minor discrepancy between the simple vegetation model and the mid-Miocene sedimentation onshore Denmark cannot it itself indicate a tectonic uplift of the hinterland.

Both rates were initially low under warm, moist, relatively stable climate conditions. The straight wave-dominated delta front gradually developed into a lobate fluvial-dominated delta front. Two high-amplitude sea-level falls affected the Pliocene units, which are characterized by widespread delta-front failures. Changes in relative sea level and climate became more frequent from the late Pliocene onward, as the system experienced the effects of glacial±interglacial transitions. Peaks in sedimentation and bifurcation rates were coeval with cold (glacial) conditions. The positive correlation between rates of supply and bifurcation on the one hand, and climate proxies (pollen and $\delta^{18}O$ records) on the other hand is highly significant. The evidence presented in this study convincingly demonstrates the control of climate on time-averaged sediment supply and channel-network characteristics, despite the expected non-uniformity and time lags in system response. The presence of a clearly discernible climate signal in time-averaged sediment supply illustrates the usefulness of integrated seismo-stratigraphic studies for basin-wide analysis of delta evolution on geological time scales. (Overeem et al., 2001)

*Deflandrea phosporitica,* a diagnostic  dinoflagellate for the top of the Oligocene

# 3. Biostratigraphy

## Approach and methodology

### Approach

In order to perform a consistent seismic interpretation and construct the temporally-resolved Wheeler diagrams, age-control is required for selected wells across the seismic transects. To this end, we have analyzed the organic-walled dinoflagellate cyst (dinocyst) content of 10 wells (table 3.1). In addition, we have included the results of previous studies of wells F17-10 and F17-12. A biostratigraphic interpretation from well G11-01 are available from the work of Köthe (2007).

Dinocysts are routinely used for biostratigraphic correlation in the Cenozoic of the North Sea area and zonation schemes with high relatively high temporal resolution and confidence are developed. For the Upper Eocene we primarily rely on the zonation schemes of Bujak and Mudge (1994), for the Oligocene that of Van Simaeys et al. (2005) and for the Miocene those of De Verteuil and Norris (1996) and Munsterman and Brinkhuis (2004). These studies have linked numerous Last Occurrence Displays (LODs) to the geological time-scale, either by calibration to calcareous nannofossils or geomagnetic polarity. The stratigraphic positions of the marker events are indicated in Figure 3.1. Note that we have only used the LODs because we rely on material from ditch cuttings, which are contaminated by downhole 'caving'.

**Table 3.1: Overview of studied wells**

| Well | Line | Interval | Samples |
|---|---|---|---|
| D12-01 | F02 Panel | 550-600 m | 4 |
| E06-01 | F02 Panel | 980-1150 m | 5 |
| F02-06 | F02 Panel | 450-1220 m | 11 |
| F04-01 | F02 Panel | 1080-1300 m | 13 |
| F15-01 | NS Panel | 950-1100 m | 7 |
| F15-06 | F17 Panel | 960-1100 m | 10 |
| K05-ENC-01 | F17 Panel | 550-750 m | 8 |
| K06-01 | F17 Panel | 793-950 m | 9 |
| K07-02 | F17 Panel | 460-600 m | 5 |
| L01-02 | F17 Panel | 920-1000 m | 3 |
| | | **Total:** | **85** |

### Sample Processing and Identification

The samples were de-oiled and processed at the TNO laboratory using the standard sample processing procedures, which involves HCl and HF treatment and sieving over a 10µm mesh sieve. The microscopy analysis was done according to standard procedures. Slides are either analyzed quantitatively or semi-quantitively. The latter includes an estimation of the numbers of the determinable sporomorphs, dinocysts and miscellaneous fossils. Diagnostic species are discussed in the report, a complete distribution chart including all species found is given as appendices.

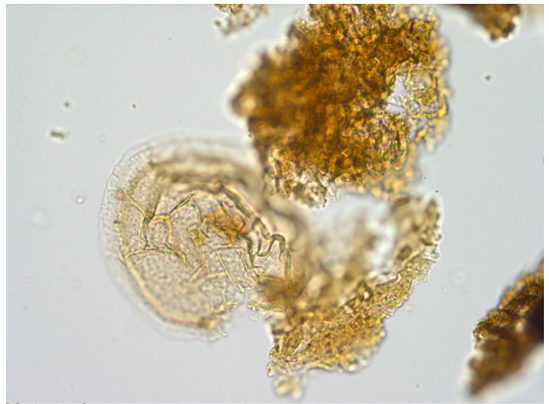

*Heteraulacacysta porosa*

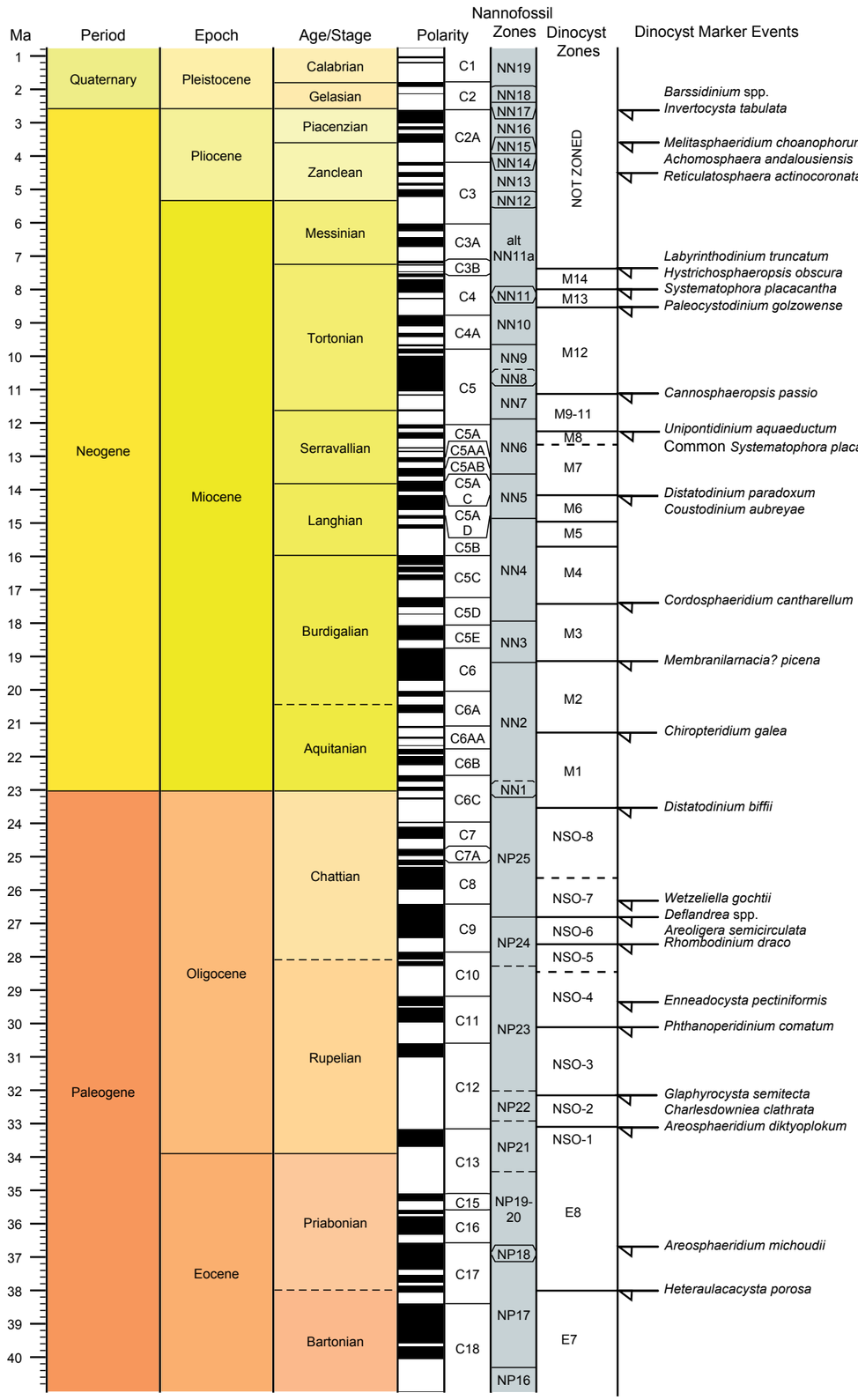


**Figure 3.1: Compilation of dinocyst zonations and LOD-marker events compared to the Geomagnetic Polarity Time Scale (GPTS) of Gradstein et al. (2012), including magnetozones (C) and calcareous nannofossil zone (NP and NN). The Eocene dinocyst Zones (E) are after Bujak and Mudge (1994), the Oligocene Zones (NSO) after Van Simaeys et al. (2005) and the Miocene Zones are after Munsterman et al. (2004). The marker events are derived from these studies augmented by the work of De Verteuil and Norris et al. (1996) for the Miocene and Kuhlmann et al. (2006) for the Pliocene.**

## Results and conclusions per well*

### D12-01

For Well D12-01 four samples were studied between 600 and 550 m depth. The samples at 600 m, 580 m and 570 depth yield late Middle Eocene (Bartonian) assemblages. This age-assignment is based on the LOD of *Heteraulacacysta porosa* and *Areosphaeridium michoudii* at 570 m depth and the composition underlying assemblage. The sample at 550 m depth is substantially younger likely of Early Pleistocene (Gelasian) Age. This is based on the absence of *Barssidinium* spp. and *Invertocysta lacrymosa* and the presence of *Reticulatosphaera actinocoronata*. Together these exclude a Pliocene age.
With Early Pleistocene deposits immediately overlying Middle Eocene deposits, all major Cenozoic unconformities known from the study merge at the location of Well D12-01.

**Table 3.2: Chronostratigraphic interpretation of D12-01**

| Sample/Interval | Age |
|---|---|
| 550 m | Early Pleistocene (Gelasian) |
| 570 – 600 m | Middle Eocene (Bartonian) |

### E06-01

For well E06-01 five samples were analyzed between 1150 and 980 m depth. The sample at 1150 m is of middle Rupelian age. Eocene markers (e.g., *Areosphaeridium diktyoplokum*) and Earliest Rupelian markers (e.g., *Glaphyrocysta semitecta*) are not recorded. The LODs of *Phthanoperidinium comatum* and *Enneadocysta pectiniformis* in this sample indicate a middle Rupelian age. The sample at 1100 m depth is of Late Chattian age. This age-assignment is based on the LOD of *Distatodinium biffii* and the absence of Early Chattian markers (e.g., *Deflandrea* spp., *Areoligera semicirculata*). The samples at 1020 and 1000 m depth are both of Langhian age. This is based on the LOD of *Distatodinium paradoxum* at 1000 m depth and the absence of older Miocene markers (such as *Cordosphaeridium cantharellum*).
The above implies that a substantial unconformity separates the Late Oligocene (Late Chattian) from the Middle Miocene (Langhian). Hence, in this well the 'Savian Unconformity' and the Early Miocene Unconformity (EMU) are merged.

**Table 3.3: Chronostratigraphic interpretation of E06-01**

| Sample/Interval | Age |
|---|---|
| 1000-1020 m | Middle Miocene (Langhian) |
| 1100 m | Late Oligocene (late Chattian) |
| 1150 m | Early Oligocene (middle Rupelian) |

***Note that palynomorph distribution charts are provided for each well as appendices to this report**

### F02-06

For well F02-06 twenty-nine samples were analyzed between 450 and 1220 m depth. The sample taken at 1220 m depth is of Late Oligocene (Chattian) age. This is based on the presence of *Svalbardella cooksoniae* and *Deflandrea phosphoritica* combined with the absence of older Oligocene markers. The sample at 1200 is substantially younger. The LOD of *Cordosphaeridium cantharellum* indicates a Burdigalian (late early Miocene) age. Subsequently, the samples at 1175 and 1185 m depth are of Langhian (middle Miocene) age based on the LOD of *Distatodinium paradoxum* at 1175 m depth. The sample at 1150 m depth is of early-middle Serravalian (middle Miocene) age, especially based on the LOD of *Unipontidinium aquaeductum*. The sample at 1125 m depth is substantially younger, of Tortonian (late Miocene) as indicated by the LODs of *Systematophora placacantha* and *Palaeocystodinium golzowense*. The sample at 1090 m depth and above up to 1020 m depth, is of early Zanclean (early Pliocene) age. This is based on the presence of *Reticulatosphaera actinocoronata* and the absence of Miocene taxa. Between 930 m and 750 m the Piacenzian (Late Pliocene) is recorded based on the presence of *Barssidinium* spp. up to 750 m depth. At 670 m depth, the Gelasian (early Pleistocene) is likely reached.
The biostratigraphic results show that late Chattian deposits are unconformably overlain by early Miocene (Burdigalian) deposits, representing the 'Savian Unconformity' between 1200 and 1220 m depth. Successively, the EMU separates these Burdigalian deposits from middle Miocene (Langhian and Serravalian) deposits between 1200 and 1185 m depth. The MMU then separates the Serravalian from late Miocene (Tortonian) deposits between 1150 and 1125 m depth. These late Miocene deposits are truncated by the Late Miocene Unconformity (LMU) between 1125 and 1090 m. The overlying lower Pliocene deposition progressed more or less continuously into the Pleistocene.

**Table 3.4: Chronostratigraphic interpretation of F02-06**

| Sample/Interval | Age |
|---|---|
| 670 m | Early Pleistocene (Gelasian) |
| 750 -930 m | Late Pliocene (Piacenzian) |
| 1020 – 1090 m | Early Pliocene (Zanclean) |
| 1125 m | Late Miocene (Tortonian) |
| 1150 m | Middle Miocene (Serravalian) |
| 1175 – 1185 m | Middle Miocene (Langhian) |
| 1200 m | Early Miocene (Burdigalian) |
| 1220 m | Late Oligocene (Chattian) |

### F04-01

For well F04-01 eleven samples were analyzed. The basal sample at 1300 m depth is of Middle Eocene (likely Bartonian), based on the LOD of *Rhombodinium perforatum* and the presence of other Eocene elements. At 1250 m depth, the middle Rupelian (Early Oligocene) is reached as Eocene species (e.g., *Areosphaeridium diktyoplokum*) are absent and *Enneadocysta pectiniformis* has a LOD at this level. The samples at 1230 and 1240 m depth are of late Rupelian to early Chattian age; *Rhombodinium draco* has a LOD at 1230 m depth. The isolated presence of *Svalbardella cooksoniae* in these samples is also in-line with this interpretation (Śliwińska et al., 2010). The sample at 1210 m depth is of Late Chattian age, based on the LOD of *Distatodinium biffii* and absence of older markers. Between 1190 and 1130 m depth we record typical early Miocene (Aquitanian to early Burdigalian) assemblages. At 1130 m depth we note the LOD of *Cordosphaeridium cantharellum*, indicating an early Burdigalian age. The samples at 1110 and 1120 m depth are clearly younger, of middle Miocene (Langhian) age, as indicated by the LOD of *Distatodinium paradoxum* at 1110 m depth. At 1090 m depth a sample of early Tortonian age is recorded, *Cannosphaeropsis passio* is present whereas Systematophora placacantha is extinct. Subsequently, at 1080 we record an early Pliocene (Zanclean) association, lacking Miocene elements but still containing *Reticulatosphaera actinocoronata*.
These biostratigraphic results imply that the Eocene-Oligocene (base Rupelian) unconformity is positioned between 1250 and 1300 m depth. A minor unconformity separating Early Oligocene (middle Rupelian) strata and Late Oligocene (early Chattian) strata is positioned between 1240 and 1250 m depth. The Savian Unconformity then separates Late Oligocene from (middle) early Miocene deposits (early Burdigalian) between 1190 and 1210 m depth. The unconformable contact between Burdigalian and Langhian strata between 1120 and 1130 m depth represents the EMU. The MMU is positioned between 1090 and 1110 m depth, separating Langhian from Tortonian strata. The LMU separates the Tortonian strata from early Pliocene (Zanclean) ones between 1080 and 1090 m depth.

**Table 3.5: Chronostratigraphic interpretation of F04-01**

| Sample/Interval | Age |
|---|---|
| 1080 m | Early Pliocene (Zanclean) |
| 1090 m | Late Miocene (early Tortonian) |
| 1110 - 1120 m | Middle Miocene (Langhian) |
| 1130 – 1190 m | Early Miocene (Aquitanian – Burdigalian) |
| 1210 m | Late Oligocene (late Chattian) |
| 1230 – 1240 m | Early-Late Oligocene (late Rupelian-early Chattian) |
| 1250 m | Early Oligocene (middle Rupelian) |
| 1300 m | Middle Eocene (Bartonian) |

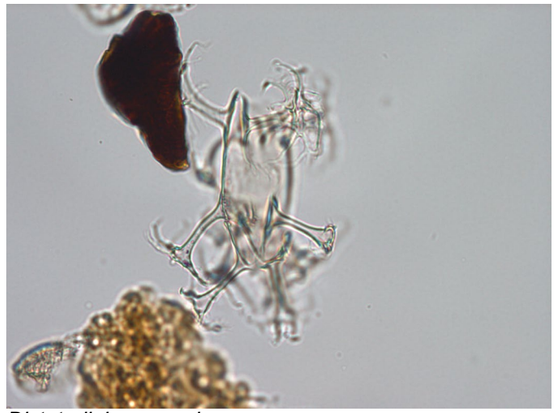

*Distatodinium paradoxum*

*Enneadocysta pectiniformis*

## Results and conclusions per well *continued*

### F15-01

Seven samples were selected from well F15-01. The lowermost sample at 1100 m depth contains Late Rupelian (Early Oligocene) assemblages. Diagnostic are the presence of *Chiropteridium galea*, *Rhombodinium draco* and absence of the Eocene marker *Areosphaeridium diktyoplokum* and the Early Rupelian marker *Enneadocysta pectiniformis*. The overlying samples at 1020 and 1050 m are of Early Burdigalian (Early Miocene) age judging on the LOD of *Cordosphaeridium cantharellum* at 1020 m depth. In the samples at 1010 m 990 m depth the dinocyst assemblages indicate a Langhian (middle Miocene) age. Diagnostic are the LODs of *Unipontidinium acquaeductum*, *Systematophora placacantha* and *Distatodinium paradoxum* at 990 m depth. The overlying samples 980 and 950 yield substantially younger assemblages. Based on the absence of Pliocene elements (*Reticulatosphaera actinocoronata*, *Barssidinium* spp.) a Gelasian (Pleistocene) age is inferred. This also supported by the abundant occurrence of 'cold-water' elements of the *Filisphaera-Habibacysta* group (Head, 1996).
The biostratigraphic results indicate that the 'Top Rupelian' and Savian unconformities merge between 1050 and 1100 m depth, separating late Rupelian from early Burdigalian deposits. Between 1010 and 1020 m the EMU separates the early Burdigalian from the Langhian. The Langhian deposits are unconformably overlain by Gelasian deposits, implying the merging of the MMU, LMU and the S1-unconformities in well F15-01. The latter is an unconformity, documented to occur in the Zanclean (early Pliocene).

**Table 3.6: Chronostratigraphic interpretation of F15-01**

| Interval | Age |
|---|---|
| 950 – 980 m | Early Pleistocene (Gelasian) |
| 990 – 1010 m | Middle Miocene (Langhian) |
| 1020 - 1050 m | Early Miocene (Burdigalian) |
| 1100 m | Early Oligocene (Rupelian) |

### F15-06

Ten samples were analyzed from well F15-06 (1100-960 m depth). The lowermost samples at 1100 and 1090 m depth are of Early Rupelian age (Zones NSO-3 and NSO-4, Early Oligocene). This is based on presence of taxa with LODs in the Early Rupelian such as *Phthanoperidinium amoenum*, *Areoligera semicirculata* and *Enneadocysta pectiniformis* and the absence of Eocene markers (e.g., *A. dikytoplokus*). The samples taken at 1060 m and 1040 m depth are of late Chattian age (Zone NSO-6 and NSO-7, Late Oligocene). Diagnostic are the LOD of *Distatodinium biffii* at 1040 m depth and the presence of elements like *Saturnodinium pansum*, *Artemisiocysta cladodichotoma*. The samples between 1000 – 1020 m depth are of Early Burdigalian age (Zone M2, Early Miocene). This interpretation is based on the LOD of *Cordosphaeridium cantharellum* at 1000 m depth. The questionable identification of *Membrinalarnacia picena* suggests an Earliest Burdigalian age at 1010 m depth. This typical Early Burdigalian association is also found at 1020 m depth. The sample taken at 990 m depth is evidently younger, of Langhian age (Zone M6, Middle Miocene). This is based on the LOD of *Distatodinium paradoxum* and *Coustodinium aubryae*. Successively, the sample at 970 m depth is of Serravalian age (Zone M7-M8, Middle Miocene). This is indicated by the abundance of *Cannosphaeropsis passio* alongside *Systematophora placacantha*. The sample at 960 m depth is likely of Zanclean (Early Pliocene) age, as *Reticulatosphaera actinocoronata* is still present and older Miocene markers are not recorded.

**Table 3.7: Chronostratigraphic interpretation of F15-06**

| Interval | Age |
|---|---|
| 960 m | Early Pliocene (Zanclean) |
| 970 m | Middle Miocene (Serravalian) |
| 990 m | Middle Miocene (Langhian) |
| 1000 - 1020 m | Early Miocene (early Burdigalian) |
| 1040 – 1060 m | Late Oligocene (late Chattian) |
| 1090 – 1100 m | Early Oligocene (early Rupelian) |

### K05-ENC-01

For well K05-ENC-01, eight samples were selected for analysis between 750 and 550 m depth. The lower five samples (610 – 750 m depth) are of Priabonian age. The LOD of *Areosphaeridium diktyoplokum* at 610 m is a diagnostic marker for the top of the Eocene. The presence of *Melitasphaeridium pseudorecurvatum* and *Cordosphaeridium funiculatum* in fact is indicative for an 'older' early Priabonian age, rather than a late Priabonian age. The samples at 570-590 m depth are of Chattian age, based on the presence of *Areoligera semicirculata* and *Deflandrea* spp. and absence of younger markers. The sample at 550 m depth lacks marine microfossils and likely corresponds to Pleistocene or younger age.
The results imply that the unconformities associated with the Eocene-Oligocene Transition and the Top Rupel merge at 610 m depth. The Savian, EMU, MMU and the LMU are merged at 560 m depth, where Chattian deposits unconformably underlie Plio- or Pleistocene deposits.

**Table 3.8: Chronostratigraphic interpretation of well K05-ENC-01**

| Interval | Age |
|---|---|
| 550 m | Undifferentiated, likely Pleistocene |
| 570 – 590 m | Late Oligocene (Chattian) |
| 610 -750 m | Late Eocene (Priabonian) |

### K06-01

For well K06-01, nine samples were selected for analysis between 793-950 m depth. The samples at 930 and 950 m depth are of Priabonian (Late Eocene) age as indicated by the LOD of *Areosphaeridium diktyoplokum* at 930 m depth. Successively at 900 m depth, an Early Rupelian (Early Oligocene) assemblage is recovered constituting the characteristic elements *Enneadocysta pectiniformis*, *Rhombodinium draco* and *Phthanoperidinium comatum*. The two samples between 850 and 890 m depth are of (early) Chattian (Late Oligocene) age, based on the presence of *Distatodinium biffii*, *Wetzeliella gochtii*, *Deflandrea* spp. and the absence of 'older' early Rupelian markers like *Enneadocysta pectiniformis* and *Phthanoperidinium comatum*. The LOD of *Wetzeliella gochtii* at 865 m indicates a definitive early Chattian age. The samples at 818 and 793 m depth are of early Burdigalian (early Miocene) age, based on the presence of *Cordosphaeridium cantharellum* and the absence of older elements.

**Table 3.9: Chronostratigraphic interpretation of well K06-01**

| Interval | Age |
|---|---|
| 793 – 818 m | Early Miocene (early Burdigalian) |
| 850 – 890 m | Late Oligocene (Chattian) |
| 900 m | Early Oligocene (early Rupelian) |
| 930 - 950 m | Late Eocene (Priabonian) |
| | |

The biostratigraphic results from well K06-01 indicate an Eocene-Oligocene contact between 900 and 930 m depth. Rupelian deposits are unconformably overlain by Chattian deposits between 900 and 890 m depth (Top Rupel Unconformity). A relatively expanded Chattian succession (850 – 890 m) is truncated by the Savian unconformity between 818 and 850 m depth. The latter separates the Chattian from Burdigalian (early Miocene) deposits.

### K07-02

For well K07-02, we studied five samples from the transect between 600 and 460 m depth. The lowermost sample at 600 m depth is of late Middle Eocene (Bartonian) to early Late Eocene Age (Priabonian, Zone E7-E8). This is based on the presence of *Areosphaeridium michoudii*. The overlying samples at 530 and 510 m depth are of definite Priabonian age (Zone E7). *Areosphaeridium diktyoplokum* is present in these samples. The sample at 490 m depth is of early Rupelian (Early Oligocene, Zone NSO-1 or NSO-2) age. *Areosphaeridium diktyoplokum* is now extinct whereas *Charlesdowniea clathrata*, *Enneadocysta pectiniformis* and other Rupelian taxa are still present. The sample at 460 m depth is substantially younger, with the presence of *Invertocysta lacrymosa* and absence of *Reticulatosphaera actinocoronata*, a late Zanclean to Piacenzian (Early-Late Pliocene) age is most likely.
The biostratigraphic results from well K07-02 thus indicate that an Eocene succession underlies a Rupelian succession. The top Rupelian, Savian, EMU, MMU, LMU and S-1 unconformities merge between 490 and 460 m, separating Rupelian from late Zanclean to Piacenzian strata.

**Table 3.10 Chronostratigraphic interpretation of well K07-02**

| Interval | Age |
|---|---|
| 460 m | Pliocene (Zanclean-Piacenzian) |
| 490 m | Early Oligocene (early Rupelian) |
| 510 -530 m | Late Eocene (Priabonian) |
| 600 m | Middle Eocene (Bartonian) |

*Cannosphaeropsis passio*

*Chiropteridium galea*

**L01-02**

Three samples were analyzed from well L01-02 (1000-920 m depth). The lowermost sample is of early Burdigalian (Zones M2-M3, Early Miocene) age. This is based on the presence/LODs of *Cordosphaeridium cantharellum*. The sample at 960 m depth is of Langhian (Zone M5-M6, Middle Miocene) age, based on the LOD of *Distatodinium paradoxum* and *Coustodinium aubryae*. The uppermost sample at 920 m is of definite Gelasian (Early Pleistocene) age; *Reticulatosphaera actinocoronata*, *Barssidinium* spp., *Invertocysta* spp. nor any other Pliocene indicator is recorded.

These results imply that the Top Rupelian and Savian unconformities are located below 1000 m depth and were not sampled. The EMU separates Early Burdigalian from Langhian strata between 960 and 1000 m depth. On top of that, the MMU, LMU and S-1 unconformities are positioned between 960 and 920 m depth.

**Table 3.11 Chronostratigraphic interpretation for well L01-02**

| Interval | Age |
|---|---|
| 920 m | Early Pleistocene (Gelasian) |
| 960 m | Middle Miocene (Langhian) |
| 1000 m | Early Miocene (Burdigalian) |

**Figure 3.2 The resultant stratigraphic subdivision gives rise to the use of age-intervals, bounded by these unconformities:**

**(A) The O1-interval corresponds to the Early Oligocene (Rupelian) sequence. It is bounded at its top by the Top Rupel.**
**(B) The O2-interval corresponds to the Late Oligocene (Chattian) sequence. It is bounded at its top by the Savian Unconformity.**
**(C) The M1-interval corresponds to the Early Miocene (Aquitanian – Burdigalian) sequence. It is bounded at its top by the EMU.**
**(D) The M2-interval corresponds to the Middle Miocene (Langhian-Serravalian) sequence. It is bounded at its top by the MMU.**
**(E) The M3-interval corresponds to the Late Miocene (Tortonian) sequence. It is bounded at its top by the LMU.**
**(F) The S-intervals refer to the Plio-Pleistocene units that are part of the Eridanos system.**

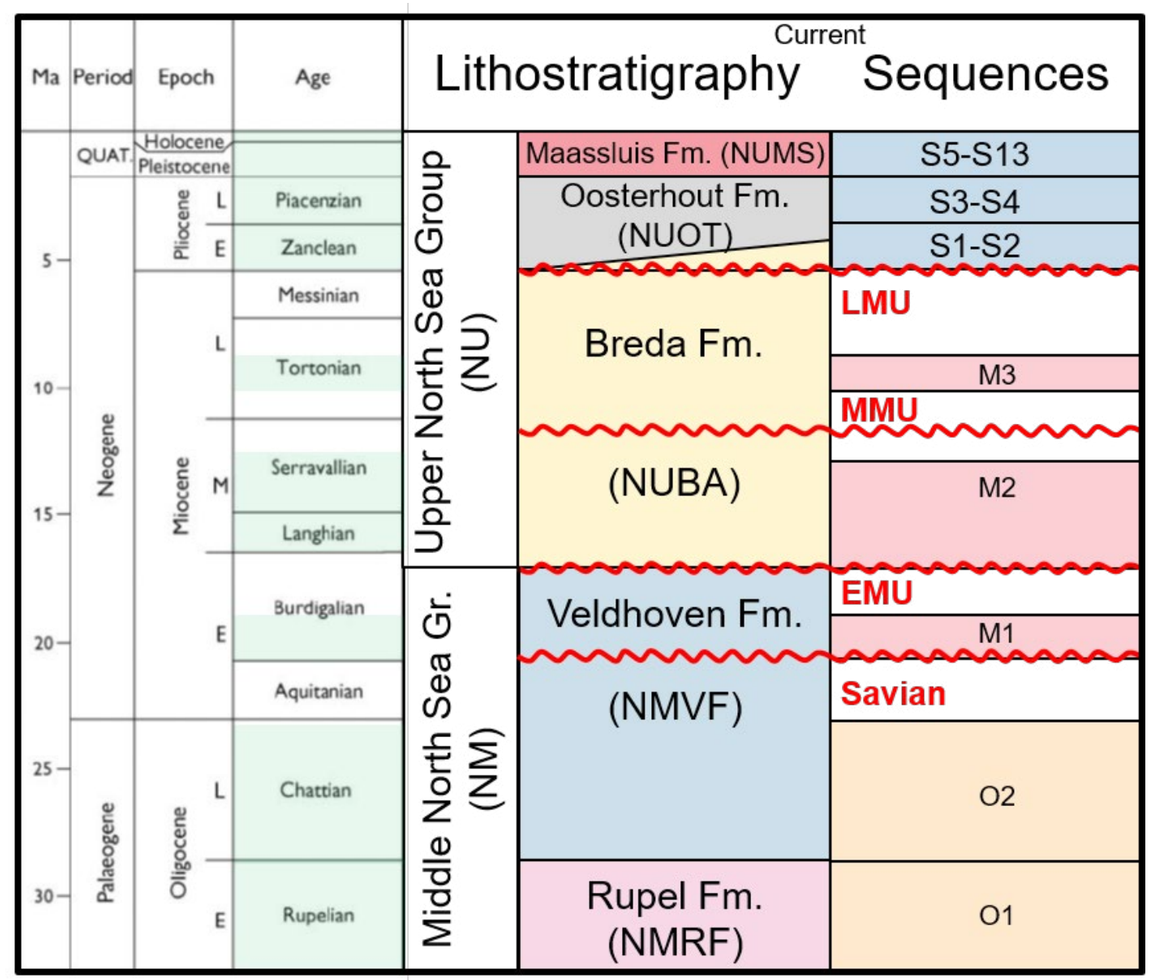


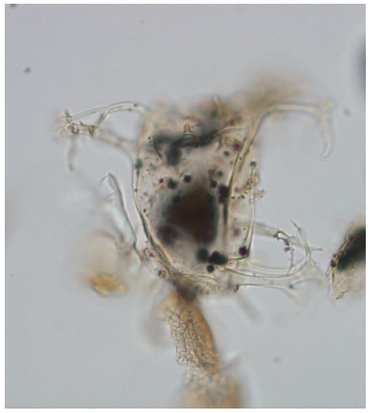

*Distatodinium biffii*

*Areosphaeridium diktyoplokus*

*Areoligera semicirculata*

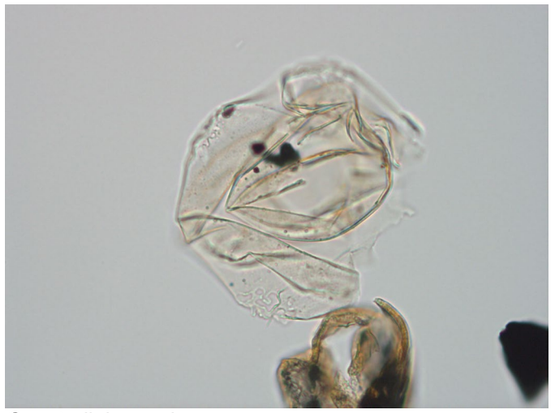

*Coustodinium aubryae*

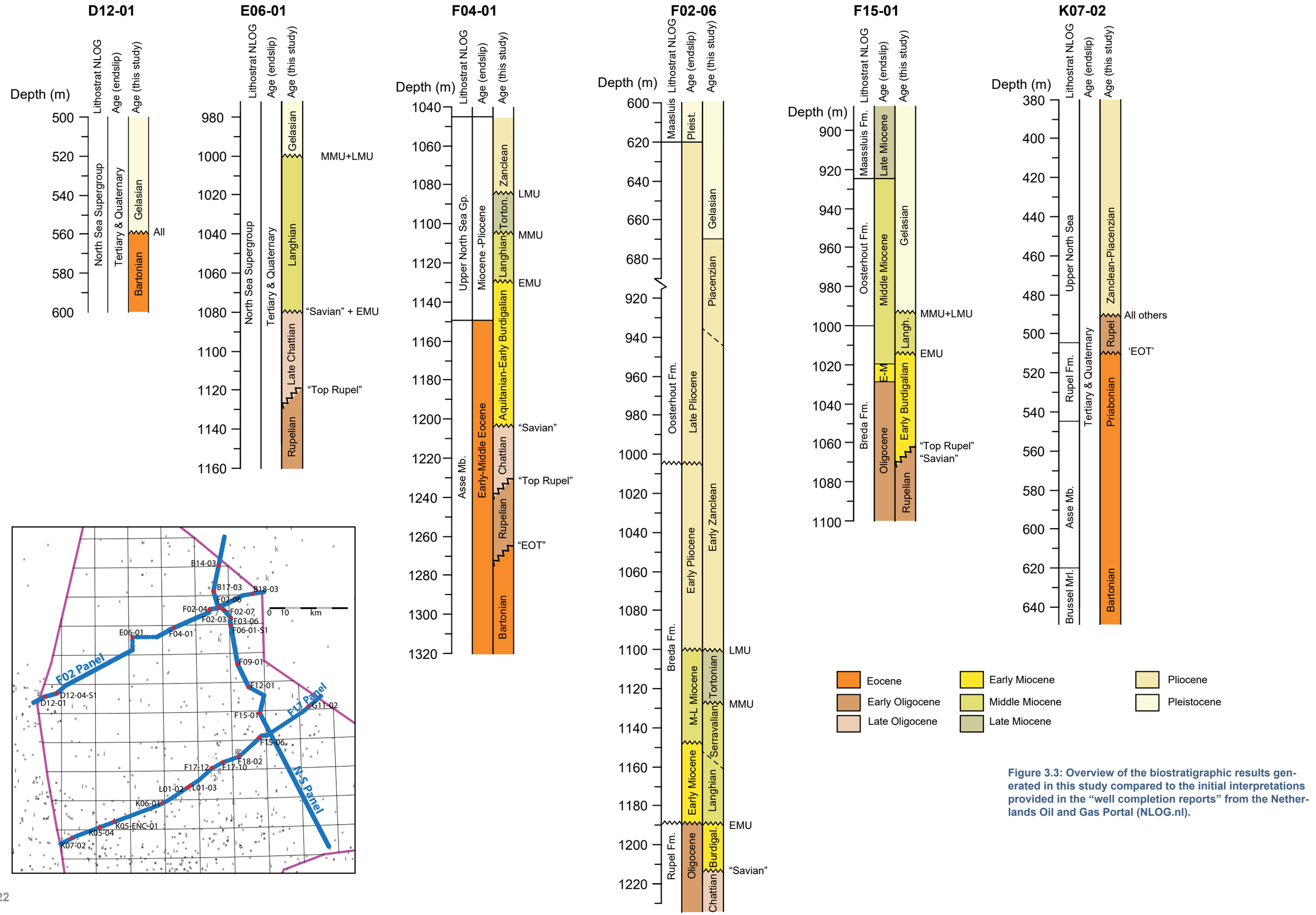





Figure 3.3: Overview of the biostratigraphic results generated in this study compared to the initial interpretations provided in the “well completion reports” from the Netherlands Oil and Gas Portal (NLOG.nl).

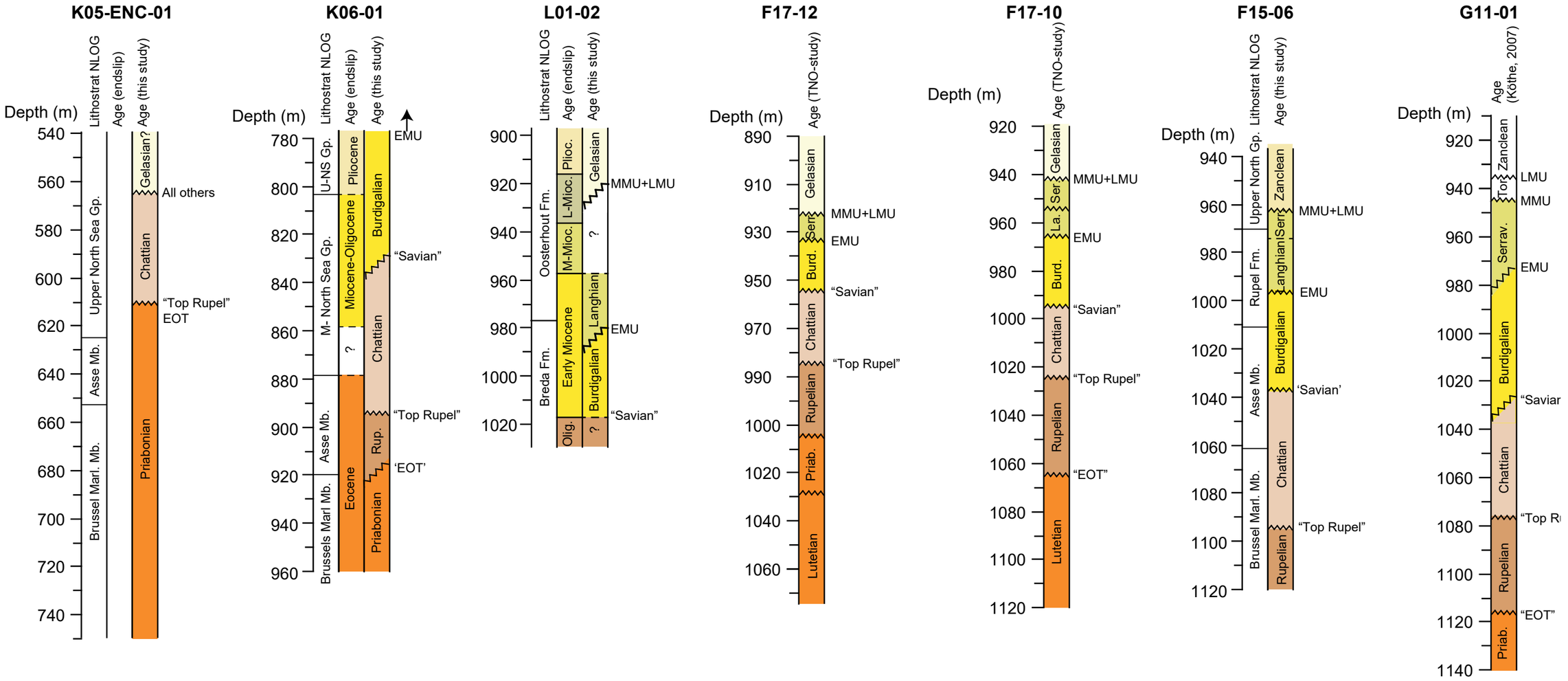


## 3. Summary and implications

The biostratigraphic results generated in this study are depicted in figure 3.3 and are markedly different from initial interpretations provided in the "well completion reports" and on the Netherlands Oil and Gas Portal (NLOG, see Figure 3.2). The following unconformities are consistently noted:

(A) The "Eocene – Oligocene Transition (EOT)" unconformity marks the top of the Eocene.

(B) The "Top Rupel" Unconformity is noted at the top of the Rupelian. Overlying deposits are typically of Late Oligocene (Chattian) age.

(C) The "Savian Unconformity" separates Late Oligocene (Chattian) from Early Miocene deposits. The often fine-grained deposits surrounding the Savian Unconformity are known as the Veldhoven Fm. in the onshore Netherlands

(D) The Early Miocene Unconformity (EMU) separates Lower Miocene (Burdigalian or older) strata from Middle Miocene (Langhian or Serravalian) strata. . In terms of lithostratigraphy, the base of the Breda Fm. coincides with this unconformity.

(E) The Mid Miocene Unconformity (MMU) separates Early Miocene strata from Middle Miocene (Langhian to Serravalian) strata. Lithostratigraphically, the MMU occurs within the Breda Fm.

(F) The Late Miocene Unconformity (LMU) separates Middle Miocene strata from Upper Miocene (Tortonian or younger) strata.

(G) Typically, Pliocene or Pleistocene sediments of the Upper North Sea Group (the Oosterhout or Maassluis Fm. respectively) unconformably overly the Oligocene-Miocene succession. The Plio- Pleistocene boundary is often also accompanied by an unconformity (see also Ten Veen et al., 2013).

*Hystrichosphaeropsis obscura*

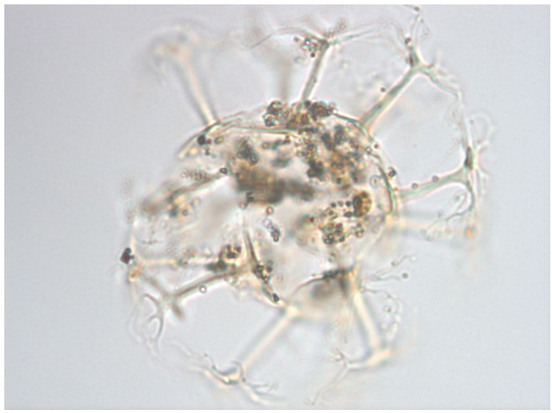

*Reticulatosphaera actinocoronata*

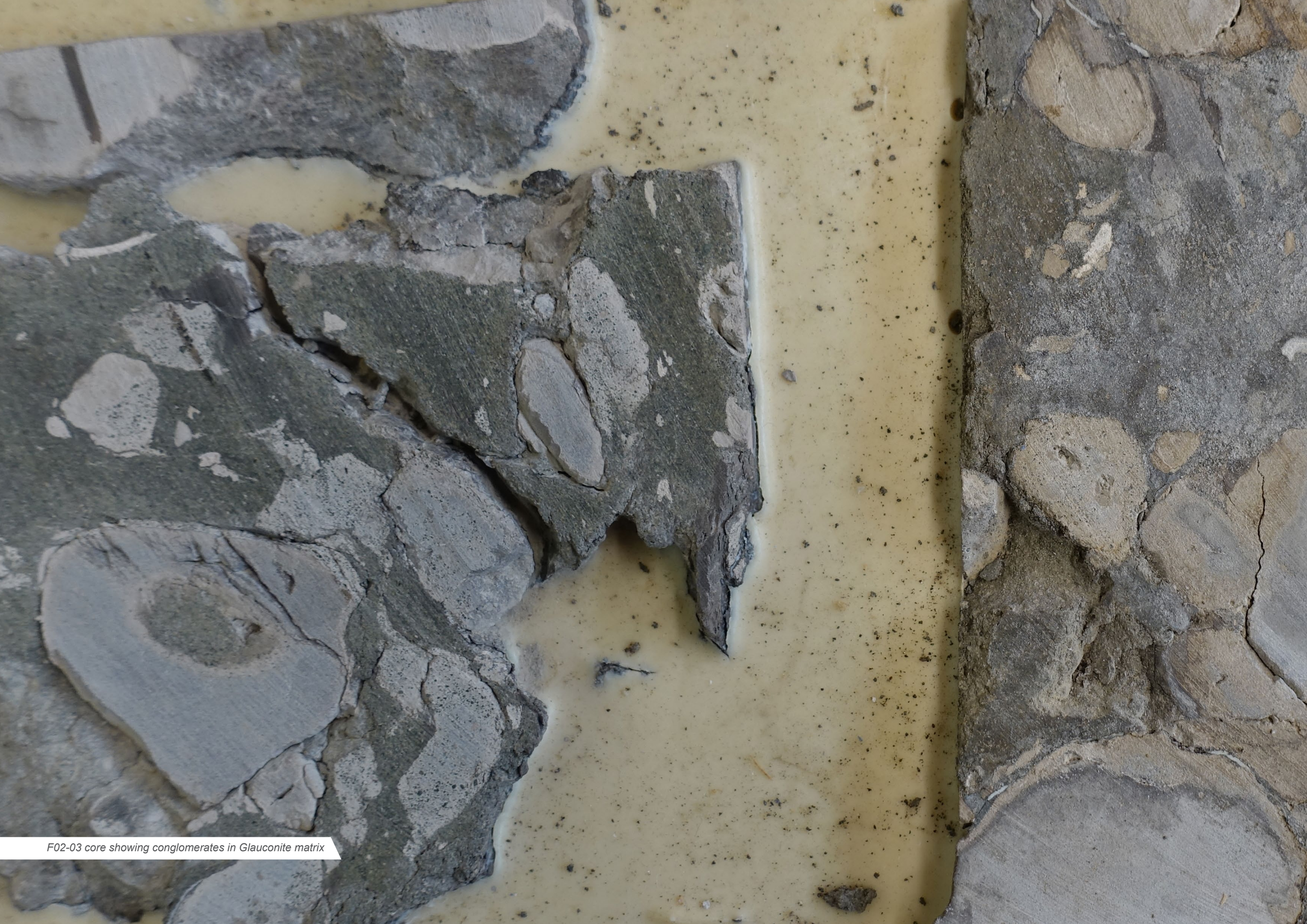

*F02-03 core showing conglomerates in Glauconite matrix*

# 4. Petrophysical analysis

# 4. PETROPHYSICAL ANALYSIS

## Introduction

The paucity of cores from the stratigraphic interval around the Mid-Miocene Unconformity (MMU) stresses the importance of using wireline logs with regards to property assessment. In general, we are interested in a number of petrophysical properties of the rocks that can be found around the MMU: porosity, permeability, and hydrocarbon content, and mineralogical composition such as sand and clay, carbonate-cemented streaks, glauconite,  and other minerals.

In a previous study that focused on shallow gas sands in the Plio-Pleistocene Eridanos delta in the Northern Offshore area (Ten Veen et al., 2013), an attempt was made to evaluate the petrophysical properties of these shallow gas sands. Even though these sands were stratigraphically younger than the sediments in the current study and therefore not completely comparable, the study yielded some interesting results, if only for the not-so-usual drilling and log acquisition setting.

One of the conclusions of that study was that evaluation of porosity, shale content, water saturation, and permeability in the Neogene strata is not straightforward, as there are several factors that complicate the process of log interpretation:

- Well to well differences. Different logging suites and log sampling rates had been used. This implies that each well needs an individual approach.
- Hole conditions. Because the studied rock sequence consists of unconsolidated sands and clays, most wells have many washout sections. This affects all contact-type logging tools and causes many aberrant readings, especially in the porosity logs.
- KCL / Polymer mud. In order to fight the instability of the unconsolidated sediments that consist for a large part of swelling clays, many operators use KCL/ Polymer additives to the drilling mud. This creates a substantial bias in the gamma-ray and spectral gamma-ray logs.
- Complex lithology. The Neogene sediments of the Eridanos delta contain many minerals that are either heavy, or radioactive, or both. A standard suite of logs (including spectral gamma ray and photon electron factor, PEF) cannot resolve all these minerals. In addition, a substantial amount of charcoal particles complicates the interpretation even further.
- Clay-Bound Water. The sediments are in general fine-grained and muddy, and they are unconsolidated. This means that they contain a considerable amount of clay-bound water. This in turn creates challenges for porosity and water saturation evaluation.

Given all these difficulties, the main recommendation of the project at the time was to use a simple shaly-sand model, preferably using the gamma-ray, neutron, and density logs to compute effective porosity (PHIE) and shale content (VSH). We will adopt this method in the current study, albeit with the notion that some room is left for a more elaborate interpretation when the input data contains more, and better logs (NMR, lithodensity and neutron, and spectral gamma ray logs).

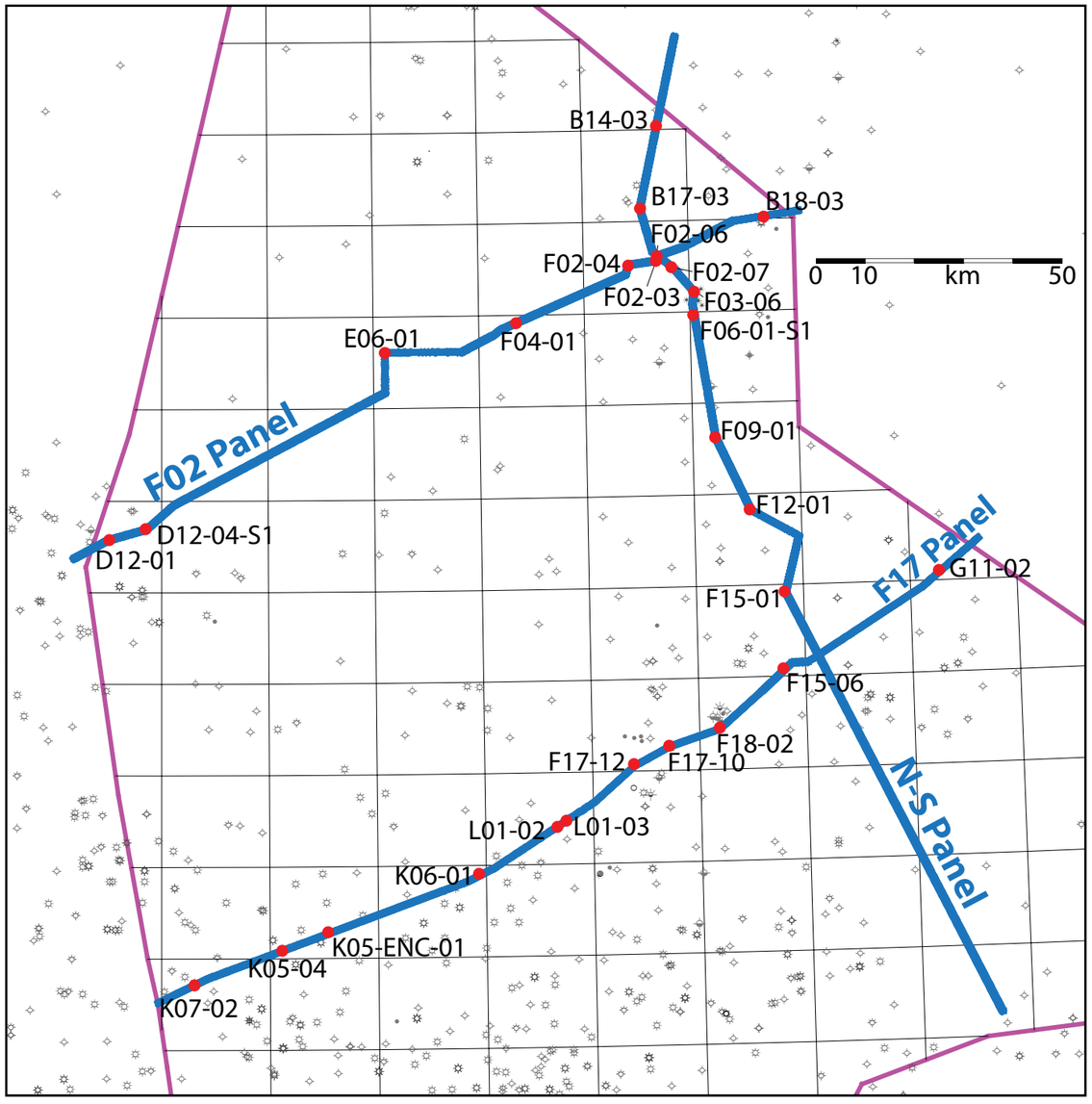


Figure 4.1: Overview map of the northern part of the Dutch offshore showing the wells that were analysed petrophysically.

| Nr | Well | Seismic | NLOG spliced logs | GR | DT | RES deep | NPHI | RHOB | PEF | SGR |
|---|---|---|---|---|---|---|---|---|---|---|
| 1 | **F09-01** | SNST87-31a | ● | ● | ● | ● | - | - | | |
| 2 | **F15-01** | SNST87-31a | ● | ● | ● | | - | - | | |
| 3 | **F02-06** | SNST87-N6a | ● | ● | | | ● | ● | ● | ● |
| 4 | **F04-01** | SNST87-N6a | ● | ● | ● | | - | - | | |
| 5 | **E06-01** | SNST87-N6a | ● | ● | ● | ● | - | - | | |
| 6 | **D12-01** | SNST87-N6a | ● | ● | ● | ● | - | - | | |
| 7 | **F15-06** | SNST83a | ● | ● | ● | ● | - | - | | |
| 8 | **F17-10** | SNST83a | - | ● | ● | ● | ● | ● | ● | ● |
| 9 | **F17-12** | SNST83a | - | ● | ● | ● | - | - | | |
| 10 | **K06-01** | SNST83a | ● | ● | ● | ● | - | - | | |
| 11 | **K05-04** | SNST83a | ● | ● | ● | ● | - | - | | |

Table 1: Overview of well logs available for petrophysical evaluation in the current project. Wells A15-03 and A15-04 did not reach MMU and were therefore not evaluated.

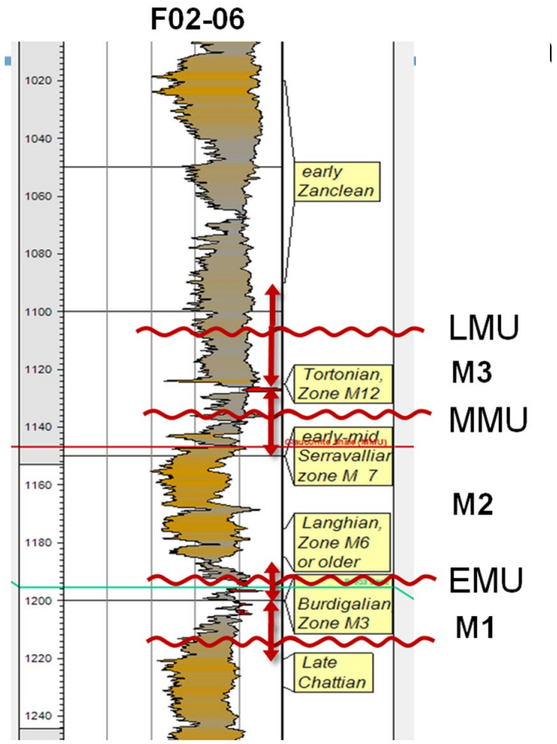


**Figure 4.2: Biostratigraphic age dating of well F02-06. Shown are the gamma ray and sonic logs with a gamma-ray colour coding, the biostratigraphic age dating, and the inferred unconformities EMU, MMU, and LMU. Red arrows show the uncertainties in the position of the unconformities**

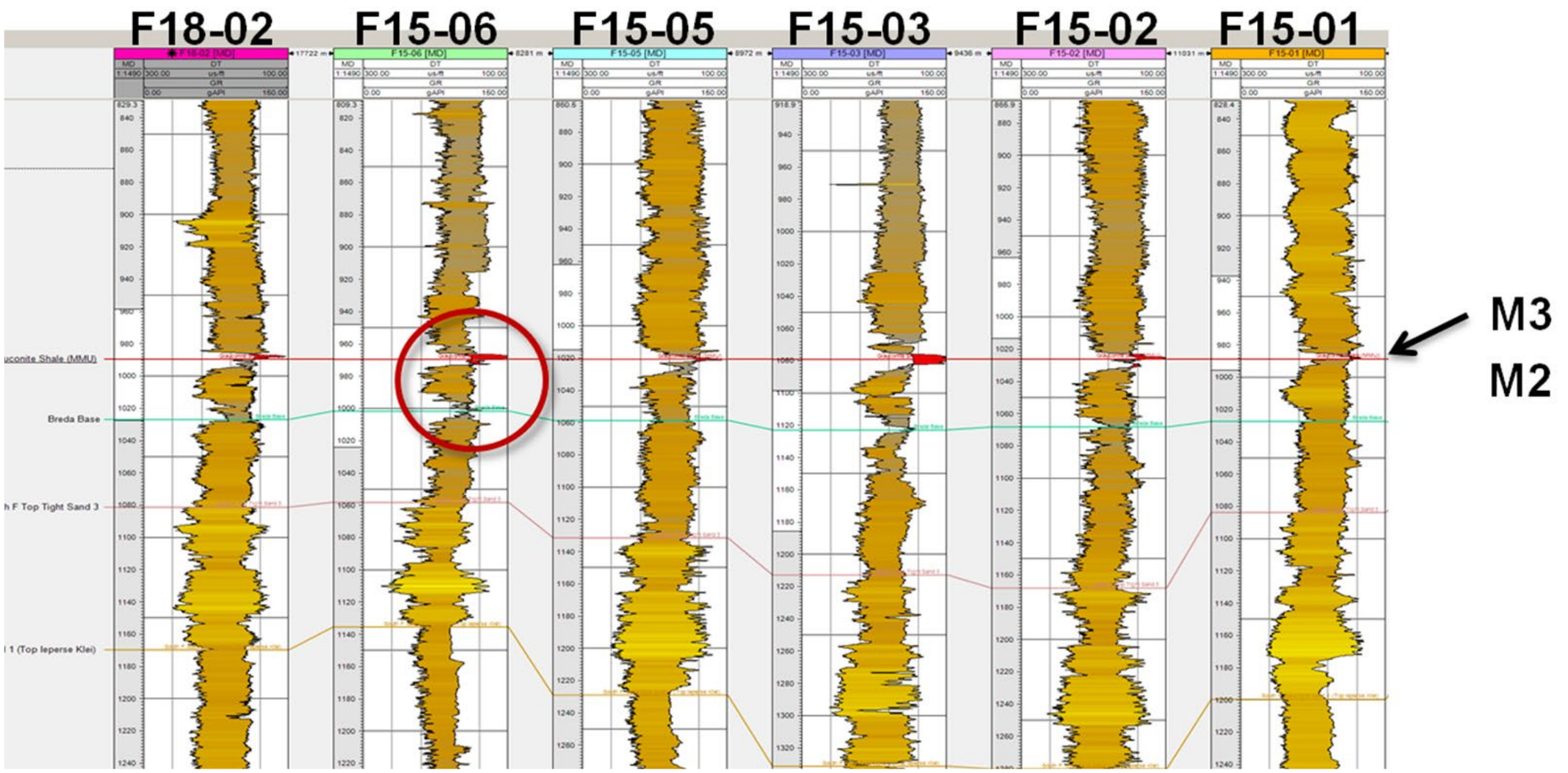


**Figure 4.3: Example of an initial correlation based on the recognition of a high gamma ray peak near the MMU. The gamma ray and sonic logs show the log character of the Breda Fm (red circle) and its overlying high gamma ray peak (red colour).**

## Data and methods

At the start of the project ten wells were selected for petrophysical examination (Table 4.1; see Figure 4.1 for well locations). These wells are located on or at a very short distance to one of the SNS seismic lines that were studied in detail. Table 1 gives an overview of the well logs that were available for each of the wells. Gamma ray, sonic, and deep resistivity logs are usually available for each well, but neutron and density logs (including PEF) and spectral gamma ray logs are generally missing, except for the wells that were drilled in the Chalk fields Hanze and Rembrandt (F02-06 and F17-10).

Because wells F02-06 and F17-10 have the largest and most extensive logging suite, these two wells were designated as key wells. Lessons learned from these two wells in a petrophysical sense were applied as much as possible to the other wells.

## Stratigraphic well-to-well correlation

Before performing a petrophysical analysis of the selected wells the stratigraphy of the formations around the MMU needs to be known. Various petrophysical parameters such as clay points, cementation factors, and water resistivity are usually specific to a certain formation.
By using these parameters, a lithostratigraphic correlation across the study area centred around the MMU. The following issues were taken into account:

- The lithostratigraphic correlation needs to be tied to the existing biostratigraphic age datings.
- Start of the definition and correlation of stratigraphic units will be preferably in the eastern part of the study area, where the sedimentary record of the Miocene is most complete and where all unconformities (EMU, MMU, LMU) are present;
- Because well spacing can be very large in the northern offshore (up to tens of kilometres), correlations can be substantially enhanced using seismic lines as guidelines. This works best if the wells have a decent velocity profile, and if there is also a synthetic seismic trace available.

Figure 4.2 shows well F02-06 with the age dating, inferred major unconformities and the stratigraphic nomenclature adopted in this study. If we expand this to other wells with biostratigraphic control in the neighbourhood, a clear log pattern emerges. The Middle Miocene M2 interval, lower Breda Fm.) consists of a coarsening/cleaning up sequence of 25-40 m thick, capped by a 2- 5 m thick shale layer with a high, sometimes very high, gamma ray peak (Figure 4.3). From previous studies (ten Veen et al, 2013; Sørensen et al, 1997) it is known that the overlying Plio-Pleistocene Eridanos delta had a source in the east, prograded in a westward direction, and that the resulting sediment bodies have a N-S elongated shape. If this basin configuration already existed in Miocene times, a first attempt to correlate the Lower Breda Fm. would be in a N-S direction.

## Regional development of the “Breda Fm”

Appendices A1 to A8 show a series of well to well correlation panels, flattened on the Glauconite Shale, the shale that usually directly overlies the Middle Miocene M2-interval. Based on these profiles, a thickness map was constructed, as shown in Figure 4.4. It is clear that there is a N-S trend in the thickness distribution, with benches running SSW-NNE and SSE NNW.
The log pattern of the M2-interval (Lower Breda Fm., see Figure 4.3) does not consist of a simple coarsening/ cleaning up cycle. Instead, it usually consists of two or more sandy packages, mostly coarsening up. Figure 4.5 summarises the main observations.

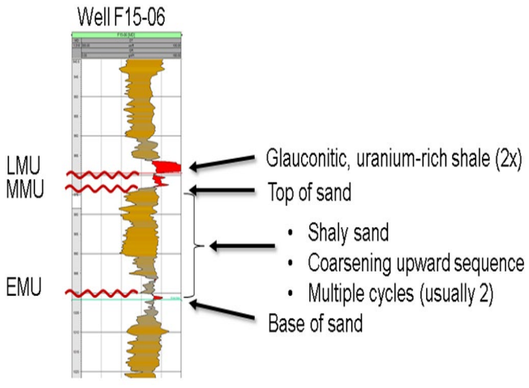


**Figure 4.5: Summary of features usually seen on the gamma ray and sonic logs in the Lower Breda Fm (M2).**

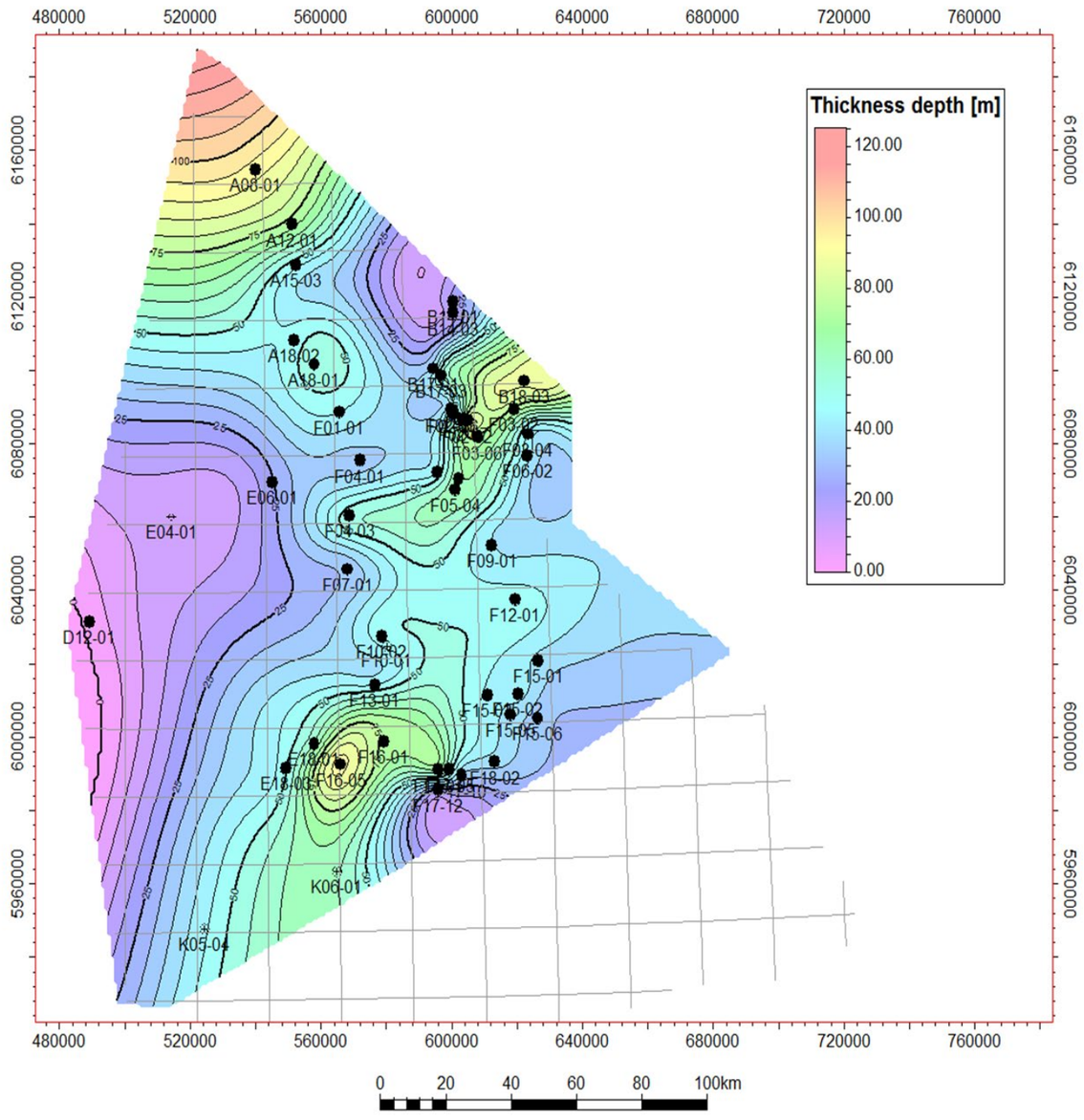


**Figure 4.4: Isochore map of the Lower Breda Fm (Sequence M2)**

## Key well F17-10

Well F17-10 was the discovery well of the Rembrandt Field, an oil-bearing structure in the Chalk. An extensive suite of well logs had been run over the Chalk section, but also over the Tertiary section. What is readily apparent from the log playback (Figure 5.6) are the high values for the neutron log and low values  for the density log, especially over the Lower Cenozoic section, pointing to high water content, and thus to high porosity values. Another conspicuous thing is the behaviour of the neutron log itself: frequently occurring streaks of about 0.5 m thick that rise to apparent porosity values of 60 to 80 p.u. The density log follows basically the same trend as the neutron log, but without the high-amplitude excursions.

Some other observations on the log playback (Figure 5.6) can be made from the components of the spectral gamma ray log. For example, the Thorium:Potassium ratio is remarkably constant over the entire Tertiary section, suggesting a non-changing sediment source (Rider, 1986). This would indicate that the Hinterland did not change over much of the Tertiary. Another striking feature are the two Uranium peaks at the top and base of the Breda Fm. Uranium in shales is known to be indicative for a relatively high TOC (Fertl & Chilingar, 1988). These two uranium-rich shales coincide with two of the unconformities in the area: the EMU and the MMU.

When we try to characterise the mineralogical constituents of the sediments around the MMU in order to get meaningful estimates for VCL, PHIE, and SW, a number of log cross-plots needs to be made. Figure 4.7 shows a neutron-density crossplot of a number of formations in F17-10. The M2 interval has by far the highest apparent porosities. It is also clear from Figure 7 that a subdivision can be made within the Breda Fm: an upper part with very high porosities (especially indicated by the neutron log which sometimes indicates more than 100 p.u.), and a lower part with slightly lower porosities. This twofold subdivision is also seen in Figure 8 and especially well in Figure 9. These crossplots show PEF against Th:K ratio. Here, the lower zone is characterized by a high PEF (4-6), indicating a. Biotite-Glauconite-Illite mineralogy. The upper zone has a low PEF (2-3), pointing to a Quartz - Muscovite-Montmorillonite mineral assemblage. Figure 4.10 shows an additional cross-plot of the gamma ray log against the density log. Again, the same two groups can be recognised in this plot and seem to support the idea of a low-density, low GR mineral assemblage at the upper half, and a high-density, high GR assemblage at the lower half of the Breda Fm. Care should be taken, however, to over-interpret these plots. Confirmation from XRD, XRF, or thin sections would be needed for a definitive answer.

It is clear, however,  that the classic Breda Fm can be subdivided into two intervals, M1 and M2. M1 is lithologically very similar  to the underlying sediments from the Rupelian to the Eocene. M2 is different, contains less clay minerals, more quartz, is less heavy and has higher porosities. Incidentally, the upper part is of Serravalian age, whereas the lower part has been dated as Langhian.

The question now is how all this translates into a shaly sand model. The more or less constant Th:K ratio basically says that the clay mineralogy remains constant over much of the Tertiary. Substantial amounts of Glauconite would in principle decrease the Th:K ratio and increase the total gamma radiation, thereby influencing the VCL computations. However, there is no way to distinguish Glauconite from the other clay minerals, so a VCL will be calculated with one fixed neutron-density wet clay point.

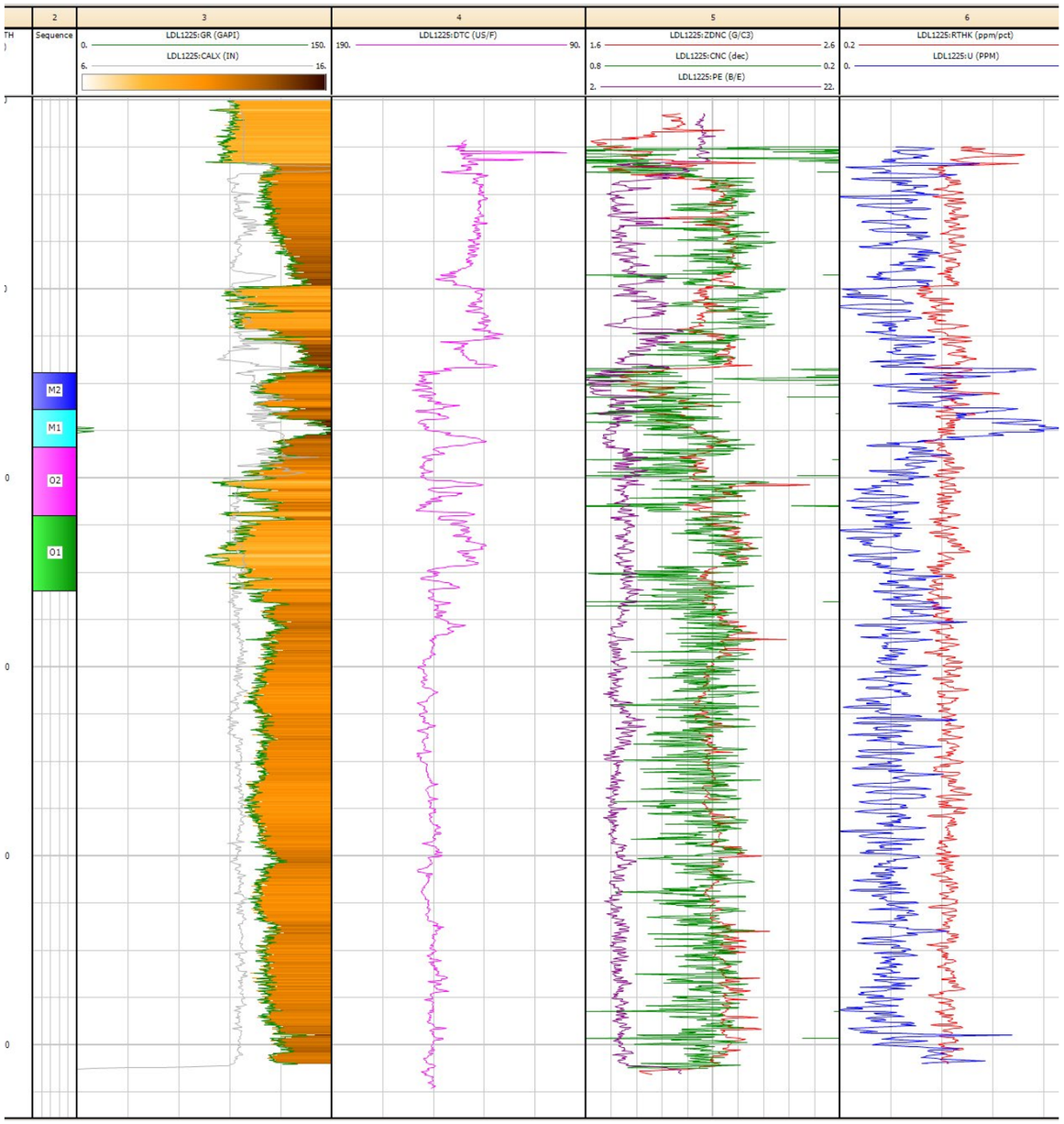


**Figure 4.6: Well F17-10. Overview of the well logs that are of interest for this study. Legend: Track 2: geological zones; Track 3: Gamma ray and caliper logs; Track 4: Sonic log; Track 5: Neutron, density and PEF logs; Track 6: Th-K ratio and U log**

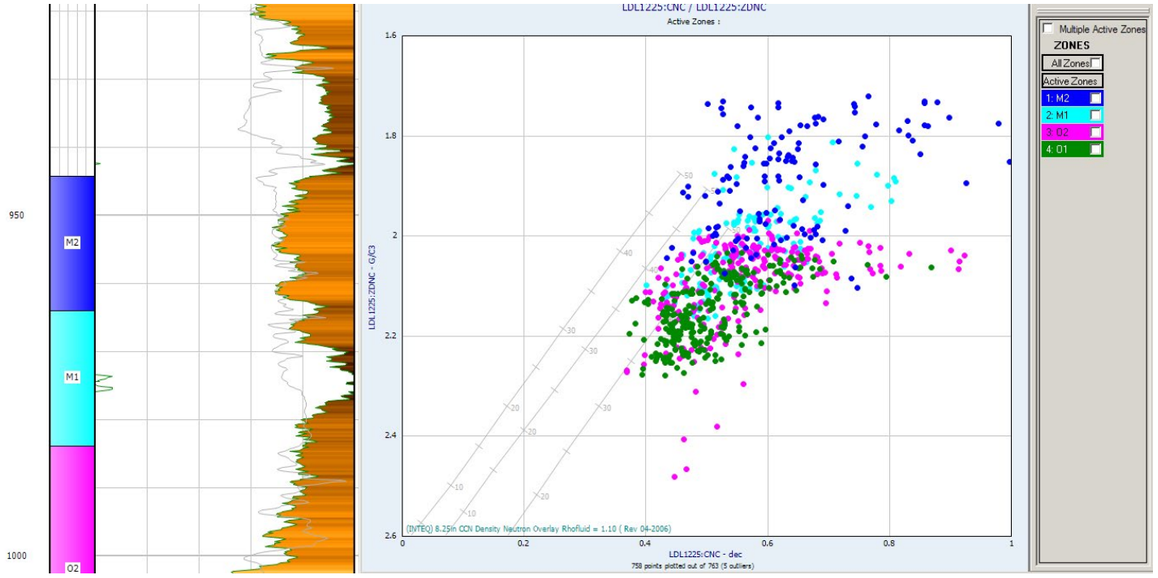


Figure 4.7: Well F17-10. Neutron-Density cross plot.

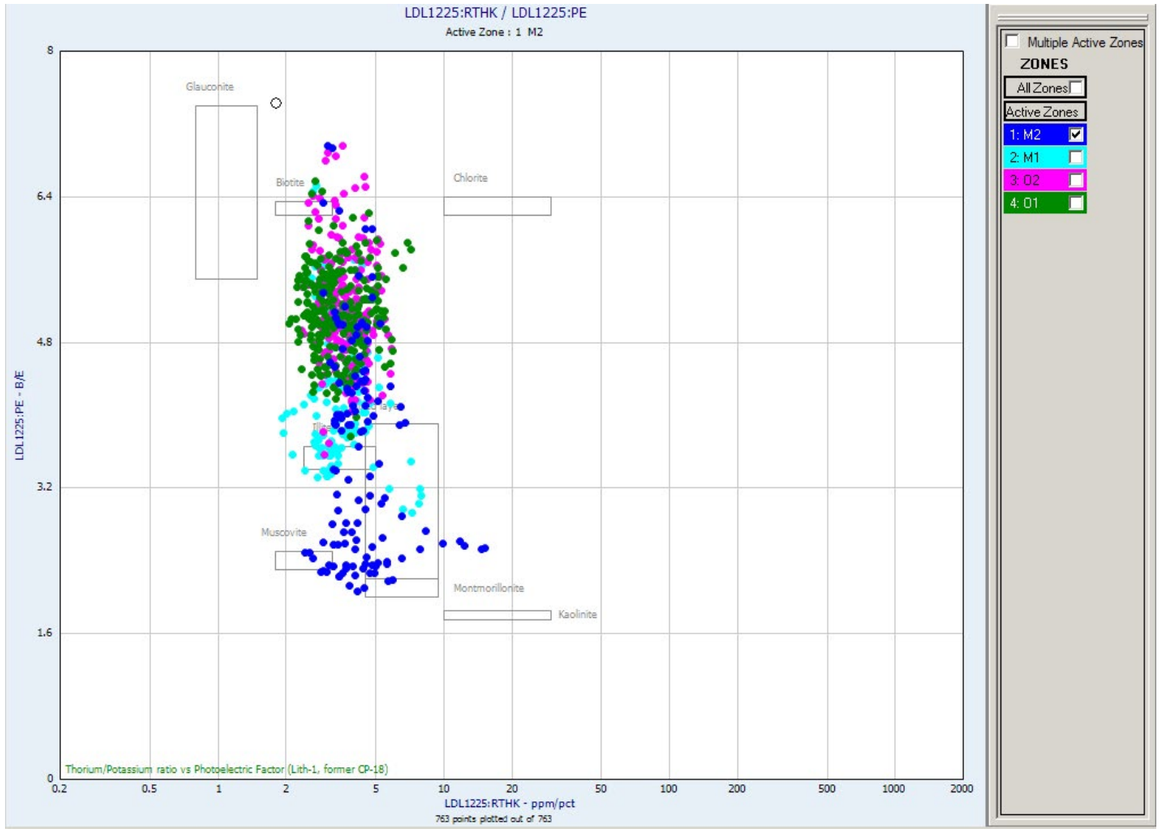


Figure 4.8: Well F17-10. Cross-plot of PEF against Th:K rati, with indications of log values for some minerals.

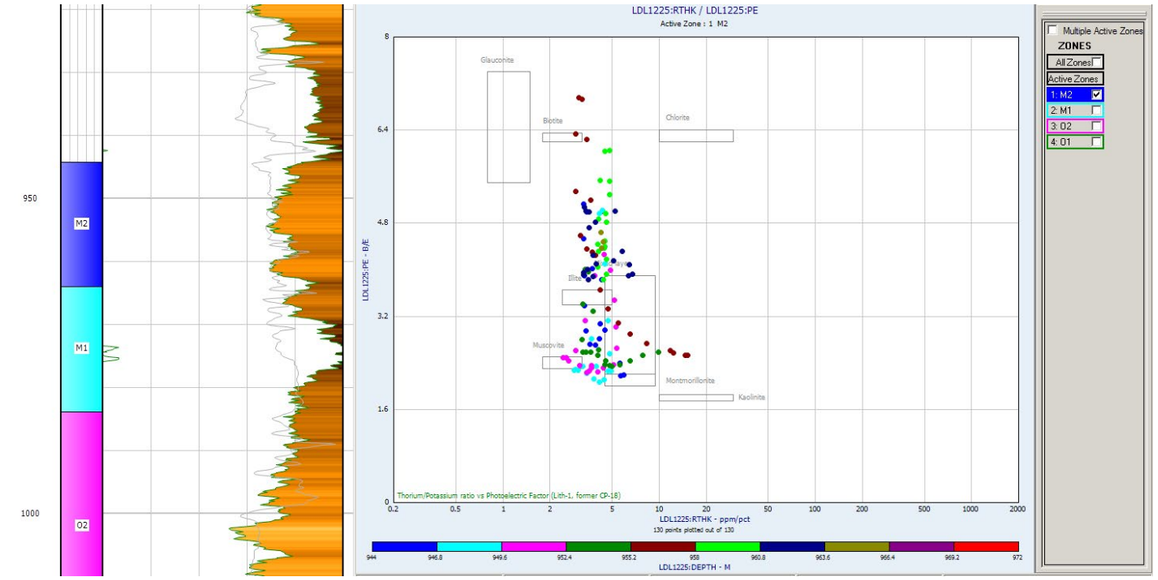


Figure 4.9: Well F17-10. Cross-plot of PEF against Th:K ratio.

The result of the VCL computations are shown in Figure 4.11. Two methods were done: one using a linear GR transform, and a second one using the neutron and density logs. There is good agreement between both curves in the upper part of the Breda Fm and younger formations, but a considerable mismatch in the lower part of the well (Figure 4.12). The lower part even shows a negative correlation between the two VCL's.

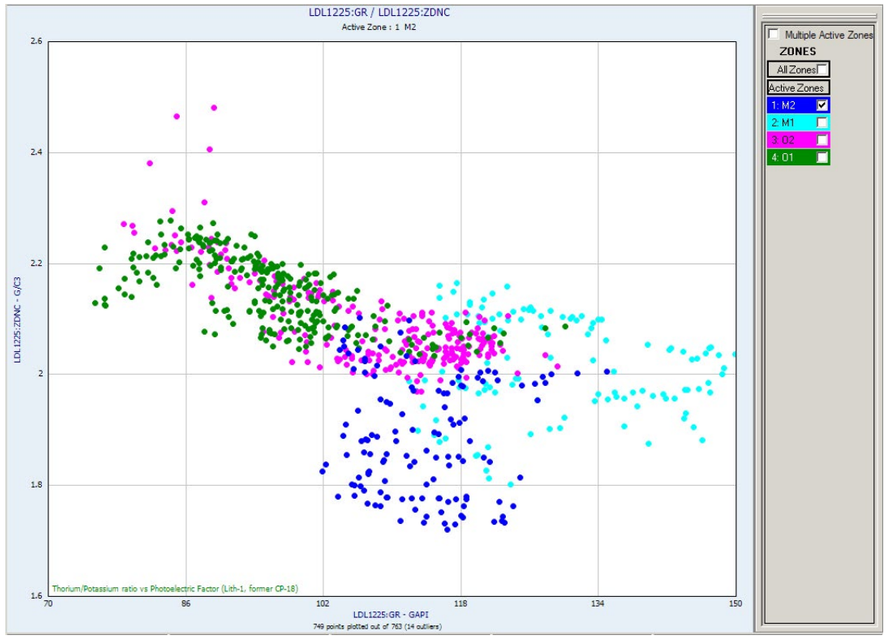


**Figure 4.10: Well F17-10. Crossplot of gamma ray against density log.**

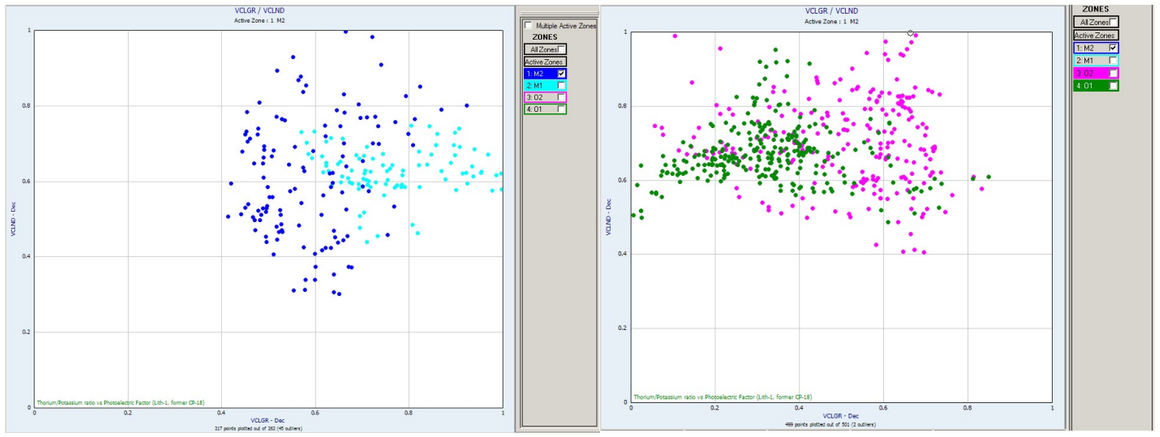


**Figure 4.12: Well F17-10. Comparison of VCL's obtained through GR and Neutron-Density transforms. Left: upper part of the well. Right: lower part of the well.**

A possible explanation for the mismatch in the lower part of the well could be that this section is overpressured, a well-known phenomenon in the Lower Tertiary and Chalk in the North Sea. Due to the thick and rapid sediment accumulation during the Plio-Pleistocene, the Lower Tertiary had no time to dewater. The result is that the sediment is overpressured and contains too much water, causing high porosities, low bulk densities, high neutron values, and long sonic travel times, thereby distorting the neutron and density values.
So it seems that the best way to estimate VCL in the entire Tertiary is through the use of an ordinary gamma ray transform. This was used in the next step, the calculation of porosity and water saturation.

## Results F17-10

The evaluation results of well F17-10 are shown in Appendix B1. With the current GR-NPHI-RHOB settings, the effective porosity is on the high side for all evaluated formations. M1 and M2 have an average effective porosity of 30 %, and shows an oil saturation of 30%. The combination of high porosity and low oil saturation strongly suggests that we are dealing with residual oil.

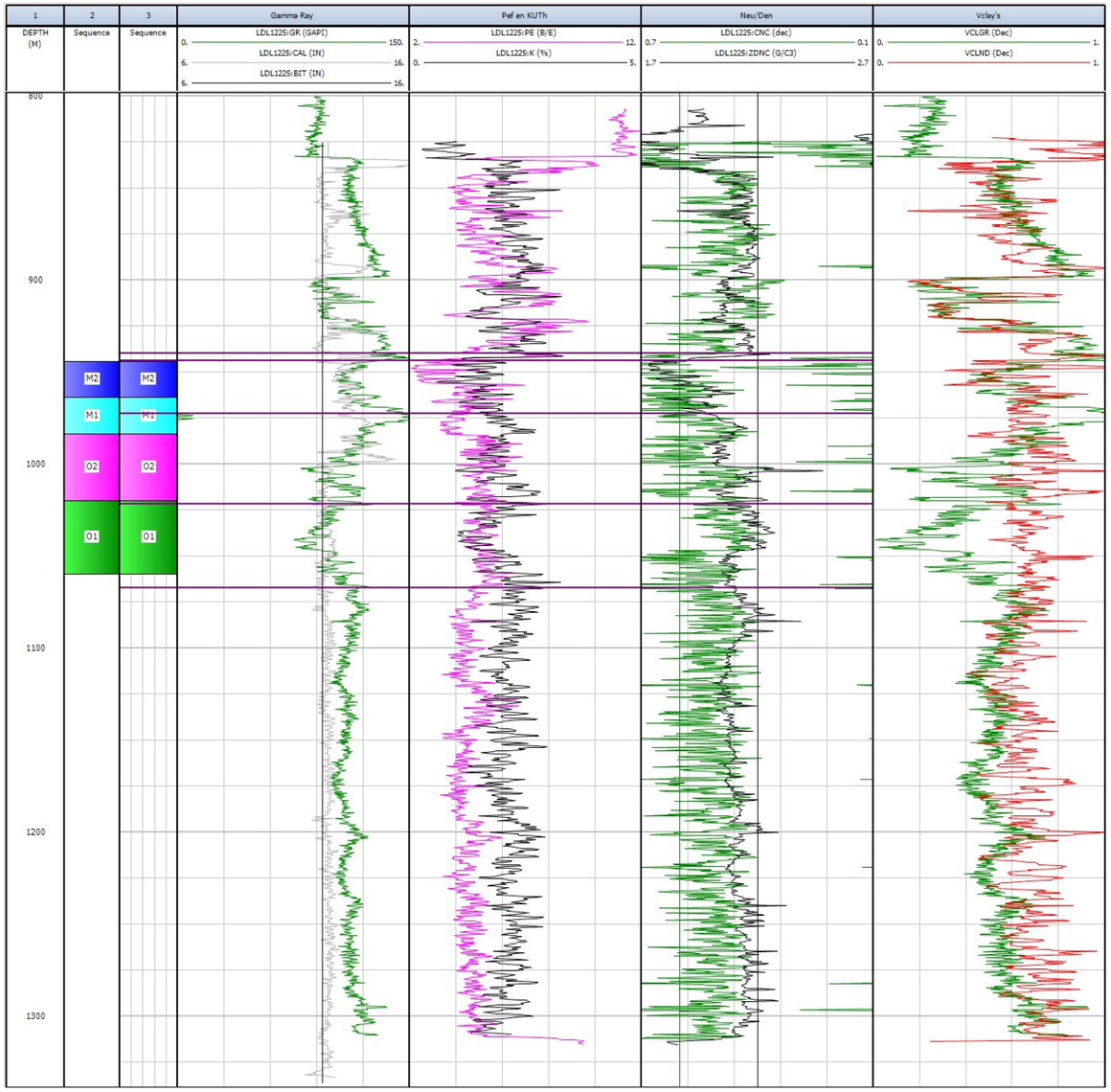


**Figure 4.11: Well F17-10. VCL computations using a linear GR transform (green curve in track 7) and a combination of neutron and density logs (red curve in track 7). Note the agreement between both curves in M2 and younger formations, and the disagreement in the lower part of the well.**

## Key well F02-06

Well F02-06 has a log suite comparable to F17-10: spectral gamma ray, neutron-density-pef, sonic, and resistivity. Inspection of the mineralogy (as far as the log readings allow) yields a rather uniform distribution of clay mineralogy: a mixture of illite and glauconite (Figure 4.13). Combining the Pef curve with the Th:K ratio (Figure 4.14) results in a slightly different view, especially when the points are colour coded according to their GR value. Illite is probably of minor importance, as the Pef values are too high. Increasing gamma radiation values move the points toward the glauconite field. Pef ranges between 2 and 20, which suggests the presence of carbonates or heavy oxides, such as iron oxide. The core from F02-03 shows indeed a mixture of limestone clasts and glauconite. Iron-bearing minerals were not seen at a quick visual inspection, but their presence cannot be ruled out.

For clay volume determination the same procedure was followed as in well F17-10: a gamma ray transform with GRmin 75, and GRmax 140; and for the neutron density the wet clay point at (2.2, 0.60); water point at (2.05, 0.3); and clean matrix point at (2.65, -0.04). The clay parameters were kept constant for all the Tertiary formations.

When comparing the two VCL curves, the same strange behaviour as in well F17-10 was seen (Figure 4.16). The VCL curves from the Plio-Pleistocene sequence and M2 are in good agreement, but the the VCL curves from the older formations even have a negative correlation. As in F17-10, the cause is unknown, as the mineralogical logs (spectral gamma ray and pef) do not really indicate very different mineralogies.

The evaluation plot of F02-06 (Figure 4.17) shows extremely high porosities in M2, even when a standard matrix density of 2.65 is chosen. Changing it to higher values to account for possible limestone or dolomite content in the matrix, would result in even higher porosities. Despite the fact that the porosities are probably too high, the fact remains that according to our calculations, residual oil (around 30%) is present in both M1 and M2.

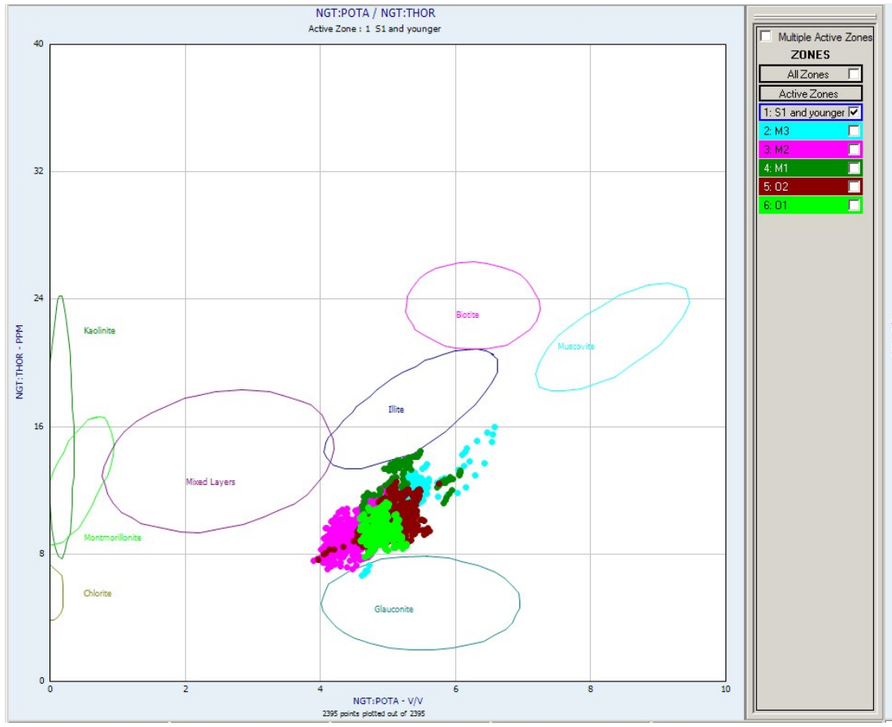


Figure 4.13: Well F02-06. Potassium-Thorium cross-plot.

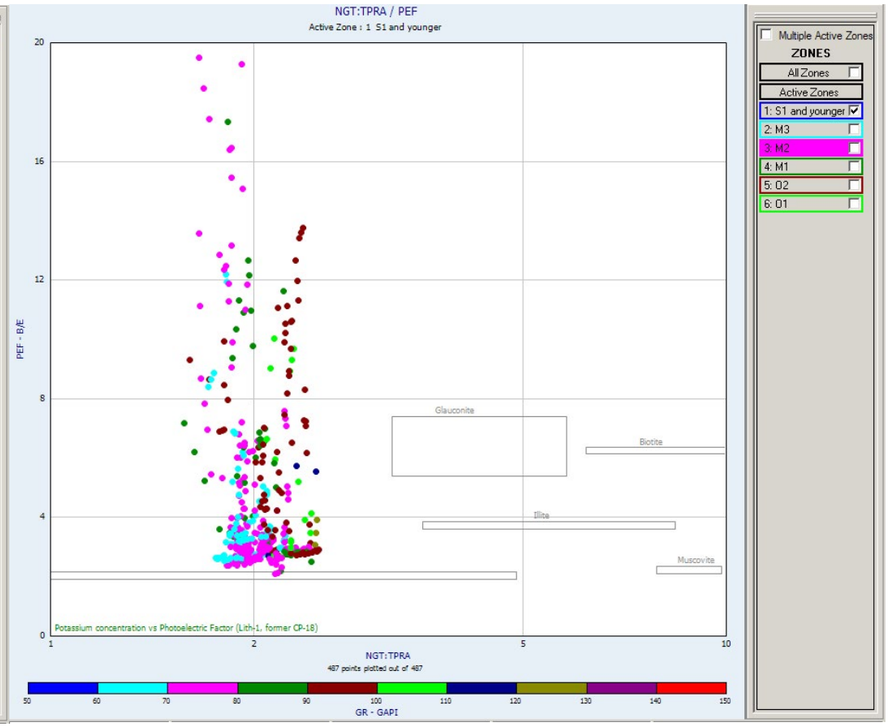


Figure 4.14: Well F02-06. Cross-plot of PEF against Th:K ratio of M2.

Figure 4.15: Left: Core cut around the MMU in well F02-03. Right: Close-up at 1203.63 m. Badly sorted glauconitic sandy shale with large rounded micritic limestone clasts. Note the yellowish crust around the limestone clasts. Irregularly distributed brownish stain is caused by bitumen.

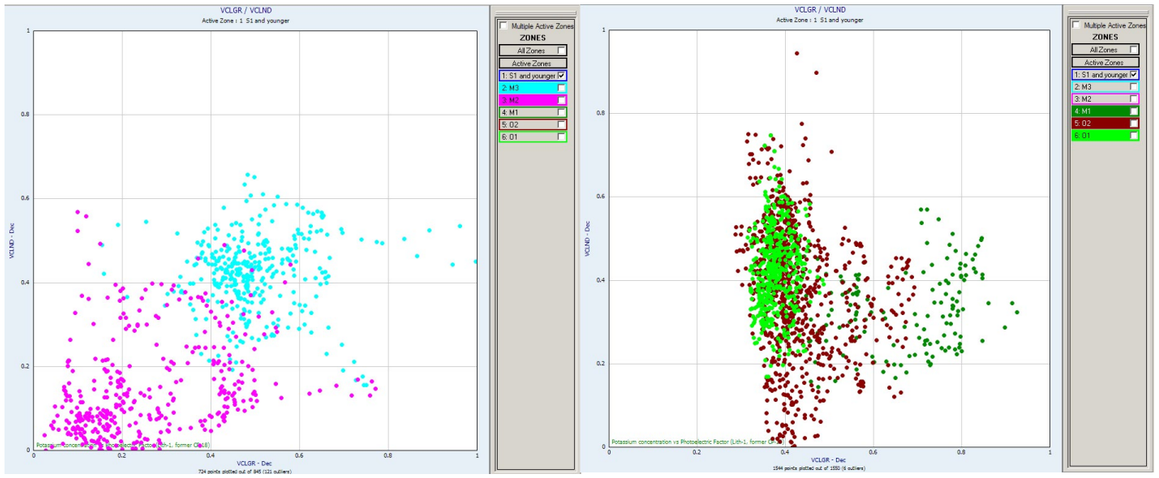


**Figure 4.16: Well F02-06. Comparison of VCL's obtained through GR and Neutron-Density transforms. Left: M2 and M3. Right: O1, O2 and M1.**

## The other wells

Apart from F02-06 and F17-10, all other wells (D12-01, E06-01, F04-01,F09-01,F15-01, F15-06, F17-12, K05-04, and K06-01) have comparable log suites, consisting of gamma ray, sonic, and resistivity logs. A simple procedure was followed for these wells: clay volume (VCL) was derived from the gamma ray log; porosity (PHIE) from the sonic log, corrected for clay effects; and water saturation (SW) from PHIE and a deep reading resistivity log, using the Indonesian shaly sand equation.
Appendices B1 to B11 show 1:500 log playbacks of the evaluations of these wells. Although the porosity in M2 varies from well to well, it is in general high, between 25 and 30 %. Several wells show amounts of residual oil in M1 and M2. Sometimes even overlying sands (Tortonian to Gelasian) show some residual oil.

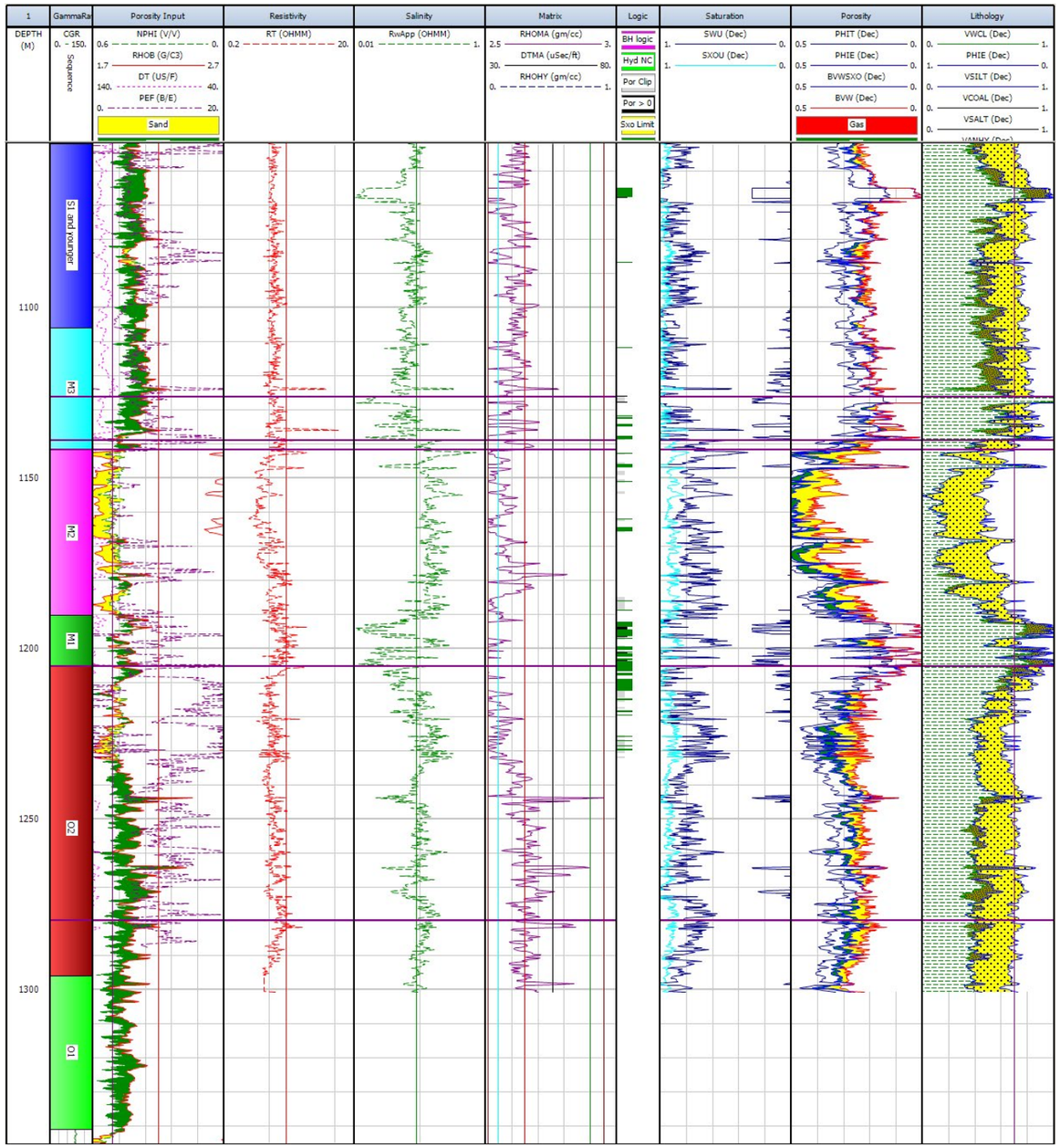


**Figure 4.17: Well F02-06 formation evaluation.**

## Core of the MMU

In well F02-03 a core was cut in the stratigraphic interval around the MMU. Although the recovery of the 9.5 m long core barrel (1202.5-1212) was only 3 m (figure 4.18), some extremely interesting observations can be made on the core fragments (Figure 4.20). The entire interval consists of a mixture of glauconitic, shaly sand and redeposited intraformational clasts of various sizes and lithologies.
The lowest preserved parts of the core (1205.50 to 1205.13 m, according to the depths on the mounted slabs) show a light brown diatomite (figure 4.19). The brownish colour could be due to oil staining, but that is unclear at the moment. Core pieces are extremely light weighted, pointing to porosities of more than 50%. The fact that these pieces show an inclined lamination (where one would expect a horizontal sedimentary dip), plus a curved lamination near the bottom, leads one to suspect that these pieces of diatomite were eroded, transported and redeposited as large diatomite boulders.
Overlying the diatomite are two large lime mudstone clasts with a diameter of some 10-20 cm. Both have rounded edges, and the upper one even has a light brown coloured coating around it. It is not known whether the coating predates the re-deposition of the clast, or that it is a diagenetic feature.
The rest of the core contains badly sorted glauconitic sandy shale with large rounded micritic limestone clasts, most of which have a light brown coating. A few chalk clasts can be recognised, e.g. at 1202.88 m. Bitumen is also present, mostly along fractures or around the limestone pebbles. Occasionally, the bitumen is present as clasts, probably eroded (e.g. around 1203.43 m).

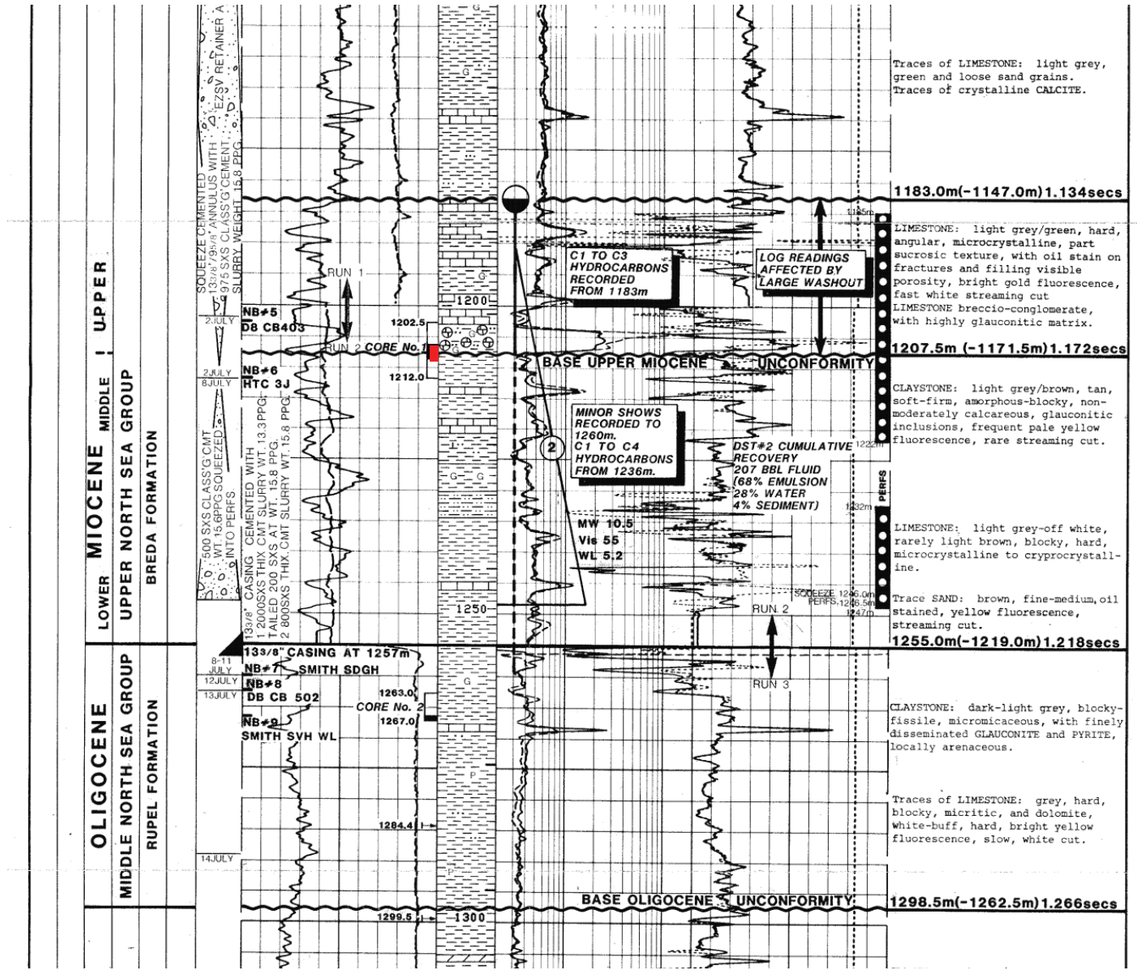


Figure 4.18: Composite log of the F02-03 well. The core is indicated in red (see also Figures 4.20, 4.19, and 4.15)


Figure 4.19: Diatomite in the F02-03 core just above the MMU

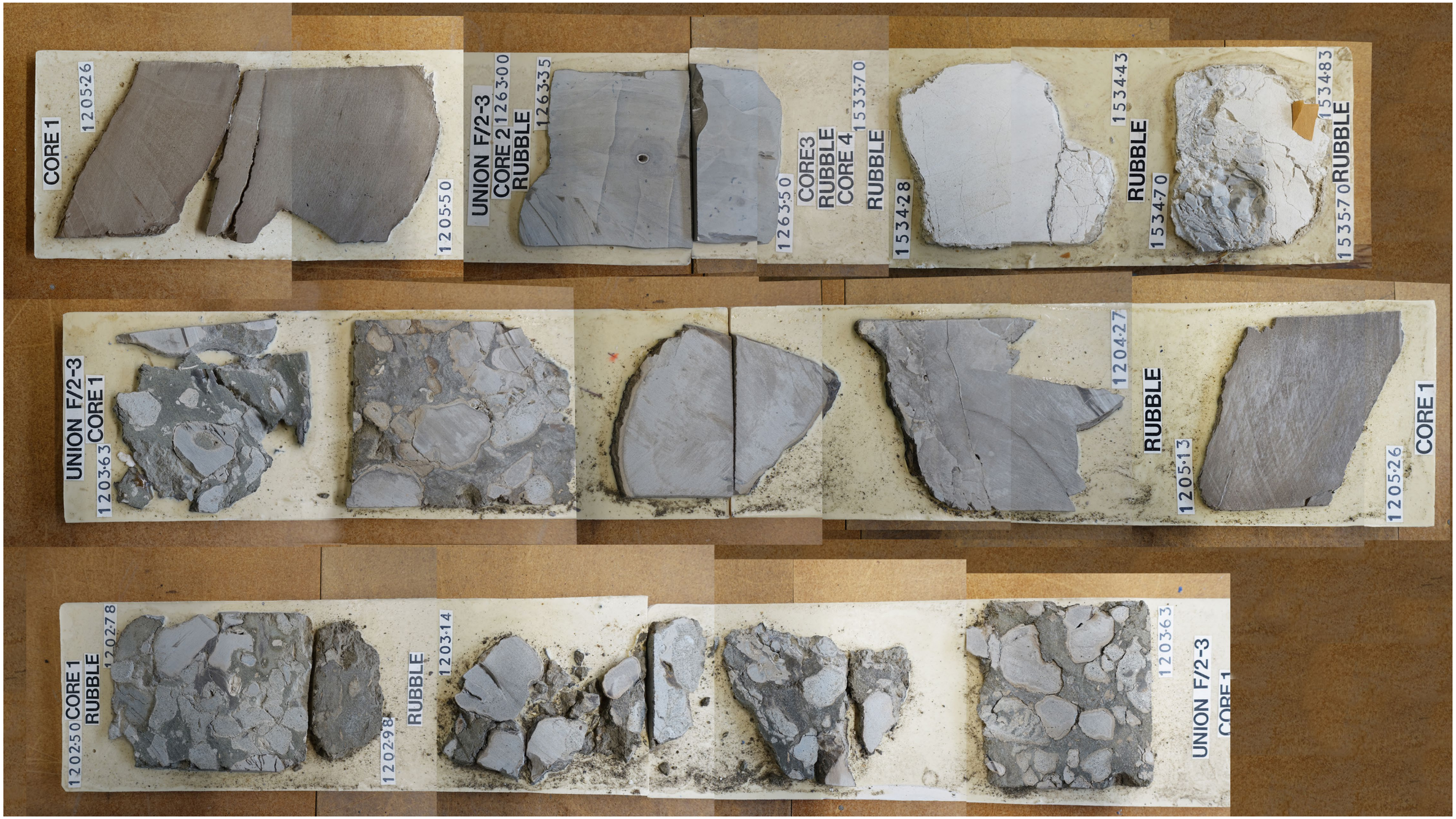


Figure 4.20: F02-03 core of the MMU

*The Pelagia shooting seismic*

# 5. Seismic Interpretation

# 5. SEISMIC INTERPRETATION

## Approach

### Seismic Transects

The seismic interpretation exercise focused on three regional composite seismic lines (see figure 5.1). These lines run between wells and are constructed from 2D and 3D seismic (table 5.1). The **F02 Panel** runs over the Hanze Field (F02) and a parallel line, the **F17 Panel**, runs over the Rembrandt field. These lines were chosen at these locations because hydrocarbon shows had been reported around the MMU at both locations. Secondly, the orientation of these two lines is parallel to the general direction of progradation of the Eridanos delta. The third line (**N-S Panel**) is a connecting line between the two lines.
All seismic data was converted to European Zero Phase convention (figure 5.2), bulk shifted to match the F02 survey, and scaled before the composite line was converted to 2D seismic lines.

### Well-to-Seismic tie (Depth Time Conversion)

Since the seismic is characterised by numerous velocity anomalies caused by shallow gas, and well-logs are often off poor quality (probably caused by mud invasion, wash-outs, or when logs are measured through the casing), tying the seismic to the wells can be extremely difficult. Consequently, synthetic to seismic matching yielded poor results. Therefore, manual adjustments where made after the wells had been tied. This was based on the expert opinions of the seismic interpreter, petrophysicist and a palynological expert. Together the well log, age-dating and seismic interpretations were assessed with respect to reliability and the tie was adjusted in order to make the best possible fit.

### Horizon Interpretation

Seismic interpretation was carried out using Petrel 2014 and OpendTect 6. Key stratigraphic horizons were identified in wells and based on bio-stratigraphic levels and/or log units. All horizons above the LMU are taken from ten Veen et al., 2013.

## Results

### Seismic Interpretation

The following seismic horizons are mapped:

- Late Miocene Unconformity (LMU)
- Mid Miocene Unconformity (MMU)
- Early Miocene Unconformity (EMU)
- Savian Unconformity
- Top Rupel Formation
- Base Rupel Fm.

Figure 5.3 depicts the relation between the mapped horizons and the lithostratigraphic units, identified intervals and ages.

**Table 5.1: List of the used seismic surveys for the constructions of the composite panels.**

| *Survey* | *Type* |
|---|---|
| **F02 Panel** | |
| SNST87 | 2D |
| D12_D15_D18_E13_Z3WIN1994A | 3D |
| E_Z2NAM1981G | 2D |
| F02_F03_Z3RWE1994A | 3D |
| F03_B18_Z3NAM1982A | 3D |
| | |
| **N-S Panel** | |
| B_Z3FUG2002A | 3D |
| F02_F03_Z3RWE1994A | 3D |
| SNST87 | 2D |
| F11_F12_Z3WES2003A | 3D |
| | |
| **F17 Panel** | |
| SNST83 | 2D |
| L01_L02_Z3NAM1991E | 3D |
| F17-F18_Z3NAM1992A | 3D |
| F15_F18_Z3PET1994A | 3D |
| G14_G14_G17_Z3NAM1997A | 3D |

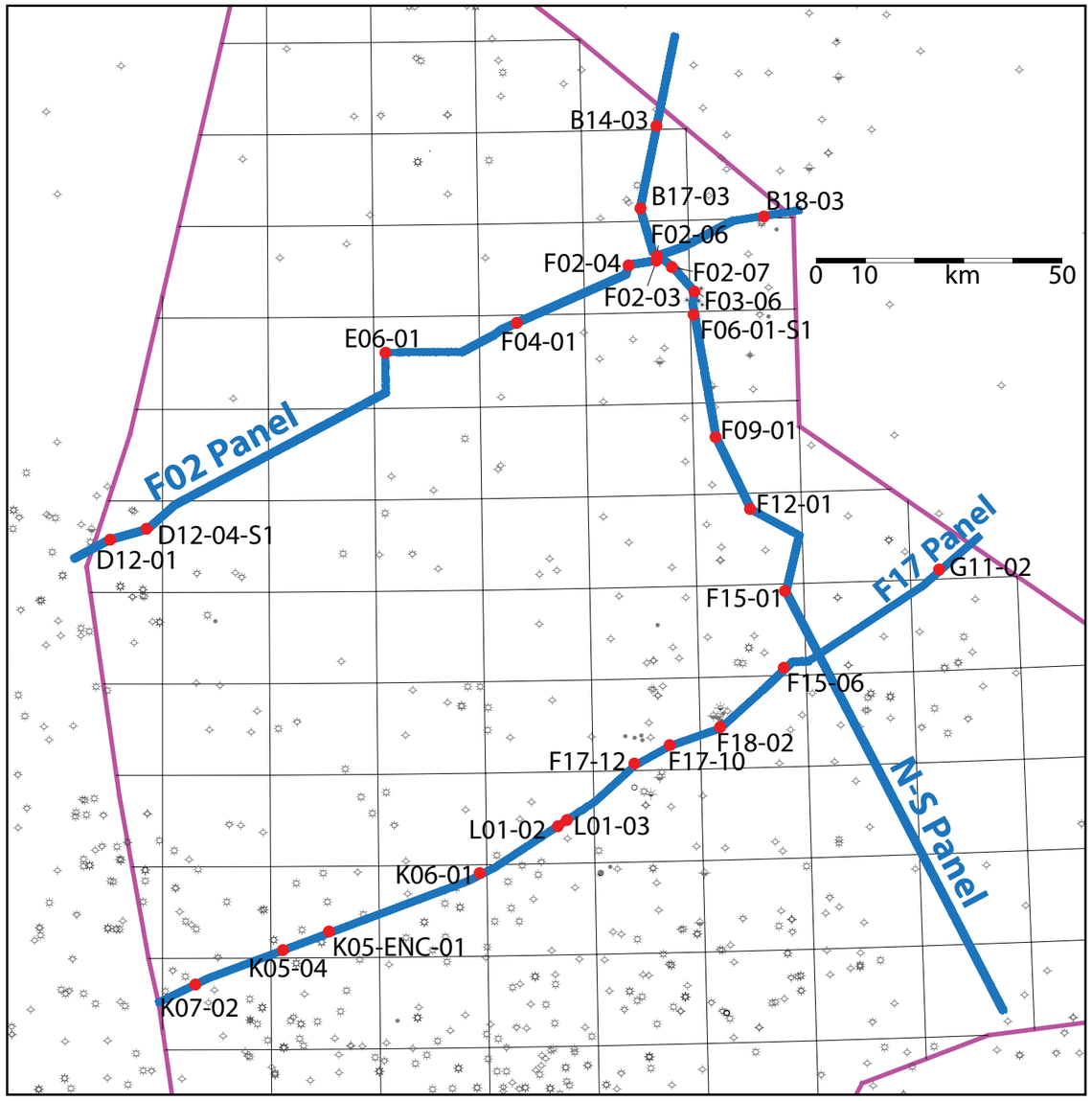


**Figure 5.1: Map of the northern Dutch offshore showing the orientation of the three panels and all wells**

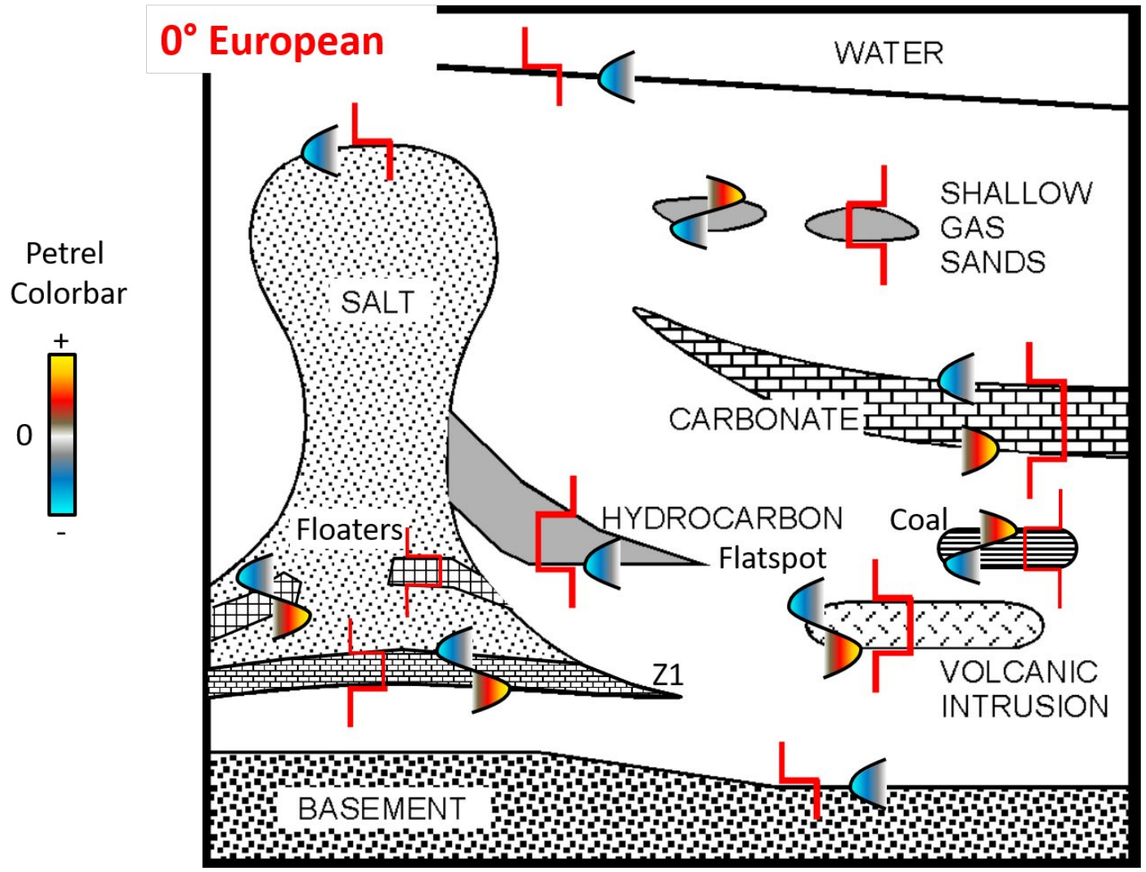


Figure 5.2: All seismic data is made European Zero phase. The relative acoustic impedance contrasts of various rock types and their corresponding seismic reflection are depicted in the Petrel colour-bar. Modified after Brown 2004

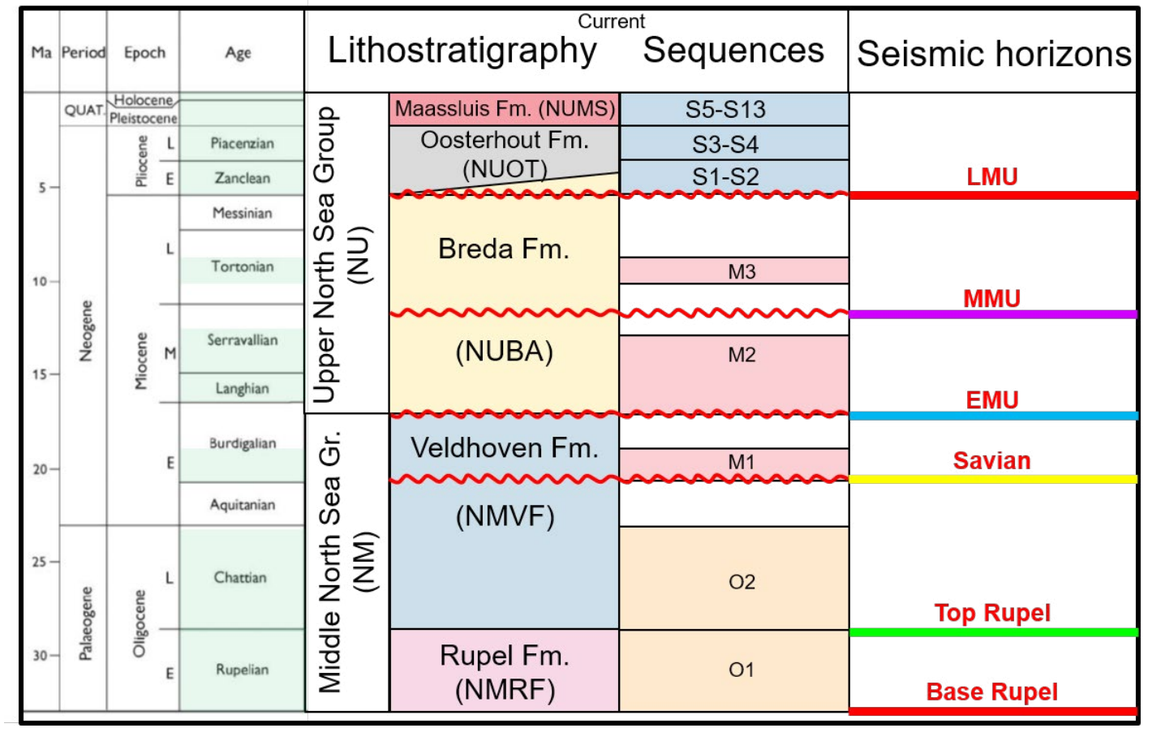


Figure 5.3 depicts the relation between the mapped horizons and the lithostratigraphic units, identified intervals and ages.

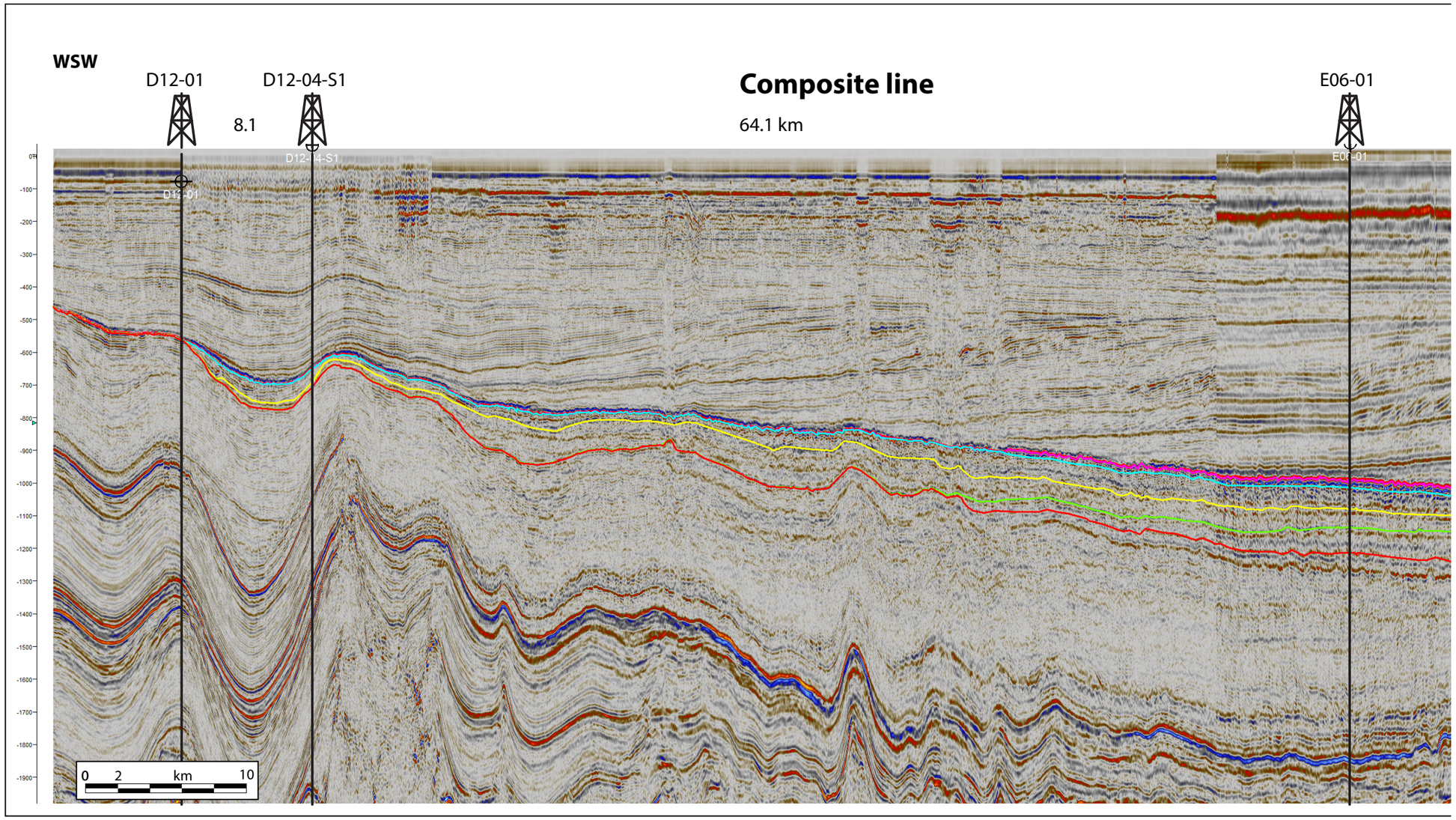


Figure 5.4: F02 Panel

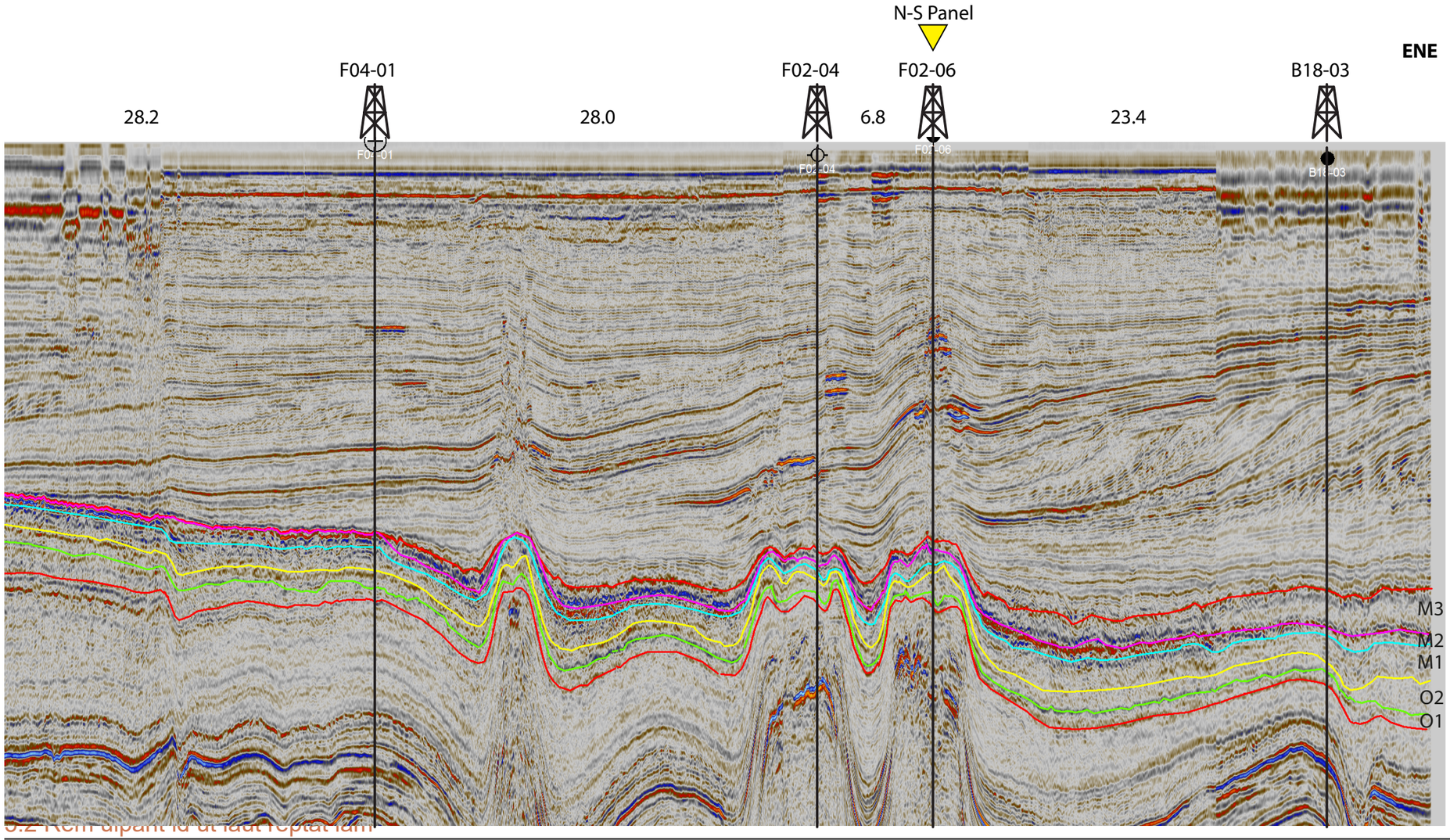
N-S Panel
ENE
F04-01
F02-04
F02-06
B18-03
28.2
28.0
6.8
23.4
LMU
M3
MMU
M2
EMU
M1
Savian
O2
Top Rupel
O1

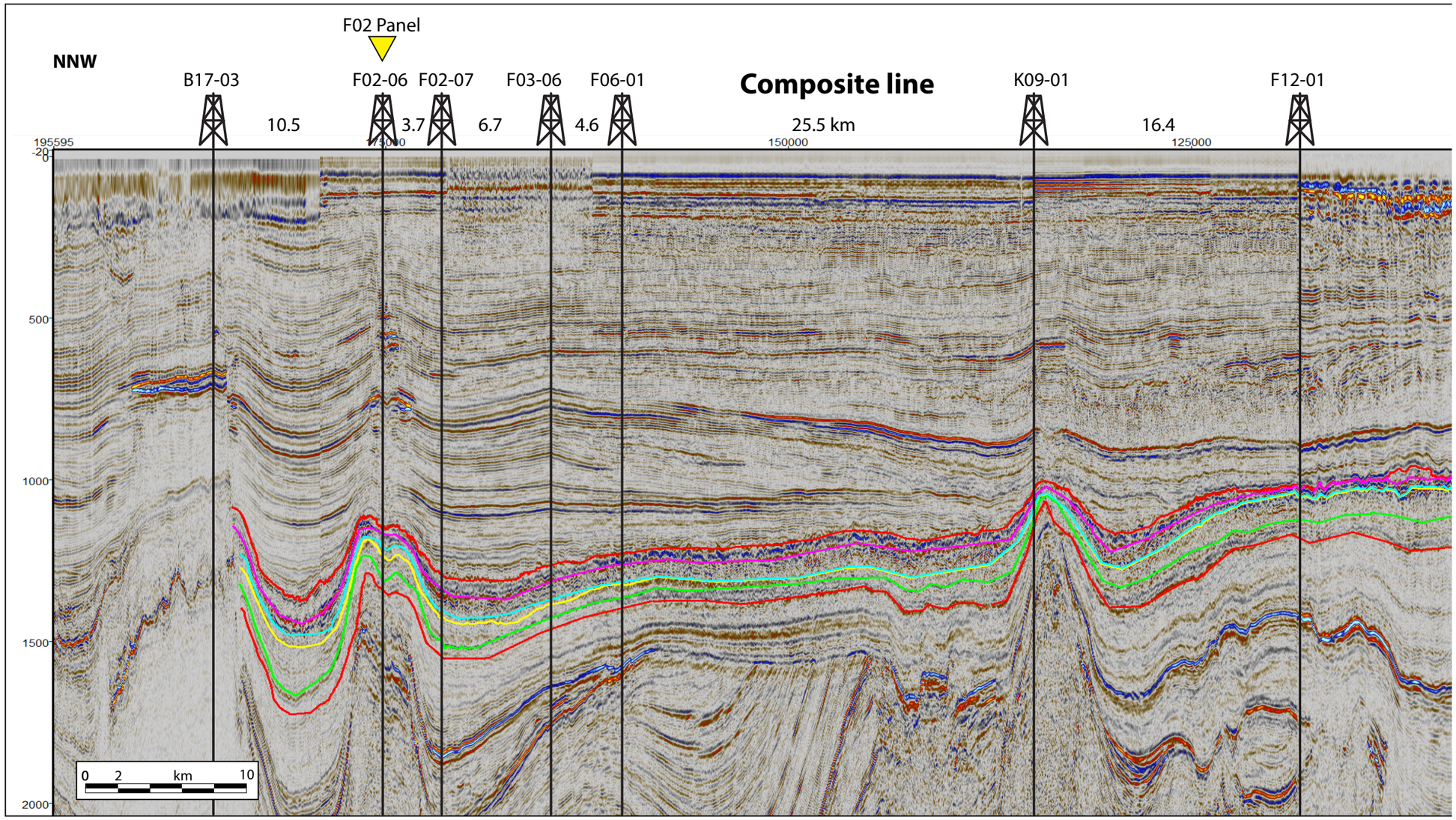


Figure 5.5: N-S Panel

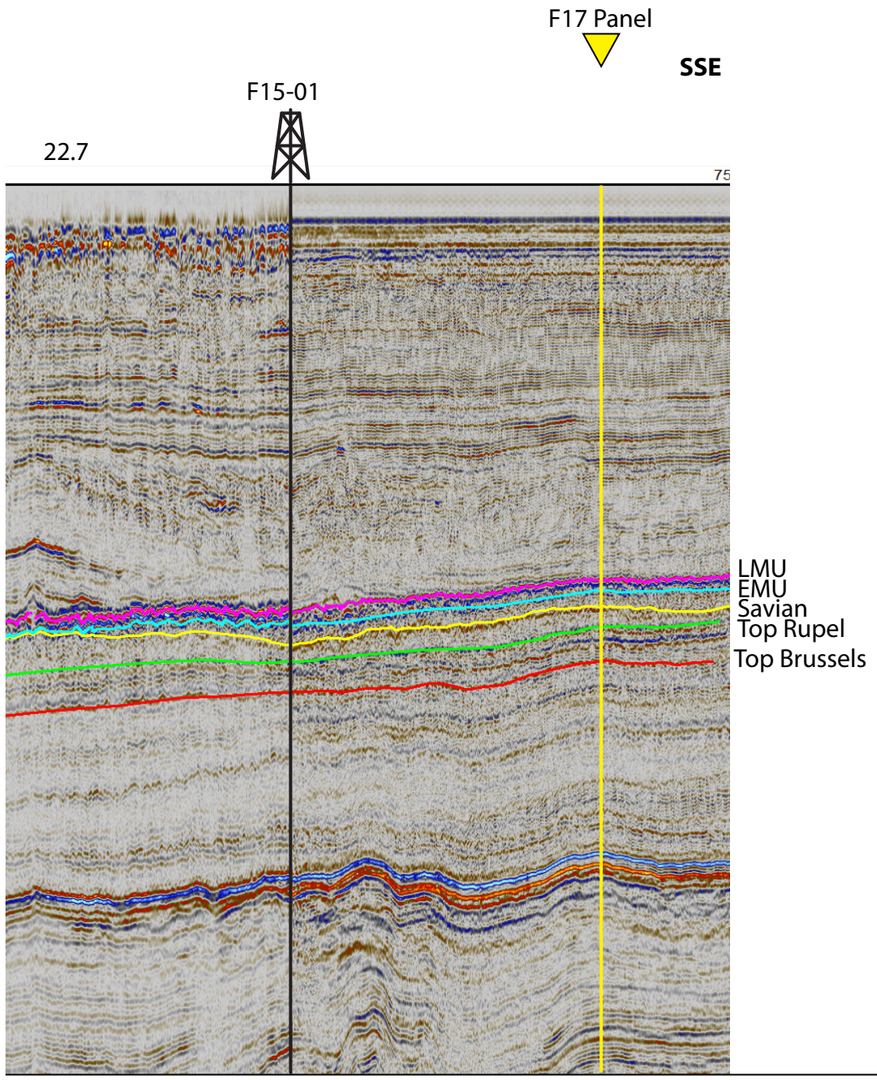
F17 Panel
SSE
F15-01
22.7
75
LMU
EMU
Savian
Top Rupel
Top Brussels

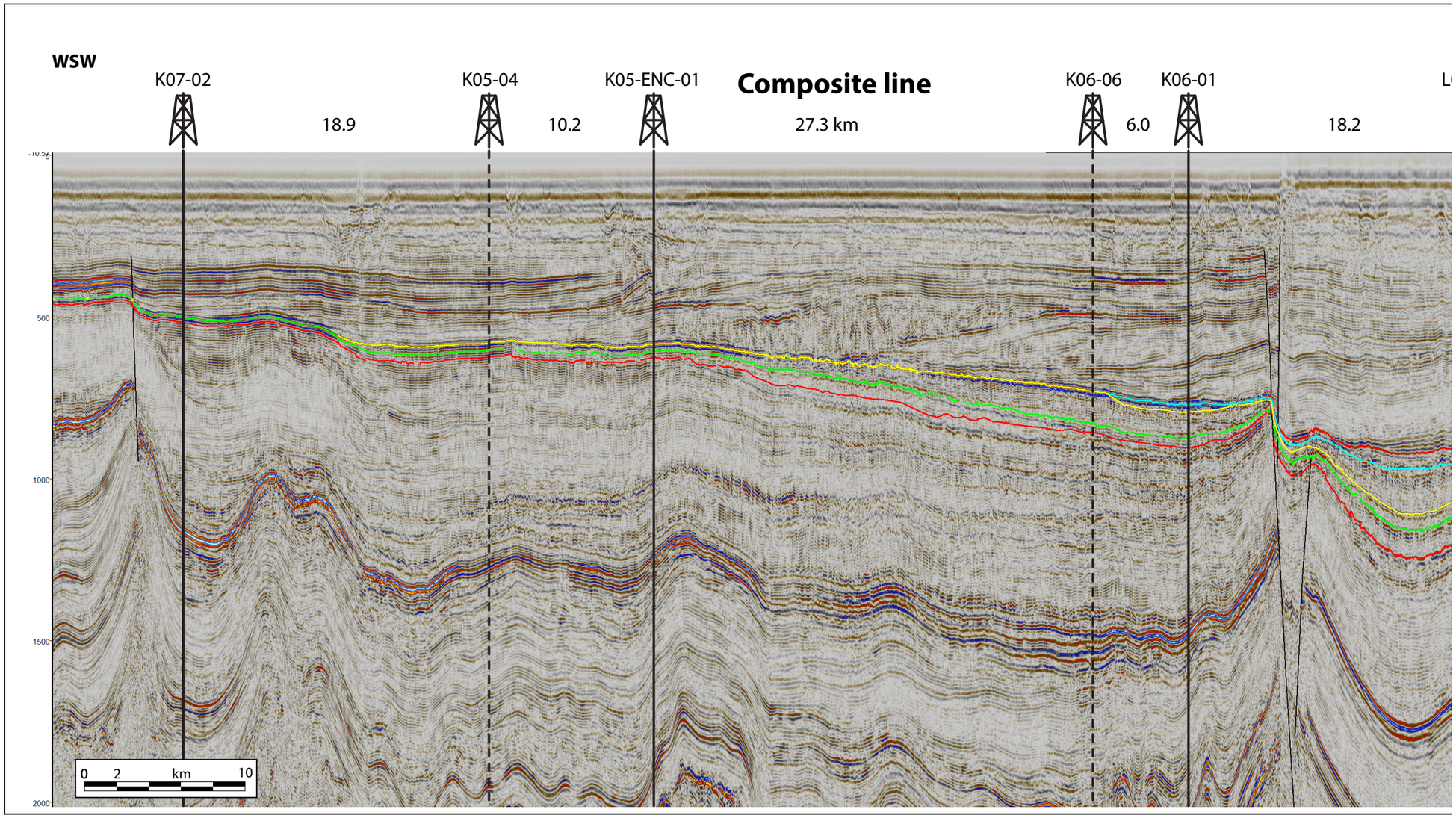


Figure 5.6: F17 Panel

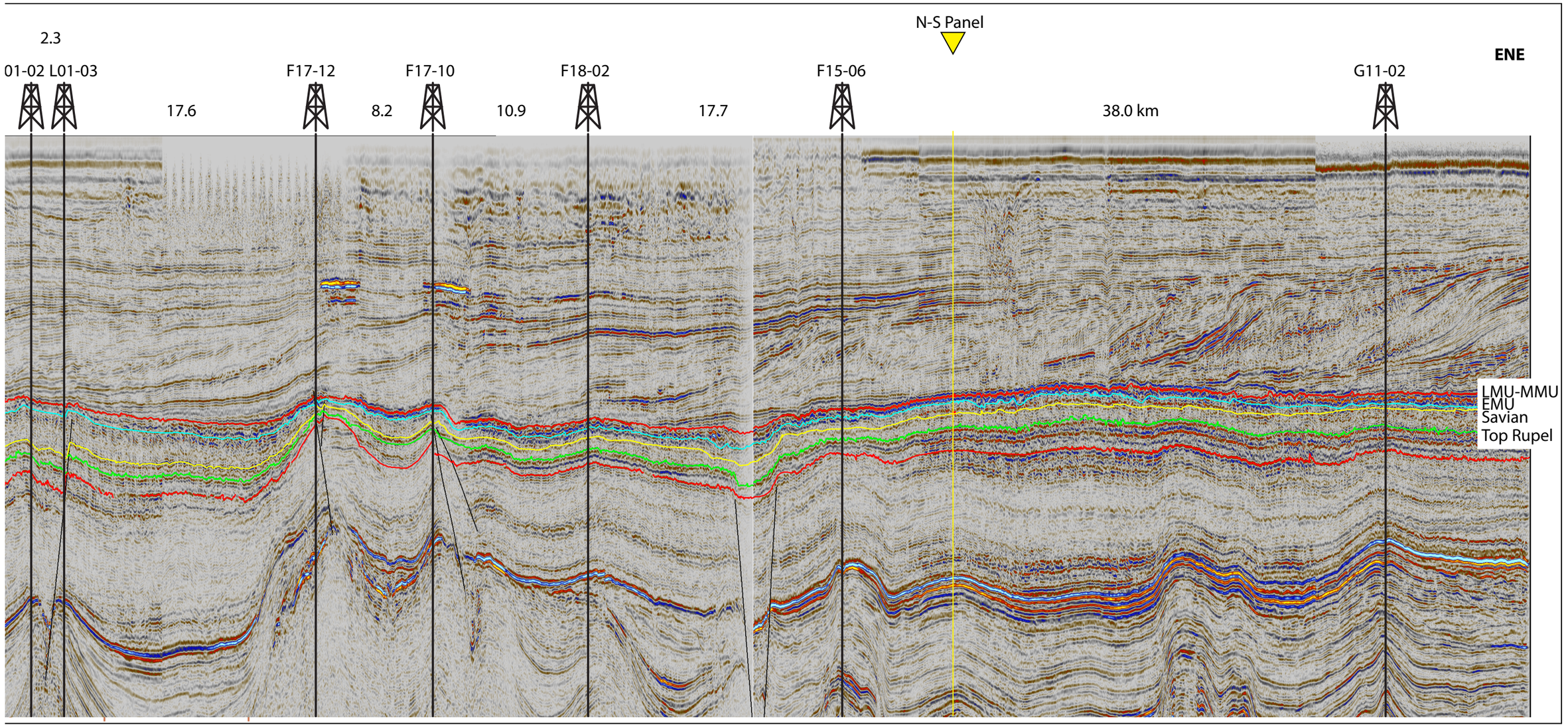
N-S Panel
ENE
2.3
01-02
L01-03
F17-12
F17-10
F18-02
F15-06
G11-02
17.6
8.2
10.9
17.7
38.0 km
LMU-MMU
EMU
Savian
Top Rupel

*Miocene Crossbedding in Denmark*

# 6. Chronostratigraphy

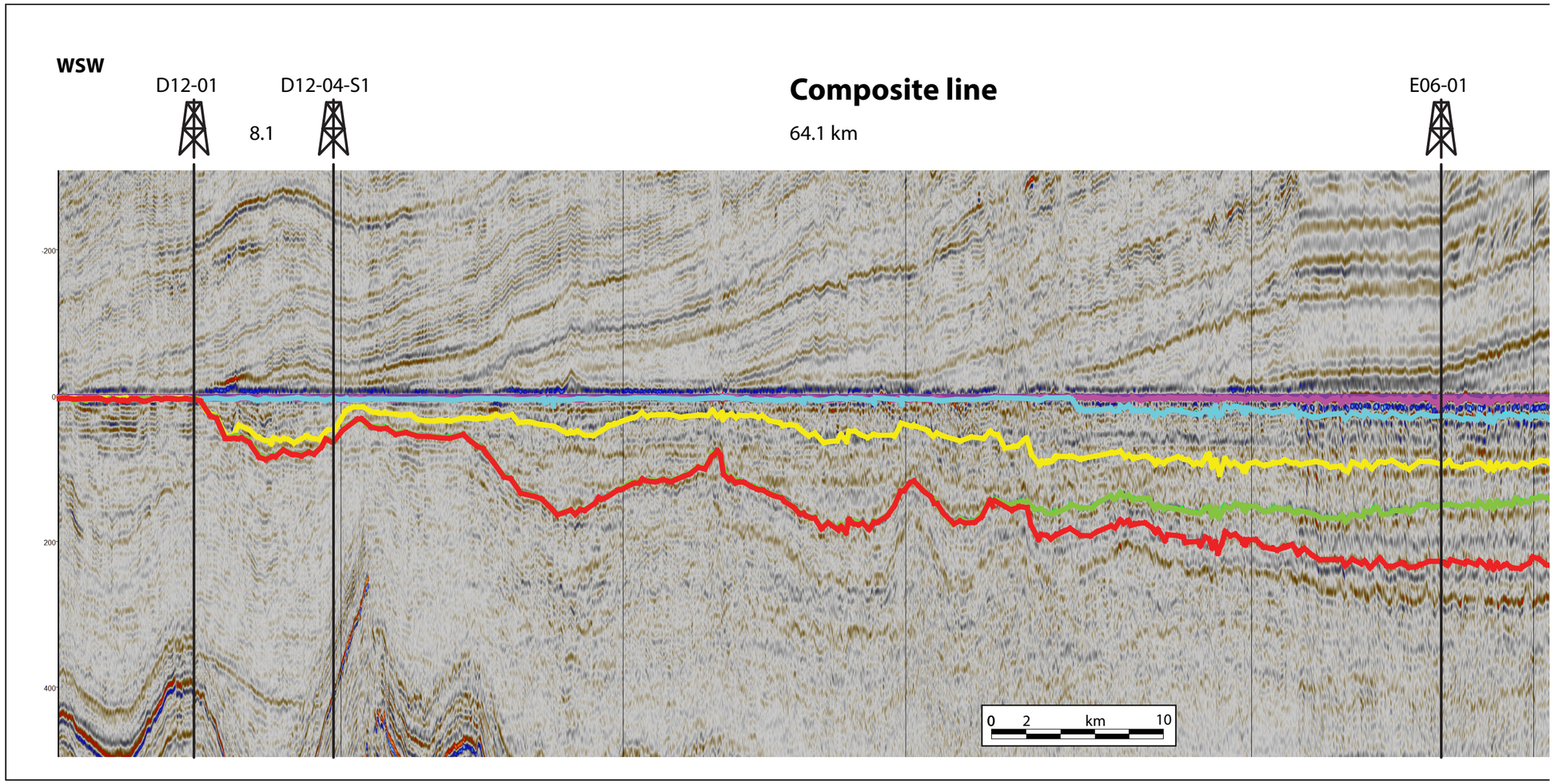


**Figure 6.1: F02 Panel flattened on the Late Miocene Unconformity (LMU)**

## Wheeler transforms methodology

The seismic transects were transformed into the Wheeler domain (geologic time domain) in order to highlight hiatuses, lateral shifts of deposition, and depositional rates.

The seismic Wheelers are made using an model driven approach. This means that the seismic is flattened according to all mapped seismic horizons and the seismic in between is transformed according to one of three models (Parallel to upper horizon, parallel to lower horizon, or linear interpolated). This approach was favoured over the data driven approach, where all seismic events between the horizons are automatically tracked. Since the data is characterised by many vertical disturbances (polygonal and normal faults, chimneys, salt domes, anomalies caused by shallow gas, tunnel valleys, and welds between seismic vintages) the tracking algorithm was unsuccessful in tracking the events properly over the entire length of the seismic lines.

The advantage of the model driven approach is that hiatuses are depicted correctly since onlap and downlap patterns are correctly handled. Furthermore, the seismic character is preserved and the correlations are consistent over larger distances (e.g. they are not hampered by vertical disturbances). Since the seismic character is preserved it allows us to place wells in the Wheeler transform.

Unfortunately, the model driven approach will results in errors when the model is not in accordance with the geological architecture (internal complexities such as clinoforms, slumps, angular unconformities, etc.). This results in dipping reflectors in the Wheeler transform, whereas in theory all events should be completely flat in a Wheeler diagram.

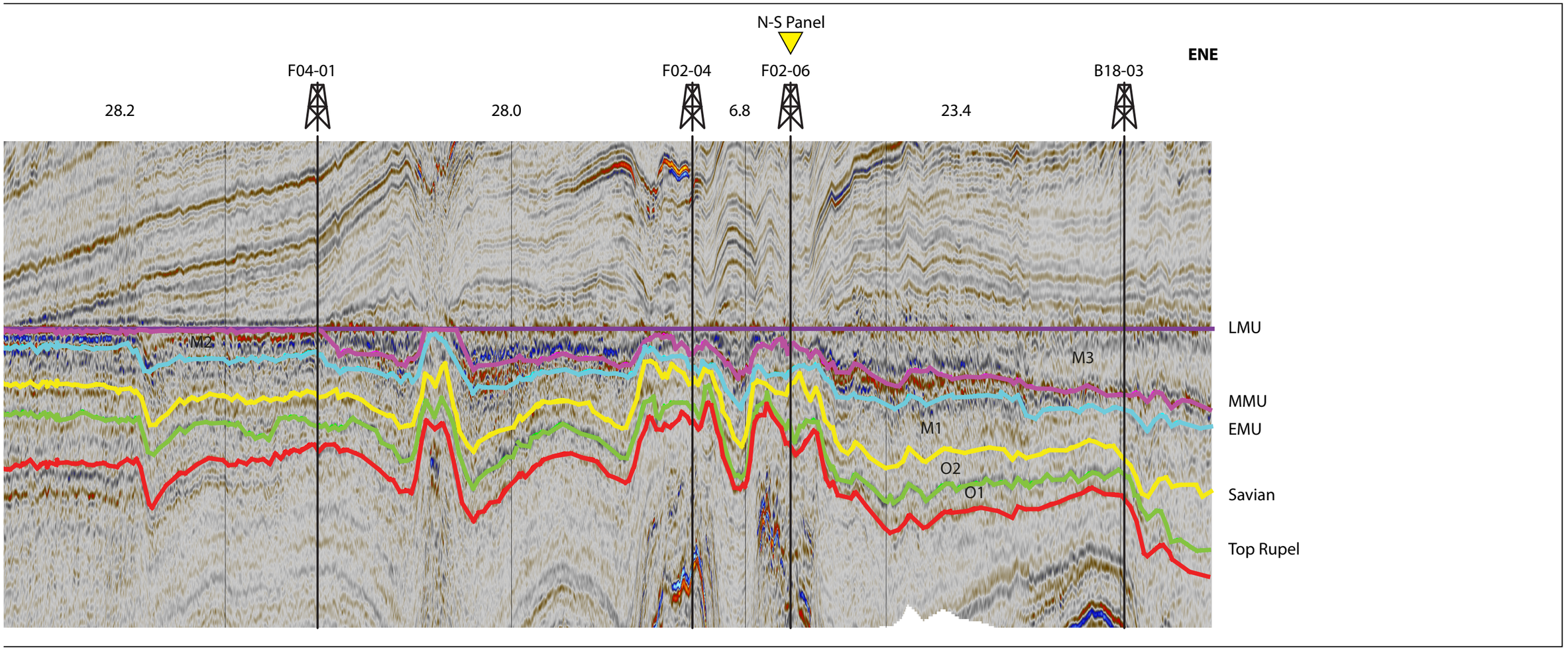


The vertical axis of this Wheeler transform is ‘relative geologic time’ (RGT). This means that the absolute ages of each seismic reflector are not depicted, but its relative age (e.g. it is older than the reflector above it and younger than the one below it). The advantage of the Wheeler in RGT is that the seismic is recognisable (since limited stretching and squeezing occurs) and depositional thicknesses are preserved. However, in order to highlight changes in sedimentation rate, the RGT Wheeler is transformed to absolute geological ages using the provided biostratigraphic ages. This stretches slowly deposited layers, and squeezes fast deposited layers. Consequently, the seismic image and the well logs become distorted.

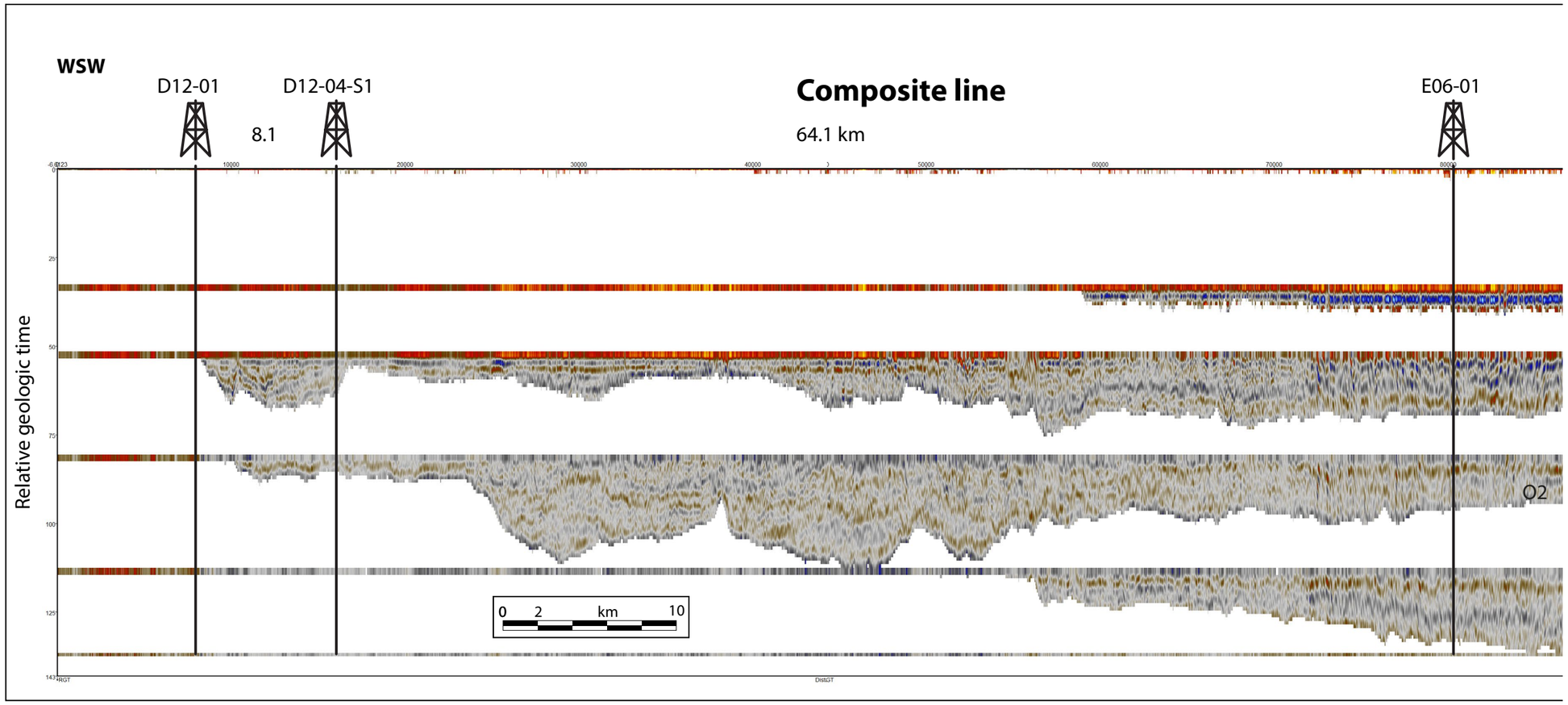


Figure 6.2: FSeismic Wheeler transform of the F02 Panel

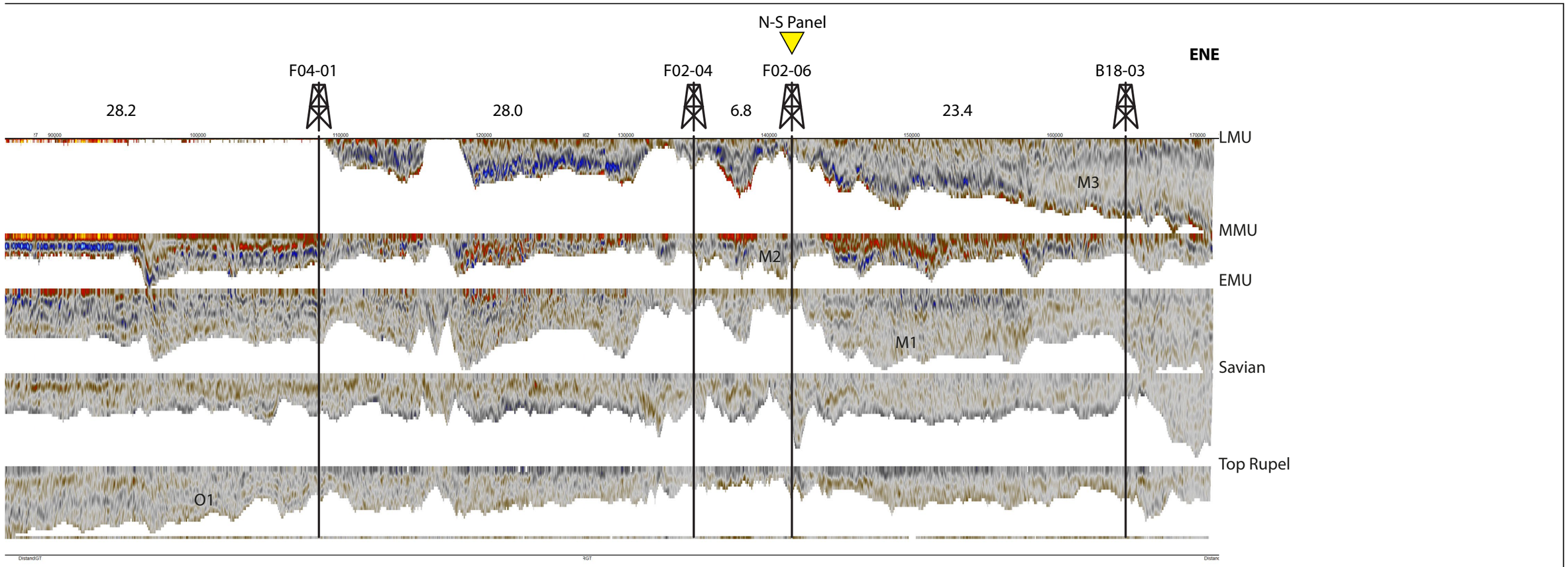
N-S Panel
ENE
F04-01
F02-04
F02-06
B18-03
28.2
28.0
6.8
23.4
LMU
MMU
EMU
Savian
Top Rupel
M3
M2
M1
O1

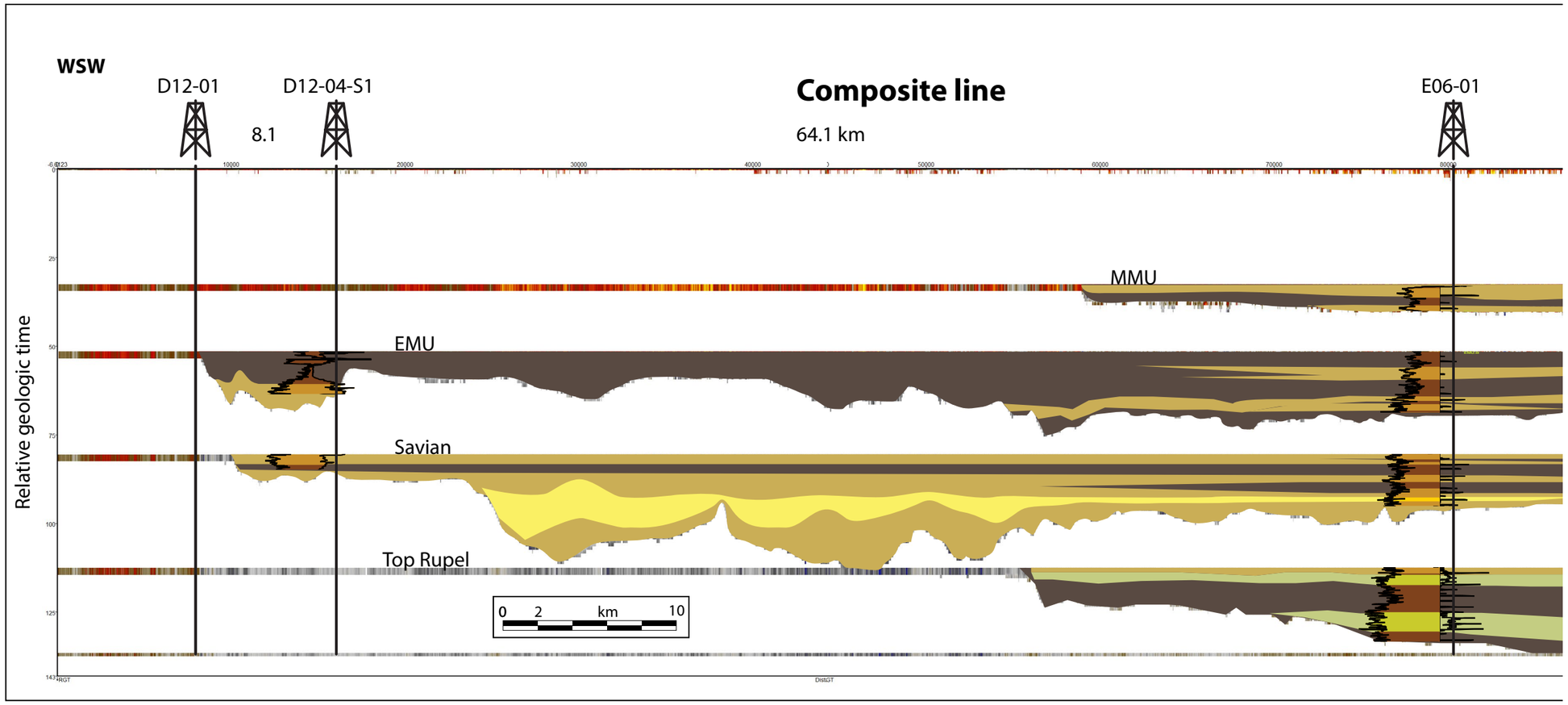


Figure 6.3: F02 Chronostratigraphic diagram of the F02 Panel

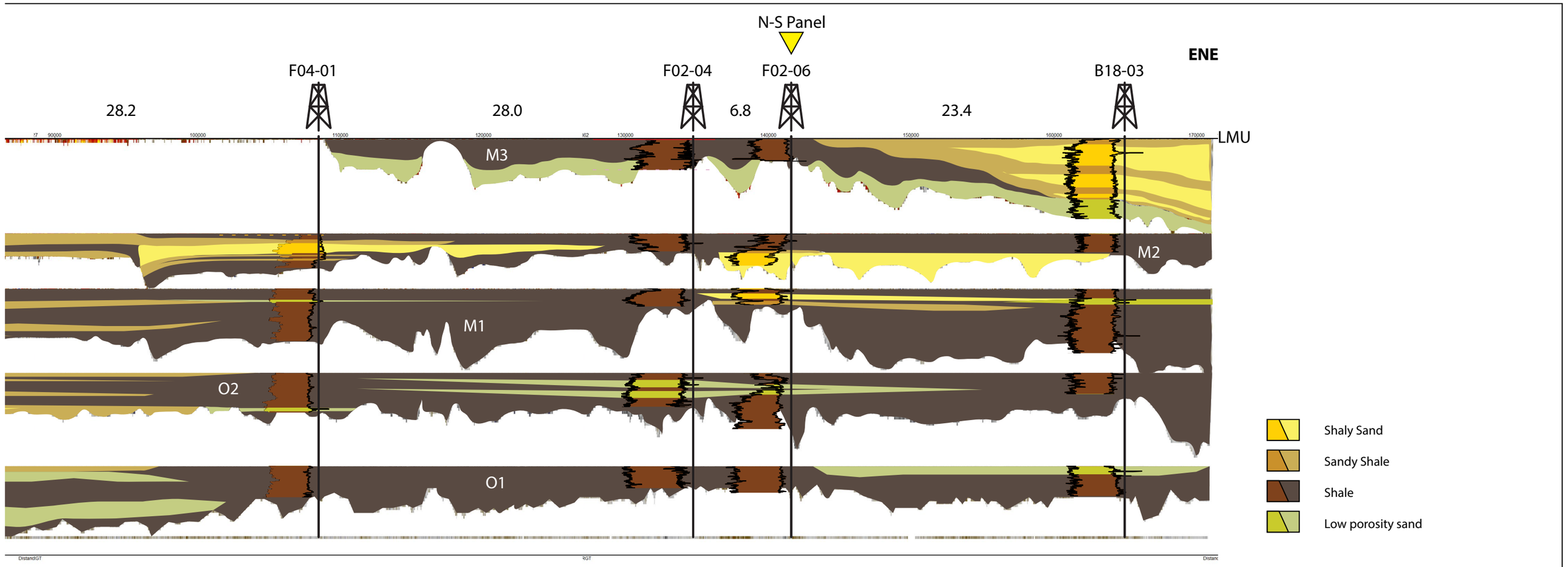


## O1 (Rupel Fm.)

The O1 interval is represented by the Rupel Formation. It consist of clay with some tight sand intervals at the top. The depo-centre is east of E06-01. The top of the unit is represented by an hiatus that is linked to thickness variations in deposition caused by salt movement (Zechstein).

## O2 (Veldhoven Fm.)

The O2 interval is represented by the lower part of the Veldhoven Fm. that is found below the Savian Unconformity. The E06-01 well shows quite some sandy shale and shaly sands. We expect that the sand content will increase towards the depo-centre, which is located between D12-04-S1 and E06-01. This means that the depo-centre has shifted westward (in respect to O1). The top of the O2 unit is the Savian unconformity.

## M1 (Veldhoven Fm.)

The M1 interval is represented by the upper part of the Veldhoven Fm. that is found below the EMU. The interval consists of shales and an occasional sandy shale layer. Although, the interval has not one distinct depo-centre, it seems that overall more deposited are found eastwards. The top of this interval is the EMU.

## M2 (Breda Fm.)

The M2 interval is represented by the lowest part of the Breda Fm. that is found below the MMU. The interval consists of shaly sand (F02-06 and F04-01), and sandy shale intervals. Shaly intervals are also present. The depo-centre is found between E06-01 and F04-01 where the most sandy intervals are found.

## M3 (Breda Fm.)

The M3 interval is represented by the middle part of the Breda Fm. that is found below the LMU. The interval consists of shale, shaly sand, sandy shale and tight sands. The depo-centre has shifted eastward to the B18-03 area. Again, the most sandy part is found in the thickest part of

this interval

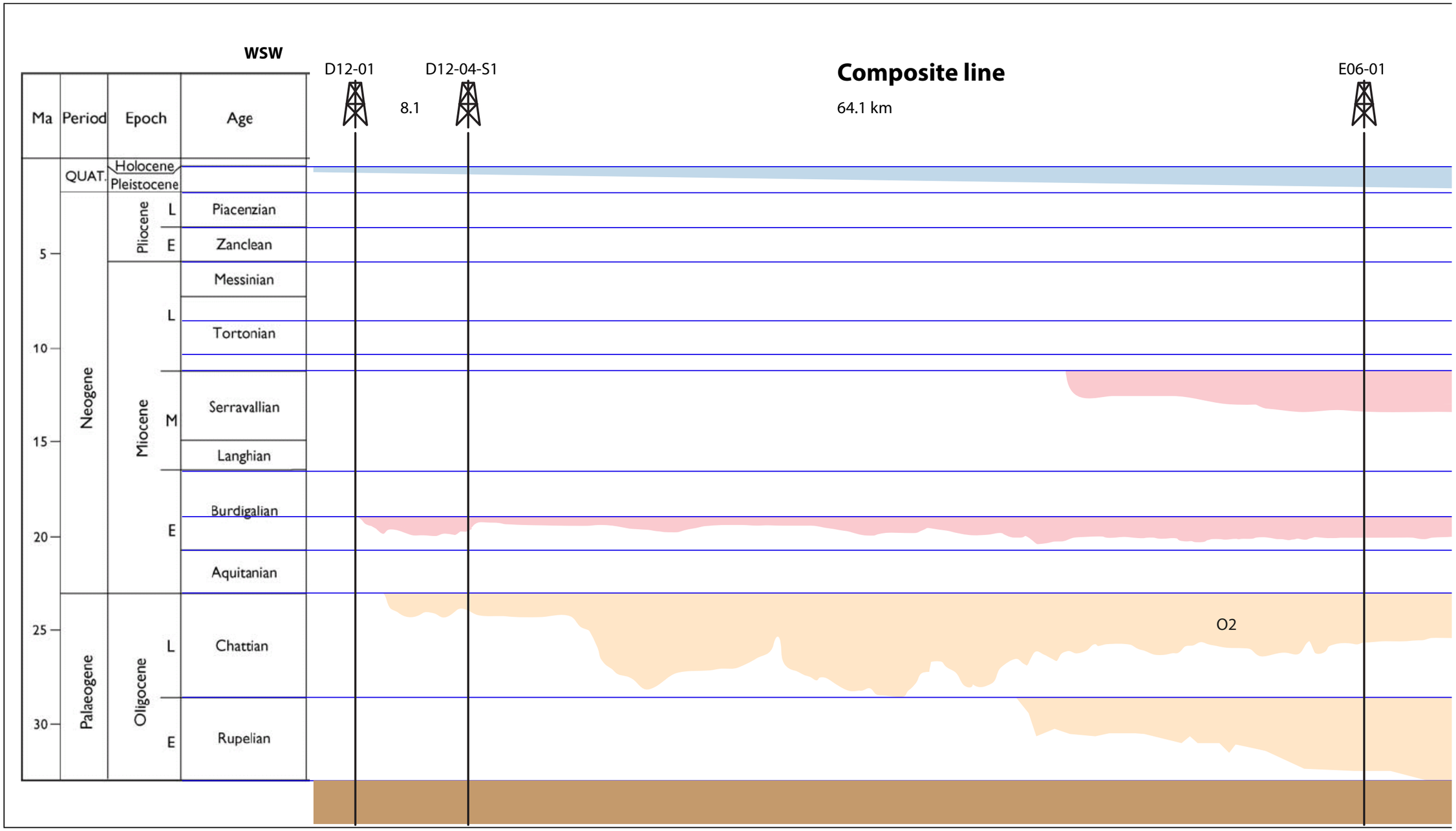


Figure 6.4: Wheeler of the F02 panel in absolute time.

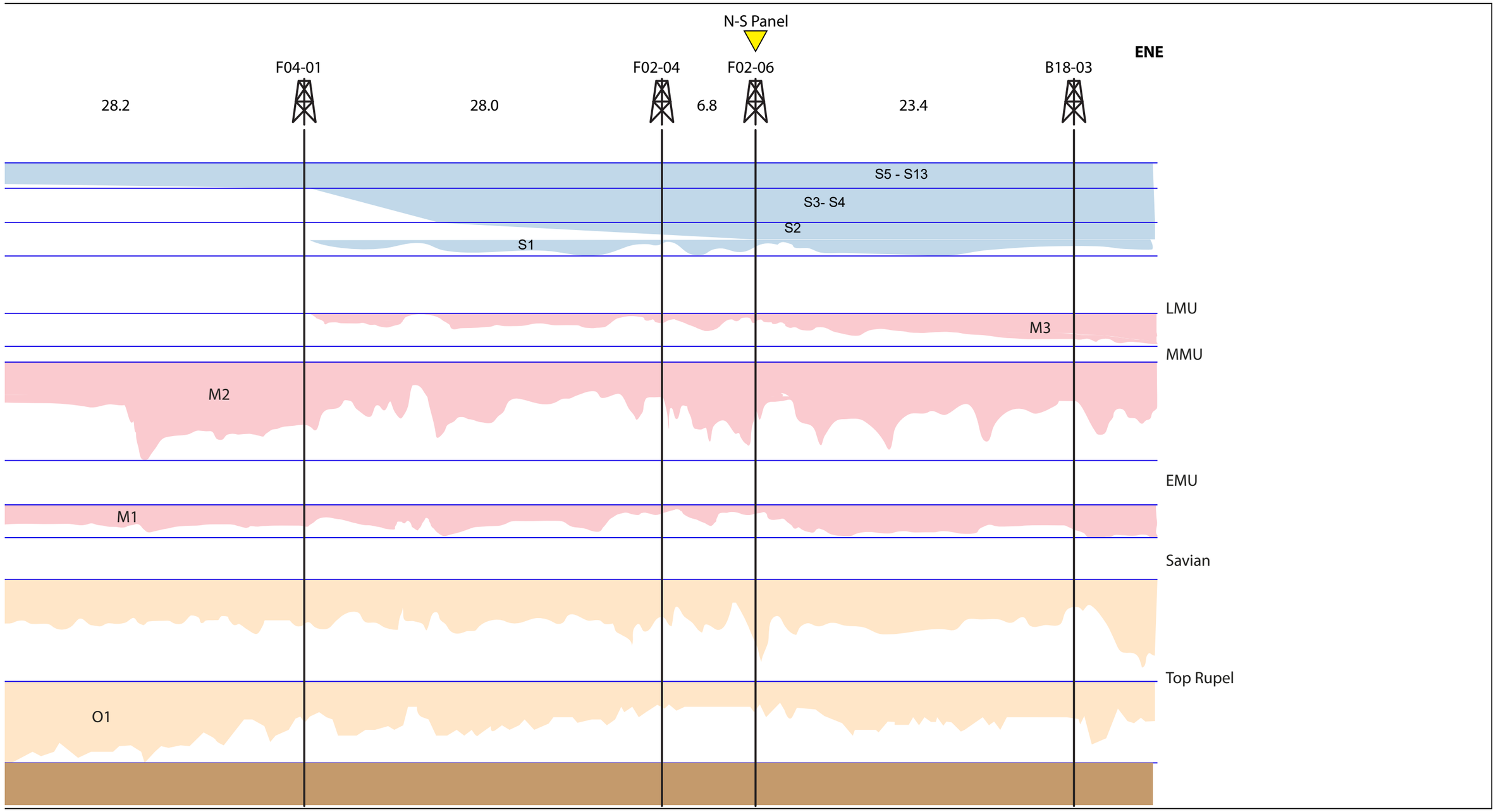


## Eridanos

The S1-S13 intervals depicted in blue (see figure 6.4) are represents the Dutch Eridanos delta. Since it was studied in great detail by Ten Veen et al. (2013) it was not part of this study. However, the S1 unit is represented by the upper part of the Breda Fm. that is found above the LMU. This unit is placed into the Eridanos delta by Ten Veen et al. (2013), but in our opinion it is part of the system below it, since it shows a different depositional trend, internal architecture (topographic infill vs clinoformal progradation) and depositional rate.

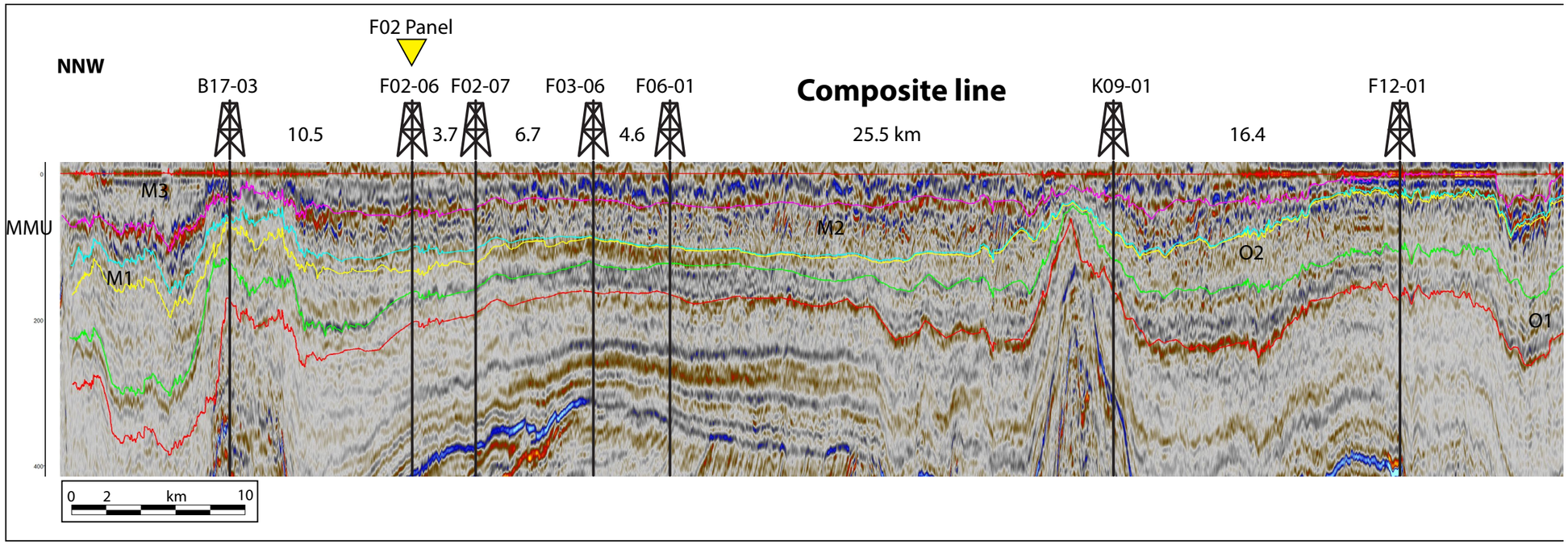


**Figure 6.5: N-S Panel flattened on the Late Miocene Unconformity (LMU)**

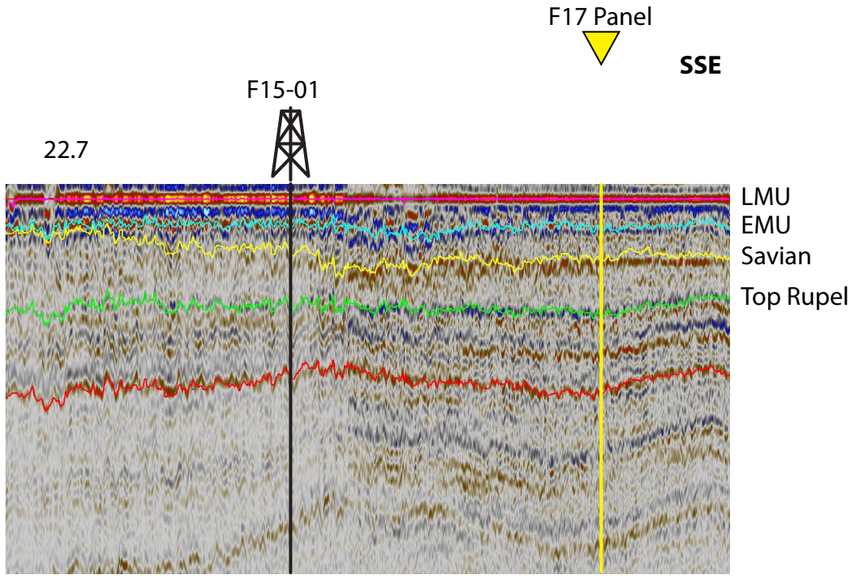
F17 Panel
SSE
F15-01
22.7
LMU
EMU
Savian
Top Rupel

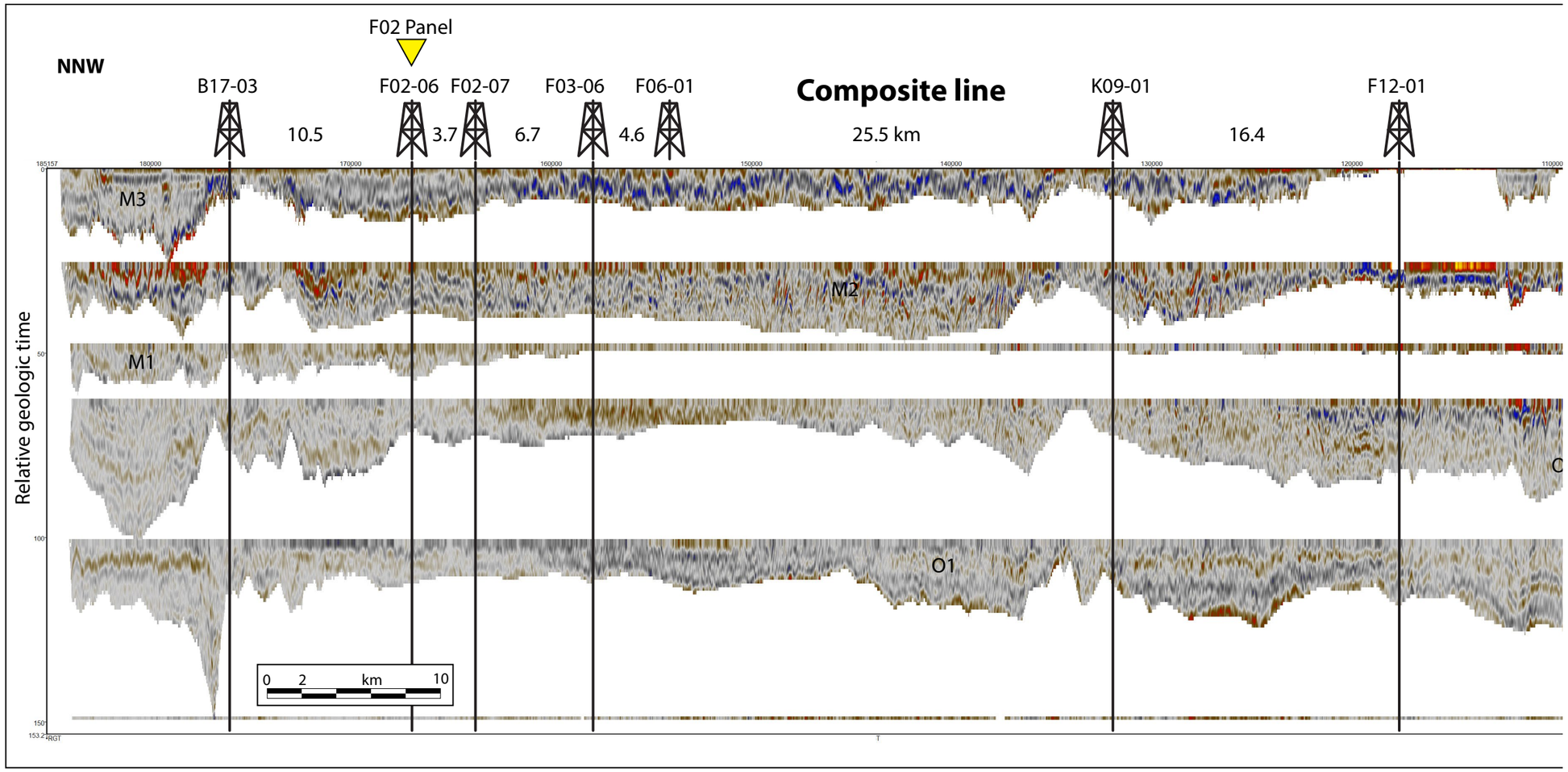


Figure 6.6: Seismic Wheeler transform of the N-S Panel.

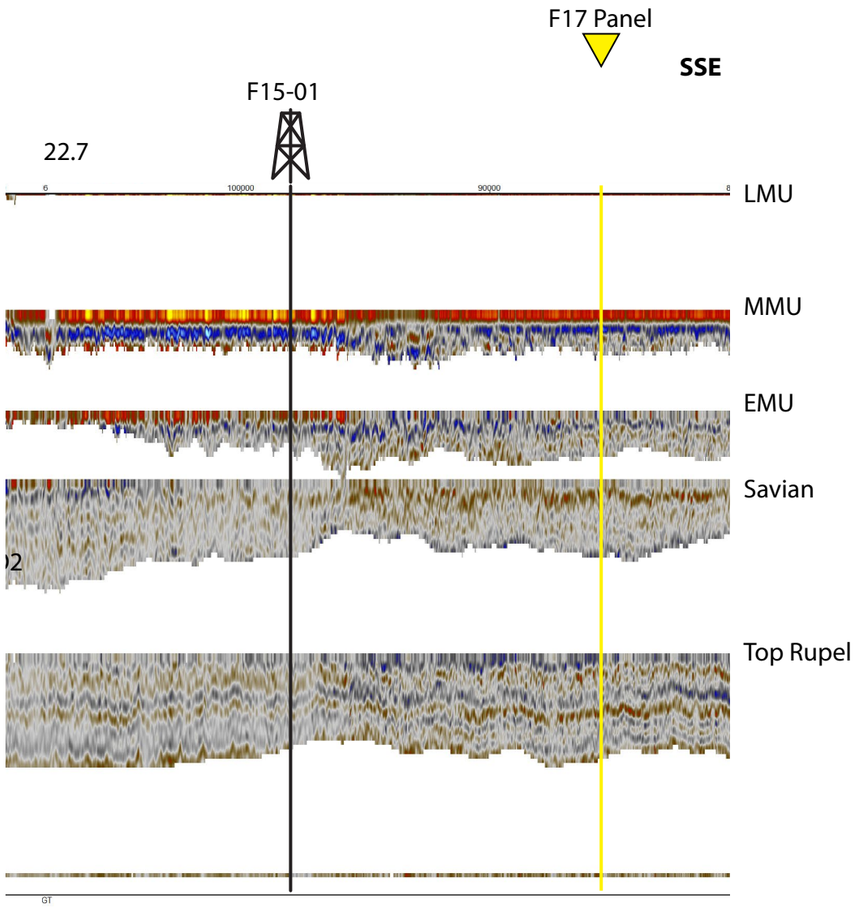
F17 Panel
SSE
F15-01
22.7
6
100000
90000
LMU
MMU
EMU
Savian
Top Rupel
GT

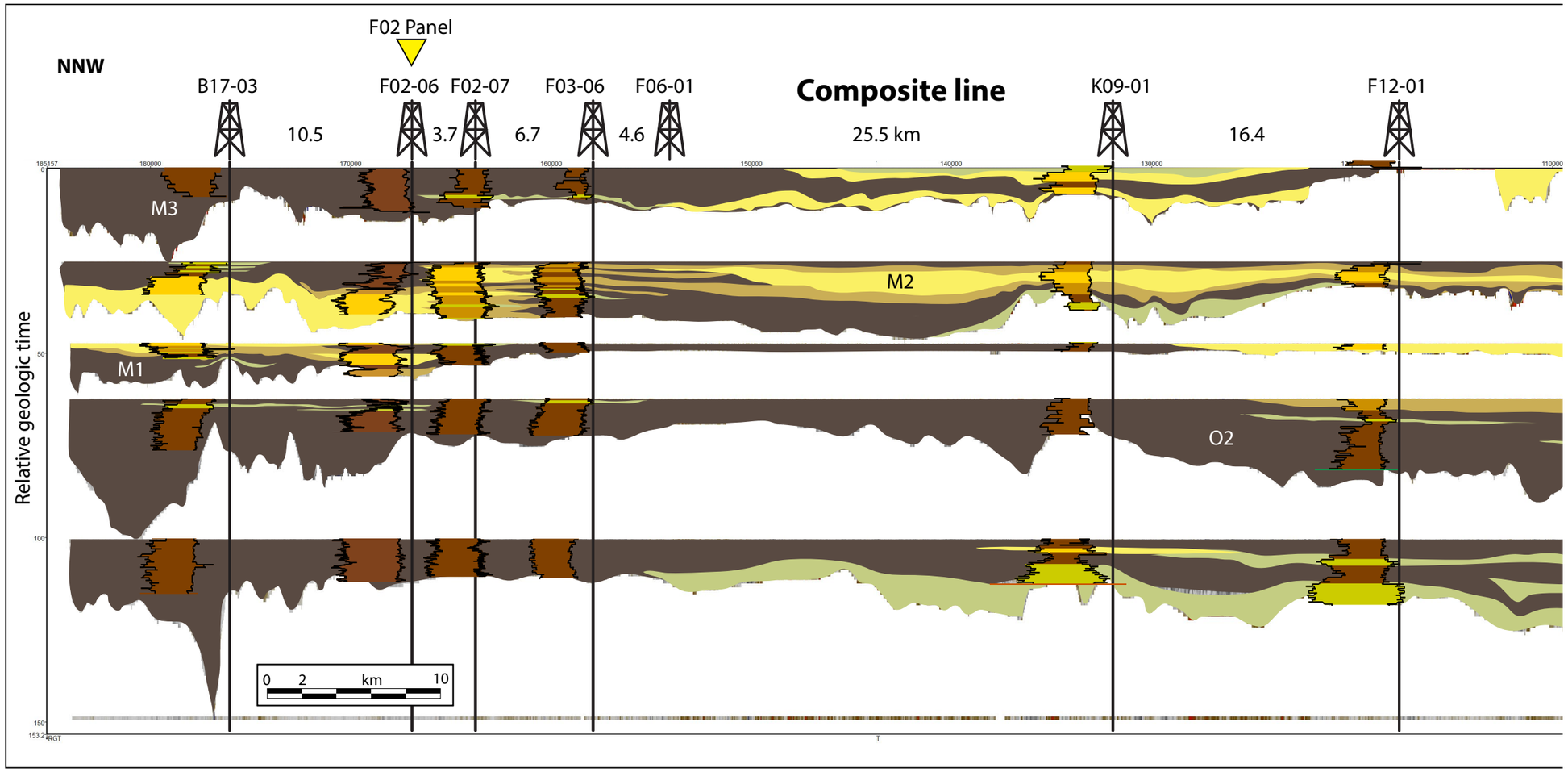


Figure 6.7: Chronostratigraphic diagram of the N-S Panel

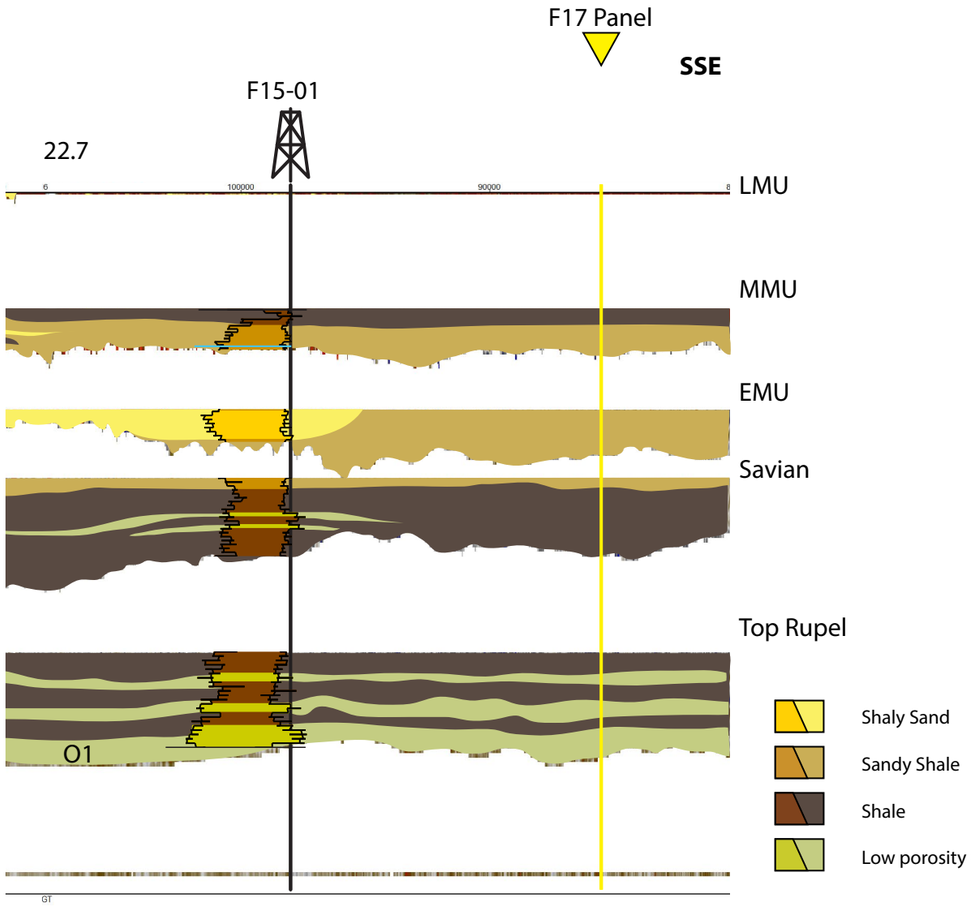


## O1 (Rupel Fm.)

The O1 interval is represented by the Rupel Formation. It consist of clay with some tight sand intervals in the south. The depo-centre is in the south, although local thickness variations are found that are related to salt tectonics . The top of the unit is represented by an hiatus that is linked to thickness variations in deposition caused by salt movement (Zechstein).

## O2 (Veldhoven Fm.)

The O2 interval is represented by the lower part of the Veldhoven Fm. that is found below the Savian Unconformity. Overall it is shaly, but some sandy shales are found in the south, and tight sand streaks are present. This means that the depo-centre has shifted Northward (in respect to O1). The top of the O2 unit is the Savian unconformity.

## M1 (Veldhoven Fm.)

The M1 interval is represented by the upper part of the Veldhoven Fm. that is found below the EMU. The interval consists of shaly sands in the depo-centre (F12-01 – F15-01), which becomes shale towards the north. The northern part also consists of an occasional sandy shale and shaly sand layer. The top of this interval is the EMU

## M2 (Breda Fm.)

The M2 interval is represented by the lowest part of the Breda Fm. that is found below the MMU. The interval consists of a complex interfingering. This can be explained by the orientation of the panel, which is running perpendicular to the depositional direction. The depo-centre is found further to the north in respect to the previous interval.

## M3 (Breda Fm.)

The M3 interval is represented by the middle part of the Breda Fm. that is found below the LMU. The interval consists of shale, shaly sand, sandy shale and tight sands. The depo-centre has shifted northwards to the B17-03 area. The most sandy parts are found in the south. This packages is not present in the south.

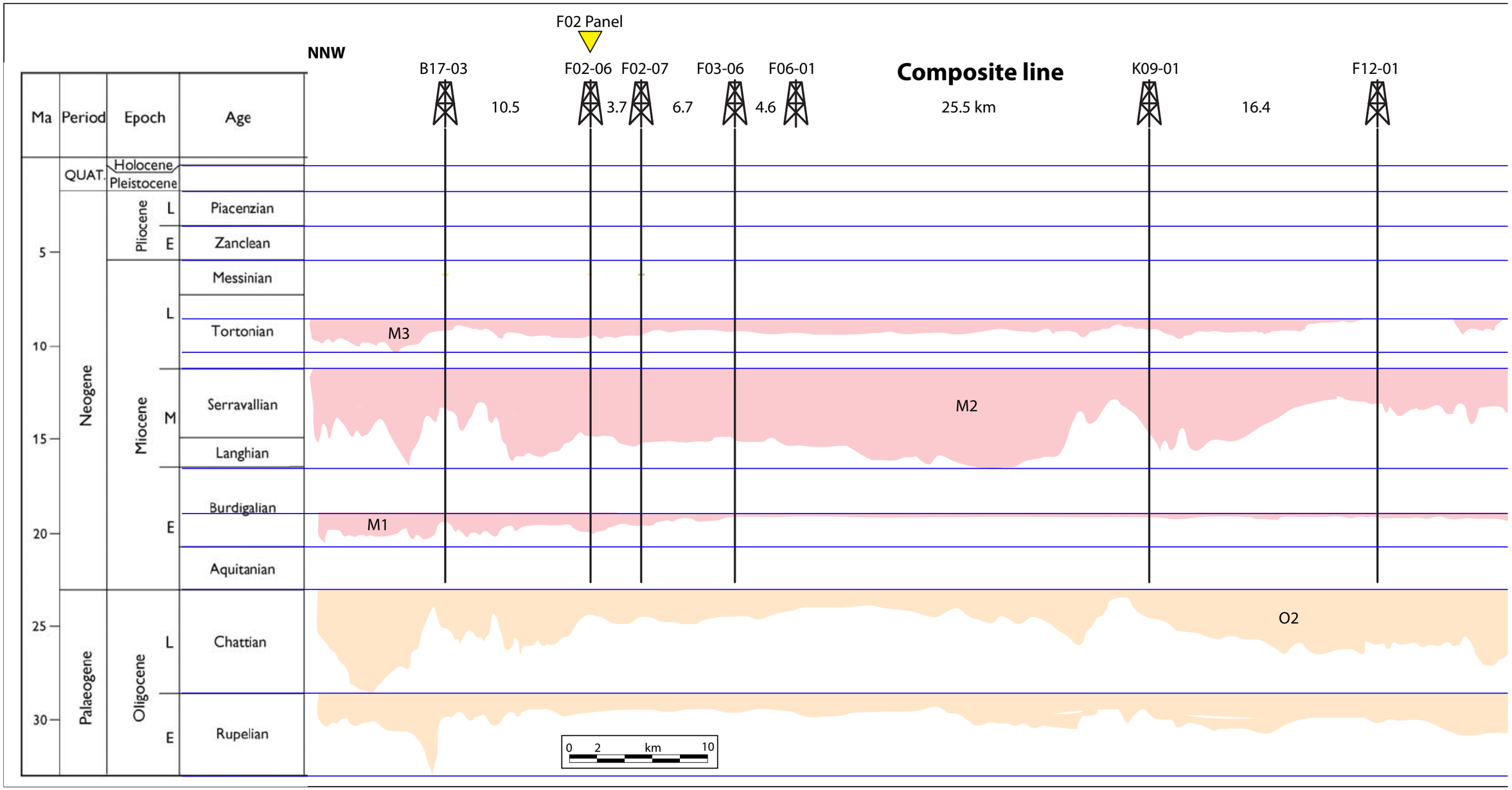


Figure 6.8: Wheeler of the N-S panel in absolute time.

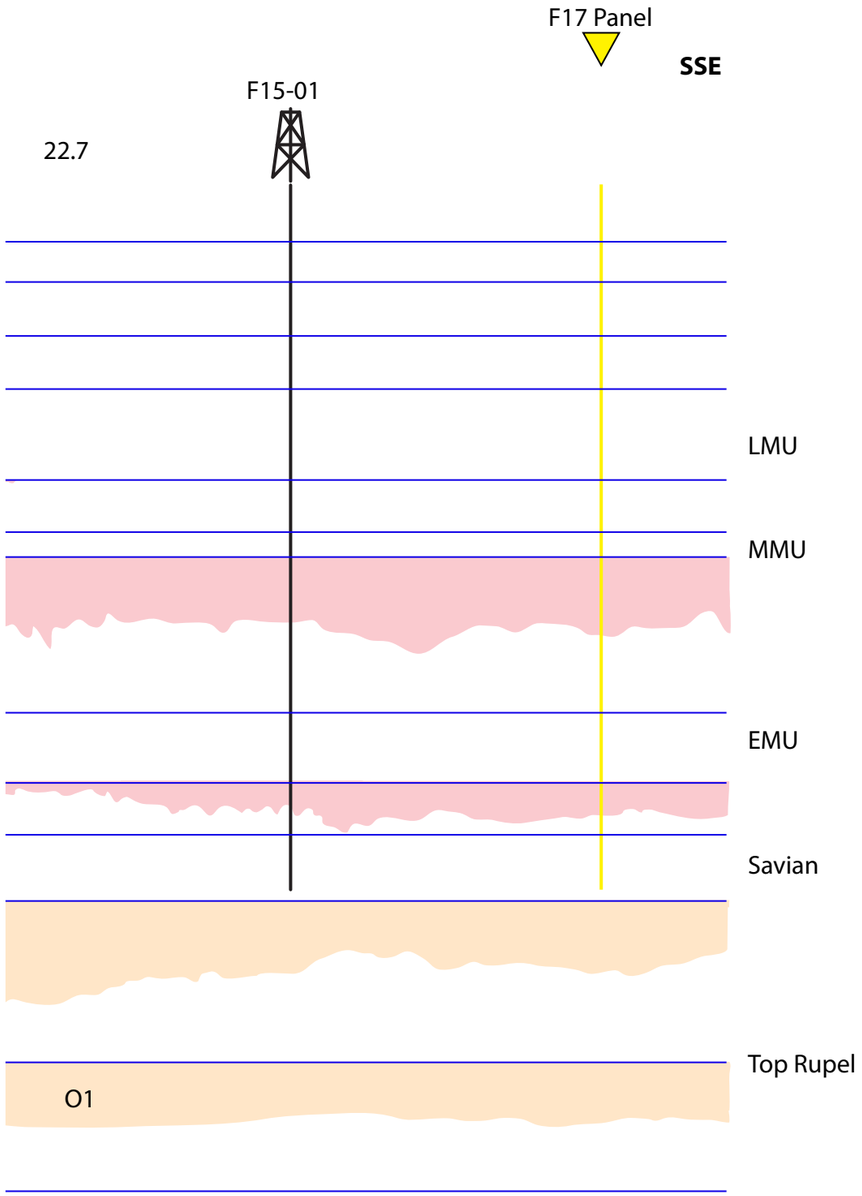
F17 Panel
SSE
F15-01
22.7
LMU
MMU
EMU
Savian
Top Rupel
O1

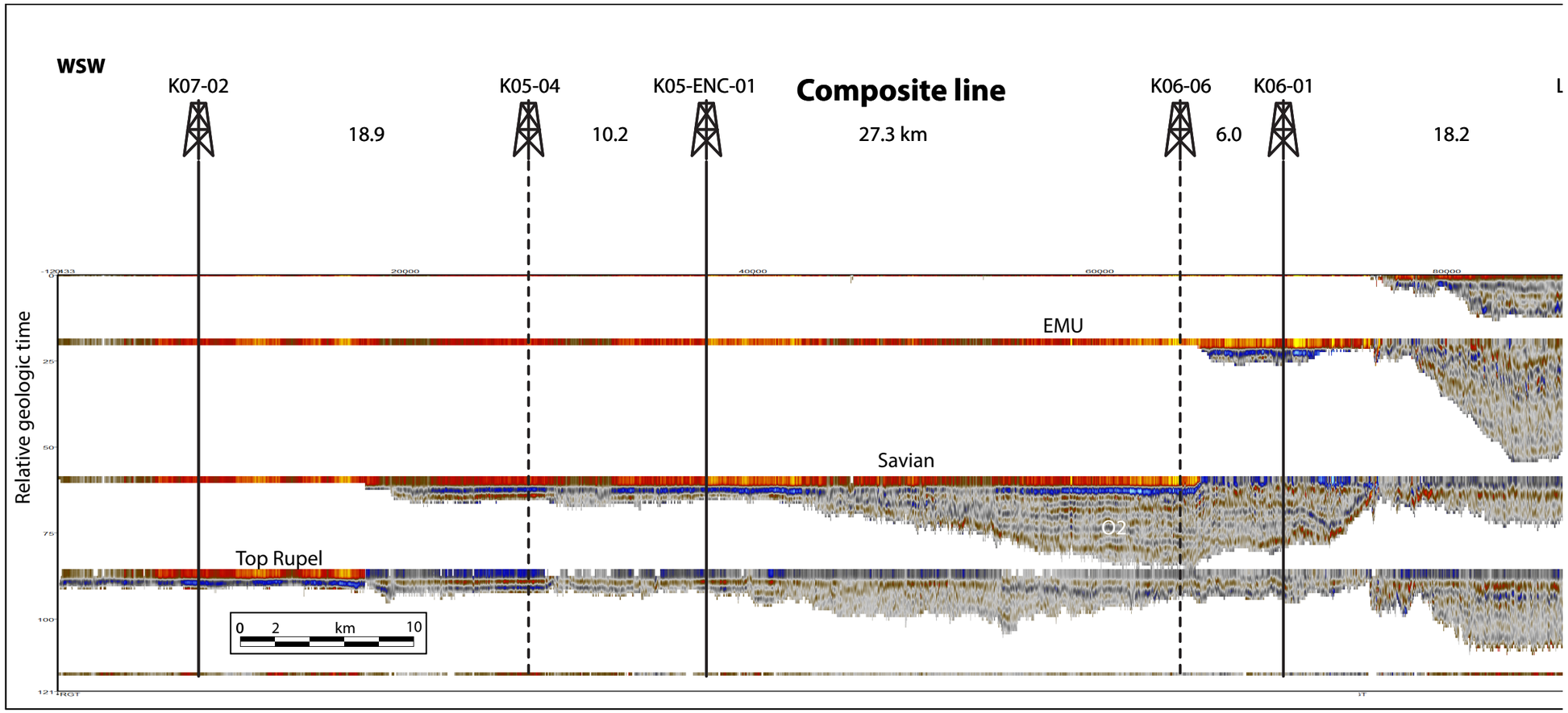


Figure 6.9: Seismic Wheeler transform of the F17 Panel.

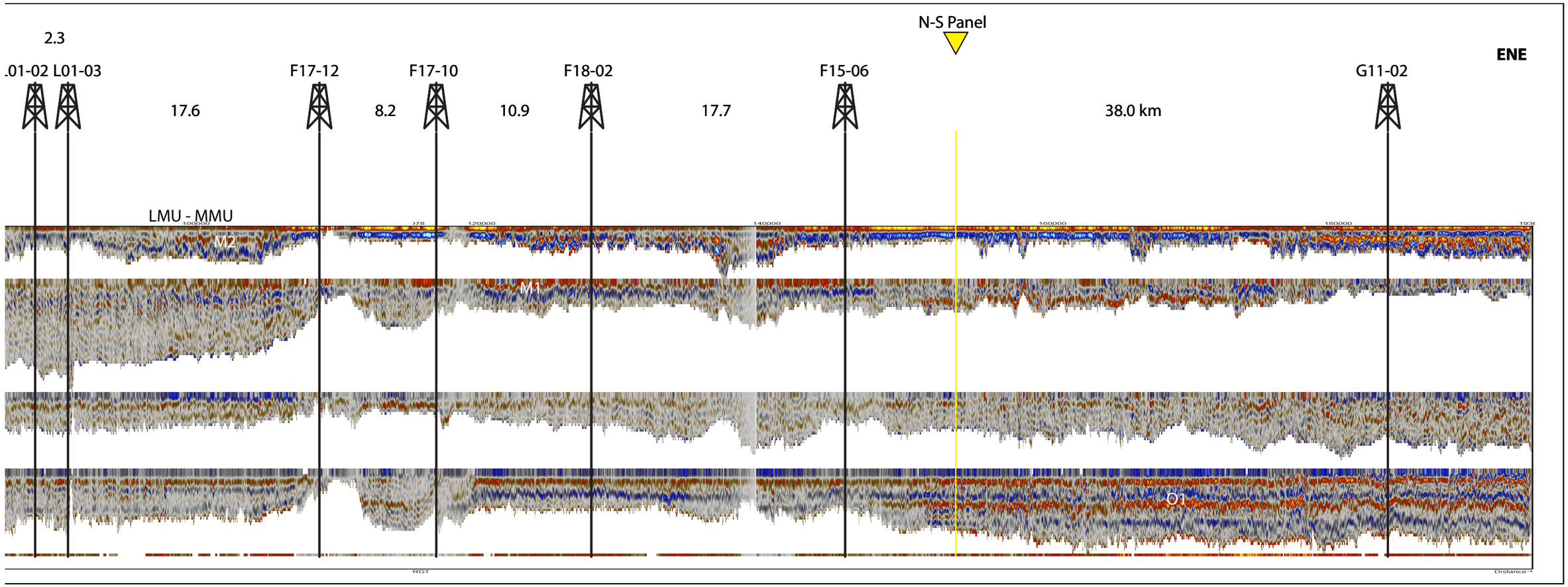
2.3
.01-02
L01-03
F17-12
F17-10
F18-02
F15-06
N-S Panel
G11-02
ENE
17.6
8.2
10.9
17.7
38.0 km
LMU - MMU
M2
M1
O1
RGT
Distance

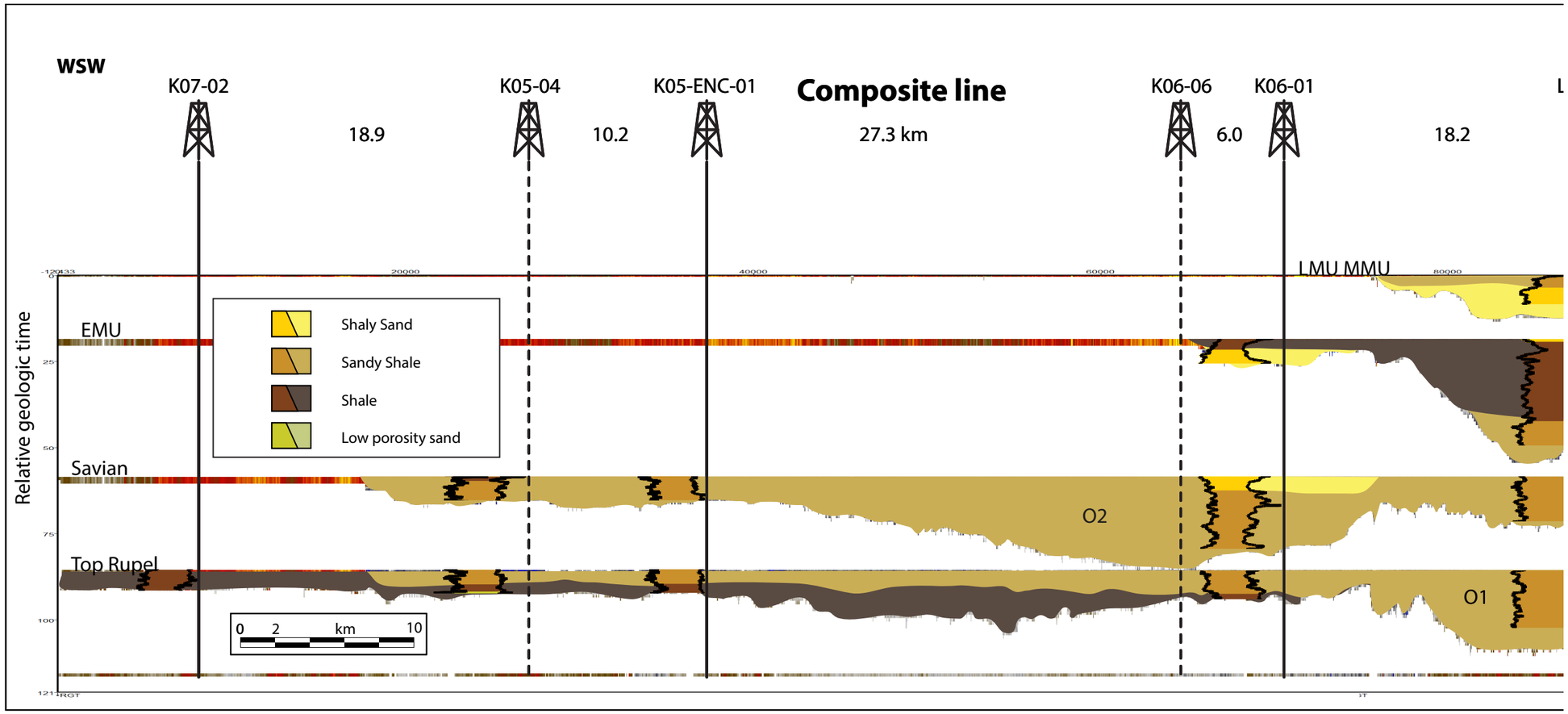


Figure 6.10: Chronostratigraphic diagram of the F17 Panel.

## O1 (Rupel Fm.)

The O1 interval is represented by the Rupel Formation. It consist of clay with some tight sand intervals in the east. The depo-centre is in the east, and the interval thins westwards. Local thickness variations are caused by salt tectonics and growth faulting. In the western part of the panel the interval contains sandy shales.

## O2 (Veldhoven Fm.)

The O2 interval is represented by the lower part of the Veldhoven Fm. that is found below the Savian Unconformity. Overall it is shaly, but some sandy shales are found in the west, and tight sand streaks are present. There is no depo-centre shift in respect to O1. The top of the O2 unit is the Savian unconformity.

## M1 (Veldhoven Fm.)

The M1 interval is represented by the upper part of the Veldhoven Fm. that is found below the EMU. The interval consists of shaly sands at the base, which becomes shale towards the top. At the very top shaly sand layers are found. The depo-centre has shifted westward (L01-02), however no sandy intervals are found there. The top of this interval is the EMU

## M2 (Breda Fm.)

The M2 interval is represented by the lowest part of the Breda Fm. that is found below the MMU. The interval consists shale, sandy shale and shaly sands. The western part contains the most sand.

## M3 (Breda Fm.)

The M3 interval is not present.

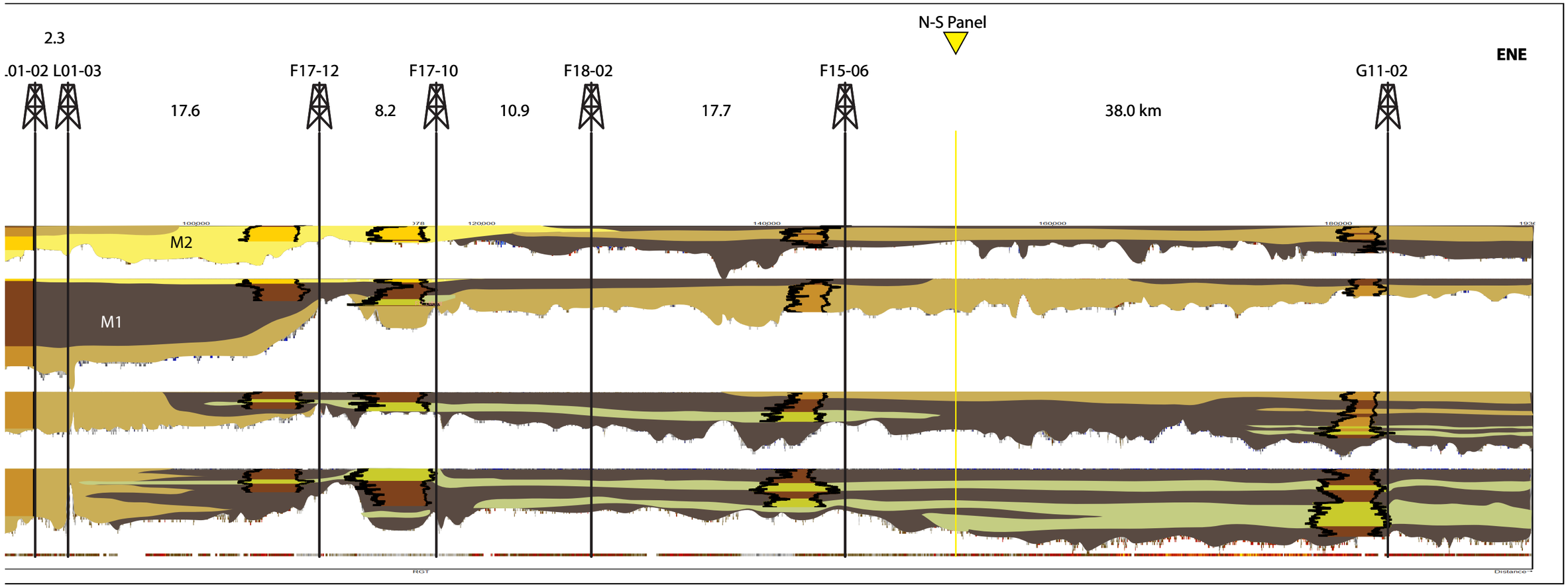


## Relative sedimentation rates

When comparing the Wheeler diagrams in absolute geological and relative geological time, relative sedimentation rates can be established (e.g. Figure 6.3 compared to figure 6.4, figure 6.7 to 6.8, and figure 6.10 is compared to 6.11). We use the term relative sedimentation rate here, since we do not take erosion into account. When an interval is vertically stretched in absolute age in comparison to relative geologic age the interval has a low relative sedimentation rate. When it is squeezed it has a high relative sedimentation rate. When there is no stretching or squeezing we speak of a medium relative sedimentation rate. A very consistent image appears for all three Panels (see table 6.1):

| | F2-Panel | N-S Panel | F17-Panel |
|---|---|---|---|
| M3 | high | high | Not present |
| M2 | low | low | low |
| M1 | high | high | high |
| O2 | medium | medium | medium |
| O1 | medium | medium | medium |

Table 6.1: Relative sedimentation rates.

## Prediction of sands

Of all intervals M2 and M3 contain the most sands. In general, the thicker parts (depo-centers) seem to contain the most sand. Unfortunately, there is no relationship between the relative sedimentation rates and the lithofacies.

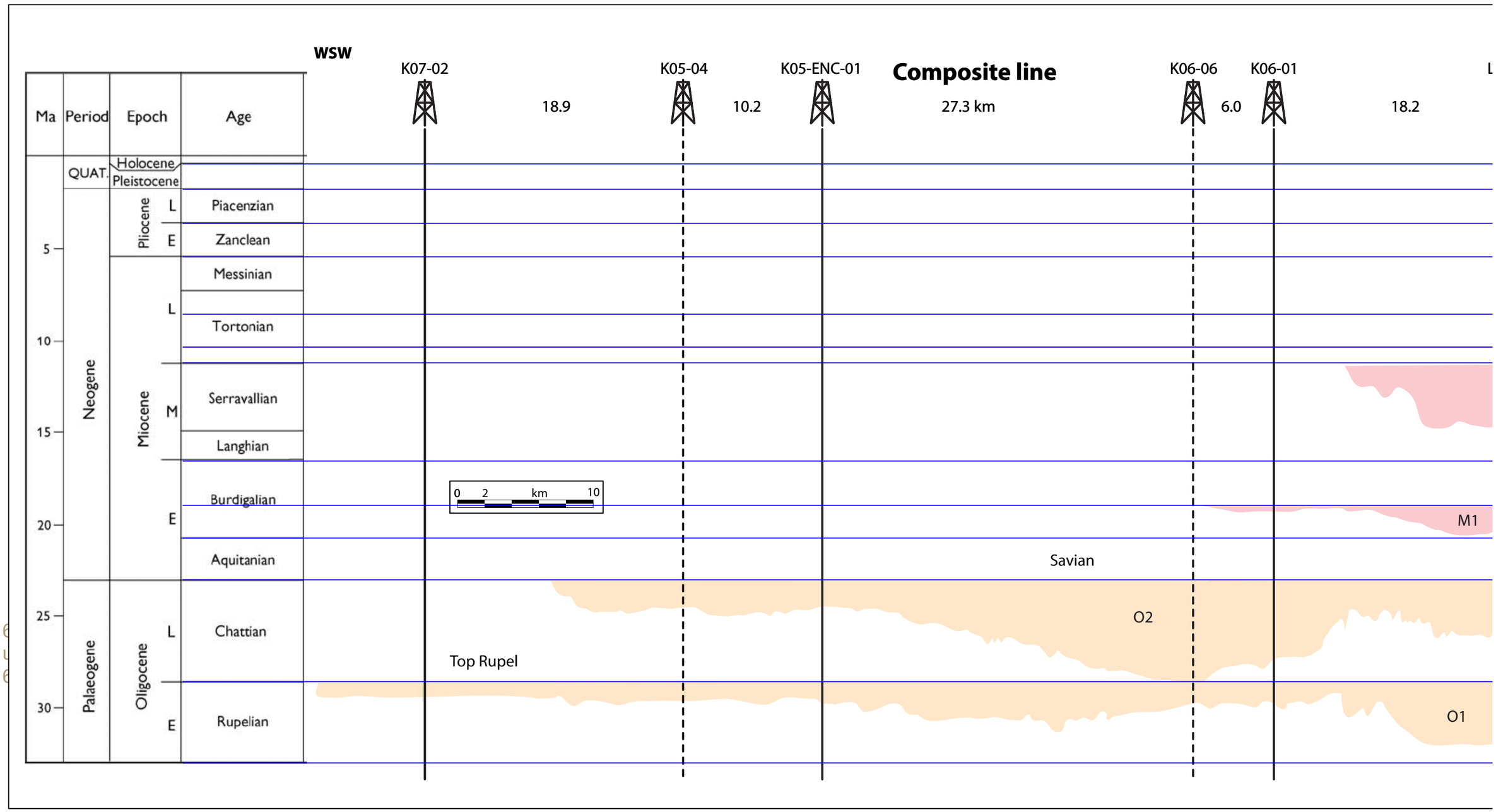


Figure 6.11: Wheeler of the F17 panel in absolute time.

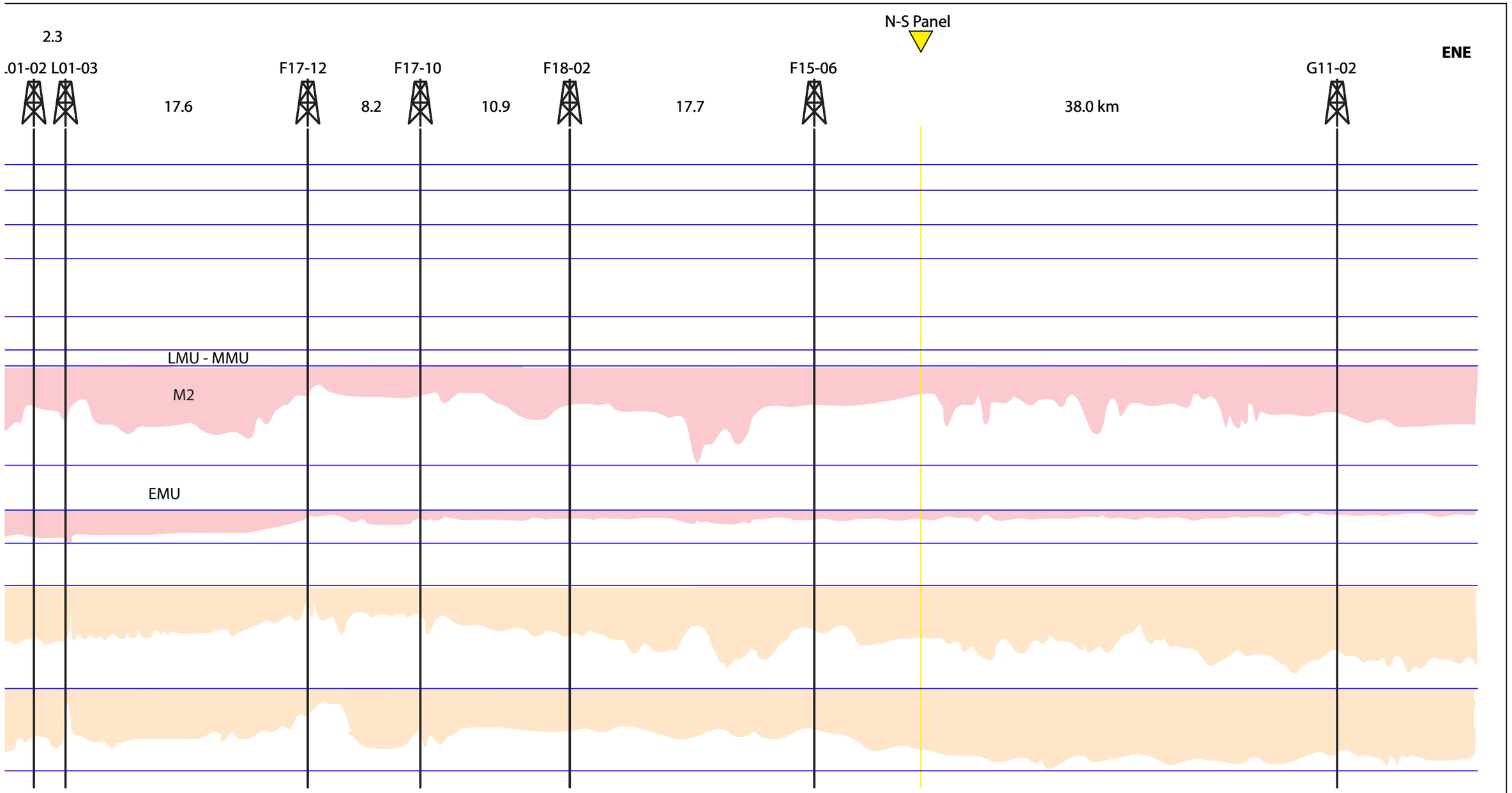
2.3
.01-02
L01-03
F17-12
F17-10
F18-02
N-S Panel
F15-06
G11-02
ENE
17.6
8.2
10.9
17.7
38.0 km
LMU - MMU
M2
EMU

*Bitumen in F02-03 core*

# 7. Petroleum in Cenozoic sequences

The spatial variations of geochemical and carbon isotopic compositions and quantity of gas in the Cenozoic sequences are assessed and evaluated in relation to geological setting and related pressure and temperature conditions to improve the understanding of the origin of the gas, gas migration conditions and the possible role of the MMU.

## Spatial variation and alteration patterns of geochemical and carbon isotopic composition of gas in Cenozoic sequences

## Data base

The gas composition and gas quantity data used include:

- Data and information provided by Wintershall:
  - Database of geochemical and carbon isotopic data from head space gas samples from F17-10,-11,-12, -13; A15-03;
  - Database of geochemical and carbon isotopic data from DST gas samples from F17-10, F17-12, F17-13, A15-03, B17-05, B17-06;
  - Gas logs, mud logs, master logs from F17-10,-11,-12,-13;
- Public gas composition and quantity data and information retrieved from www.nlog.nl.

## Approach

One of the objectives of this study is to assess the origin of the gas in the Cenozoic sequences. The main types of possible origin are:

1. Primary microbial gas formed in-situ from - thermogenically immature - organic matter in the Cenozoic sequences;
2. Gas migrated into Cenozoic sequences from underlying sequences/reservoirs. These gases in turn may have different origins:
   a. Thermogenic unassociated gas;
   b. Thermogenic oil associated gas;
   c. Thermogenic condensate associated gas;
   d. Secondary microbial origin: gas resulting from biodegradation of oil or biodegradation of thermogenic gas (James and Burns, 1984; Larter et al., 2005);
   e. Primary microbial gas;
3. Mixed gases.

The geochemical gas composition by itself will not provide sufficient information to fully evaluate the origin of the gas.

The isotopic abundances of the heavy isotope of carbon ($^{13}C$) of hydrocarbon gas components play an important role in studying the origin of gas. The ratio difference (δ) between $^{13}C$ and $^{12}C$ in parts per thousand (‰), relative to standard:

$\delta^{13}C = [\{(^{13}C/^{12}C)sample/(^{13}C/^{12}C)standard\}-1]*1000$

The ratio of $^{13}C$ to $^{12}C$ is conventionally compared to the standard 'Peedee Formation belemnite' and the result is given in a per mil quantity ($\delta^{13}C$ ‰ PDB).

In addition we use the heavy isotope of hydrogen, deuterium (D or 2H). The standard for D is mean ocean water (SMOW).

A combination of the following plots are used to characterize the observed gas properties

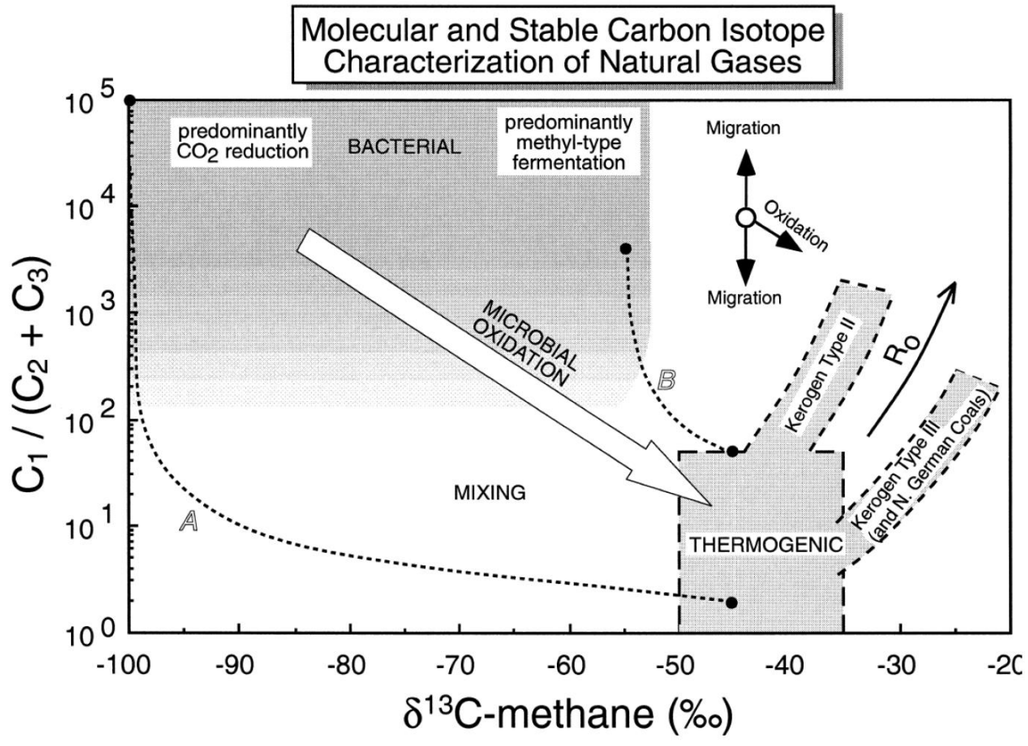


Figure 7.1: The 'Bernard' diagram (from Whiticar, 1999; after Bernhard, 1976).

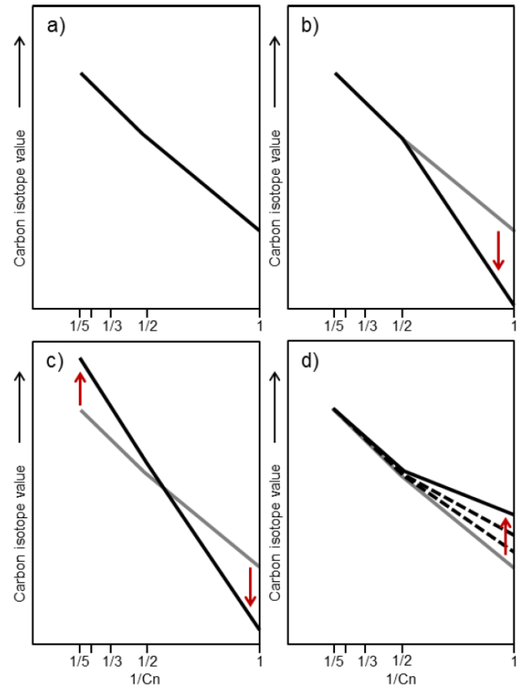


Figure 7.2. Chung's natural gas plot (from Zou et al., 2007; after Chung et al., 1988): a) near linear relation between $\delta^{13}C$ (‰) and 1/Cn representative of unaltered thermogenic gas; b) a sharp decrease of the methane isotopic value in comparison with the unaltered thermogenic linear relation indicative of mixing of microbial gas with thermogenic gas; c) $^{13}C$ enrichment of the higher molecular weight hydrocarbon gases (C2+ and especially propane) and a depletion of $^{13}C$ of methane is indicative of biodegraded gas; d) $^{13}C$ enrichment of methane is indicative for methane leakage/diffusion.

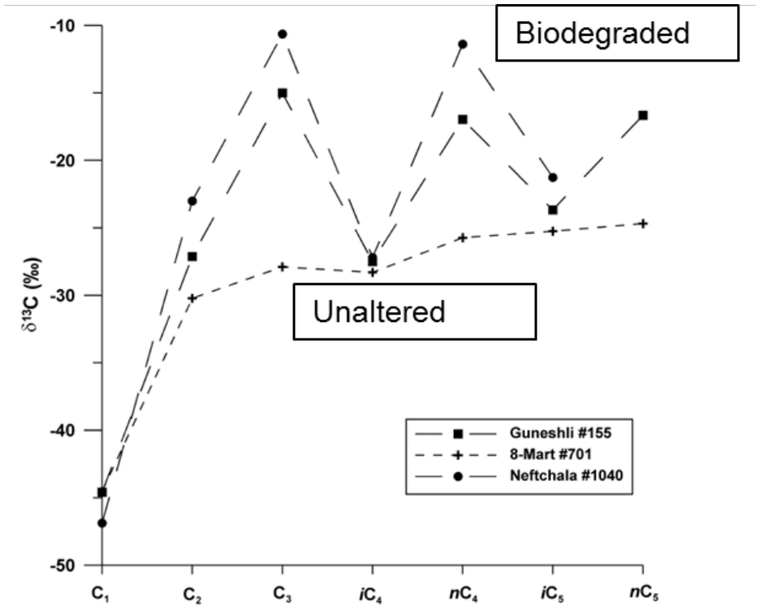


Figure 7.3. Example of the application of a compound specific cross plot of δ $^{13}$C versus hydrocarbon gas components showing the difference between the isotopic signature of an unaltered gas (8-Mart#701) and biodegraded gases (Neftchala#1040 and Guneshli#155) of the South Caspian Basin (From Katz et al., 2002). The biodegraded gases display enrichment in $^{13}$C of C3, nC4 and nC5, in particular, as a result of microbial alteration.

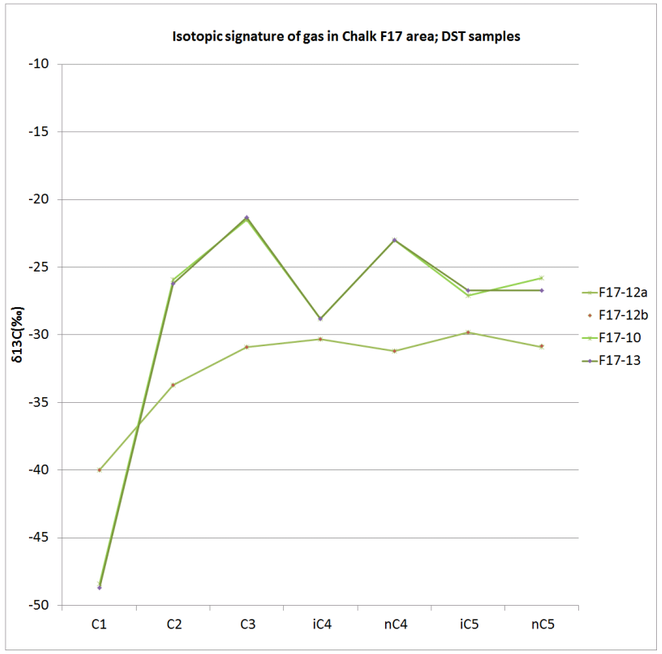


Figure 7.4 Compound specific carbon isotopic composition of DST samples from gas in the Chalk Group at 3 different well locations (F17-10, F17-13, and 2 samples from F17-12).

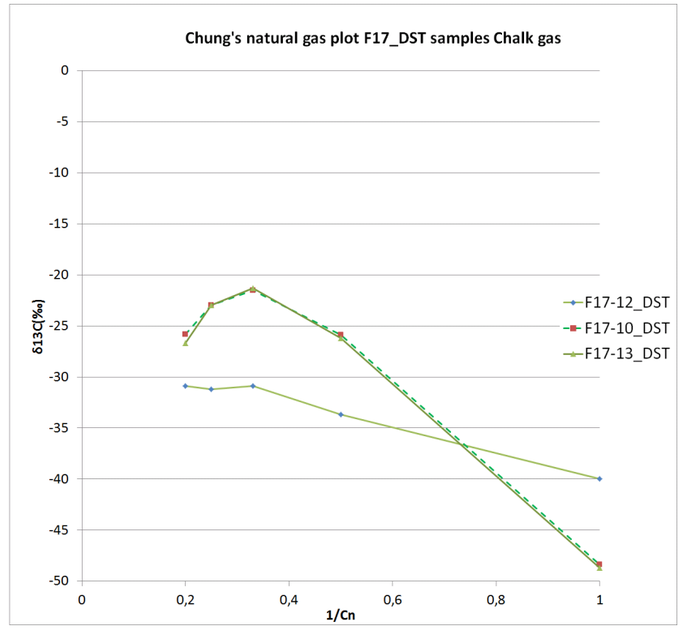


Figure 7.5 Chung's natural gas plot of compound specific carbon isotopic composition of DST samples from gas in the Chalk Group at 3 different well locations (F17-10, F17-13, F17-12). Linear relation between δ$^{13}$C (‰) and 1/Cn indicative of non-biodegraded nature of gas sample from F17-12; shift to heavier δ$^{13}$C (‰) for C2+ in combination with increased depletion of δ$^{13}$C (‰) for methane is indicative for biodegraded gas samples from F17-10 and F17-13.


Figure 7.6 Compound specific carbon isotopic composition of head space samples from gas in the Chalk Group at 4 different well locations (F17-10, F17-11, F17-12, F17-13). The legend shows, between brackets, the depth of the gas samples.

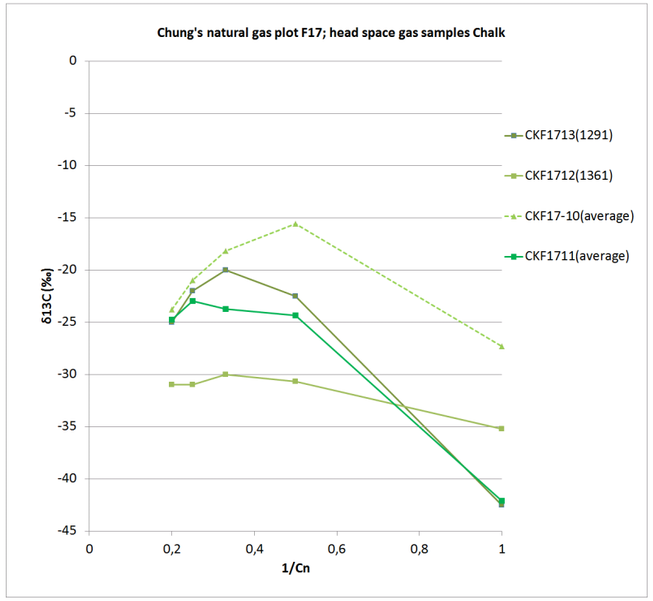


**Figure 7.7. Chung's natural gas plot of compound specific carbon isotopic composition of head space samples from gas in the Chalk Group at 4 different well locations (F17-10, F17-11, F17-12, F17-12). The linear relation between $\delta^{13}C$ (‰) and 1/Cn is indicative of non-biodegraded nature of gas sample from F17-12; shift to less depleted $\delta^{13}C$ (‰) for C2+ in combination with increased depleted $\delta^{13}C$ (‰) for methane is indicative for biodegraded gas samples from F17-10, F17-11 and F17-13.**

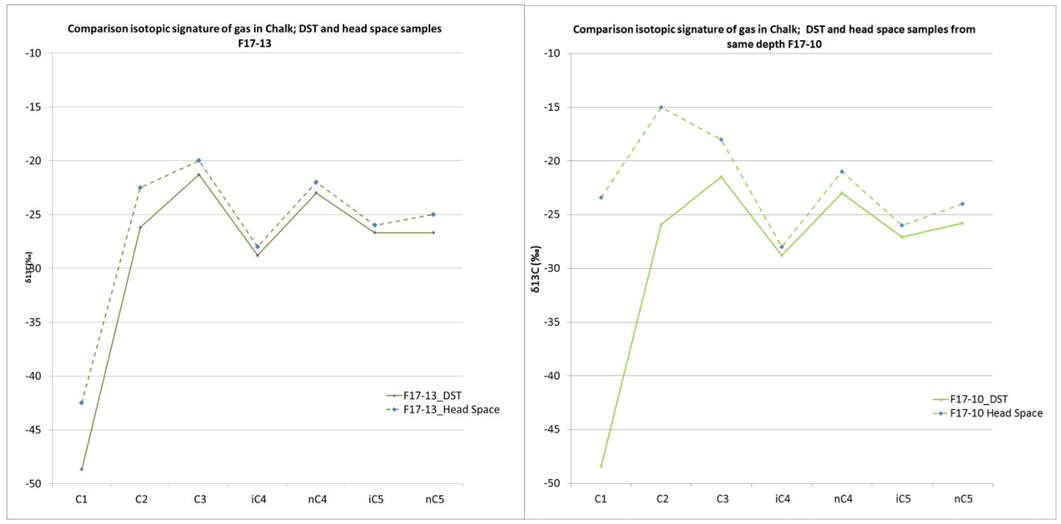


**Figure 7.8. Compound specific carbon isotopic composition of a DST and a head space sample from gas in the Chalk Group at the same depth in F17-13 and F17-10 (plot on the left). The plot shows the difference in carbon isotopic values for the 2 types of gas samples. The head space and DST gas samples of F17-10 show a large difference in carbon isotopic values for methane and ethane, in particular (plot on the right).**

and to identify their alteration patterns and origins:

- The 'Bernard' diagram (after Bernard et al., 1976): this cross plot of C1/(C2+C3) versus $\delta^{13}C\_C1$ can be used to identify the origin of gas based on the dryness of microbial gas (C1/(C2+C3)> 200) and its lighter isotopic ratio of methane (between $\delta^{13}C$ =-90‰ and $\delta^{13}C$= -60‰) in comparison with thermogenic gas (between $\delta^{13}C$ =-60‰ and $\delta^{13}C$ =-30‰) (Figure 7.1);
- The 'Schoell' diagram (after Schoell, 1980, 1983; Whiticar et al., 1986): this cross plot of $\delta^{13}C\_C1$ versus $\delta D\_C1$ provides insight into the origin of the gas (microbial gas, thermogenic nonassociated gas, thermogenic gas associated with oil or condensates, mixed gases);
- The natural gas plot of Chung (after Chung et al., 1988; Zou et al., 2007); this cross plot of $\delta^{13}C$ of individual gas components (methane, ethane, propane, n-butane and n-pentane) versus the inverse carbon number of the component (1/Cn) is helpful in the identification of origin and possible mixing of gases (Figure 7.2):
  - Chung's indicative plot of unaltered gas of thermogenic origin shows a near linear relation between $\delta^{13}C$ (‰) and 1/Cn (Figure 7.2 a);
  - Biodegradation of a thermogenic gas results in a $^{13}C$ enrichment of the higher molecular weight hydrocarbon gases (C2+ and especially propane) and a depletion of methane in the biodegraded gas; these changes in gas composition are visualized in Figure 7.2c);
  - Mixing of thermogenic gas with primary microbial gas results in a sharp decrease of the methane isotopic value in comparison with the unaltered thermogenic linear relation (Figure 7.2b);
  - Leakage of gas may result in less negative C isotope values in the residual gas (as suggested by Clayton et al., 1997; Prinzhofer and Pernaton, 1997) (Figure 7.2d);
- Compound specific cross plot of $\delta^{13}C$ versus C1, C2, C3, iC4, nC4, iC5, nC5 (Katz et al., 2002; Prinzhofer and Deville, 2013; Vandré et al., 2007). This cross plot allows to distinguish between unaltered thermogenic gas and biodegraded gas (Figure 7.3). Biodegradation of a wet gas involves the preferential removal of propane, n-butane and n-pentane.
- Cross plots of C1/(C2+C3) versus depth;
- Plots based on gas and mud log gas readings, for example cross plots of Total Gas (ppm) versus depth, and C1 (ppm) versus depth.

## Alteration patterns of gas properties in the F17 area

The characterization and interpretation of the spatial variation in geochemical and carbon isotopic composition of gas encountered in the Cenozoic sequences and underlying Chalk reservoir are based on data and information from wells F17-10, -11, -12, -13. The provided data include geochemical and isotopic analyses of head space gas samples from the Chalk Group and from different depths in the Cenozoic sequences, as well as analyses of DST gas samples from the Chalk Group and one DST shallow gas sample.

### Geochemical and carbon isotopic characteristics of gas in Chalk

The compound specific carbon isotopic signature of gas in the Chalk based on DST samples shows a clear difference in pattern of the carbon isotopic composition of the gas sample from well F17-12 in comparison with that of the gas samples from wells F17-10 and F17-13 (Figure 7.4 and Figure 7.5). The carbon isotopic signature of the Chalk gas in F17-12 is largely that of an unaltered thermogenic gas. The carbon isotopic compositions of the gas samples from wells F17-10 and F17-13 are enriched in $^{13}C$ for C2+ and for propane (C3) and normal butane (nC4), in particular, and depleted in $^{13}C$ for methane. These characteristics are indicative for biodegraded gas.

Figure 7.6 and Figure 7.7 are the same indicative plots for the head space gas samples from the Chalk. These plots also show the difference between the non biodegraded character of the gas samples from F17-12 and the biodegraded characteristics of the gas samples from F17-10, F17-13, and also F17-11.

In addition, all the DST gas samples are more depleted in $^{13}C$ of methane and ethane in comparison with the head space gas samples. This difference is most apparent for the samples from F17-10 (Figure 7.8). In addition, the DST samples from F17-10 and F17-13 show a similar compound specific carbon isotopic signature of gas (Figure 7.4), while the head space gas samples from these wells show very different characteristics (Figure 7.6), especially for the carbon isotopic compositions of methane and ethane. Differences in geochemical and isotopic composition of gases derived from analyses of head space and DST samples are well known (e.g. Abrams, 2013; Dolson, 2016); general causes for these differences include, amongst other things, the effects induced by preferential loss of lightest hydrocarbons as cuttings are being circulated to the surface, resulting in heavier (less negative) carbon and hydrogen isotopic values in head space gas samples. The head space samples of F17-10 not only show a large shift towards less depleted $\delta^{13}C$ values, but also a shift in $\delta D$ from $\delta D$ = -194‰ (DST sample) to $\delta D$ = -171‰ to -181‰. The analyses results of head space gas samples of F17-10 report very high % of N2 in total gas suggesting that the samples were contaminated with air; this might explain the difference of the analyzing results of F17-10 in comparison with those of F17-11 and F17-13.

### Vertical alteration pattern of geochemical and carbon isotopic composition of gas

First we use the head space gas data from the Chalk and Cenozoic sequences of F17-10, -11, -12, -13 to characterize and interpret the

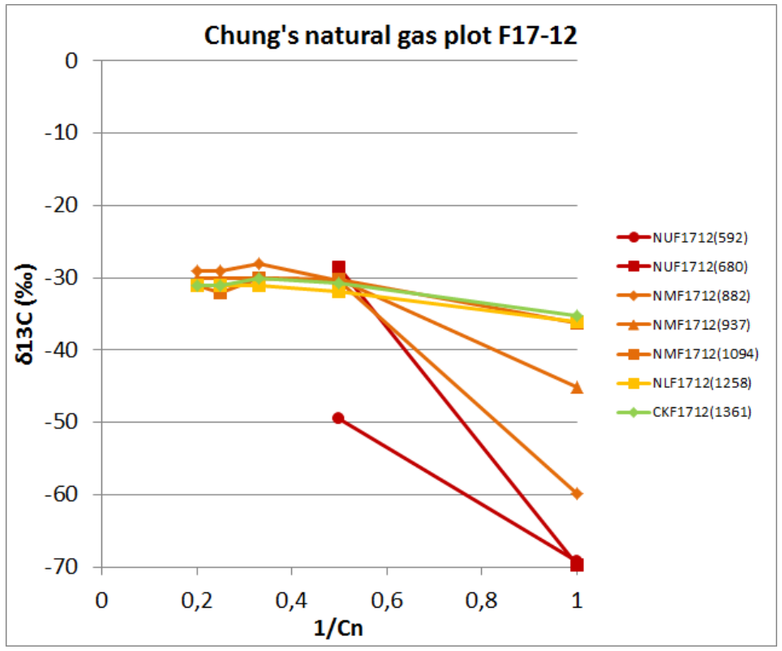


**Figure 7.9. Chung's natural gas plot of compound specific carbon isotopic composition of head space samples from gas at different depths in F17-12. The legend shows, between brackets, the depth of the sample in TVDss. The plot shows that the isotopic composition remains approximately unaltered until a depth of 1094 m. At shallower depths the $^{13}C$ of methane, in particular, becomes increasingly depleted.**

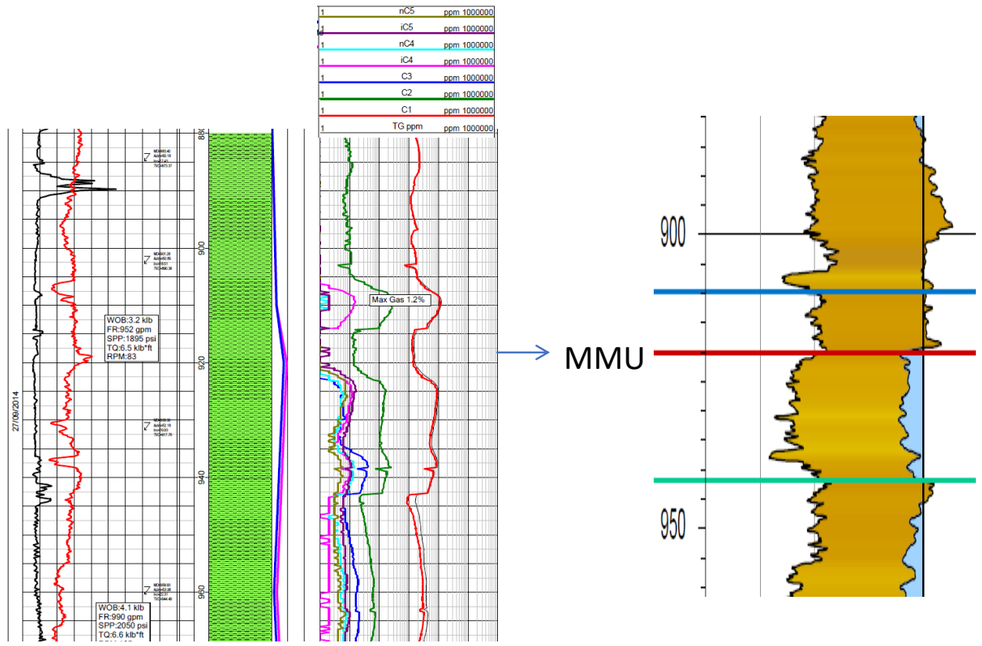


**Figure 7.10. Copy of part of the Masterlog of F17-12 (figure at the left) showing the relatively high content of Total Gas and methane at 910 mMDRT and between 925 and 940 mMDRT, and the sharp decrease in Total Gas and methane to much lower values in combination with the disappearance of the C3+ components at 905 mMDRT. The sharp decrease in TG and methane occurs close to the depth of the MMU.**

observed vertical alteration of geochemical and carbon isotopic composition of the gases per well. In order to compare the changes in geochemical and carbon isotopic composition we only use the analyses of one type of gas sample from these wells in the indicative Chung plots; the uncertain carbon isotopic compositions, reported between brackets in the provided gas composition database, were not taken into account in the evaluation.

### Vertical alteration pattern F17-12

The compound specific carbon isotopic compositions of head space gas samples from the Chalk, and Lower, Middle and Upper North Sea groups (Figure 7.9) show that the isotopic compositions are very similar in the Chalk, Lower North Sea Group and in the Middle North Sea Group until a depth of 1094 mTVDss. This suggests that during leakage of gas of Chalk origin into the Cenozoic sequences the composition of the gas remains unaltered in the Lower North Sea Group and also in the Middle North Sea Group until a depth of 1094 mTVDss. The plot shows that the $\delta^{13}C$ of methane is increasingly depleted in gas samples from shallower depths, while the $\delta^{13}C$ of ethane does not change much until a depth of 680 mTVDss.

The observed changes in carbon isotopic compositions at depths shallower than 1094 m point initially to increasing mixing of the migrated gas of Chalk origin with gas of - primary - microbial origin. Assuming that gas of primary microbial origin is characterized by $\delta^{13}C\_C1$ = -70‰ and gas of Chalk origin by $\delta^{13}C\_C1$ = -36‰, the percentage of primary microbial gas at 937 m and 882 mTVDss is ± 33% and 75%, respectively. The gas at 592 m depth with a methane content of 99.8 Mol% and $\delta^{13}C\_C1$ = -69.2‰ and $\delta^{13}C\_C2$ = -49.5‰ can be considered a gas of primary microbial origin.

The very minor shift of $\delta^{13}C$ of C3, nC4 and nC5 to less depleted values at 882 mTVDss compared to those of the Chalk gas might indicate that, in addition to mixing with primary microbial gas, biodegradation of the migrated Chalk gas also affected the gas composition to a minor extent at this depth.

The gas composition on the master log of F17-12 (Figure 7.10) shows that the total gas (TG) and C1 content at 930 mMDRT (=882 mTVDss) and 910 mMDRT (TG = 1.2 %) are relatively high at these depths around the MMU, i.e just below and above the glauconite shales. The TG decreases rapidly above the MMU to much lower values at 905 mMDRT.

### Vertical alteration pattern F17-11

The compound specific carbon isotopic compositions of head space gas samples from the Chalk and North Sea groups (Figure 7.11) show that the isotopic compositions are very similar in the Chalk and the North Sea Supergroup until a depth of 1149 mTVDss. A major shift of $\delta^{13}C\_C1$ towards more depleted values occurs between 1149 and 944 mTVDss. This major shift of $\delta^{13}C\_C1$ without changes in the carbon isotopic composition of ethane, propane, n-butane and n-pentane is indicative of mixing of gas of Chalk origin with primary microbial generated gas. Assuming that gas of primary microbial origin is characterized here by $\delta^{13}C\_C1$ = -70‰ and gas of Chalk origin at F17-11 by $\delta^{13}C\_C1$ = -40‰, the percentage of primary microbial gas at 944 mTVDss with $\delta^{13}C\_C1$ = -57.40‰, is ± 50%. There are no head space gas analyses available for the Upper North Sea Group at F17-11.

### Vertical alteration pattern F17-13

The compound specific carbon isotopic compositions of head space gas samples from the Chalk, and Lower, Middle and Upper North Sea groups (Figure 7.12) show that the isotopic compositions change between a depth of 1291 mTVDss in the Chalk and 964 mTVDss in the North Sea Supergroup. Assuming that gas of primary microbial origin is characterized by $\delta^{13}C\_C1$ = -70‰ and gas of Chalk origin at F17-11 by $\delta^{13}C\_C1$ = -43‰, the percentage of primary microbial gas at 964 mTVDss with $\delta^{13}C\_C1$ = -56‰, is ± 50%. Increasing depletion of $^{13}C$ of methane and also ethane and n-butane occurs with decreasing depth in the Upper North Sea Group. The plot suggests that the head space gas at 520 mTVDss in the Upper North Sea Group still has the characteristics of a mixed gas, i.e not 100% microbial. At the very

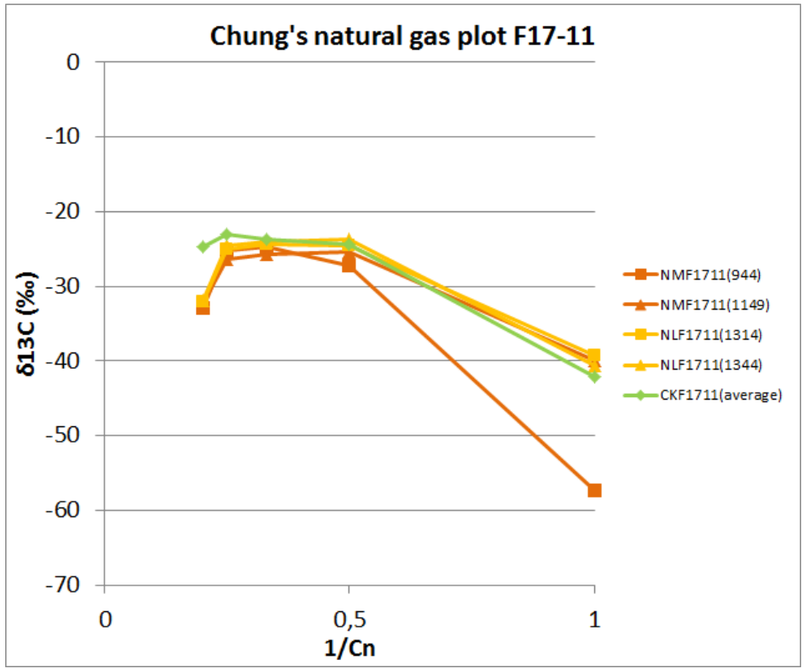


**Figure 7.11. Chung's natural gas plot of compound specific carbon isotopic composition of head space samples from gas at different depths in F17-11.**

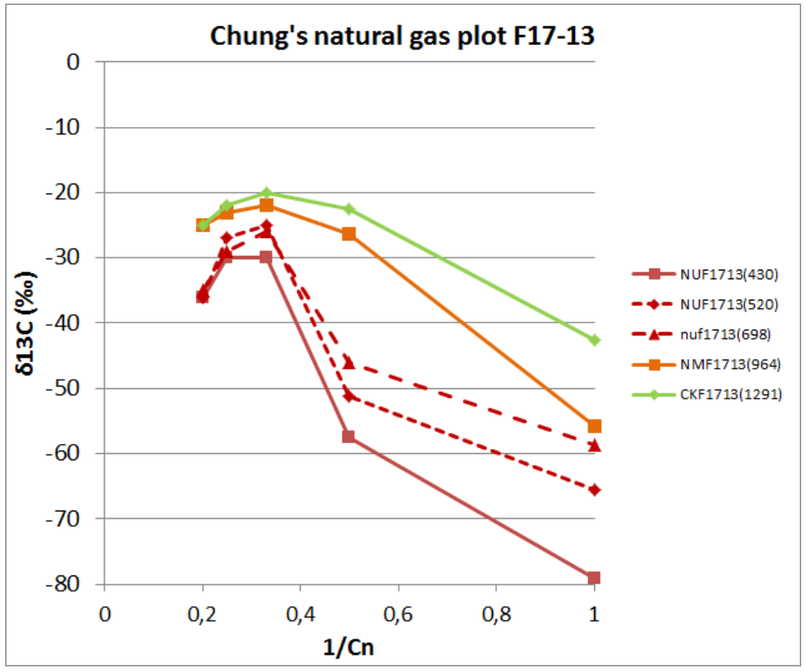


**Figure 7.12. Chung's natural gas plot of compound specific carbon isotopic composition of head space samples from gas at different depths in F17-13.**

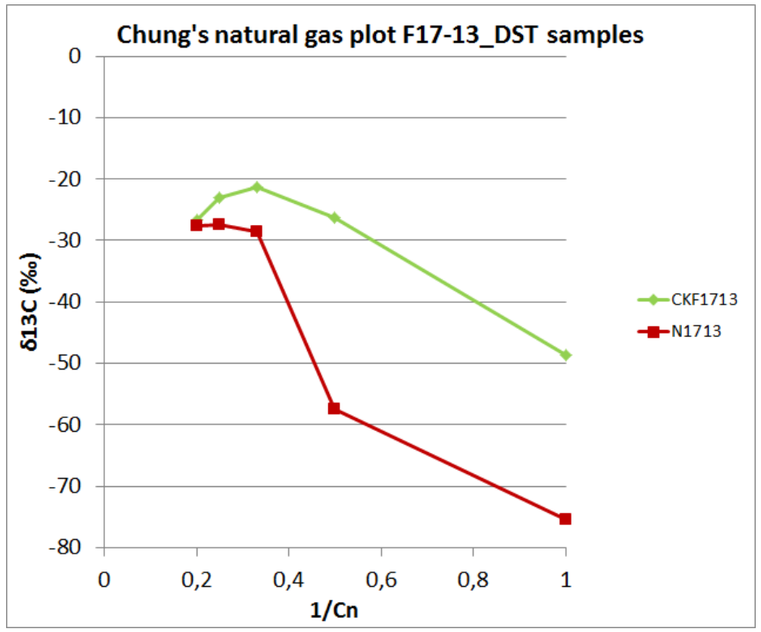


Figure 7.13. Chung's natural gas plot of compound specific carbon isotopic composition of DST samples from gas in the Chalk and from shallow gas in F17-13.

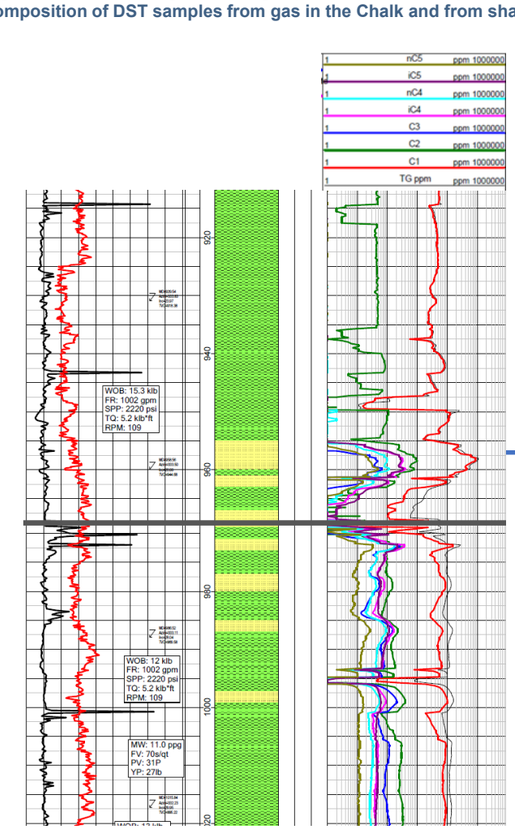


Peak TG and C1; C3+ not present at depths < 950 mMD

Figure 7.14. Copy of part of the Masterlog of F17-13 showing the relatively high content of Total Gas, methane and other gas components at 956-960 mMDRT, and the sharp decrease in Total Gas and disappearance of the C3+ components in the gas at depths of less than 950 mMDRT.

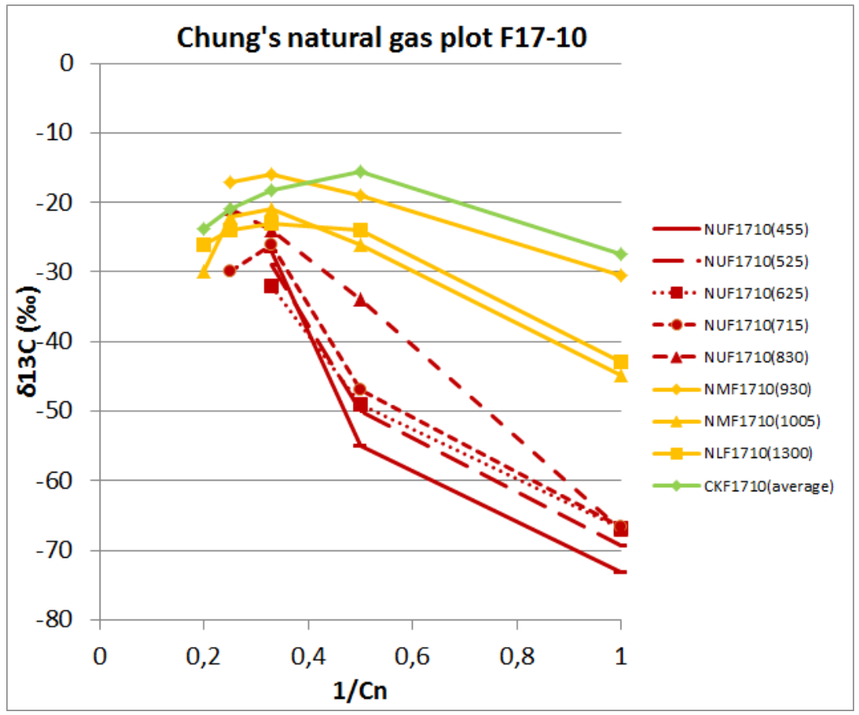


Figure 7.15. Chung's natural gas plot of compound specific carbon isotopic composition of head space samples from gas at different depths in F17-10.

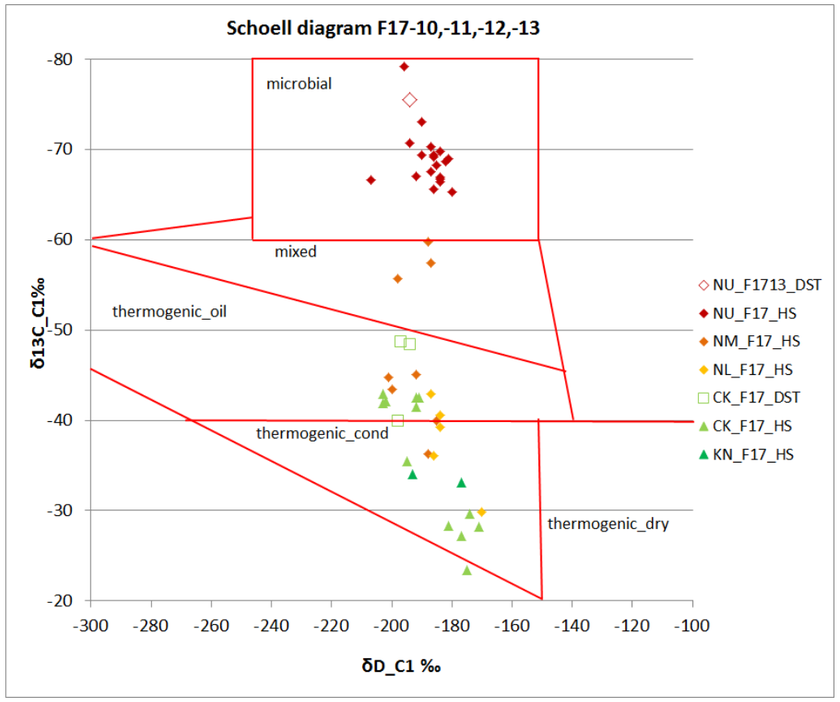


Figure 7.16. Schoell's indicative cross plot of $\delta^{13}C\_C1$ versus δD_C1 for head space (HS) and DST gas samples from F17-10, F17-11, F17-12 and F17-13.

shallow depth of 420 mTVDss the $^{13}C\_C1$ is very depleted $\delta^{13}C\_C1$ = -80‰.

Figure 7.13 presents the compound specific carbon isotopic composition of a DST sample from the Chalk and a DST sample of shallow gas from an unknown depth. The shallow gas sample is strongly depleted in $^{13}C$ of methane and ethane. The carbon isotopic composition of methane changes from $\delta^{13}C\_C1$ = -48.7‰ in the Chalk gas sample to $\delta^{13}C\_C1$ = -75.5‰ in the shallow gas sample. The C1/(C2+C3) of the shallow gas exceeds 8000.

The gas composition presented on the masterlog of F17-13 (Figure 7.14) shows a relatively high content of Total Gas, methane and other gas components at 956-960 mMDRT (=907.5-911.5 mTVDss) , corresponding to the depth with reported oil shows. The log shows a sharp decrease in total gas in combination with the disappearance of the C3+ components in the gas at depths < 950 mMDRT (= 901.5 mTVDss). The head space gas composition at depths < 900 mTVDss is dominated by C1 (=99.9 Mol%), but still includes very minor amounts of C3+.

### Vertical alteration pattern F17-10

Figure 7.15 presents the compound specific carbon isotopic compositions of head space gas samples from the Chalk, and Lower, Middle and Upper North Sea groups for F17-10. The overall observed relative changes in carbon isotopic composition show about the same pattern as in the other F17 well locations. The compound specific isotopic composition of the gas at 930 mTVDss deviates from the general trend: it is much more enriched in $^{13}C$ in comparison with the samples from greater depths, 1300 and 1005 mTVDss. All samples from the Upper North Sea Group have a strong microbial signature. The gas composition presented on the masterlog of F17-10 shows a peak of Total Gas, methane and other gas components at 930 mMDRT (~ 895 mTVDss), followed by a sharp decrease in total gas in combination with the disappearance of the C3+ components in the gas. The MMU is located at 942.35 mMDRT and the sharp decrease in TG seems to coincide with the top of the glauconite shales.

### Other indicative plots showing alteration of gas properties in F17 area

All gas samples from the Upper North Sea Group from F17-10, -11,-12, -13 fall within the area of microbial gas on Schoell's indicative plot (Figure 7.16). Three samples from the Middle North Sea group indicate mixing of thermogenic generated gas with gas of microbial origin. All the other gas samples from Middle and Lower North Sea Group, Chalk and Rijnland Group are thermogenic in origin according to Schoell's indicative plot.

The cross plot of C1/(C2+C3) versus depth for head space gas samples from F17-10, -11,-12, -13 (Figure 7.17) indicates that all, but one, gas samples from the Upper North sea Group are dry gases. The outlier concerns a gas sample from F17-10 at a depth of 405 m and C1= 91.9 Mol%, and a very low % of C1 in total gas (0.0026%).

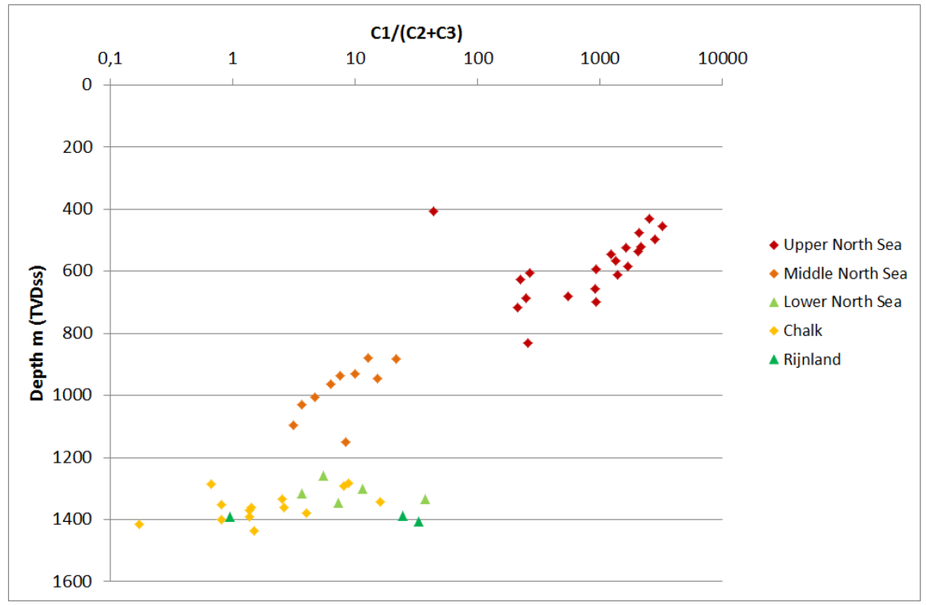


**Figure 7.17. Cross plot of C1/(C2+C3) versus depth for head space gas samples from F17-10, -11,-12, -13.**

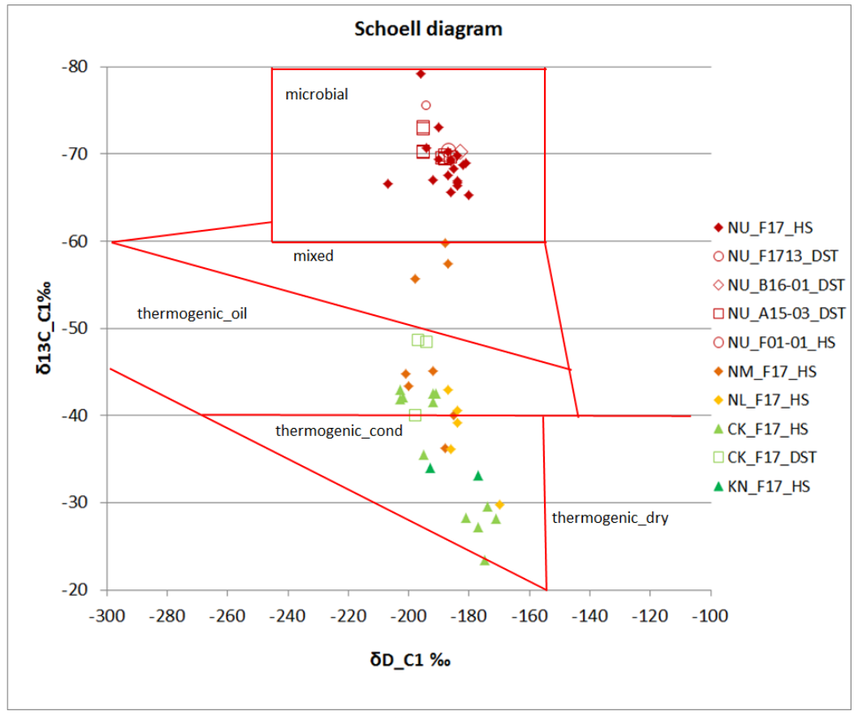


**Figure 7.18. Schoell's indicative cross plot of $\delta^{13}C\_C1$ versus δD_C1 for head space (HS) and DST gas samples from F17-10, F17-11, F17-12, F17-13, B16-01, A15-03 and F01-01.**

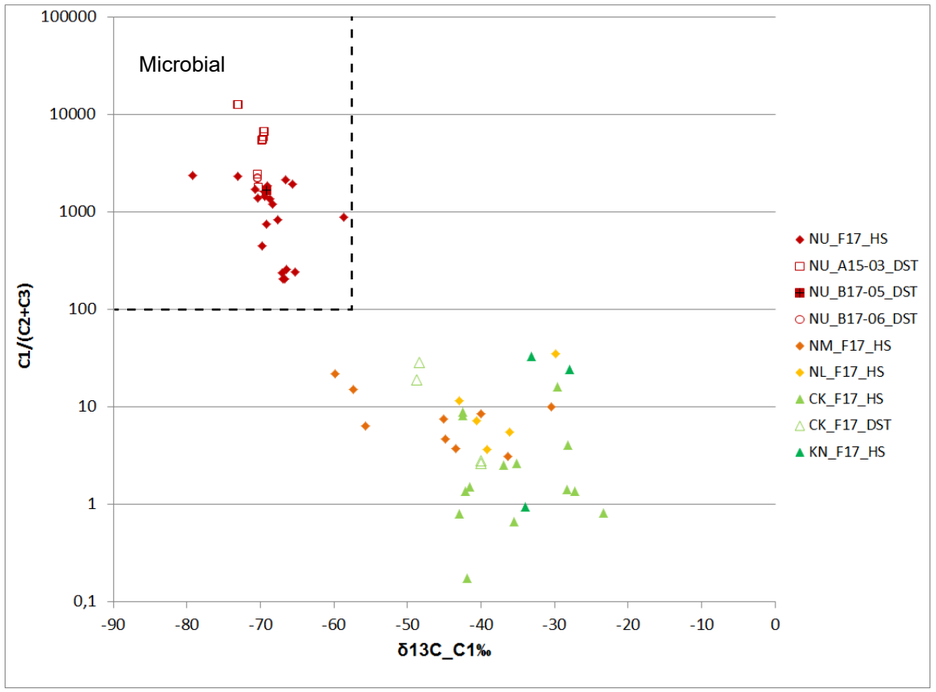


Figure 7.19. Bernard cross plot of C1/(C2+C3) versus $\delta^{13}C\_C1‰$ (see also figure 7,1) showing the $^{13}C$ depleted and dry nature of the gas samples in the Upper North Sea Group from different locations.

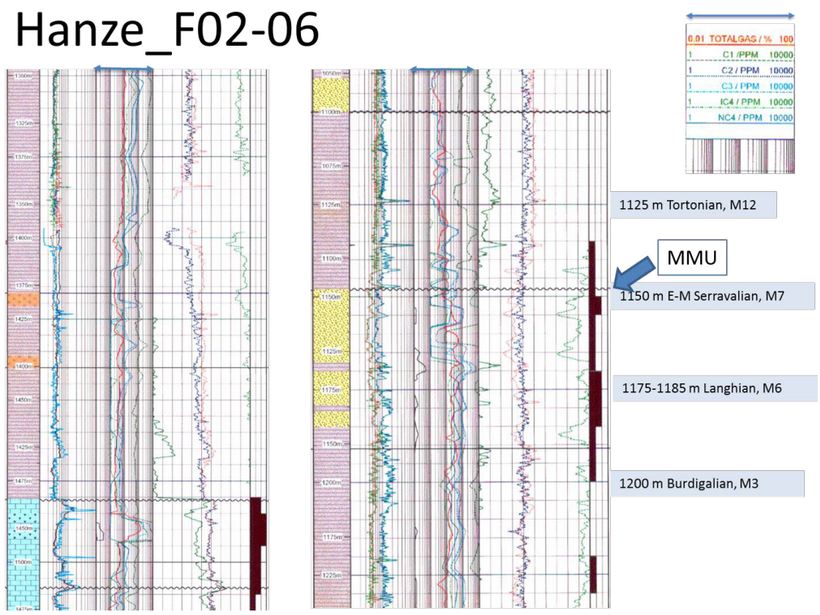


Figure 7.20. Selected parts of the composite log of F02-06, showing that all gas components were detected in the Chalk and in Cenozoic sequences below the MMU and oil shows (in black) were identified in Cenozoic sequences between 1135 – 1230 mMDRT.

## Alteration patterns of gas properties in Cenozoic sequences

The geochemical and carbon isotopic composition of the F17 wells in combination with those of B16-01, A15-03 and F01-01 are presented in the indicative Schoell plot (Figure 7.18). Figure 7.19 presents a cross plot of C1/(C2+C3) versus $\delta^{13}C\_C1‰$ showing the $^{13}C$ depletion and dry nature of the gas samples in the Upper North Sea Group from the different well locations.

Both figures indicate that the properties of the gas samples from different locations in the Upper North Sea Group all point to a microbial origin of the gas .

The alteration pattern of gas properties in the northern offshore outside the F17 area is described below at selected well locations that represent different geological settings.

### Vertical alteration pattern in Cenozoic sequences overlying the Hanze field

The composite logs from F02-06 (Figure 7.20 and 7.21) show that a full suit of gas components are present in the Chalk and in Cenozoic sequences until a short distance above the MMU. At depths of less than 1035 mMDRT, methane is the only detected gas component. A rather abrupt change in geochemical composition of gas is also apparent at about 1075 mMDRT (~1034 mTVDss) on the gas log of F02-05.

The average gas composition of 3 samples retrieved from the interval between 595-702 mTVDss in F02-B-01 is a dry gas characterized by C1 = 99.5 Mol% and C1/(C2+C3) = 2140.

The logged gas compositions indicate that gas from the Chalk reservoir leaked into the Cenozoic sequences and moved through the Cenozoic sequences until a short distance above the MMU. The sequences above the MMU are dated as Early Zanclean. In addition, the fault crossing the Hanze field may have played a role as a focused migration path. The gas pressure kick encountered at 1222 mTVDss below the MMU while drilling the F02-A-02 borehole close to the fault might be an indication.

Oil shows are reported in well F02-06 at 1135-1230 mMDRT in (Figures 7.21 and 7.22). In well F02-05 oil shows were encountered at different depth intervals between about 1080 mMDRT and top Chalk (1406 mMDRT), suggesting that in this location not only gas, but also oil was also able to migrate vertically through the Cenozoic caprock of the Hanze oil field.

### Gas in Cenozoic sequences in spatial relation with seismic chimneys

#### A15-03

Block A15 and well A15-03 are selected to show an example of such a situation. Seismic section in block A15 shows a number of stacked flat spots in the Upper North Sea Group and a seismic chimneys that extends from the flat spots to greater depth following the right hand side of the Zechstein salt structure to the location where the Zechstein salt is missing (Figure 7.22). The seismic chimney suggests the existence of a current or paleo pathway for vertical leakage from sub-salt into the Cenozoic sequences. The vertical migrating fluids might consist of deep thermogenic gas generated from Carboniferous source rocks.

The geochemical and carbon isotopic composition of head space and DST samples of shallow gas in the Upper North Sea Group in A15-03 have a strong microbial signature from the MMU upward ($\delta^{13}C\_C1 = \pm -70‰$; Figure 7.23). The DST gas samples show an increase in dryness from C1/(C2+C3) = 1774 at 900 m depth to C1/(C2+C3) = 12398 at 449 m depth. No C4 and C5 components were encountered in the DST samples at depths shallower than about 900 m. Hence, the properties of the gas above the MMU are indicative of a microbial origin. Figure 7.23 also shows gas properties of thermogenic origin of 2 different maturities. It is clear that the observed gas composition in the Upper North Sea Group at A15-03 is not indicative for a thermogenic origin.

### A18-02

Figure 7.24 shows the location of shallow gas accumulations in the Upper North Sea Group. The gas accumulations occur above a Zechstein salt structure. The seismic section (Figure 7.24) also shows the presence of a seismic chimney below the shallow gas occurrences.

The geochemical gas composition of shallow gas in the Upper North Sea Group obtained from a surface production test at A18-02-S2 has a very high methane content of 99.57 Mol % and a C1/C2 = 9957 (no C3 has been reported), i.e. a strong microbial signature.

### B16-01

The shallow gas accumulation tapped by B16-01 is located above a Zechstein salt structure (Figure 7.25 ). The signature of a DST sample from the shallow gas accumulation in the Upper North Sea Group is that of gas of microbial origin (C1 = 99.6Mol%, $\delta^{13}C\_C1 = -70.3‰$, $\delta D = -183‰$; see also Figure 7.18). Because the total depth of B16-01 is only 1245 mTVDss, no information is available on gas content and composition in the Lower North Sea Group.

### Gas in Cenozoic sequences which are not top seals for oil or gas fields

### F02-07

F02-07 is located outside the Hanze oil field area and is not on top of a salt structure. The cross-plot of methane content (in ppm) versus depth for the Chalk, Lower, Middle and Upper North Sea groups (Figure 7.26) show a very low methane content in the Lower and Middle North Sea groups and increasing amounts of methane in the Upper North Sea Group. This indicates that there is no charging of the Lower North Sea Group from below and the shallow gas in the Upper North Sea Group is probably generated in-situ.

### F01-01

The Cenozoic sequences at F01-01 do not directly overly an oil or gas field; the top of the Zechstein at this location is at 1924 mTVDss. Figure 7.27 shows that the gas content in the Lower North Sea Group is very low and increases in the Upper North Sea Group. In addition, the isotopic signature of shallow gas at 683 mMDRT ($\delta^{13}C\_C1 = 70.5‰$ and $\delta D\_C1 = -187‰$) as well as the gas dryness in the Upper North Sea Group point to a microbial origin of the gas.

### B18-03

Wet gas is present in the Rijnland Group and Lower Graben Formation (Figure 7.28). The total gas content reported on the gas log of B18-03 is low in the Lower North Sea Group and does not support gas leakage from deeper sequences into the Cenozoic. Total gas content is significantly higher above the MMU (located here at 1346.77 mMDRT ~1316.52 mTVDss).

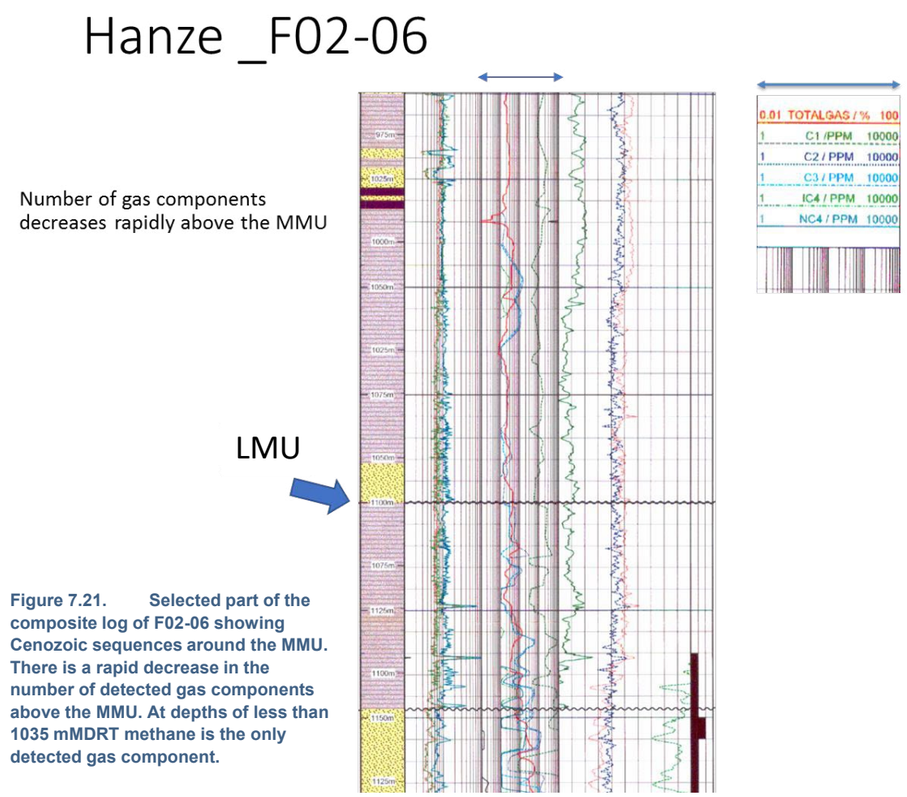


**Figure 7.21. Selected part of the composite log of F02-06 showing Cenozoic sequences around the MMU. There is a rapid decrease in the number of detected gas components above the MMU. At depths of less than 1035 mMDRT methane is the only detected gas component.**

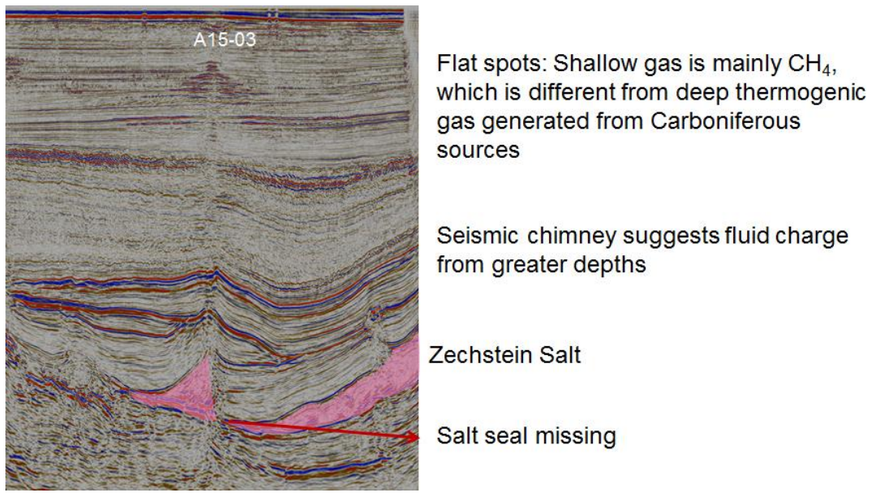


**Figure 7.22. Seismic section crossing A15-03.**

## Discussion & conclusions observed alteration pattern of gas properties

- In areas with current or paleo input of gas from deeper pre-Cenozoic sources:
  - Gas composition in Lower North Sea Group (from head space and mud gas data mostly) is indicative of a predominant thermogenic origin;
  - The occurrence of thermogenic gas in immature North Sea Group infers migration (leakage) of gas into the Cenozoic Lower North Sea Group. This leakage has been observed in locations where the Cenozoic caprock directly overlies petroleum reservoirs (Chalk oil reservoirs: F17-10,-11,-12,-13, F02-06, F2-05).
  - There is no apparent change in gas composition during migration through the Lower North Sea Group;
  - Abrupt changes in gas composition from predominantly thermogenic to predominantly microbial signature occur at a small distance above the MMU/LMU (in F17 the abrupt changes occur in sequences of Gelasian age; above Hanze oil field in sequences of Early Zanclean age);
  - Gas composition in the Upper North Sea Group above the MMU has a strong microbial signature.
- In areas without input of gas from deeper pre-Cenozoic sources:
  - Gas is largely absent in Lower and Middle North Sea groups (as apparent from low values of TG and C1 on mud and gas logs);
  - Gas is present in the Upper North Sea Group (F01-01, B18-03, F02-07);
  - Gas in Upper North Sea Group has a microbial signature (e.g. F01-01).
- Seismic chimneys might indicate the existence of vertical migration paths of gas from pre-Cenozoic sources into the Cenozoic sequences in present or past (A15-03, A18-02). This could not be verified due to lack of geochemical and carbon isotopic data of gas occurrences in the Lower North Sea Group at these locations.

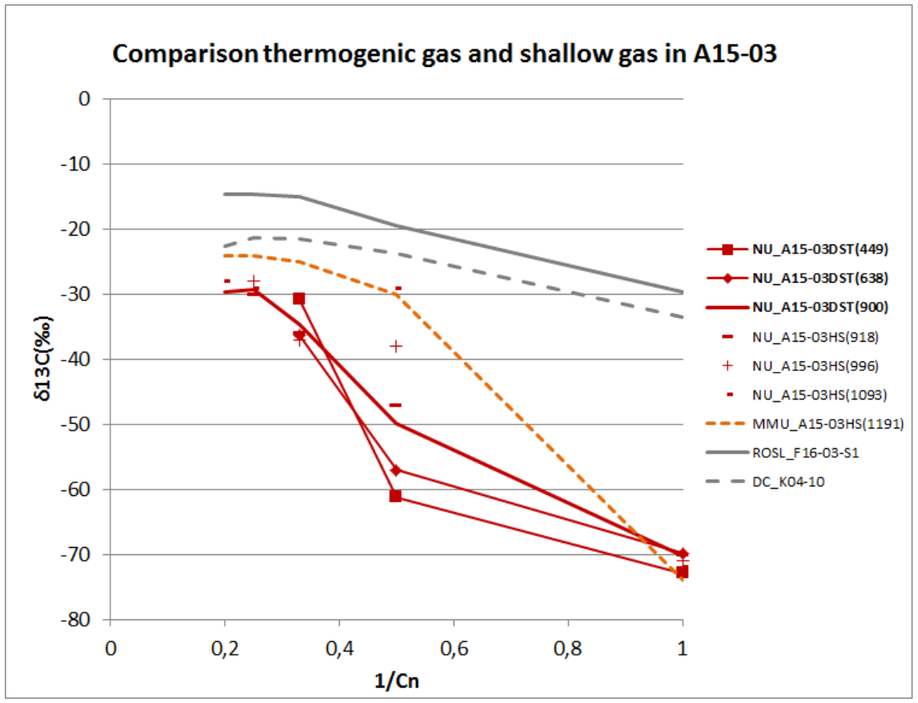


Figure 7.23. Chung's natural gas plot of compound specific carbon isotopic composition of head space (HS) and DST gas samples from different depths in A15-03. Two compound specific carbon isotopic compositions of gas samples from Upper Rotliegend and Carboniferous reservoirs show a typical signature for gas of thermogenic origin.

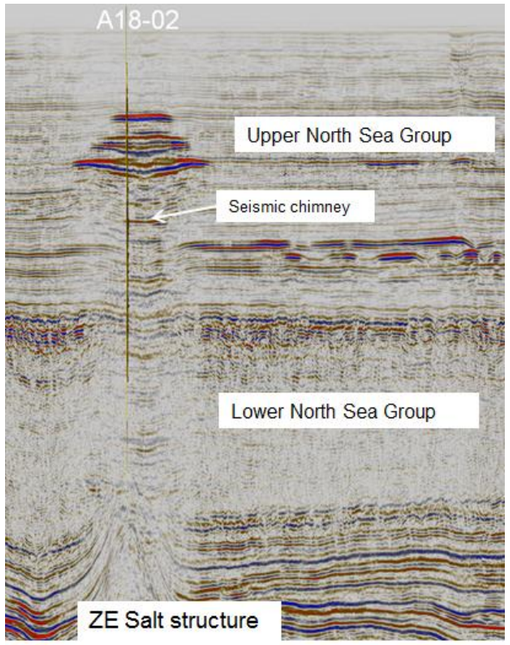


Figure 7.24. Seismic cross section running through well A18-02 tapping shallow gas accumulations. A seismic chimney seems to extend from the Zechstein salt structure towards the shallow gas accumulations.

## Biodegradation and primary microbial gas generation

### Basic conditions

A number of basic conditions need to be fulfilled to enable biodegradation or primary microbial gas generation by methanogenesis. In addition to the presence of a petroleum accumulation for biodegradation and the presence of organic matter for microbial gas generation, microbial activity of methanogens requires that the following conditions are fulfilled:

- Anoxic condition;s
- Temperatures < 80°C
    - Optimal temperatures for microbial activity: 35-45 °C (Katz, 2011); 30-50 °C (Clayton, 2010); activity slows down fast at temperatures exceeding 65 °C;
- Water; sufficient pore water and pore space for microbial population to grow;
- Near absence of sulphate;
- Absence of high salinity pore water: high salinity might slow down or hinder biodegradation and might reduce the maximum temperature at which methanogenesis takes place, (Head et al., 2014).

### Biodegradation

The Hanze oil is light (37°API); hence the oil is not or hardly affected by biodegradation. The present-day temperature of the Hanze Chalk reservoir is 74 °C. Present-day temperature in combination with the probably high salinity and high sulphate content (TDS of the formation water in Zechstein caprock immediately underlying the Chalk reservoir is 234000 mg/l; and sulphate content is 1791 mg/l) exclude biodegradation of the oil at present-day. Probably the reservoir was filled after the reservoir reached temperatures higher than optimum temperature for biodegradation (at latest phases of Eridanos delta sedimentation or more recent; the reservoir was probably filled not before the Gelasian (S5: 2.44-2.58 Ma).

In contrast, the gas samples from the Chalk at F17-10 and F17-13 are characterized as biodegraded gas. The current high temperature of the Chalk reservoir in F17-10, -11 and -13 (measured temperatures range between 61 – 74 °C) does not favour widespread biodegradation of the oil at present-day. In addition, the Chalk reservoir at F17-10,-11 is also overlying a salt structure and salinity and sulphate content is also be high in the Chalk. Given the biodegraded nature of the gas from samples in the Chalk, it can be concluded that the generation of this gas composition took place in the past when the Chalk was buried less deeply and temperatures of the reservoir were lower.

The gas samples from the Chalk at F17-12 show no signs of biodegradation. This may indicate that the reservoir was filled later than the Chalk reservoir at the location of F17-10 and F17-13, i.e. at times when the reservoir reached temperatures too high for biodegradation to take place. If the reservoirs at the two locations were filled at the same time and at comparable reservoir temperature conditions, other differences in reservoir conditions influencing biodegradation may also provide an explanation (such as differences in extent of HC/water interface, in water leg and pore space below the contact; differences in water salinity, sulphate content; rate of trap filling).

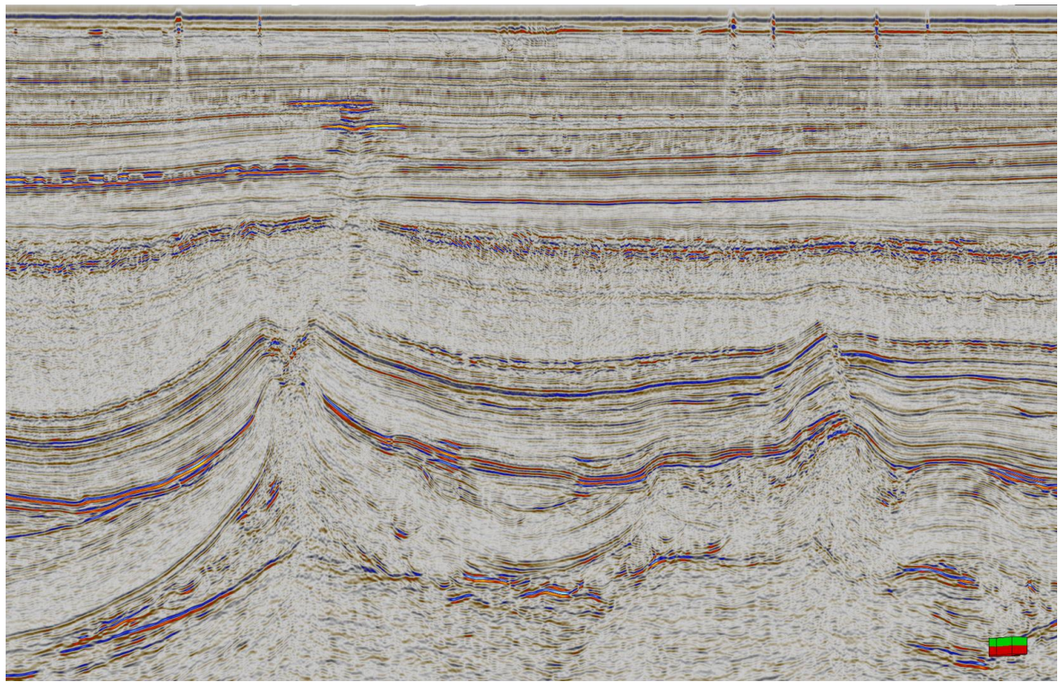

Figure 7.25. The seismic section in the B16 area shows DHI's of shallow gas occurrences in the Upper North Sea Group above a salt structure, a seismic chimney extending vertically below the DHIs' and the location of a tilted fault extending from the Zechstein salt structure towards the DHIs.

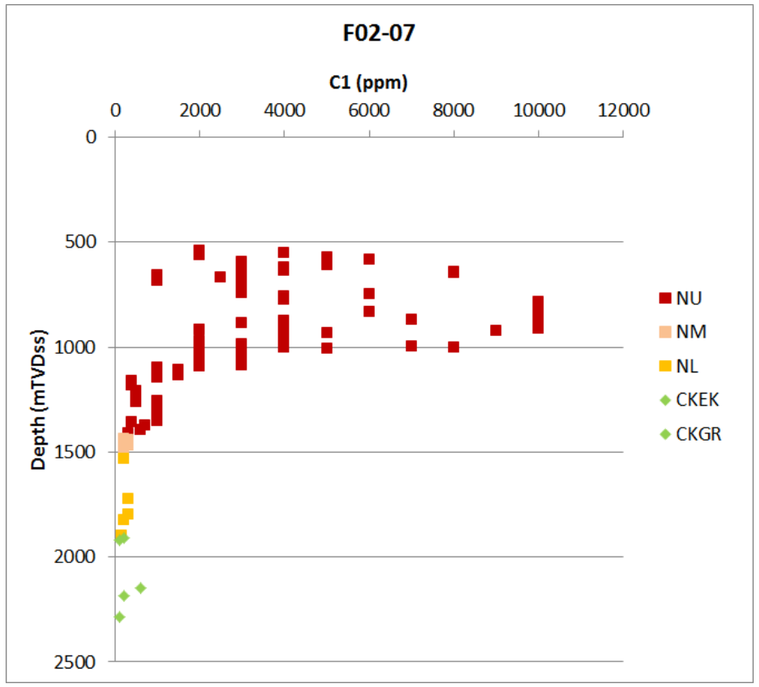


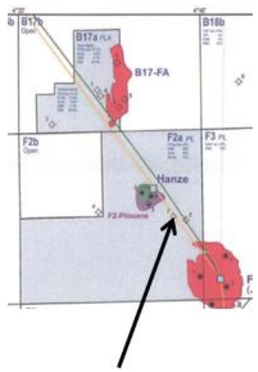


Figure 7.26. Cross plot of methane content (ppm) versus depth in F02-07; the methane content is derived from the gas log of F02-07.

### Primary microbial gas generation

Lithologs of wells in the F17 area as well as in northern offshore report the occurrence of organic matter in Upper North Sea Group sequences, including the Eridanos delta deposits. In contrast no or hardly any organic matter has been observed in the Lower North Sea Group sequences, explaining the absence of microbial gas in the Lower North Sea Group.

In general the salinity of the pore water in the Eridanos is relatively low and porosity relatively high. The other key condition for enabling microbial generation of gas from organic matter in Eridanos Delta deposits is temperature. The temperature in the subsurface varies for the same depth of measurement, especially large lateral variations in temperature and geothermal gradient exist between sedimentary sequences on top of large salt structures and outside such structures.

Assuming that the optimum window for methanogenesis is: 30-50 °C. The corresponding optimum depth window for methanogenesis is:

- In Cenozoic sequences above a salt structure. The geothermal gradient above a salt structure is relatively high. For example, assuming the gradient is constant, the geothermal gradient is 45.7 °C/km in sediments above the Hanze field (based on the Hanze reservoir temperature of 74 °C at 1400 m, and a surface temperature of 10 °C). This gives the following depth interval for the optimum window; 30 °C at about 450 m and 50 °C at about 900 m;
- In Cenozoic sequences outside salt structures. Assuming a geothermal gradient of 30 °C and surface temperature of 10 °C; the optimum window occurs between 650 m and about 1300 m;

In reality the geothermal gradient in sedimentary sequence overlying a salt structure will be higher, but not constant: the gradient is high close to the top of the salt structure and will be lower at shallower depths.

The above calculations show that the optimum depth interval is smaller and located at shallower depths above a salt structure. In between salt structures the optimum depth window is located at greater depths and will be larger.

Measured temperatures at B17-05 show that 30 °C is reached at about 700 m (Figure 7.29). At B17-05 a depth of 700 m corresponds with seismo-stratigraphic unit S4 and Piacenzian age (Pliocene).

Modeling of primary microbial gas generation in the Eridanos delta deposits in the northern offshore (Step Graben and northern half of the Central Graben) showed that microbial gas generation in the optimum window started at the beginning of the Pleistocene and continues until present-day (Verweij and Nelskamp, 2014). The modeling also showed that temperature fluctuations do not have a large influence on the history of the optimum window for microbial gas generation.

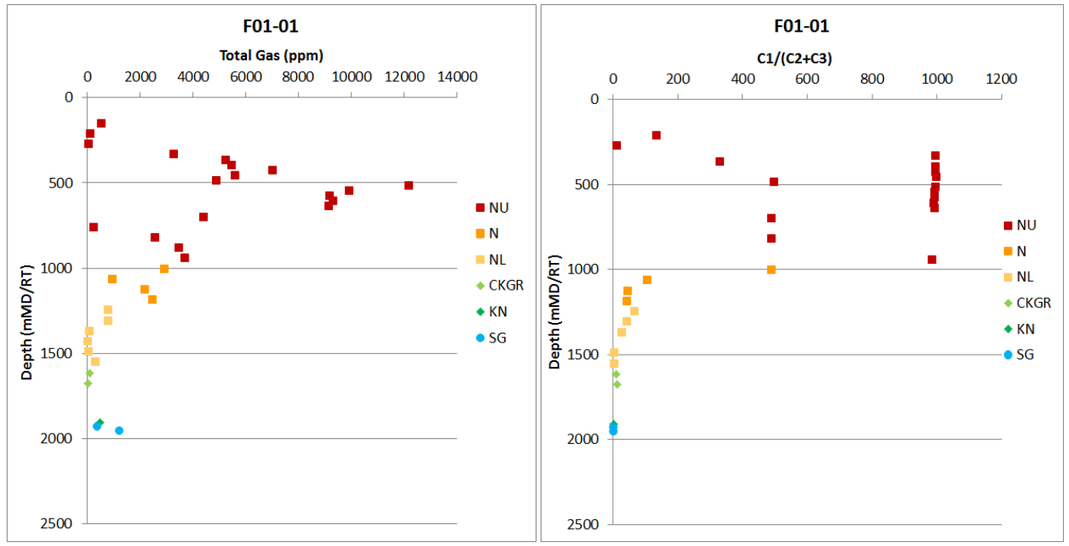


Figure 7.27. Cross plot of total gas content (ppm) versus depth in F01-01 (plot on the left) and cross plot of C1/(C2+C3) versus depth in F01-01 (based on air space gas analyses from cuttings) (plot on the right).

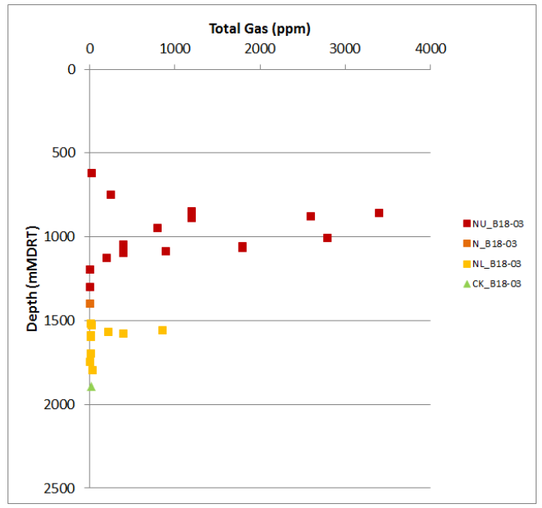


Figure 7.28. Cross plot of total gas content (ppm) versus depth in B18-03 (left). Sharp peaks in Total Gas appear at 1560, 1568, and 1580 mMDRT. The MMU is located at 1346.77 m MDRT (~ 1316 mTVDss). The table shows the geochemical composition of gas in the Rijnland and Schieland groups in B18-03.

| Depth | Stratigraphy | C1 | C2 | C3 | C4 | C4+ | CO2 | N2 |
|---|---|---|---|---|---|---|---|---|
| mMD/RT | | % | % | % | % | % | % | % |
| 2220 | KN | 92 | 6 | 2 | tr | | | |
| 2300 | KN | 76 | 18 | 6 | tr | | | |
| 2776-2797 | SLCL | 79.73 | 10.52 | 4.88 | | 1.81 | 1.78 | 1.28 |

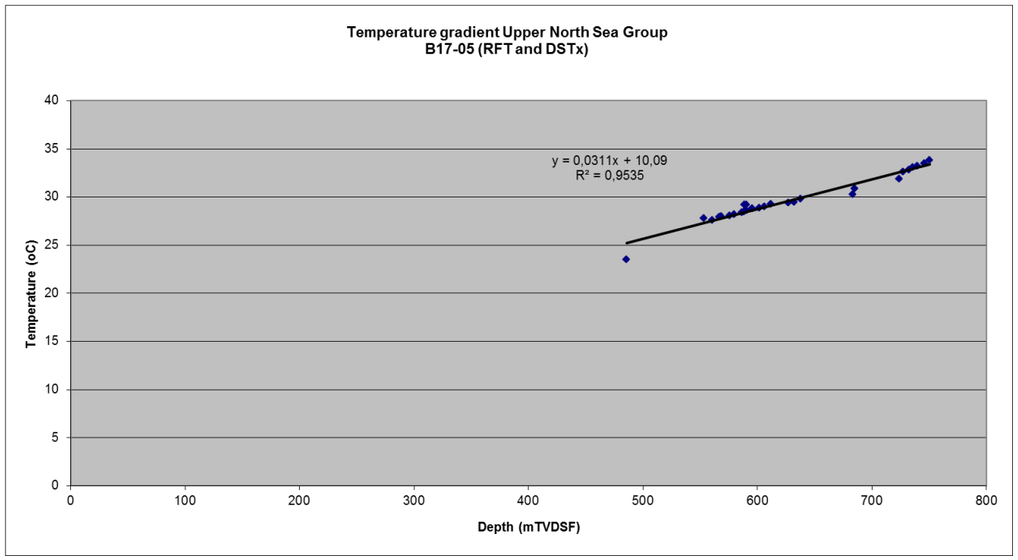


**Figure 7.29. Cross plot of temperature versus depth in B17-05. The temperature reaches 30°C at 650 m below the sediment water interface, i.e. at about 700 m below sea surface. Hence, the optimum temperature for methanogenesis (30-50°C) is reached at about 700 mTVDss.**

## Influence of overpressure distribution on petroleum system in Cenozoic sequences

Migration and trapping of gas and oil in the Cenozoic sequences are influenced directly and indirectly by the pore (over)pressure condition in the sequences at present-day and in the past.

First, we assess and evaluate the present-day spatial variation in pore pressure in the Cenozoic sequences using measured pore pressures as well as mudweight pressures.

### Approach to assess overpressure distribution

There are only a limited number of pore pressure measurements available for the Cenozoic sequences in the study area and these principally cover the Upper North Sea Group in the northern offshore (A, B, and northern F blocks). No pore pressure measurements are available for the Cenozoic in the Cleaverbank Platform. Therefore, we also use mudweight pressures as proxy for pore pressure in order to extent our insight into the pressure condition of the Cenozoic sequences.

Previous studies in the Dutch North Sea and surrounding areas provide background information on factors of influence that individually or in combination provide insight in understanding current (over)pressure condition in Cenozoic sequences:

1. Sedimentary loading has been identified as an important pressure generating mechanism for the Cenozoic sequences (and Chalk) in the Dutch North Sea and surrounding areas (Verweij et al., 2012). The competition between sedimentary loading and pressure-dissipating mechanism (such as water flow, compaction and dewatering of the rock framework) will control an overpressure distribution. When sediments are unable to dewater during sedimentary loading and subsidence, the pore water will bear part of the increase in overburden load and become overpressured.

2. Type of pore fluid. Measurements of pore pressure include measurement of water pressure, oil or gas pressure. The magnitude pore pressure in gas column will be higher than the pore water pressure at the same depth of measurement.

3. Lithologies - such as mudstones - with high rock matrix compressibilities as well as low permeabilities are especially susceptible to overpressuring. Cenozoic mudstones are known to be susceptible to overpressuring in environments of rapid sedimentation worldwide, including the Dutch northern offshore (Verweij et al., 2012) and surrounding UK, Danish and Norwegian North Sea sectors (Japsen, 1999; Evans et al., 2003). Lithologies such as sandstones and limestones, with relatively low matrix compressibilities and high permeabilities (aquifers), allow water flow and redistribution of overpressures.

4. Disequilibrium compaction: Overpressuring in lithologies such as mudstones is accompanied by a slow down or even stop of compaction (a process known as disequilibrium

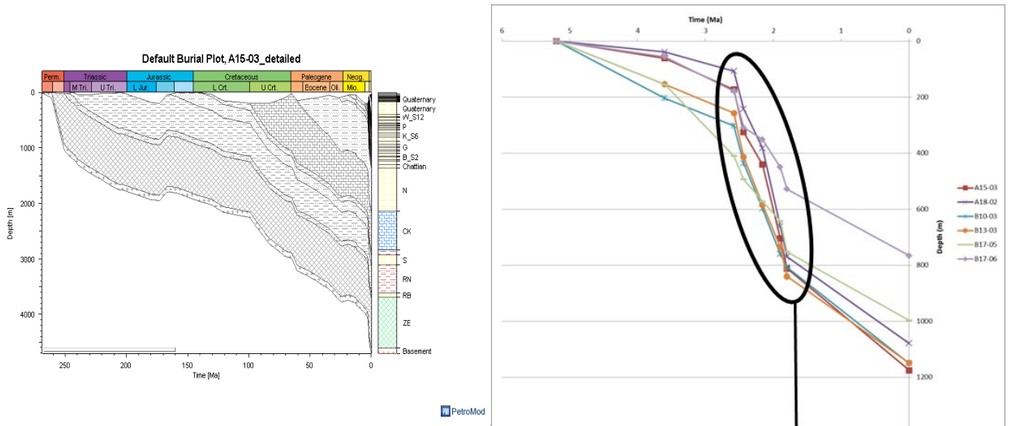


**Figure 7.30** Figure on the left shows the burial history in the northernmost offshore (A block). Figure on the right shows the non-decompacted burial history in A & B blocks since the start of the Pliocene. Both figures illustrate the sharp increase in late burial rate.

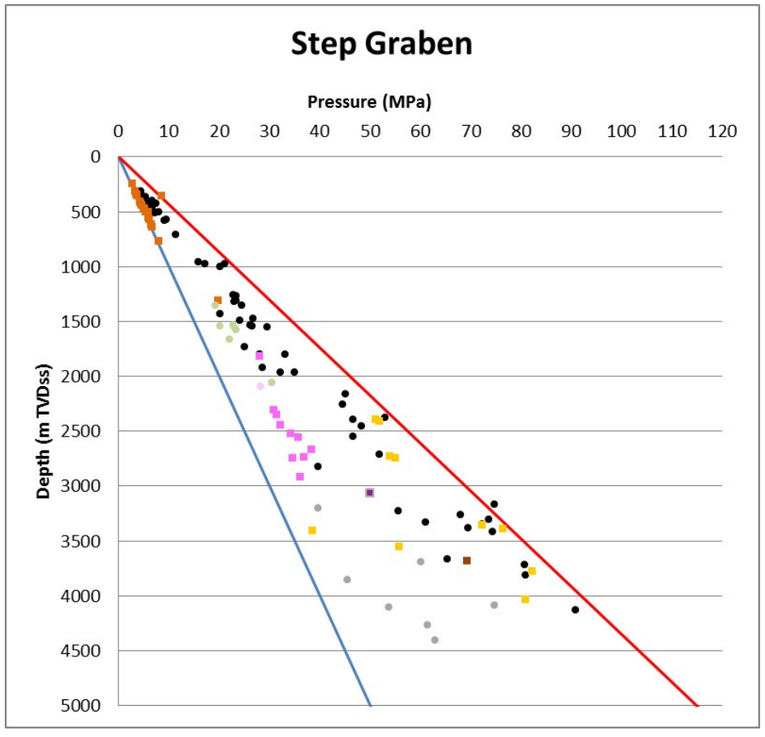


**Figure 7.31.** Cross plot of pore pressure (coloured dots) and leak-off pressure (black dots) versus depth for different stratigraphic units in the Step Graben (From Verweij et al., 2012) . The pore pressures in the Upper North Sea Group (orange dots) are normally pressured, while the Chalk (green dots) and older stratigraphic units are overpressured.

compaction) and preservation of porosity (porosity will be relatively high for its depth of burial). Japsen's (1999) study of interval velocities of the Cenozoic identified an area of relatively low velocities for the depth of burial of the Paleogene in the A and B blocks and northern F blocks in the Dutch offshore and adjacent Central North Sea area. Japsen suggested that the identified velocities of the Paleogene are low relative to depth because of overpressured and undercompacted conditions related to rapid Late Cenozoic loading. The analysis of sonic and 3D seismic data in the southern Dutch Central Graben by Winthaegen & Verweij (2003) confirmed such regional undercompaction and overpressuring of the mudstones of the Lower North Sea Group. The petrophysical analyses of this project also suggest that porosity in the Lower North Sea group is relatively high for the current burial depth (Chapter 4).

5. Polygonal fault systems can have an important impact on the properties of sediments by increasing the permeability of fine-grained sediments and decreasing their mechanical strength and sealingness. Vejbeak (2008) suggested that the top of current overpressured conditions in the Paleogene sediments in the Danish North Sea coincides with a layer of intra-formational faulting. Verweij et al. (2012) indicated that the polygonal fault system in Paleogene sediments below the Miocene unconformities in offshore Netherlands also seem to coincide with the top of current overpressuring in Paleogene mudrocks.

6. Pockmarks are created by expulsion of fluids (oil, water, gas to the seafloor (e.g. Judd and Hovland, 2007; Schroot et al., 2005). Andresen et al. (2008) inventoried a large number of paleo pockmarks in Eridanos delta deposits of Mid –Oligocene and Late Miocene age in the Danish part of the North Sea and suggested that these pockmarks were created by thermogenic gas venting. This project identified paleo pockmarks at the top of the S1 sequence in the Dutch offshore on the F02 panel between F02-06 and B18-03.

With regard to sedimentary loading, there are important regional differences in sedimentary loading of the Lower Cenozoic mudrocks after the periods of non-deposition/erosion related to the MMU/LMU, exemplified by the thickness variation of the Neogene sedimentary package: the largest thickness of Neogene sediments (> 1350 m) occur in the B blocks and northernmost F blocks and thickness decreases rapidly towards the southwest. In the northernmost offshore very high sedimentation rates of over 1000m/My were reached during deposition of the Eridanos delta deposits, while sedimentation rates remained high (> 200 m/My) since then (Figure 7.30). The thickness of the Lower Cenozoic mudstone sequences is another factor of influence on overpressure generation and preservation in the study area. The thickness is highly variable: it is reduced above salt structures and relatively thin over large part of the Central Graben (except for the south western most part where it reaches > 900 m), while in the A blocks of the Step Graben the sequence reaches a thickness of more than 900 m.

### Regional variation in pressures

The pore pressures in the Upper North Sea Group indicate that hydrostatic/close-to-hydrostatic pressure conditions prevail in the Upper North Sea Group, while the pre-Cenozoic units (Chalk and older) are overpressured to a greater or lesser extent (Figure 7.31). Pore pressure measurements are largely lacking for the predominantly mudrock sequences of the Lower North Sea Group (Figure 7.31 and Figure 7.32). Pore pressure measurement of P= of 21.173 MPa at 1528 mTVDss in the Basal Dongen Tuffite at F17-06 and a kick measurement of P= 20.71 MPa at 1224 mTVDss at the base of the Rupel in F02-02A indicate that significant

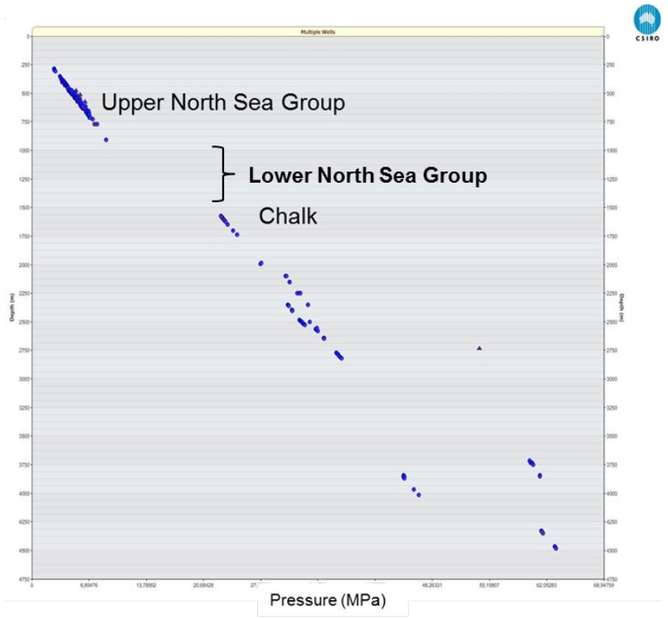


**Figure 7.32. Multiple-well cross plot of pore pressure versus depth shows that pore pressure measurements are lacking for depths between the normally pressured Upper North Sea Group and the overpressured Chalk and older stratigraphic units.**

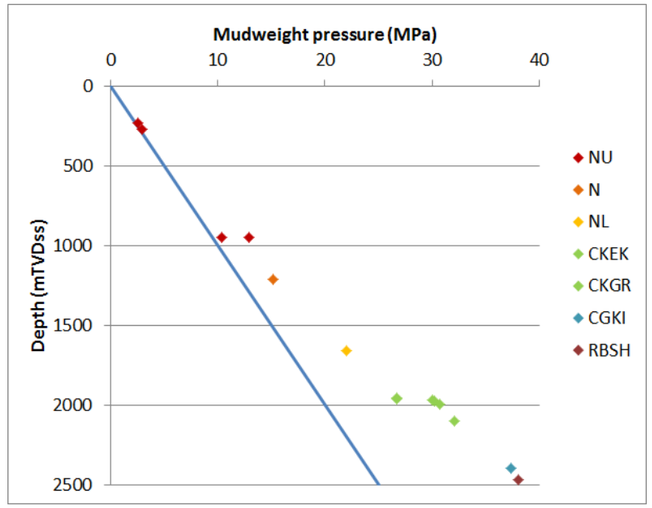


**Figure 7.33. Cross plot of mudweight pressure versus depth at A12-02. The mudweight overpressure has a magnitude of 3.08 – 5.4 MPa in Cenozoic sequences below the MMU. The Glauconite shale/MMU in A12-01 is located at a depth of 1075.38 mTVDss. Note the pressure transition zone between the largely normally pressured Upper North Sea Group and overpressured pre-Cenozoic stratigraphic units.**

overpressures do occur in the Lower North Sea Group.

Mudweight pressures are used as proxy for pore pressure in order to extent our insight into the pressure condition of the Cenozoic sequences between the normally pressured conditions at shallow depth and the overpressured condition in the pre-Cenozoic sequences (Figure 7.33). Figures 7.34, 7.35 and 7.36 show the change of mudweight pressure with depth in the Cenozoic sequences in the Step Graben and Dutch Central Graben and Cleaverbank Platform, respectively. These pressure depth plots indicate that there is a pressure transition zone in the Cenozoic sequences between the normally pressured Upper North Sea Group at shallow depths and overpressured pre-Cenozoic units. The mudweight pressures reach highest values in the Step Graben. The plots also show that there is lateral variation of mudweight pressures at the same burial depth.

### Variation in pressures along SW-NE seismic section North (Figures 7.37 to 7.42)

The seismic section from southwest to northeast runs through the Cleaverbank Platform (D12-01; Figure 7.39), Step Graben (F04-01; Figure 7.38), and Dutch Central Graben (F02-03,-05,-06,-07; Figure 7.39 and Figure 7.40; and B18-03; Figure 7.42). Comparison of the mudweight pressure - depth plots shows that the mudweight overpressures increase for the same burial depth in the Cenozoic between D12-01 and F04-01, i.e. from west to east. The main difference, however, can be observed in the mudweight overpressures in the more basal parts of the Lower North Sea Group: i.e. 0.977 MPa at 835 mTVDss in D12-01 versus 8.424 MPa at 1483 mTVDss in F04-01 (Figure 7.37 and Figure 7.38, respectively). Relatively high mudweight overpressures were also observed further east in the Hanze area (Figure 7.39 and 7.40) and at B18-03 (Figure 7.42). The regional difference between mudweight overpressures in the Cleaverbank Platform and the Step and Dutch Central Graben are spatially related with the west to east increase in thickness of the Cenozoic sequences both below and above the MMU/LMU. More local variations in mudweight overpressures also occur, for example, between overpressures in Cenozoic sequences overlying the Hanze field (F02-03,-05,-06) and at F02-07 outside the Hanze field (Figure 7.41): at the same depth of measurement the mudweight pressure is lower at F02-07 (note that this is based only on one measurement value).

Sometimes abrupt increases in mudweight pressure have been reported, for example: at D12-01: the increase is Pmw = 0.052 to 0.977 MPa at 835 mTVDss (the Glauconite shale/MMU is located at a depth of 522.02 mTVDss (Figure 7.37); at F02-07: the increase is Pmw = 16.567 to 19.053 MPa at a depth of 1408.2 mTVDss , hence below the Glauconite shale/MMU which is located at 1333.52 mTVDss (Figure 7.40).

### Variation in pressures along SW-NE seismic section South

The southern seismic section runs from southwest to northeast through the Cleaverbank Platform (K05-04, K06-01,K06-06), Dutch Central Graben (F17-06, F17-07), Terschelling Basin (F18-02), Schillgrund High (F15-06). The regional increase in mudweight overpressure from the Cleaverbank Platform to the Dutch Central Graben as observed along the northern cross section is also apparent along this southern section: low overpressure values at the base of the Lower North Sea Group in K05-04 (OPmw= 1.135MPa at 1165 mTVDss; Figure 7.43); to increased overpressures in the Dutch Central Graben: OPmw=3.542MPa at 1206.6 mTVDss in F17-07 (Figure 7.44); pore fluid overpressure OP=5.432MPa at 1528 mTVDss in F17-06 (Figure 7.45). More towards the north east, the mudweight overpressures in the Cenozoic decrease again, reaching values of OPmw = 1.407 MPa at 1444.5 mTVDss in F18-02 in the Terschelling Basin (Figure 7.46) and OPmw = 1.136 MPa at 1124.88 mTVDss on the Schillgrund High in well F15-06 (Figure 7.47).

It is interesting to note that mudweight pressures and WFT pore pressure measurements in F17-06 show that the overpressures in the Scruff, Schieland, Chalk groups and lowermost part of the Lower North Sea Group have the same magnitude and follow a hydrostatic gradient. This suggests

| Well Name | Depth (mMDRT) | Depth (mTVDss) | Age Strat. Unit Overlying MMU | Depth (mMDRT)MMU* | Depth (mTVDss) |
|---|---|---|---|---|---|
| F17-10 | 930 | | Gelasian | 942,35 | 908,1 |
| F17-11 | 1162*** | | | | |
| F17-12 | 905 | | Gelasian | 920,09 | 884,59 |
| F17-13 | 955 | | | | |
| F02-06 | 1040** | | Early Zanclean | 1147,9 | 1108,9 |
| F02-03 | 1183 | 1147 | | 1207,46 | 1171,46 |
| F02-05 | 1075 | 1034 | | 1177 | 1136 |
| F02-05 | 1075 | 1034 | | 1135 (LMU) | 1094 |

* 'MMU' corresponding to depth of glauconite shale
** Complete suit HCs present until depth 1138mMDRT
***Complete suit HCs present until depth 1345mMDRT (gradual decrease of iC5, nC4 and C3 between 1345 and 1162 mMDRT)

**Table 7.1 Location of abrupt changing geochemical gas composition in Cenozoic sequences in relation to the location of the MMU**

that the Lower North Sea Group sediments do not act as a pressure barrier in this location. The mudweight pressures decrease at shallower depth in the North Sea Supergroup.

### Variation in pressure along S-N seismic section

The S-N seismic section runs through the Schillgrund High (F15-06) and Dutch Central Graben (F12-01/F12-02, F09-02, F09-01, F02-07). Figures 7.48 and 7.49 show that the mudweight overpressures in the Cenozoic sequences are higher in the Dutch Central Graben in comparison with those in the Schillgrund High (Figure 7.47). In addition, the mudweight overpressures vary at the same burial depth in the Dutch Central Graben (OPmw = 2.330MPa at 1430 mTVDss at F12-02, OPmw = 5.666MPa at 1378 mTVDss at F12-01; OPmw = 3.439 MPa at 1406.5 mTVDss at F09-02).

### Discussion and conclusion Influence of overpressure distribution on petroleum system

The increase in – mudweight – overpressure starts in the Upper North Sea Group above the EMU/MMU/LMU. The depth at which the mudweight overpressuring starts in the Upper North Sea Group roughly corresponds to the depth at which gas content increases. Probably the mudweight was increased during drilling in order to decrease the flow of gas into the borehole. The mudweight pressure in the Upper North Sea Group downward from depths where gas is present, is clearly not not representing the real pore pressure. The real pore pressure measurements indicate that the pore pressures are close to normal at least to a depth of 700 m (B13-03, A18-02).

The observed - mudweight - overpressure conditions in the Cenozoic sequences in most locations inventoried in the project do show a rather gradual increase of mudweight overpressure from the normally pressured condition in the Upper North Sea Group until the base of the Lower North Sea Group. The mudweight pressure data do not reveal the existence of a regionally extensive pressure barrier confining the overpressured Cenozoic sequences. At some locations abrupt increases in mudweight have been reported close to the Miocene unconformities (A12-02, F01-01, F02-07) . Pressure kicks indicate that locally there exists either a vertical connection with higher overpressures at greater depths (via faults), or lateral connection with deeper overpressures at greater depth via lateral continuous carrier rocks. In addition, petrophysical interpretation of the logs results in relatively high apparent porosities in the Breda Formation.

Assuming that the pattern of mudweight pressures is a proxy for the pattern of pore pressures in the Middle and Lower North Sea Group, with the exception of locations where gas leakage has been observed (i.e. F17, Hanze), the observed pattern of mudweight overpressures suggests that dewatering of the Lower & Middle North Sea Group is not fast enough to keep up with the previous and ongoing sedimentary loading.

The highest mudweight overpressures in the Cenozoic sequences occur at the base of the Lower North Sea Group in the Step and Dutch Central Graben, where thick packages of Lower and Middle as well as Upper North Sea sequences occur. These high overpressures continue into the pre-Cenozoic Chalk or Jurassic sequences. Vertical hydraulic continuity between pre-Cenozoic and Cenozoic sequences could be identified at F17-06, suggesting that the Lower Cenozoic mudrocks are not a pressure barrier, at least not in this location. Local pressure kicks have been encountered at the top of the Chalk, though.

The observed overpressure condition in the Cenozoic and underlying Chalk or Jurassic sequences for gas/oil might influence gas/oil leakage and migration:

- The fluid overpressures in the Chalk in the Step Graben and Dutch Central Graben are close to the leak-off pressures (Verweij et al., 2012); the overpressures in the basal parts of the mudrocks of the Lower North Sea Group reach similar magnitudes as those in the Chalk and will also reach

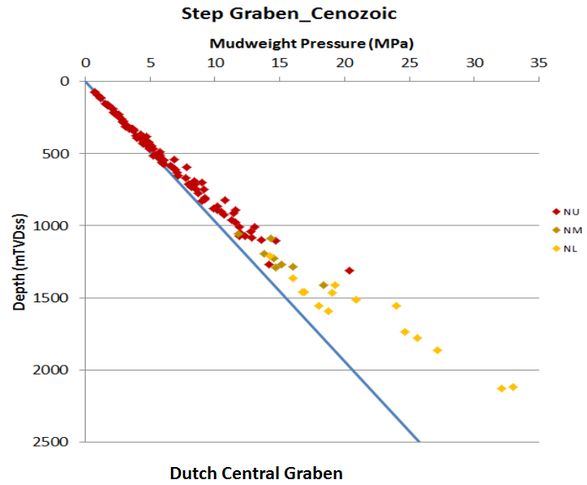


Figure 7.34. Cross plot of mudweight pressure versus depth in Cenozoic sequences in the Step Graben.

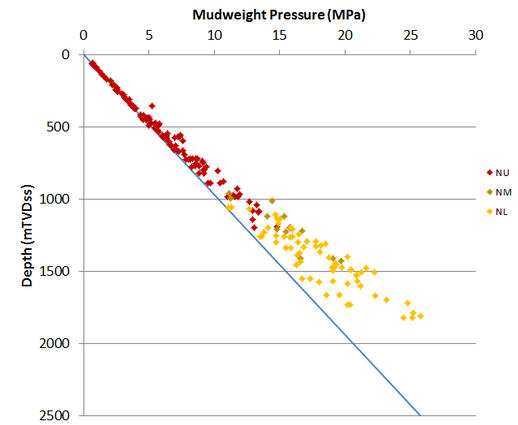


Figure 7.35. Cross plot of mudweight pressure versus depth in Cenozoic sequences in the Dutch Central Graben.

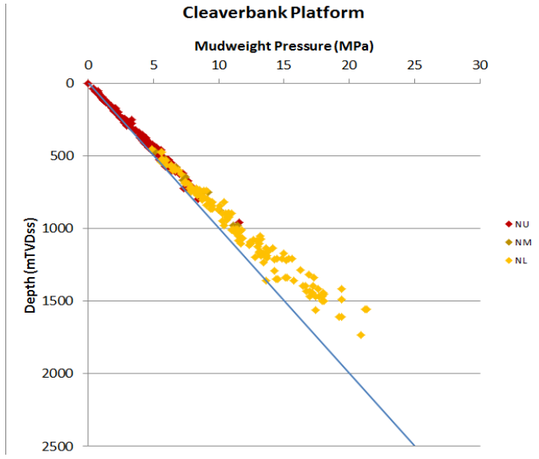


Figure 7.36. Cross plot of mudweight pressure versus depth in Cenozoic sequences in the Cleaverbank Platform.

leak-off pressures. Such high overpressures might have induced fracturing or reopen fractures of the Cenozoic caprock and/or reactive faults facilitating leakage (see also Verweij et al., 2008). Locations on top of salt structures are particularly susceptible, because of fracturing and faulting of Chalk reservoir and Cenozoic caprocks due to salt movements.

- Decrease in overpressure with decreasing depths in the Cenozoic caprock is an additional driving force for upward migration of gas/oil;
- A decrease in hydrostatic pressure with decreasing burial depth cause gas to be exsolved from migrating oil; decrease in overpressure will enhance this process;
- A decrease in hydrostatic pressure with decreasing burial depth reduces the density of migrating gas; decrease from overpressure to normally/hydrostatic pressure will enhance this process

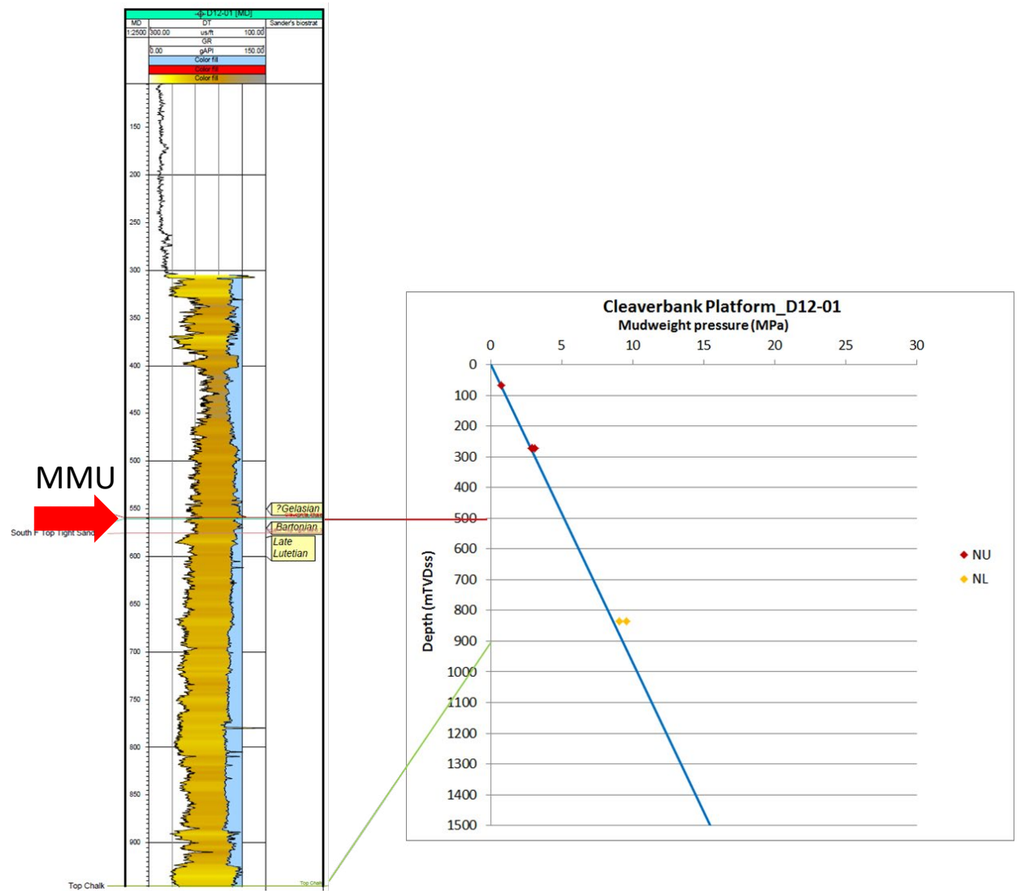


**Figure 7.37. Cross plot of mudweight pressure versus depth in Cenozoic sequences at D12-01: maximum mudweight overpressure changes in magnitude from 0.486 to 0.977 MPa at 835 mTVDss . The small inset cross plot shows mudweight pressures in Cenozoic sequences of D12-04, -05,-01,-A-02,-03). The petrophysical logs shows the location of the Glauconite shale/MMU.**

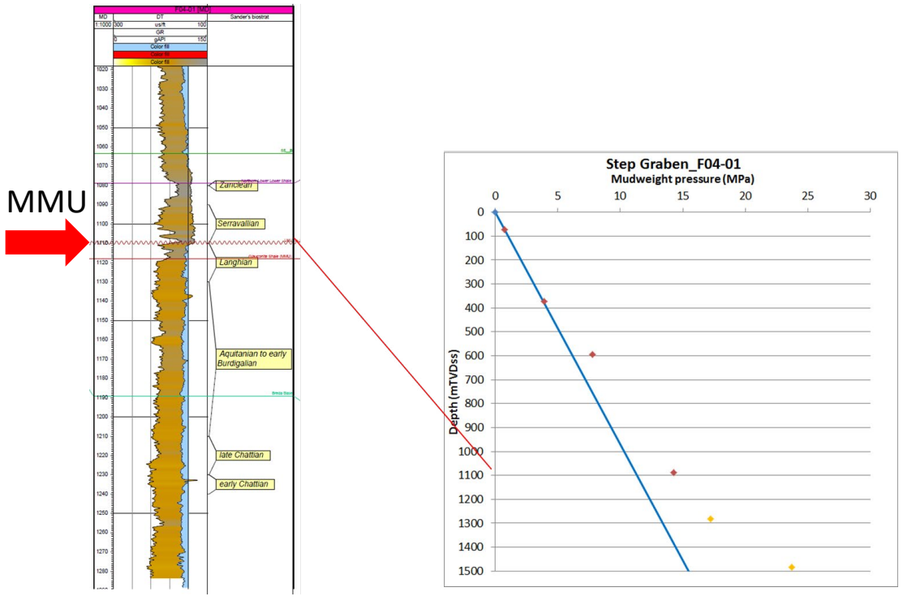


Figure 7.38. Cross plot of mudweight pressure versus depth in Cenozoic sequences at F04-01. The base of the North Sea Supergroup is at 1725 mTVDss. The petrophysical log shows the location of the Miocene unconformities (LMU at 1110 mMD = 1083 mTVDss; Glauconite shale/MMU at 1118.04 mMD = 1091.14 mTVDss) The LMU is located just above lowermost measurement in the Upper North Sea Group.

Figure 7.39. Multiple well cross plot of mudweight pressure versus depth in Cenozoic sequences above the Hanze oil field. Cross plot includes mudweight pressures measured at F02-03,-05,-06. The maximum mudweight overpressure OPmw = 4.148 MPa in the Lower North Sea Group. The petrophysical log of F02-06 shows the location of the Glauconite shale/MMU (1108.9 mTVDss = 1147.9 mMDRT).

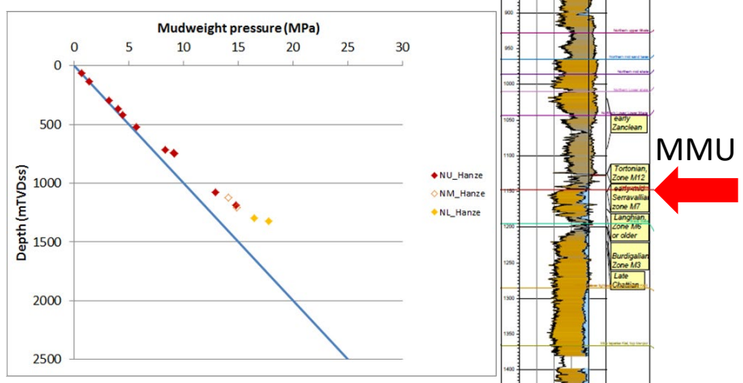


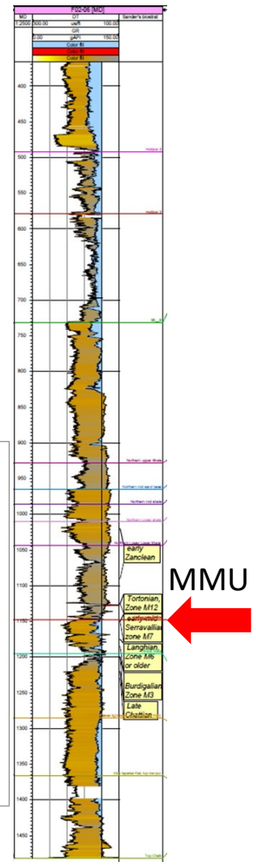


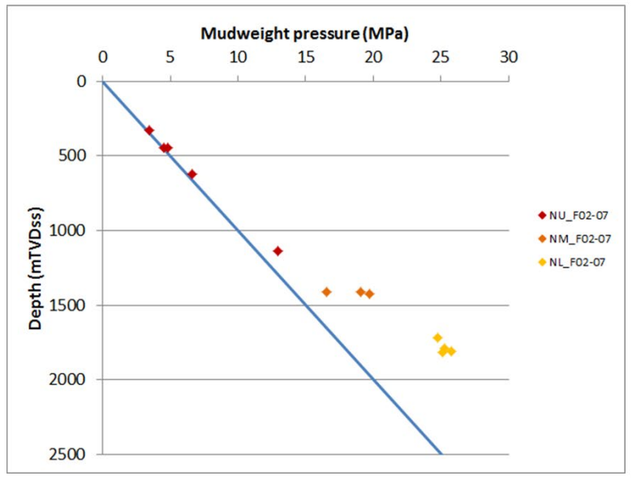


Figure 7.40. Cross plot of mudweight pressure versus depth of Cenozoic sequences in F02-07, located in the Dutch Central Graben, outside the Hanze oil field. Note the sharp increase in mudweight just below the MMU from 16.56 –> 19.05 –> 19.71 MPa. The petrophysical log shows the location of the Glauconite shale/MMU.

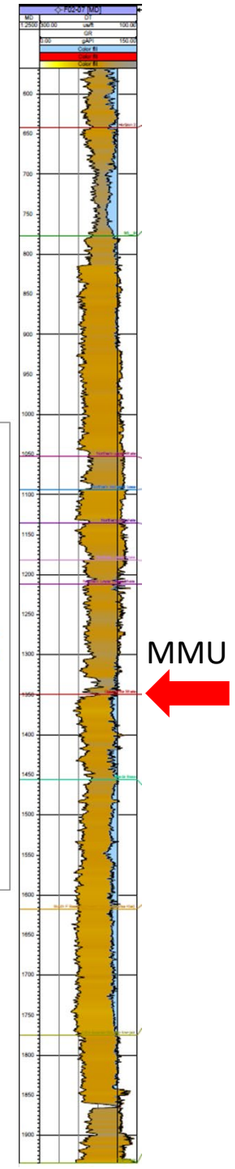

Vertical leakage of thermogenic gas into the Cenozoic sequences and its abrupt changing geochemical composition at short distance above the ‘MMU’

### Apparent migration front of thermogenic gas

The apparent migration front of thermogenic gas above the F17 and Hanze oil fields is located at short distance above the MMU (Table 7.1). Although gas composition from F17-12 (non-degraded thermogenic gas) and F17-10, 11, 13 (biodegraded gas) are different, the apparent sharp migration front of the gases of Chalk origin above both F17-12 and F17-10,11,-13 is located at short distance above the MMU in sequences of Gelasian age. Below the migration front, the geochemical composition of the gas in the Cenozoic caprock does not change much, i.e. the gas composition seems not to have been affected noticeably by biodegradation, water washing or adsorption during migration.

The geochemical and isotopic composition of the gas at shallower depth in the Upper North Sea Group is indicative for gas of microbial origin.

### Timing of vertical leakage of thermogenic gas

The above table shows that migrating thermogenic gases reached sequences of Gelasian age (2.58-1.8) above the F17 area. The Hanze reservoir was probably filled not before the Gelasian (S5: 2.58-2.44 Ma), and leakage into the Cenozoic caprock will not have started before that time. Hence leakage of thermogenic gas from the F17 and Hanze Chalk fields into the Cenozoic caprock occurred in Gelasian times and/or later. Hence after the times of formation of the Miocene unconformities.

We indicated that the main phase of microbial gas generation in the Eridanos Delta deposits started at the beginning of the Gelasian and continues until present-day. Hence microbial gas generation is active during leakage of thermogenic gas from the Chalk oil reservoirs.

The calculated present-day depth interval for the optimum temperature window for microbial gas generation above the Hanze oil field, assuming a constant high geothermal gradient, is from about 450 m to about 900 m.

### Scenarios to explain abrupt changes in geochemical composition of gas

Microbial generation of gas in the Eridanos delta deposits started at the beginning of the Gelasian and continues until present-day. This indicates that thermogenic gases passing the Miocene unconformities and leaking into the Eridanos delta deposits will have encountered microbial generated gases, whether the thermogenic gas leakage occurred in one event, several events, or continuesly until present-day. The timing of the thermogenic gas leakage (e.g.in Early Gelasian or related to glaciation and deglaciation of the Dutch North Sea) and type of leakage (events or continues leakage) will have influenced the geochemical composition of the end result of mixing of the thermogenic gas and the microbial gas:

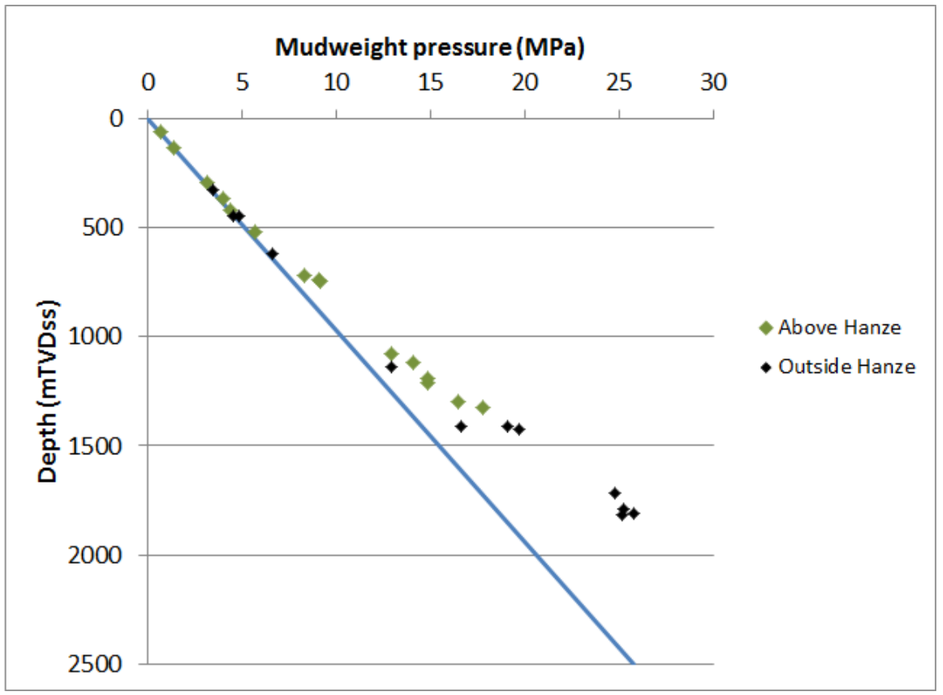


Figure 7.41. Multiple well cross plot of mudweight pressure versus depth in Cenozoic sequences overlying the Hanze field (F02-03,-05,-06) and outside the Hanze field (F02-07).

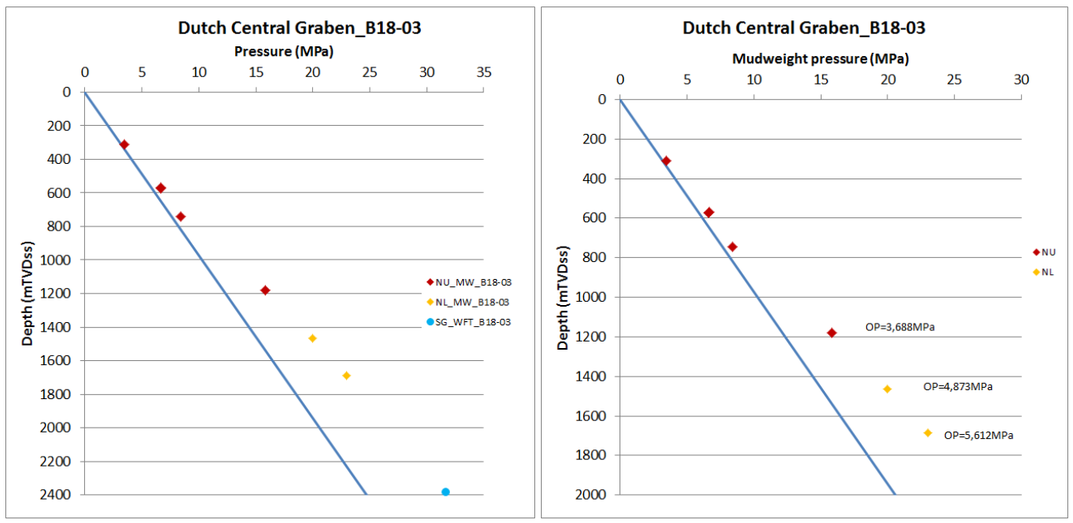


Figure 7.42. Cross plot of mudweight pressure versus depth in Cenozoic sequences and WFT pressure versus depth in Jurassic sequence (SG) (left). Cross plot of mudweight pressure versus depth in Cenozoic sequences in well B18-03 (right). The base of the North Sea Supergroup is located at 1893 mMD = 1863 mTVDss, and MMU/glauconite shale is located at = 1346.77 mMD = 1316.52 mTVDss. The mudweight overpressure seems more dependent on depth than on location of Miocene unconformities.

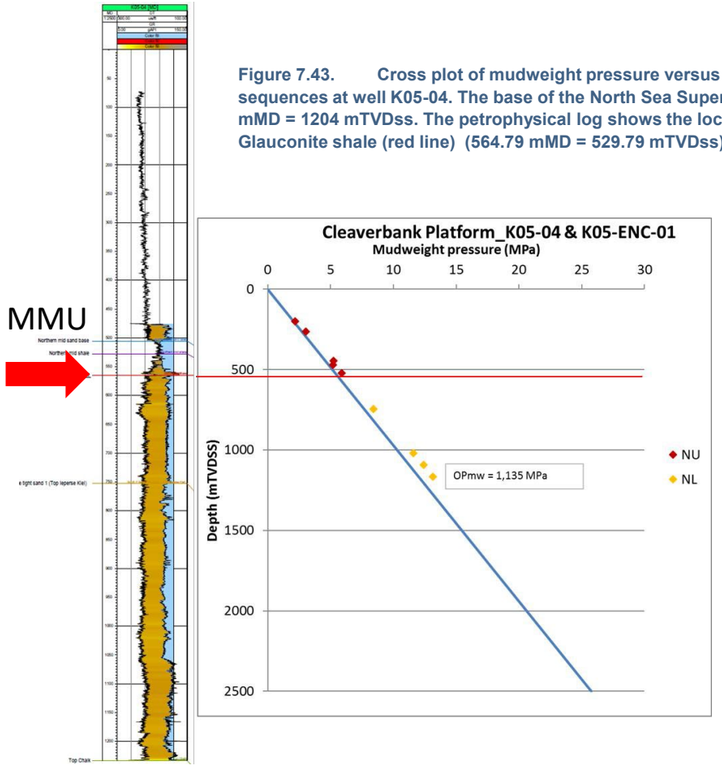


Figure 7.43. Cross plot of mudweight pressure versus depth in Cenozoic sequences at well K05-04. The base of the North Sea Supergroup is at 1229 mMD = 1204 mTVDss. The petrophysical log shows the location of the Glauconite shale (red line) (564.79 mMD = 529.79 mTVDss).

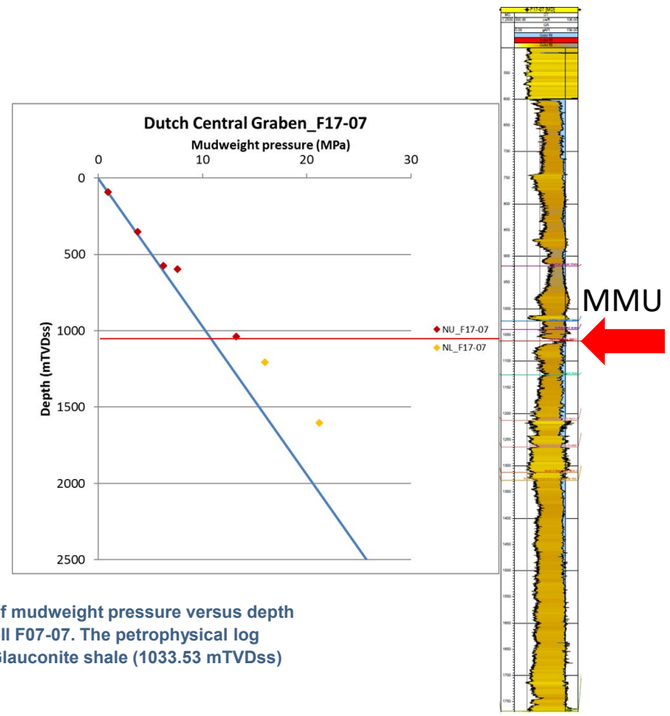


Figure 7.44 Cross plot of mudweight pressure versus depth in Cenozoic sequences at well F07-07. The petrophysical log shows the location of MMU/Glauconite shale (1033.53 mTVDss) (red line).

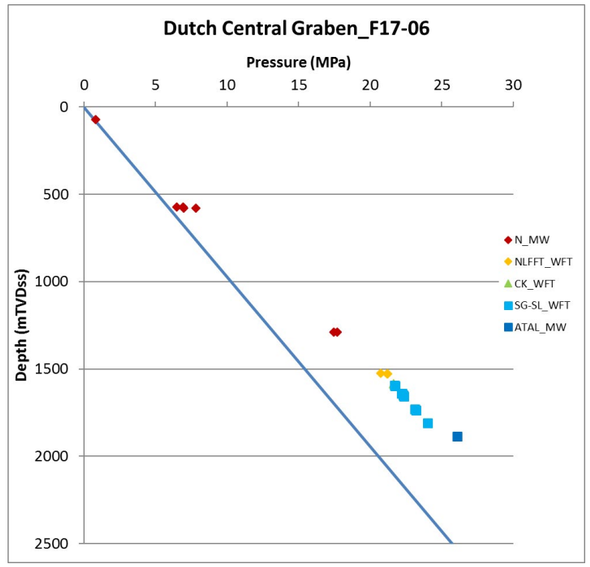


Figure 7.45. Cross plot of of mudweight and WFT pore water pressures versus depth in Cenozoic and underlying Chalk and Jurassic sequences. The WFT pressures in Jurassic (SG-SL) and Chalk sequences follow a hydrostatic gradient and the overpressures in Jurassic and Chalk sequences extend into the Lower North Sea Group (NLFFT).

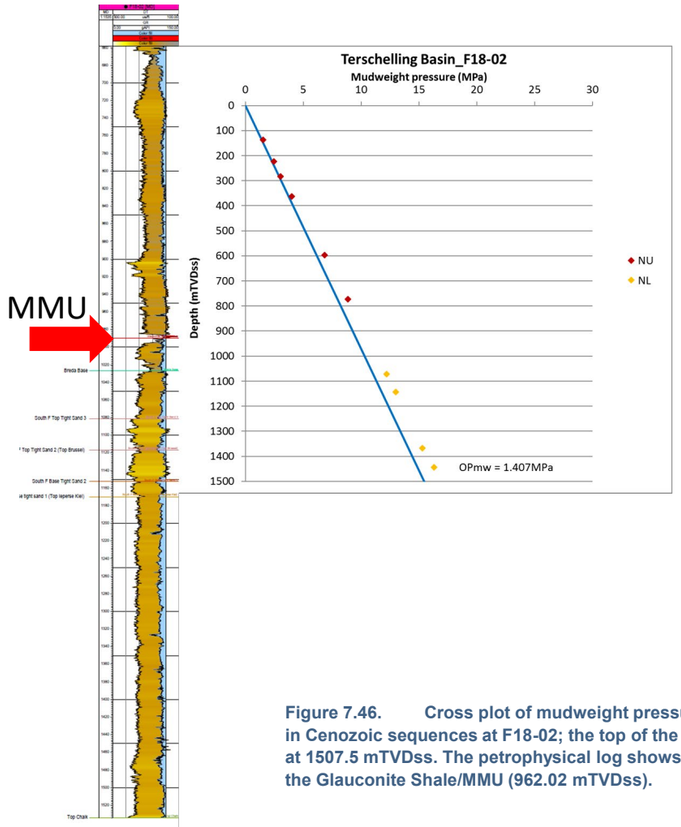


Figure 7.46. Cross plot of mudweight pressure versus depth in Cenozoic sequences at F18-02; the top of the Chalk is located at 1507.5 mTVDss. The petrophysical log shows the location of the Glauconite Shale/MMU (962.02 mTVDss).

Scenario 1: Leakage of thermogenic gas from the Chalk petroleum reservoirs is ongoing, but amount of microbial gas generated in the Eridanos delta deposits is much larger than the amount of vertically leaking gas of Pre-Cenozoic sources. The mixing of both gases masks/conceals the thermogenic component in the shallow gas;

Scenario 2: Leakage of thermogenic gas from the Chalk petroleum reservoirs occurred during one or more events in the past, while microbial gas generation continues until present-day. The amount of microbial gas generated in the Eridanos delta deposits is much larger than the amount of residual thermogenic gas in the delta deposits that was trapped during the leakage events and preserved. The mixing of both gases masks/conceals the thermogenic component in the shallow gas. If so, there is no/hardly any thermogenic gas leakage occurring after this event. The observed presence of gas below the migration front can be considered to be residual gas;

Scenario 3: Leakage of thermogenic gas from the Chalk petroleum reservoirs occurred during one or more events in the past, and most of the gas that entered the recently deposited and porous Eridanos delta deposits escaped to the atmosphere; microbial gas generated after the thermogenic leakage event is trapped in the sediments and preserved. The observed presence of gas below the migration front can be considered to be residual gas;

Scenario 4: The thermogenic gas leaks through the Cenozoic caprock overlying the Chalk petroleum reservoir, crosses the Miocene unconformities, enters a relatively permeable unit of the Eridanos delta deposits and migrates laterally updip. Given the fact that the structural geometry of the permeable unit above the MMU will have been influenced by salt movement to a greater or lesser extent, such a permeable unit may initially have formed a trap for the gas. After such a trap was filled to spill point the additional gas might have migrated laterally updip in the delta deposits. This will only happen if lateral migration of the gas is more easy than leaking through the intra-delta unit overlying the trap. In this case no or only very little thermogenic gas will have leaked into shallower delta deposits, and microbial gas is the dominant gas.

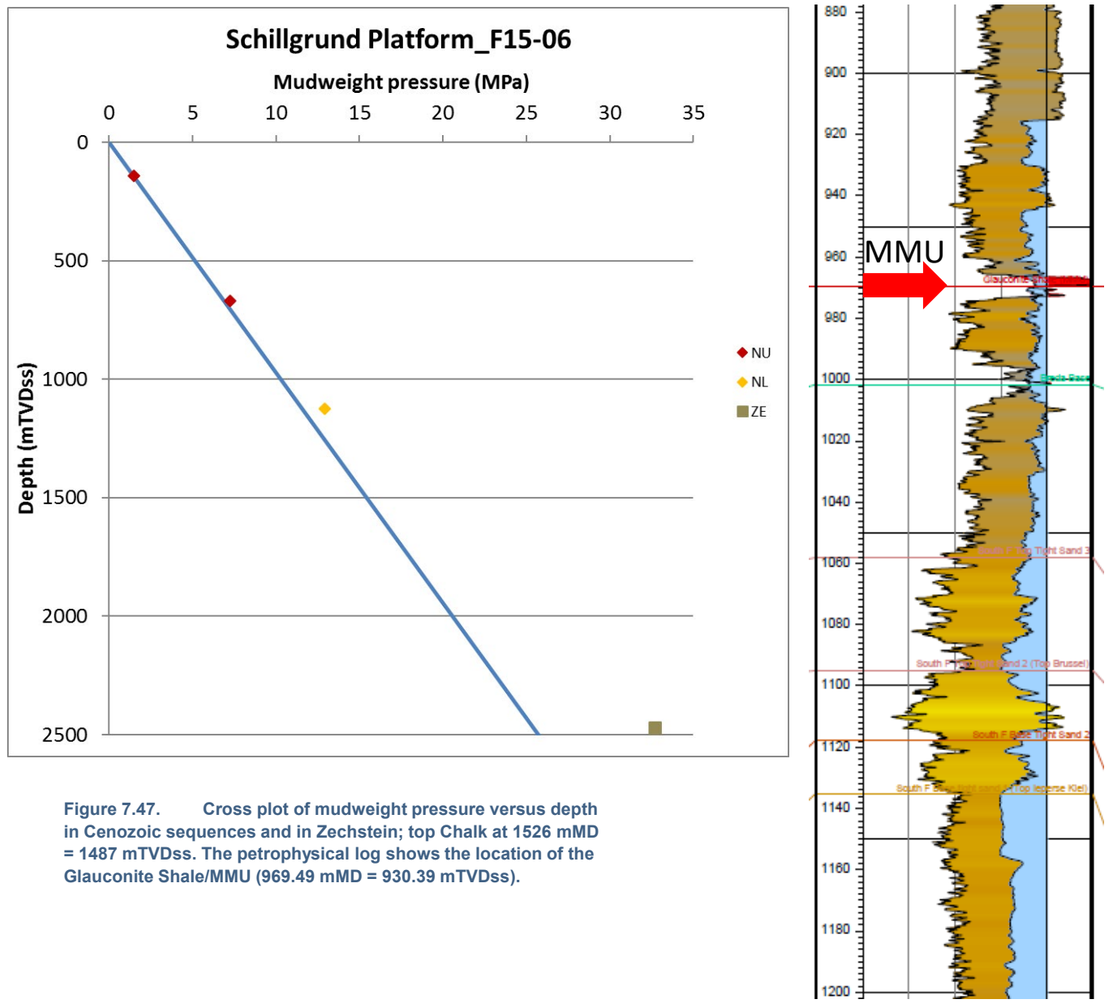


**Figure 7.47. Cross plot of mudweight pressure versus depth in Cenozoic sequences and in Zechstein; top Chalk at 1526 mMD = 1487 mTVDss. The petrophysical log shows the location of the Glauconite Shale/MMU (969.49 mMD = 930.39 mTVDss).**

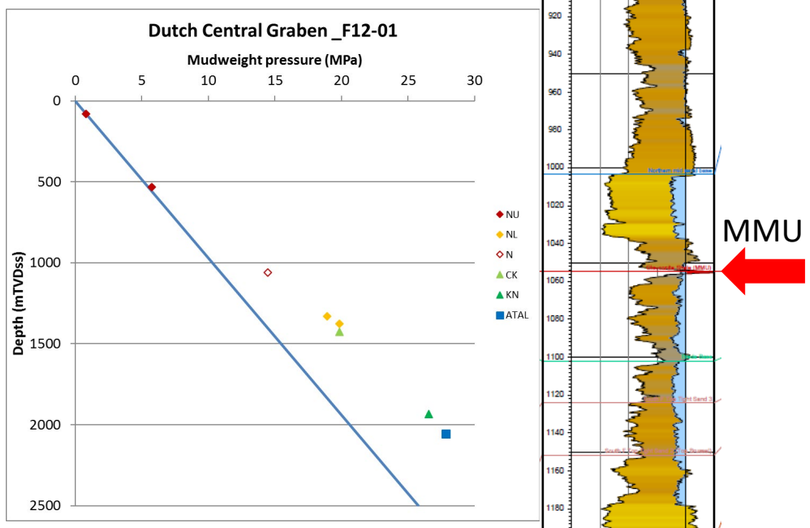


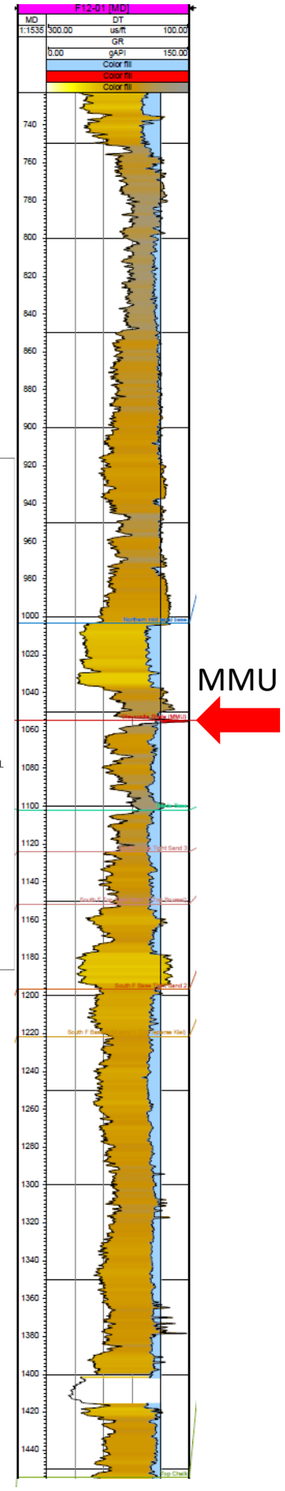


Figure 7.48. Cross plot of mudweight pressures versus depth for different stratigraphic sequences at well F12-01. Petrophysical log shows the location of the Glauconite Shale/MMU (1023.48 mTVDss).

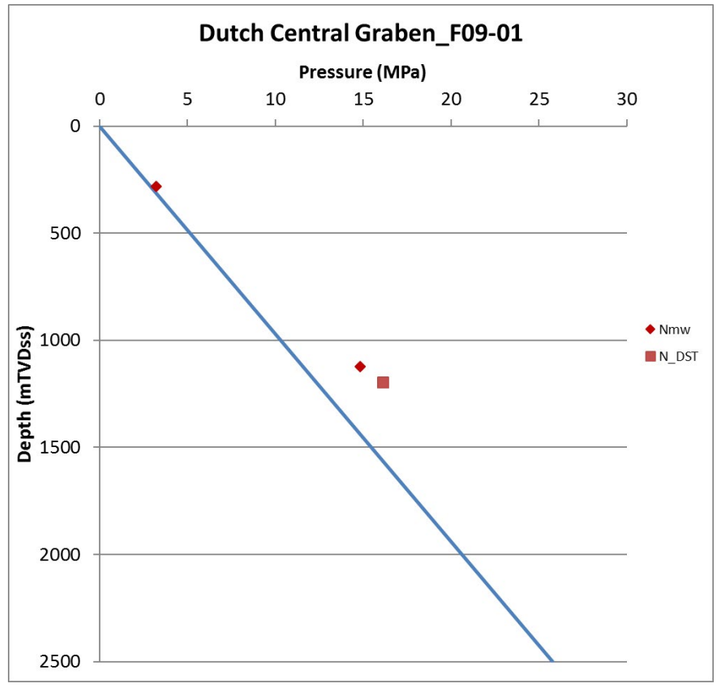


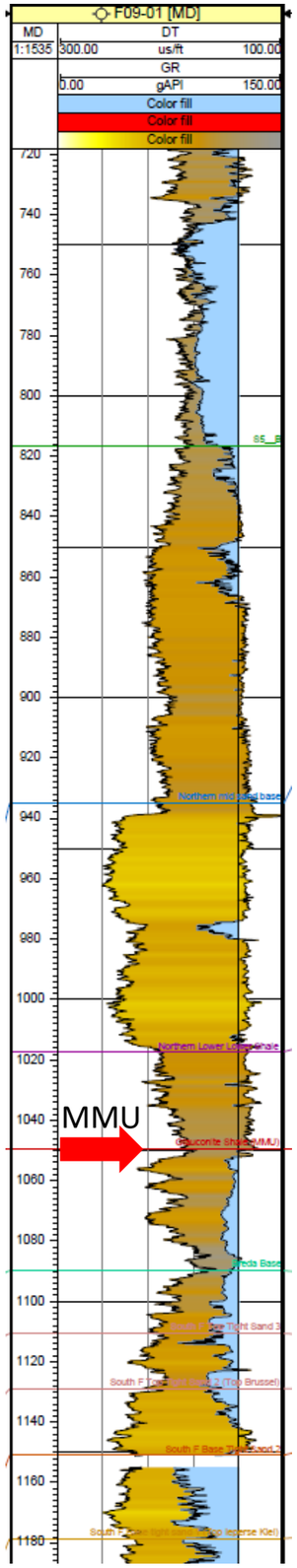


Figure 7.49. Cross plot of mudweight and DST pressures in Cenozoic sequences at well F09-01. Petrophysical log shows the location of the Glauconite Shale/MMU (1051.44 mMD = 1014.04 mTVDss).

*Miocene outcrop in Denmark*

## 8. Conclusions

# 8. CONCLUSIONS

## MMU Petroleum play

The aim of this project is to investigate whether a petroleum play is present around the MMU. One of the hypotheses that was tested, encompasses the presence of a basin floor fan of Serravalian age. Unfortunately, no single petroleum play was found. The hydrocarbons encountered in F02 are found in Serravallian aged strata while the hydrocarbons in F16 are found in Pliocene strata. However, in F02 there are also gas accumulations in the Pliocene, but these are 400 meters above the MMU.

Interpretation of the gas composition data revealed the existence of two petroleum systems around the Miocene unconformities. Gas of predominant thermogenic origin occurs in Cenozoic sequences below the MMU/LMU (and slightly above it) overlying the F17 and Hanze Chalk fields. There is no apparent change in thermogenic gas composition in the Lower North Sea Group sequences. Abrupt changes in gas composition from predominant thermogenic to predominant microbial signature occur above the MMU/LMU. Gas composition in the Eridanos Delta deposits above the MMU/LMU has a strong microbial signature. Leakage of thermogenic gas from the F17 and Hanze Chalk fields into the Cenozoic caprocks occurred in Gelasian times and/or later. Microbial generation of gas in the Eridanos Delta deposits started at the beginning of the Gelasian and continuous until present day. Loading-induced overpressured conditions in Cenozoic sequences below the MMU/LMU and underlying Chalk will have affected past and present leakage of thermogenic gas.

## Stratigraphic development

At the start of the project we knew that the studied interval has never been of major interest for drillers. This is reflected in the lack of accuracy of the lithostratigraphic interpretations that are provided on the NLOG.nl website. The biostratigraphic results obtained in this project showed that all lithostratigraphic interpretations were wrong to some extent. Either, the provided interpretation is to coarse (e.g. only naming the super groups), or contains errors. As a consequence, well markers (tops) are not reliable and wells can have apparent mis-ties, although tied correctly. For this interval, we advise not to use the well markers as provided on the NLOG website.

The cause of these inaccuracies is not only the lack of interest by drillers, but also the use of lithostratigraphy in a complex depositional system. For example, the presence of green sands, is interpreted as “Breda Fm.”, which is not diagnostic. Moreover, these lithostratigraphic units are defined in the south of the Netherlands, where they are part of the Rhine Meuse system, while the strata in our study area are sourced from Scandinavia. Consequently, the use of lithostratigraphy yields very poor results.

The new subdivision into intervals shows a very complex regional facies development. The chronostratigraphic diagrams show a complex pattern of sandy shales, shaly sands, tight sands and shales, and abrupt sedimentary shifts. However, when the lithofacies of these diagrams are plotted on maps (figures 8.1a-e) in a simplified way, the relationship between the panels is shown and the lateral development of the system becomes clear. Unfortunately, the sparsity of the data analyzed does not allow to draw hard conclusion on the sedimentary development, provenance or depositional environment. The palynological analysis, forming the basis for the biostratigraphic interpretations, also present a glimpse into the depositional environment, even in the absence of reliable cored sections. The entire Eocene – Miocene succession, is characterized by persistently marine depositional settings. The diversity of dinoflagellate cysts is high and persistently encompasses outer neritic to open marine taxa, such as Spiniferites. An exception is the Langhian-Serravalian interval, which reflects an increase in abundance of restricted dinoflagellate cyst taxa (i.e., predating the MMU, see also Donders et al., 2009). In addition, a clear increase in terrestrial components is recognized above the LMU (in the Plio-Pleistocene). This is related to the inception of the Eridanos System.

## Old vs New

Figure 8.2 shows the Wheeler of Panel F02. In red the old interpretations are depicted, while the new interpretations are depicted in green. The old lithostratigraphy is replaced by the subdivision in intervals. We prefer the use of intervals over lithostratigraphy, but in order to compare the results the new lithostratigraphic subdivision is shown in grey. In the new interpretation the Rupel is subdivided into the Veldhoven and Rupel Formation.

The naming and age of surfaces has changed dramatically. Especially the base of the Upper North Sea Group (NU) had 3 different definitions. Seismically is was defined (NLOG.nl) at the LMU (which was erroneously called MMU), lithostratigraphically it was defined as the base of the Breda formation, while its age was defined as base Miocene (Savian). We propose to abandon these definitions and use the Savian unconformity, Early Miocene unconformity, Mid Miocene unconformity, and Late Miocene unconformity. Furthermore, the base of the Dutch Eridanos is better placed at the top of S1 instead of the LMU

## Recommendations

We advise a comprehensive study that incorporates all wells in the northern Dutch offshore, including biostratigraphic age dating of this interval, in order to develop a usable stratigraphic subdivision. In the mean time we advise not to use the well markers (tops) as provided on the NLOG website for this interval, since they are most likely wrong.

To improve our understanding of the spatial distribution of overpressured conditions in the Cenozoic sequences, we recommend to derive additional pressure data from analyses of sonic and density logs. Such analyses will also provide understanding of the spatial distribution of porosity ‘anomalies’ identified in the present petrophysical study.

**Figure 8.1a: Simplified litho-facies distribution of M3**

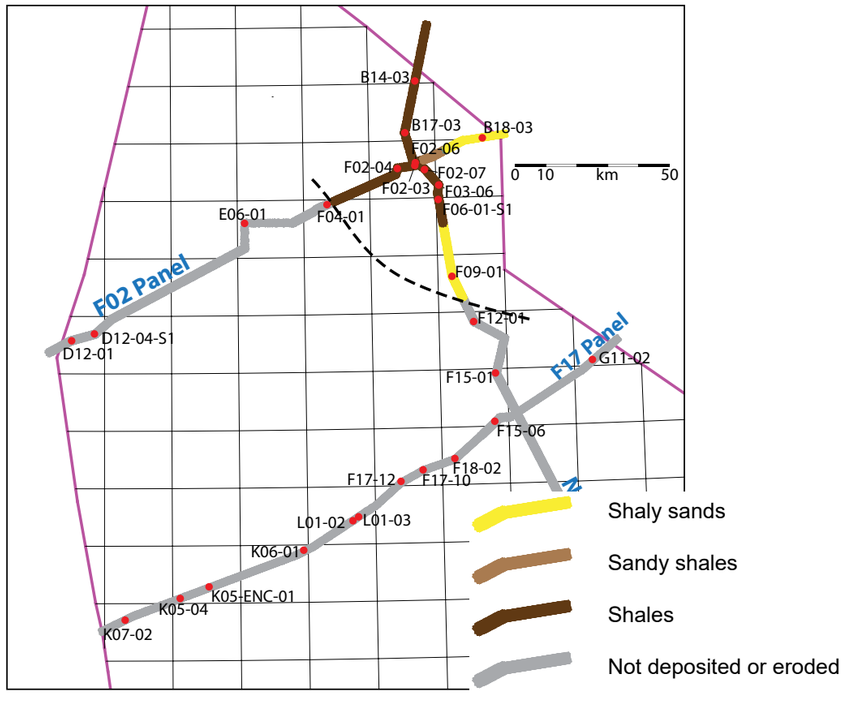


**Figure 8.1b: Simplified litho-facies distribution of M2**

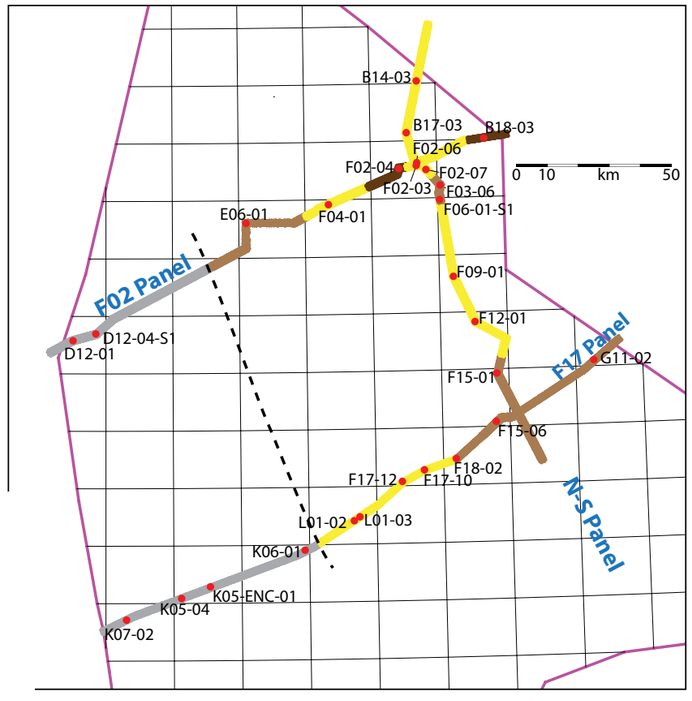

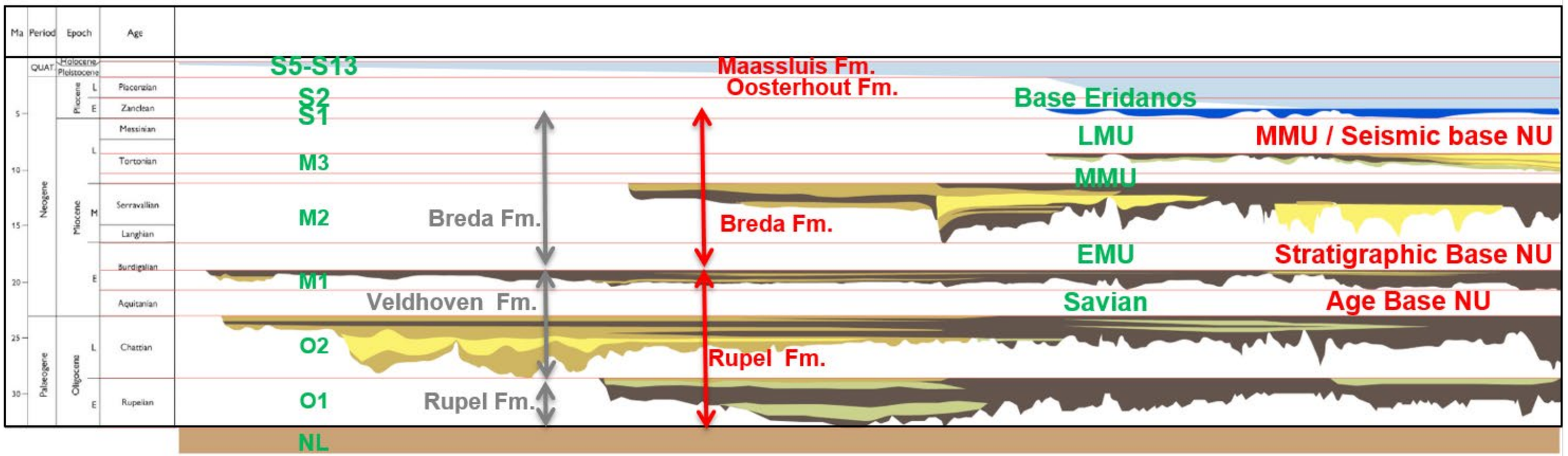


Figure 8.2: Chronostratigraphic diagram of the F02 panel depicting the old terminologies and the new subdivision.

Figure 8.1c: Simplified litho-facies distribution of M1

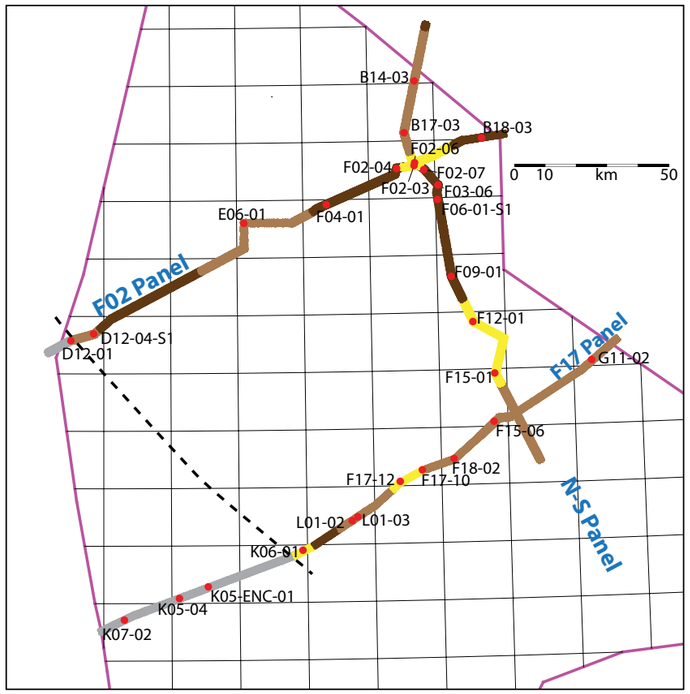


Figure 8.1d: Simplified litho-facies distribution of O2

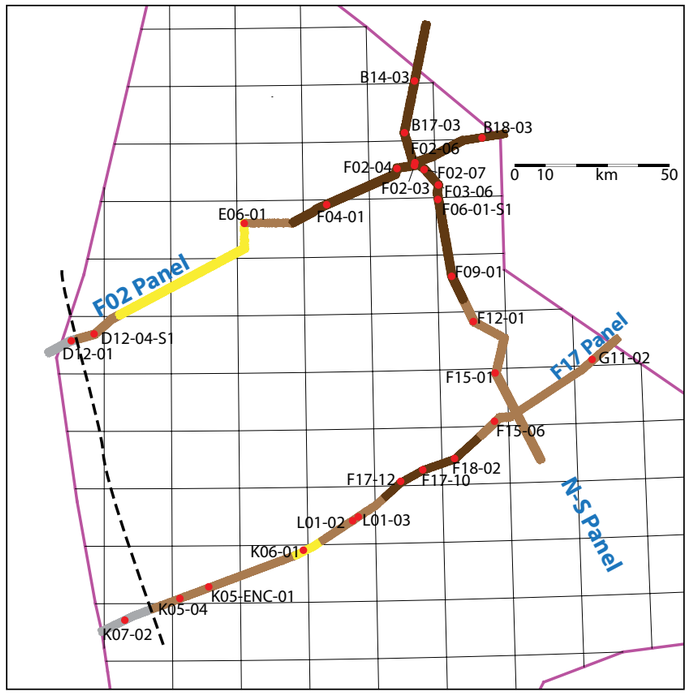


Figure 8.1e: Simplified litho-facies distribution of O1

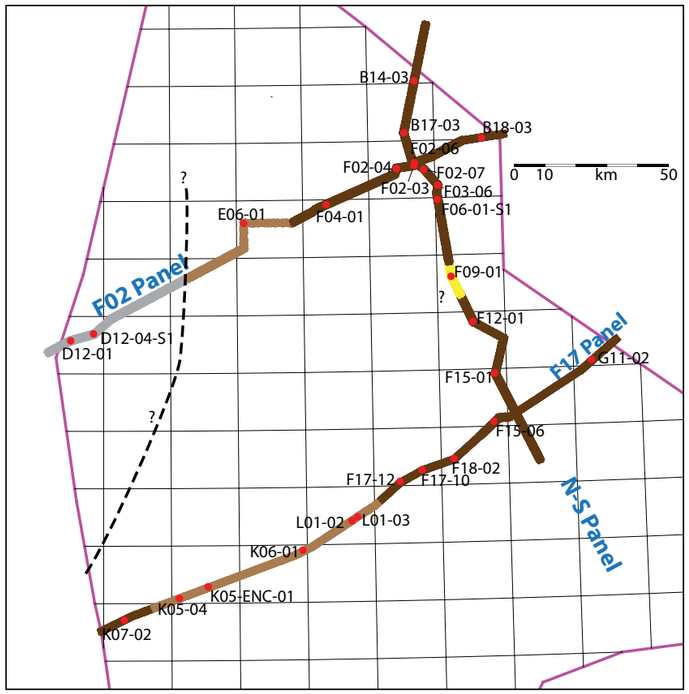

*Rasmussen showing the Danish Miocene*

# 09

## References

# 9. REFERENCES


Abrams, M.A., 2013. Best practices for the collection, analysis, and interpretation of seabed geochemical samples to evaluate subsurface hydrocarbon generation and entrapment. Paper OTC-24219 prepared for presentation at the Offshore Technology Conference, Houston, 6-9 May 2013, 21 pp.

Anell, I., Thybo, H., Rasmussen, E., 2012. A synthesis of Cenozoic sedimentation in the North Sea. Basin Res. 24, 154-179, doi: 10.1111/j.1365-2117.2011.00517.x.

Anell, I., Thybo, H., Stratford, W., 2010. Relating Cenozoic North Sea sediments to topography in southern Norway: The interplay between tectonics and climate. Earth Planet. Sci. Lett. 300, 19-32, doi: 10.1016/j.epsl.2010.09.009.

Andresen, K.J., Huuse, M., Clausen, O.R., 2008. Morphology and distribution of Oligocene and Miocene pockmarks in the Danish North Sea – implications for bottom current activity and fluid migration. Basin Research 20, 445-466.

Benvenuti, A., Kombrink, H., ten Veen, J.H., Munsterman, D.K., Bardi, F., Benvenuti, M., 2012. Late Cenozoic shelf delta development and Mass Transport Deposits in the Dutch offshore area – results of 3D seismic interpretation. Neth. J. Geosci. 91, 591-608, doi: doi:10.1017/S0016774600000391.

Bernhard, B.B., Brooks, J.M., Sackett, W.M., 1976. Natural gas seepage in the Gulf of Mexico. Earth and Planetary Science Letters, 31, 45-54.

Brown, A. ,2011. Interpretation of Three-Dimensional Seismic Data. AAPG Memoir 42 / SEG Investigations no. 9

Bujak, J., & Mudge, D., 1994. A high-resolution North Sea Eocene dinocyst zonation. Journal of the Geological Society, 151(3), 449-462.

Cameron, T., Crosby, A., Balson, P., Jeffery, D., Lott, G., Bulat, J., Harrison, D., 1992. The geology of the southern North Sea. United Kingdom offshore regional report. British Geological Survey and HMSO, London.
Dybkjær, K., Piasecki, S., 2010. Neogene dinocyst zonation for the eastern North Sea Basin, Denmark. Review of Palaeobotany and Palynology 161, 1-29, doi: http://dx.doi.org/10.1016/j.revpalbo.2010.02.005.

Chung, H.M., Gormly, J.R., Squires, R.M., 1988. Origin of gaseous hydrocarbons in subsurface environments: theoretical considerations of carbon isotope distribution. Chemical Geology 71, 97-103.

Clayton, C., 2010. Incorporation of biogenic gas generation into petroleum system models. Oral presentation at the Geological Society of London meeting ‘ Modelling sedimentary basins and their petroleum systems’ , London, 22-23 April 2010.

Clayton, C.J., Hay, S.J., Baylis, S.A., Dipper, B., 1997. Alteration of natural gas during leakage from a North Sea salt diapir field. Marine Geology 137, 69-80.

Dolson, J., 2016. Understanding oil and gas shows and seals in the search for hydrocarbons. Springer International Publishing, Switzerland, 485 pp.

De Verteuil, L., & Norris, G., 1996. Miocene dinoflagellate stratigraphy and systematics of Maryland and Virginia (Vol. 42). Micropaleontology Press.

Evans, D., Graham, C., Armour, A., Bathurst, P., 2003. The Millennium Atlas, Petroleum Geology of the Central and Northern North sea. The Geological Society of London (London), 389 pp.

Fertl, W.H. & G.V. Chilingar, 1988. Total organic carbon content determined from logs. SPE Formation Evaluation,1988, p. 407-419.

Gołędowski, B., Clausen, O.R., Nielsen, S.B., 2014. Reply to comment of E. S. Rasmussen and K. Dybkjær on Patterns of Cenozoic sediment flux from western Scandinavia, by B. Gołędowski, S. B. Nielsen and O. R. Clausen, Basin Research (2012), 24(4), 377–400. Basin Res. 26, 347-350, doi: 10.1111/bre.12046.

Gołędowski, B., Nielsen, S.B., Clausen, O.R., 2012. Patterns of Cenozoic sediment flux from western Scandinavia. Basin Res. 24, 377-400, doi: 10.1111/j.1365-2117.2011.00530.x.

Head, M. J., 1996. Late Cenozoic dinoflagellates from the Royal Society borehole at Ludham, Norfolk, eastern England. Journal of Paleontology, 70(04), 543-570.
Head, I.M., Gray, N.D., Larter, S.R., 2014. Life in the slow lane; biogeochemistry of biodegraded petroleum containing reservoirs and implications for energy recovery and carbon management. Frontiers in Microbiology. Vol. 5, article 566, 1-23.

Hillis, R.R., Holford, S.P., Green, P.F., Doré, A.G., Gatliff, R.W., Stoker, M.S., Thomson, K., Turner, J.P., Underhill, J.R., Williams, G.A., 2008. Cenozoic exhumation of the southern British Isles. Geology 36, 371-374, doi: 10.1130/g24699a.1.

Holford, S.P., Green, P.F., Duddy, I.R., Turner, J.P., Hillis, R.R., Stoker, M.S., 2009. Regional intraplate exhumation episodes related to plate-boundary deformation. Geol. Soc. Am. Bull. 121, 1611-1628, doi: 10.1130/b26481.1.

Houben, A. J., van Mourik, C. A., Montanari, A., Coccioni, R., & Brinkhuis, H. (2012). The Eocene–Oligocene transition: Changes in sea level, temperature or both?. Palaeogeography, Palaeoclimatology, Palaeoecology, 335, 75-83.

Huuse, M., Clausen, O.R., 2001. Morphology and origin of major Cenozoic sequence boundaries in the eastern North Sea Basin: top Eocene, near-top Oligocene and the mid-Miocene unconformity. Basin Res. 13, 17-41, doi: 10.1046/j.1365-2117.2001.00123.x.
James, A.T., Burns, B.J., 1984. Microbial alteration of subsurface natural gas accumulations. AAPG Bulletin 68, 957-960.

Japsen, P., 1999. Overpressured Cenozoic shale mapped from velocity anomalies relative to a baseline for marine shale, North Sea. Petroleum Geoscience 5: 321-336.

Japsen, P., 1997. Regional Neogene exhumation of Britain and the western North Sea. J. Geol. Soc. 154, 239-247, doi: 10.1144/gsjgs.154.2.0239.

Japsen, P., Green, P.F., Bonow, J.M., Erlström, M., 2015. Episodic burial and exhumation of the southern Baltic Shield: Epeirogenic uplifts during and after break-up of Pangaea. Gondwana Res., doi: 10.1016/j.gr.2015.06.005.

Japsen, P., Rasmussen, E.S., Green, P.F., Nielsen, L.H., Bidstrup, T., 2008. Cenozoic palaeogeography and isochores predating the Neogene exhumation of the eastern North Sea Basin. Geological Survey of Denmark and Greenland Bulletin 15, 25-28.
Judd, A., Hovland, M., 2007. Seabed fluid flow – impact on geology, biology and the marine environment. Cambridge University Press, Cambridge, 400 pp.

Katz, B.J., Narimanov, A., Huseinzadeh, R., 2002. Significance of microbial processes in gases of the South Caspian basin. Marine and Petroleum geology 19, 783-796.

Katz, B.J., 2011. Microbial processes and natural gas accumulations. The Open Geology Journal 5, 75-83.

Köthe, A., 2007. Cenozoic biostratigraphy from the German North Sea sector (G-11-1 borehole, dinoflagellate cysts, calcareous nannoplankton) [Känozoische Biostratigraphie aus dem Deutschen Nordsee-Sektor (Bohrung G-11-1, Dinoflagellatenzysten, Kalknannoplankton)]. Zeitschrift der deutschen Gesellschaft für Geowissenschaften, 158(2), 287-327.

Köthe, A., Gaedicke, C., Lutz, R., 2008. Erratum: The age of the Mid-Miocene Unconformity (MMU) in the G-11-1 borehole, German North Sea sector [Berichtigung: Das Alter der Mittelmiozän-Diskordanz in der Bohrung G-11-1, Deutscher Nordsee-Sektor]. Zeitschrift der Deutschen Gesellschaft für Geowissenschaften 159, 687-689, doi: 10.1127/1860-1804/2008/0159-0687.

Kuhlmann, G., Langereis, C., Munsterman, D., Jan van Leeuwen, R., Verreussel, R., Meulenkamp, J., Wong, T., 2006. Chronostratigraphy of Late Neogene sediments in the southern North Sea Basin and paleoenvironmental interpretations. Palaeogeography, Palaeoclimatology, Palaeoecology 239, 426-455, doi: 10.1016/j.palaeo.2006.02.004.

Kuhlmann, G., Wong, T.E., 2008. Pliocene paleoenvironment evolution as interpreted from 3D-seismic data in the southern North Sea, Dutch offshore sector. Mar. Pet. Geol. 25, 173-189, doi: 10.1016/j.marpetgeo.2007.05.009.
Larter, S.R., Head, I.M., Huang, H., Bennett, B., Jones, M., Aplin, A.c., Murray, A., Erdmann, M., Wilhelms, A., Di Primio, R, 2005. Biodegradation, gas destruction and methane generation in deep subsurface petroleum reservoirs: An overview. In: Dore, A.G., Vining, B.A. (eds). Petroleum Geology: North-West Europe and Global Perspectives – Proceedings of the 6th Petroleum Geology Conference. Geological Society London, 633-639.

Miller, K. G., Feigenson, M. D., Wright, J. D., & Clement, B. M. (1991). Miocene isotope reference section, Deep Sea Drilling Project Site 608: an evaluation of isotope and biostratigraphic resolution. Paleoceanography, 6(1), 33-52.

Miller, K. G., Kominz, M. A., Browning, J. V., Wright, J. D., Mountain, G. S., Katz, M. E., ... & Pekar, S. F. (2005). The Phanerozoic record of global sea-level change. Science 310, 1293-1298.

Munsterman, D. K., & Brinkhuis, H., 2004. A southern North Sea Miocene dinoflagellate cyst zonation. Netherlands Journal of Geosciences, 83(04), 267-285.

Overeem, I., Weltje, G.J., Bishop-Kay, C., Kroonenberg, S.B., 2001. The Late Cenozoic Eridanos delta system in the Southern North Sea Basin: a climate signal in sediment supply? Basin Res. 13, 293-312, doi: 10.1046/j.1365-2117.2001.00151.x.

Pälike, H., Norris, R. D., Herrle, J. O., Wilson, P. A., Coxall, H. K., Lear, C. H., ... & Wade, B. S. (2006). The heartbeat of the Oligocene climate system. science, 314(5807), 1894-1898.

Prinzhofer, A., Pernaton, E., 1997. Isotopically light methane in natural gas: bacterial imprint or diffusive fractionation? Chemical Geology 142, 193-200.

Prinzhofer, A., Deville, E., 2013. Origins of hydrocarbons seeping out from offshore mud volcanoes in the Nile delta. Tectonophysics 591, 52-61.

Rasmussen, E. S. (2004). Stratigraphy and depositional evolution of the uppermost Oligocene–Miocene succession in western Denmark. Bulletin of the Geological Society of Denmark, 51(2), 89-109.

# 9. REFERENCES


Rasmussen, E.S., Dybkjær, K., 2014. Patterns of Cenozoic sediment flux from western Scandinavia: discussion. Basin Res. 26, 338-346, doi: 10.1111/bre.12024.

Rickers, F., Fichtner, A., Trampert, J., 2013. The Iceland–Jan Mayen plume system and its impact on mantle dynamics in the North Atlantic region: Evidence from full-waveform inversion. Earth Planet. Sci. Lett. 367, 39-51, doi: 10.1016/j.epsl.2013.02.022

Rider, M.H.(1986) The geological interpretation of well logs. Blackie, 175 p.

Schoell, M., 1980. The hydrogen and carbon isotopic composition of methane from natural gases of various origins. Geochim. Cosmochim. Acta 44, 649-661.

Schoell, M., 1983. Genetic characterization of natural gases . AAPG Bulletin 67 (12), 2225-2238.

Schroot, B.M., Klaver, G.T., Schüttenhelm, R.T.E., 2005. Surface and subsurface expressions of gas seepages to the seabed – examples from the Southern North Sea. Marine and Petroleum Geology 22, 499-515.

Simaeys, S. Van, Munsterman, D., & Brinkhuis, H., 2005. Oligocene dinoflagellate cyst biostratigraphy of the southern North Sea Basin. Review of Palaeobotany and Palynology, 134(1), 105-128.

Śliwińska, K. K., Clausen, O. R., & Heilmann-Clausen, C., 2010. A mid-Oligocene cooling (Oi-2b) reflected in the dinoflagellate record and in depositional sequence architecture. An integrated study from the eastern North Sea Basin. Marine and Petroleum Geology, 27(7), 1424-1430.

Sørensen, J.C., U. Gregersen,M. Breiner & O. Michelsen, 1997 High-frequency sequence stratigraphy of Upper Cenozoic deposits in the central and southeastern North Sea areas. Marine and Petroleum Geology 14, p. 99–123

Thöle, H., Gaedicke, C., Kuhlmann, G., Reinhardt, L., 2014. Late Cenozoic sedimentary evolution of the German North Sea – A seismic stratigraphic approach. Newslett. Stratig. 47, 299-329, doi: 10.1127/0078-0421/2014/0049.

Thöle, H., Kuhlmann, G., Lutz, R., Gaedicke, C., 2016. Late Cenozoic submarine slope failures in the southern North Sea – Evolution and controlling factors. Mar. Pet. Geol. 75, 272-290, doi: http://dx.doi.org/10.1016/j.marpetgeo.2016.04.028.

Vandré, C., Cramer, B., Gerling, P., Winsemann, J., 2007. Natural gas formation in the western Nile delta (Eastern Mediterranean): Thermogenic versus microbial. Organic Geochemistry 38, 523-539.

Van Simaeys, S. (2004). The Rupelian-Chattian boundary in the North Sea Basin and its calibration to the international time-scale. Netherlands Journal of Geosciences, 83(03), 241-248.

Veen, J. ten, Verweij, H., Donders, T., Geel, K., Bruin, G. de, Munsterman, D. Verreussel, R., Daza Cajigal, V., Harding, R., 2013. H. Cremer Anatomy of the Cenozoic Eridanos Delta Hydrocarbon System. TNO 2013 R10060

Vejbaek, O.V., 2008. On dis-equilibrium compaction as the cause for Cretaceous-Paleogene over-pressures in the Danish North Sea. AAPG Bulletin 92, 165-180.

Verweij, J.M., Nelskamp, S.N., 2014. Focus on shallow gas systems. Extended abstract. First EAGE Workshop on Basin & Petroleum Systems Modeling Advances of Basin and Petroleum Systems Modeling in Risk and Resource Assessment 19-22 October 2014, Dubai, UAE.

Verweij, J.M., Simmelink, H.J., Underschultz, J., Witmans, N., 2012. Pressure and fluid dynamic characterisation of the Dutch subsurface. Netherlands Journal of Geosciences — Geologie en Mijnbouw 91 (4), 465 – 490.

Whiticar, M.J., Faber, E., Schoell, M., 1986. Biogenic methane formation in marine and freshwater environments: CO2 reduction vs. acetate fermentation – isotope evidence. Geochimica et Cosmochimica Acta 50, 693-709.

Whiticar, M.J., 1999. Carbon and hydrogen isotope systematics of bacterial formation and oxidation of methane. Chemical geology 161, 291-314.

Winthaegen, P.L.A., Verweij, J.M., 2003. Estimating regional pore pressure distribution using 3D seismic velocities in the Dutch Central North Sea Graben. Journal of Geochemical Exploration 78-79: 203-207.

Zou, Y-R., Cai, Y., Zhang, Ch., Zhang, X., Peng, P., 2007. Variations of natural gas carbon isotope-type curves and their interpretations – a case study. Organic Geochemistry 38, 1398-1415.

**TNO Applied Geosciences**
Princetonlaan 6
3584 CB Utrecht
The Netherlands

For more information and
questions, please contact:

**Friso Veenstra**
friso.veenstra@tno.nl

TNO innovation for life